

University of Nottingham
UK | CHINA | MALAYSIA

Immune Instructive Materials For Dendritic Cell Modulation

Submitted by

Lisa Kämmerling

Thesis submitted to the University of Nottingham for the degree of Doctor of Philosophy at the Faculty of Medicine

July 2021

Abstract

With most cytokine-based immunotherapies not fulfilling the promise of efficacy seen in pre-clinical experiments and often being associated with severe dose-limiting toxicities, biomaterial-based immunotherapies have emerged as powerful tools in different clinical settings including cancer vaccines and inflammatory diseases. Dendritic cells (DCs) play a central role in regulating adaptive immune responses making them ideal targets for immune modulation.

To study the effect of polymer chemistry on DCs a screening of a polymer library constituted of acrylates, methacrylates and acrylamides was performed. Both stimulatory and regulatory polymers that instructed or inhibited DC activation respectively were identified. Polymers such as HFiPMA instructed an immunogenic DC phenotype in the absence of any other exogenous stimuli leading to improved interaction with T cells, while polymers such as ZnA rendered DCs less responsive to TLR-4 stimulation and induced limited T cell proliferation. To elucidate the mechanisms of the observed polymer induced modulation in behaviour and phenotype of DCs, the coating stiffness and thickness of adsorbed proteins from serum supplemented culture medium on scaled up polymers were investigated. Two stimulatory hit polymers were additionally tested in an *in vitro* breast cancer-based tumour assay, showing the successful induction of tumour specific cytotoxic T lymphocytes that killed breast cancer cells efficiently. To investigate molecular changes of DCs cultured on stimulatory polymers, microarray analysis was performed to detect the expression levels of more than 21,000 genes.

A short study into topography-induced DC modulations revealed that certain topographies render DC less responsive to LPS stimulus as well as slowed down DC motility, presenting a clear relationship between feature spacing and speed.

In summary, findings from this study demonstrate the ability of polymer surfaces to modulate DC phenotype and function. The observations presented and discussed in this study provide a framework through which immune-instructive therapeutics for vaccine adjuvants, cancer therapies or auto-immune diseases could be developed.

Publications and Conference Proceedings

Manuscripts in preparation

Lisa Kämmerling, Joris Meurs, Francesco Pappalardo, Morgan R. Alexander, Amir M. Ghaemmaghami. “Discovery of immune instructive polymers with ability to modulate dendritic cell phenotype and downstream adaptive immune responses”.

Lisa Kämmerling, Laurence Burroughs, Steven Vermeulen, Britta Koch, Jan de Boer, Morgan R. Alexander, Amir M. Ghaemmaghami. “Topography conditioning renders DCs tolerogenic and limits DC motility.”

Matthew Vassey, Le Ma, **Lisa Kämmerling**, Chidimma Mbadugha, Gustavo F Trindade, Grazziela P. Figueredo, Francesco Pappalardo, Robert Markus, Seema Rajani, Qin Hu, David A. Winkler, Derek Irvine, Richard Hague, Amir M. Ghaemmaghami, Ricky Wildman and Morgan R. Alexander. “Instruction of innate immune cells using micron-scale 3D features of controlled chemistry and architecture: The ChemoArchiChip”.

Manuscripts submitted

Leanne E. Fisher, **Lisa Kämmerling**, Morgan R. Alexander, Amir M. Ghaemmaghami. (2021). “Immune instructive materials for medical applications.” **Current opinion in Biotechnology.**

Manuscripts published

Rostam, Hassan M., Leanne E. Fisher, Andrew L. Hook, Laurence Burroughs, Jeni C. Luckett, Grazziela P. Figueredo, Chidimma Mbadugha, Alvin C. K. Teo, Arsalan Latif, **Lisa Kämmerling**, Mitchell Day, Karen Lawler, David Barrett, Somaia Elsheikh, Mohammad Ilyas, David A. Winkler, Morgan R. Alexander, and Amir M. Ghaemmaghami. (2020). "Immune-Instructive Polymers Control Macrophage Phenotype and Modulate the Foreign Body Response In Vivo." **Matter** 2(6):1564–81.

Lisa Kämmerling, Leanne E. Fisher, Ezgi Antmen, Gorkem M. Simsek, Hassan M. Rostam, Nihal E. Vrana, Amir M. Ghaemmaghami. (2021). "Mitigating the foreign body response through 'immune-instructive' biomaterials." **Journal of Immunology and Regenerative Medicine** 12:100040.

Conferences/Meetings attended

1. Lisa Kämmerling, Adam Dundas, Valentina Cuzzucoli Crucitti, Derek Irvine, Morgan R. Alexander, Amir M. Ghaemmaghami. (2020). Oral presentation – "New instructive biomaterials to direct the adaptive immune system via dendritic cell modulation". 11th World Biomaterials Congress, Virtual platform.

2. Lisa Kämmerling, Adam Dundas, Valentina Cuzzucoli Crucitti, Derek Irvine, Morgan R. Alexander, Amir M. Ghaemmaghami. (2019). Poster presentation - "New instructive biomaterials to direct the adaptive immune system via dendritic cell modulation". British Society for Immunology Congress 2019, Liverpool, United Kingdom.

3. Lisa Kämmerling, Morgan R. Alexander, Amir M. Ghaemmaghami. (2019) Poster presentation – “Dendritic cell immunomodulation by novel polymers”. 1st joint conference of TCES-UKSB, Nottingham, United Kingdom.

4. Lisa Kämmerling, Adam Dundas, Valentina Cuzzucoli Crucitti, Derek Irvine Morgan R. Alexander, Amir M. Ghaemmaghami. (2019) Oral presentation – “Immune instructive polymers for dendritic modulation.” Post Graduate Research Symposium, School of Life Sciences, University of Nottingham, United Kingdom.

5. Lisa Kämmerling, Britta Koch, Jan de Boer, Morgan R. Alexander, Amir M. Ghaemmaghami. (2018) Poster presentation – “Topography-induced modulation of dendritic cell motility and phenotype”. 29th Annual Meeting of the European Society for Biomaterials, Maastricht, the Netherlands.

6. Lisa Kämmerling, Britta Koch, Jan de Boer, Morgan R. Alexander, Amir M. Ghaemmaghami. (2018) Poster presentation – “Topography induced modulation of dendritic cell motility”. Post Graduate Research Symposium, School of Life Sciences, University of Nottingham, United Kingdom.

Acknowledgements

The work presented here would not have been possible without the support, encouragement, and guidance of many individuals around me:

First and foremost, I am extremely grateful to *my supervisors Professor Amir M Ghaemmaghami and Professor Morgan R Alexander* for their invaluable advice, continuous support and patience during my PhD study. Their immense knowledge and guidance have been vital in my development as an independent researcher.

I would also like to acknowledge all *past and present members of the Immunology and Immuno-bioengineering group*, *and the Laboratory or Biophysics and Surface Analysis.* Specifically, I would like to thank the postdocs (Dr Constantin Tanase, Dr Matthew Vassey, and Dr Leanne Fisher), as well as my fellow PhD colleagues Dr Arsalan Latif, Dr Chidimma Mbadugha, and Mitchell Day for always being open for scientific discussions, offering new perspectives on research approaches and giving challenging feedback on experimental design. It was a pleasure to work with and alongside them, as they created a friendly laboratory environment that encouraged creative thinking and had me looking forward to every day in the lab.

I would like to express my gratitude to *collaborators within and outside the University of Nottingham* for their endless support in my studies. Special thanks goes to Professor Paddy Tighe for his support with the gene microarray analysis , Professor Derek Irvine for answering my endless polymer chemistry questions, Professor Jan de Boer and the MERLN laboratory for fabricating

topographic surfaces used in this study, Dr Laurence Burroughs for helping me with polymer questions, Dr David Scurr for support with surface analysis, Dr Craig Stoppiello for performing the XPS sample acquisition, Dr Marcos Castellanos Uribe and Iqbal Khan for acquiring my gene microarrays, Dr Adam Dundas and Dr Valentina Cuzzucoli Crucitti for fabricating polymeric microparticles for this study, Dr Joris Meurs for performing the LESA analysis and Dr Francesco Pappalardo for performing AFM measurements for me. I thank them all for sharing their expertise and facility in progressing the depth of this project, while widening my research projective.

I would also like to thank Dr David Onion and Nicola Croxall from the *Flow Cytometry Facility, all members of SLIM imaging unit as well the nmRC, University of Nottingham* for their technical support and patience in training troubleshooting, and their valuable advice in developing analysis routines.

Thank you to *my friends and support team* here in the UK. Without their kind help and support my life in the UK would have been lacking something.

Lastly, I would like to express my endless gratitude to *my parents and my husband*. Without their tremendous understanding and encouragement in the past few years, it would be impossible for me to complete my doctoral studies and I would not be the person I am today.

I. Table of contents

Abbreviations XVIII

Chapter 1 General Introduction 2

1.1 The immune system 2

1.1.1 Innate immune system 2

1.1.1.1 The role of dendritic cells in the immune system 6

1.1.1.2 DC origin and subsets 10

1.1.1.3 Monocyte-derived DCs as an experimental model 12

1.2 Adaptive immune system 13

1.2.1.1 T cells: origin and selection 14

1.2.1.2 T cell subsets and their function in health and disease 15

1.2.1.3 Dendritic cells and their interaction with T cells 18

1.3 Biomaterials in immunomodulation 19

1.4 Surface chemistry 22

1.5 Surface topography 24

1.6 Modulating macrophage cell responses using biomaterials 27

1.7 Biomaterial-based DC modulation 28

1.8 Screening strategies for biomaterial discovery 37

1.9 Hypothesis and aims 38

Chapter 2 General Methods 40

2.1 Cellular and molecular techniques 40

2.2 Monocyte isolation 40

2.2.1 Dendritic cell generation 40

2.2.2 Enzyme linked immunoglobulin linked assay (ELISA) 41

2.2.3 Flow cytometry 41

2.3 Surface characterisation methods 43

2.3.1 X-ray photoelectron spectrophotometry (XPS) 43

2.3.2 Time of flight – secondary ion mass spectrometry (ToF-SIMS) 44

Chapter 3 Screening of an acrylate and methacrylate library for immunomodulation of DCs 46

3.1 Introduction 46

3.2 Methods 49
3.2.1 Monocyte isolation 49
3.2.2 Monomer to polymer polymerisation by UV 49
3.2.3 Polymer plate washes for cell culture 49
3.2.4 Determination of cell viability 50
3.2.5 DC culture on polymer coated surfaces 51
3.2.6 Flow cytometry staining 51
3.2.7 Cytokine analysis 51
3.2.8 Endocytosis assay 52
3.2.9 Statistical analysis 52
3.3 Results 53
3.3.1 Evaluation of DC viability on polymer surface 53
3.3.2 Identification of polymers that induce DC activation 56
3.3.3 Identification of polymers that suppress surface marker upregulation 61
3.3.4 Cytokine production in response to polymers 66
3.3.5 Endocytosis 73
3.4 Discussion 75
Chapter 4 Surface characterisation of selected hit polymers and their functional effect on DCs 82
4.1 Introduction 82
4.2 Methods 85
4.2.1 Monocyte isolation 85
4.2.2 Monomer to polymer polymerisation by UV 85
4.2.3 Polymer plate washes for cell culture 85
4.2.4 Cell culture 85
4.2.5 XPS analysis 85
4.2.6 ToF-SIMS 87
4.2.7 AFM 88
4.2.8 DC culture on polymer coated surfaces 88
4.2.9 Flow cytometry staining 88
4.2.10 Cytokine analysis 89
4.2.11 Sample preparation for Microarrays 89
4.2.12 Microarray data analysis 90
4.2.13 Bioinformatics analysis 90
4.2.14 T cell co-cultures 91
4.2.15 IDO activity 91
4.2.16 Tumour killing assay 91

4.2.17 Statistical analysis 92
4.3 Results 94
4.3.1 Material characterisation 94
4.3.1.1 Bio-adsorbate layer thickness on polymers 94
4.3.1.2 Atomic force microscopy (AFM) 98
4.3.2 Cytokine secretion on scaled up polymer coatings 100
4.3.3 Surface marker expression on scaled up polymer coatings 103
4.3.4 Gene microarray analysis supports relevance of stimulatory polymers for cancer immunotherapy 106
4.3.4.1 DEAEA treated DCs upregulate genes involved in antigen presentation and DC maturation 109
4.3.4.2 HFiPMA culture activates genes and canonical pathways involved in adaptive immune responses and induction of anti-tumour responses 119
4.3.5 T cell co cultures 131
4.3.5.1 Polymer culture influences DC interaction with CD3+ T cells 132
4.3.5.2 Stimulatory polymers significantly improve DC ability to activate naïve T cells and induce higher proliferation levels 135
4.3.5.3 Memory T cells expand more rapidly when DCs have been cultured on stimulatory polymers 138
4.3.6 Tumour killing assay 142
4.3.7 Immunomodulatory properties of ZnA 145
4.4 Discussion 149
Chapter 5 From 2D to 3D structures – Polymeric scaffolds as new tools for immunomodulation 156
5.1 Introduction 156
5.2 Methods 161
5.2.1 Scaffold fabrication 161
5.2.2 Monocyte isolation 162
5.2.3 Viability assay 162
5.2.4 Cell culture 162
5.2.5 ELISA 162
5.2.6 SEM 163
5.2.7 Statistical analysis 163
5.3 Results 164
5.3.1 Optimisation of pore size 164
5.3.2 HFiPMA scaffold did not negatively impact DC viability 167

5.3.3 DCs cultured in HFiPMA scaffold increase cytokine secretion 168
5.4 Discussion 172
Chapter 6 Particulate system - Is 2D effect of polymer coatings translated into 3D particulates? 176
6.1 Introduction 176
6.2 Methods 181
6.2.1 Monocyte isolation 181
6.2.2 Viability assay 181
6.2.3 Cell culture 181
6.2.4 Microparticle fabrication 181
6.2.5 Immunofluorescence staining 182
6.2.6 Flow cytometry 182
6.2.7 Single step nanoprecipitation 182
6.3 Results 185
6.3.1 Polymeric microparticles for DC modulation 185
6.3.1.1 Assessing impact of microparticles on dendritic cell viability 185
6.3.1.2 Microparticles induce differential attachment behaviour of DCs 186
6.3.1.3 Microparticles induce upregulation of CD86 on DCs 188
6.3.1.3.1 DEAEA MP increase CD86 mean fluorescence intensity 188
6.3.1.3.2 Assessed by flow cytometry 189
6.3.1.4 Microparticle induce modulated cytokine secretion 192
6.3.2 Polymeric nanoparticles for DC modulation 194
6.4 Discussion 200
Chapter 7 Investigation of topography – induced modulation of DC behaviour and function 204
7.1 Introduction 204
7.2 Methods 209
7.2.1 Topography fabrication 209
7.2.2 Topography preparation 209
7.2.3 Cell culture on topographies 210
7.2.4 DC staining 210
7.2.5 Live cell imaging 210
7.2.6 Flow cytometry staining 210
7.2.7 ELISA 211

7.2.8 $CD3^+$ T cell co-culture 211
7.2.9 T cell proliferation assay 211
7.2.10 Statistics 212
7.3 Results 213
7.3.1 Motility of immature dendritic cells on topographic features 213
7.3.2 Topography culture decreases HLA-DR expression on iDCs 219
7.3.3 LPS stimulation DCs on topographies leads to less activated DCs 221
7.3.4 Assessing cytokine secretion on topographies 224
7.3.5 Effect of topography culture on DC ability to initiate T cell response 225
7.4 Discussion 228
Chapter 8 General Discussion 234
Chapter 9 References 243
Appendix 1: Polymer library with viability values 263
Appendix 2: Cytotoxicity of monomer in media 269
Appendix 3: Comparison of monomer effect to polymerised surface coatings on iDCs 270
Appendix 4: DEAEA vs TCP – summary of IPA analysis 271
Appendix 5: HFiPMA vs TCP – summary of IPA analysis 272
Appendix 6: Canonical pathways summary 273
Appendix 7: LPS stimulated DCs lead to typical maturation gene responses 287
Appendix 8: Mini TopoChip unit numbering with corresponding features 289
Appendix 9: Phenome topographies with corresponding topography IDs 299

II. Table of figures

Figure 1-1 Overview schematic of PRR sub-families 4

Figure 1-2: TLRs and their ligands 5

Figure 1-3: Overview of monocyte to DC differentiation, maturation and the polarisation of T lymphocytes..... 7

Figure 1-4: Brief overview of immature and mature DC functions and the role they play in the tolerance-immunity spectra. 8

Figure 1-5: Schematic overview of human DC hematopoiesis 11

Figure 1-6: Overview of T cell polarisation dependant from perpetrators. 16

Figure 1-7: The costimulatory signals between DCs and T lymphocytes. 19

Figure 3-1: Viability comparison of pre-culture procedure 54

Figure 3-2: Viability assay of DCs cultured on polymer coatings in 96 well-plates with plates prepared as described in Table 3. 56

Figure 3-3: Polymers increase CD83 expression on DCs 58

Figure 3-4: Polymers increase CD86 expression on DCs 60

Figure 3-5: Correlation of CD83 and CD86 expression on polymer cultured DCs ...61

Figure 3-6: Polymers render DCs less susceptible to CD83 upregulation upon LPS stimulaton 63

Figure 3-7: Polymers render DCs less susceptible to CD86 upregulation upon LPS stimulation 65

Figure 3-8: Correlation of polymer CD83 and CD86 expression in LPS presence...66

Figure 3-9: Cytokine secretion by DCs after polymer culture 68

Figure 3-10: Polymers suppress cytokine secretion in presence of stimulus 70

Figure 3-11: DCs modulate uptake ability after polymer culture 74

Figure 4-1: Schematic overview of tumour killing experiment.....92

Figure 4-2: DEAEA TOF-SIMS overview 96

Figure 4-3: Bio-adsorbate layers on polymer coatings 98

Figure 4-4 AFM Force-Displacement curve of representative force curves extracted from polymer films, acquired by Francesco Pappalardo. 99

Figure 4-5 Young's modulus of wet polymer films 100

Figure 4-6: Polymer treatment modulates DCs cytokine secretion 102

Figure 4-7: Polymer treatment modulates surface marker expression on DCs 105

Figure 4-8: Differentially expressed genes of DEAEA, HFiPMA and TCP + LPS vs TCP 106

Figure 4-9: MAP Prediction legend 111

Figure 4-10: DEAEA - OX40L signalling pathway 112

Figure 4-11: DEAEA- Antigen presentation Pathway 113

Figure 4-12: DEAEA- DC maturation part1 114

Figure 4-13: DEAEA- DC maturation part2 115

Figure 4-14: DEAEA -DC maturation part3 115

Figure 4-15: DEAEA-DC maturation part 4 116

Figure 4-16: DEAEA - TLR signalling 118

Figure 4-17: HFiPMA – Antigen presentation pathway 121

Figure 4-18: HFiPMA - TLR signalling 123

Figure 4-19: HFiPMA - Integrin signalling 124

Figure 4-20: HFiPMA - NFκB signalling 125

Figure 4-21: HFiPMA – DC maturation part 1 127

Figure 4-22: HFiPMA- DC maturation part 2 128

Figure 4-23: HFiPMA – Th1 and Th2 activation pathway 130

Figure 4-24: HFiPMA - Pattern recognition receptors 131

Figure 4-25: Polymer treatment influences the outcome of DC-T cell interactions134

Figure 4-26: Polymer treatment influences DC interaction with naïve T cells and modulates naïve T cell proliferation rates 136

Figure 4-27: Polymer treatment influences DC interaction with naïve T cells and modulates naïve T cell IFN gamma secretion 138

Figure 4-28: Polymer treatment influences DC interaction with memory T cells and modulates their proliferation rates 140

Figure 4-29: Polymer treatment influences interaction of DCs with memory T cells and modulates their IFN-γ secretion 142

Figure 4-30: MCF7 monolayer shows dead cells after CTL-coculture 144

Figure 4-31: Tumour specific lysis is increased ratio-dependent in conditions where DCs were conditioned on polymers.....145

Figure 4-32: ZnA modulates HLA-DR and PD-L2 expression.....147

Figure 4-33: ZnA treatment increased IDO activity.....148

Figure 5-1 Methodology of scaffold fabrication.....161

Figure 5-2: HFiPMA-Comparison of pore size between different weight percentages and freezing temperatures.....165

Figure 5-3: HFiPMA-scaffolds comparison between fabrication days.....166

Figure 5-4: Representative images of HFiPMA scaffolds by SEM.....167

Figure 5-5: Impact of HFiPMA scaffolds on DC viability.....168

Figure 5-6: TNF-α secretion within scaffolds.....169

Figure 5-7: IL-1β secretion within scaffolds.....170

Figure 5-8: IL-6 secretion within scaffolds.....171

Figure 6-1: Single step nanoprecipitation methodology.....184

Figure 6-2: Impact of microparticles on DC viability.....186

Figure 6-3: DC attachment to polymer microparticles.....187

Figure 6-4: CTCF of DCs adhered to microparticles.....189

Figure 6-5: Effect of 2.5 mg/mL microparticle culture on DC activation.....191

Figure 6-6: Comparison between 2.5 mg/mL and 10 mg/mL microparticle culture on DC activation.....192

Figure 6-7: TNFα secretion after microparticle culture.....193

Figure 6-8: IL-1β secretion after microparticle culture.....194

Figure 6-9: Preliminary fabrication of DEAEA nanoparticles.....195

Figure 6-10: Preliminary fabrication of HFiPMA nanoparticles.....196

Figure 6-11: Preliminary fabrication of THFuA nanoparticles.....197

Figure 6-12: HFiPMA nanoparticle aggregates by SEM.....198

Figure 6-13: TEM of HFiPMA nanoparticle.....199

Figure 7-1: Mean speed per Track from each topographic pattern.....214

Figure 7-2: Track displacement from each topographic pattern.....214

Figure 7-3: Correlation between mean speed and track displacement of cells on topographies. 215

Figure 7-4: Five fastest and five slowest motility generating topographies 216

Figure 7-5: Five topographic features that support the most movement and five that support least cell movement 216

Figure 7-6: Mean speed can be correlated to feature spacing 217

Figure 7-7: Examples of feature spacing classes 218

Figure 7-8:Mean speed vs track displacement 219

Figure 7-9: Modulation of HLA-DR expression on immature DCs following 24 hours culture on topographies. 220

Figure 7-10: No modulation of PD-L1, CCR7, CD83 and CD86 after iDC topography culture 221

Figure 7-11: HLA-DR expression is modulated when DCs are stimulated with LPS on topographies 222

Figure 7-12: CCR7, PD-L1, CD83 and CD86 expression in LPS-stimulated DCs on topographies 223

Figure 7-13: IL-10 and IL-12 secretion after DC culture on topographies with and without LPS stimulation 225

Figure 7-14: CD3+ T cell proliferation for topography modulated DCs. 226

Figure 7-15: Topography-treated DCs induce modulated T cell secretion 227

III. Table of tables

Table 1: Literature known surface coating effects on DCs 31

Table 2: List of used flow cytometry antibodies 42

Table 3: Polymer plates preparation for cell culture 53

Table 4: Liquid extraction surface analysis – mass spectrometry of monomer remnants in priming media from 5 selected polymers, by Joris Meurs 55

Table 5: Polymer structures 72

Table 6: Atomic percentages of polymers films after media incubation (by XPS), acquired by Craig Stoppiello 96

Table 7: Top canonical pathways for DEAEA and HFiPMA cultured DCs 108

Table 8: DEAEA vs TCP – Top 10 upregulated genes 109

Table 9: DEAEA vs TCP - Top 10 downregulated genes 117

Table 10: HFiPMA- Top 10 upregulated genes 119

Table 11: HFiPMA- Top 10 downregulated genes.....122

Table 12: Nanoparticle single step nanoprecipitation volumes and addition rates .183

Table 13: TCP + LPS - Top 10 upregulated genes 287

Table 14: TCP + LPS - Top 10 downregulated genes 288

Abbreviations

°C	Degree Celsius
ALP	Alkaline phosphatase
AML	Acute myeloid leukaemia
APC	Antigen presenting cell
Ar	Argon
BE	Binding energy
BSA	Bovine serum albumin
CCL19	Chemokine (C-C) motif ligand 19
CCR	C-C chemokine receptor 7
CD	Cluster of differentiation
CLR	C type Lectin receptor
CpG-ODN	CpG oligodeoxynucleotides
CTL	Cytotoxic T lymphocyte
CTLA4	Cytotoxic T-lymphocyte associated protein 4
DC	Dendritic cell
DC-SIGN	Dendritic cell – specific intercellular adhesion molecule -3-Grabbing Non-integrin

DMPA	2,2-diemethoxy-2-phenylacetophenon
EAE	Experimental autoimmune encephalomyelitis
ECM	Extracellular matrix
ELISA	Enzyme linked immunosorbent Assay
FasL	Fas Ligand
FBGC	Foreign body giant cells
FBR	Foreign body response
FBS	Foetal bovine serum
FcγRI	Fc gamma receptor I
FOXP3	Forkhead Box Protein P3
GM-CSF	Granulocyte-macrophage colony stimulating factor
HA	Hyaluronic acid
HEV	High endothelial venules
HIV	Human immune deficiency virus
HSC	Hematopoietic stem cell
ICAM-1	Intercellular adhesion molecule 1
IDO	Indoleamine 2,3-dioxygenase
IFNγ	Interferon γ

IL-10	Interleukin-10
IPA	Propan-2-ol
IPEX	Immunodysregulation polyendocrinopathy enteropathy X-linked syndrome
iPSCs	Induced pluripotent stem cells
KE	Kinetic energy
LC	Langerhans cell
LPS	lipopolysaccharide
MACS	Magnetic cell separation
MHC	Major histocompatibility complex
MMC	Mitomycin C
moDC	Monocyte derived dendritic cell
MSC	Mesenchymal stem cell
mTEC	Medullary thymic epithelial cells
NALP3	NACHT, LRR and PYD domains containing protein 3
NFκB	Nuclear factor κ B
NLR	Nod like receptor
O_2	Oxygen
PAMPs	Pathogen associated molecular pattern

PBS	Phosphate buffered saline
PCL	Poly(caprolactone)
PCR	Polymerase chain reaction
PEG	Polyethylene glycol
PFA	Paraformaldehyde
PGA	Poly(glycolic acid)
pHEMA	Polyhydroxyethylmethacrylate
PI	Photo initiator
pIBTMA	Poly(isobutyl-co-benzyl-co-terahydrofurfuryl) methacrylate
PLA	Poly(lactic acid) (PLA)
PLGA	Poly(lactic-co-glycolic acid)
PRR	Pattern recognition receptor
PS	Polystyrene
RA	Rheumatoid arthritis
RLR	Retinoic acid-inducible gene-I-like receptors
RNA	Ribonucleic acid
SLE	Systemic lupus erythematosus
TCP	Tissue culture plastic

TGF-β	Transforming growth factor β
TLR	Toll like receptor
TNF-α	Tumour necrosis factor α
UV	Ultraviolet
XPS	X ray photoelectron spectroscopy

Chapter 1: General Introduction

Chapter 1 General Introduction

1.1 The immune system

The immune system has evolved to protect us against environmental insults with the ability to recognise and fight pathogens such as bacteria or viruses. The immune system consists of an innate and an adaptive arm [1]. The innate arm fights invading pathogens as the body's first line of defence in a non-specific manner, to give the adaptive arm enough time to build a specific immune response against particular pathogens.

1.1.1 Innate immune system

The innate immune system, initially engages with invading pathogens by sensing bacterial, fungal or viral components through a set of pattern recognition receptors (PRRs) and leads to NFκB activation and innate cytokine production [2], [3]. The innate immune response is characterised by its rapid speed and non-specificity against foreign invaders, solely directed to clear foreign pathogens or materials, while limiting tissue damage and removing apoptotic cells. This defence consists of conserved effector functions such as the complement system, whereby foreign entities are marked by opsonising fragments that can be recognised by phagocytes (e.g., neutrophils, macrophages) for clearance and destruction of the invading pathogens.

The host organism can also recognise pathogen-associated molecular patterns (PAMPs), associated only with microorganisms. Professional antigen presenting cells (APCs) such as dendritic cells (DCs), and macrophages

recognise PAMPS via PRRs on their surface [4]. Macrophages are phagocytic and plastic cells, that can be classified into a pro-inflammatory M1 phenotype and an anti-inflammatory (pro-wound healing) M2-phenotype. M1 macrophages utilise Warburg metabolism and M2 macrophages oxidative metabolism [5].

There are four major sub-families of PRRs- the Toll-like-receptors (TLRs), the nucleotide-binding oligomerisation domain (NOD)-Leucin Rich Repeats (LRR) – containing receptors (NLRs), the retinoic acid-inducible gene 1 (RIG-1)-like receptors (RLRs) and the C-type lectin receptors (CLRs) [3]. Humans have 10 different TLRs, which have specificity to a broad array of microbial molecular signatures [6]–[8]. CLRs, which bind to carbohydrates, are specific to a variety of polyanionic ligands [9], [10]. NLRs recognise intracellular pathogens or pathogenic components, while RLRs belong to the RNA helicases family that specifically detects RNA species derived from viruses in the cytoplasm [11]–[13]. An overview of the PRR groups and their ligands can be found in Figure 1-1.

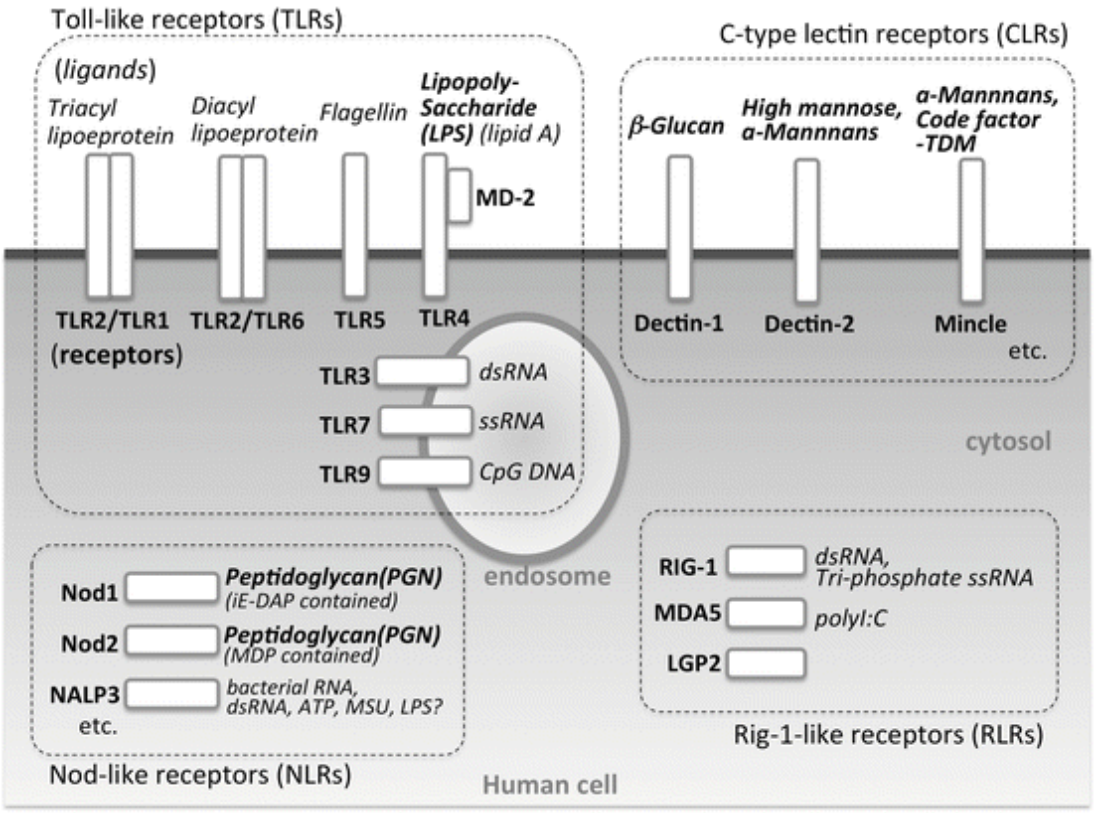


Figure 1-1 Overview schematic of PRR sub-families

4 classes of PRR families and binding of their ligands (microbical products or endogenous danger signals) trigger downstream signalling pathways. TLRs and CLRs are transmembrane PRRs, while NLRs and RLRs are cytosolic PRRs. Taken from [14].

An example for CLRs is CD209 (also known as DC-SIGN). DC-SIGN is a transmembrane protein and recognises N-linked high-mannose oligosaccharides and branched fucosylated structures on host cells (e.g. ICAM-2, , ICAM-3 on T cells) or pathogens (e.g. HIV) [15]–[19]. It is primarily expressed on human DCs. DC-SIGN is highly expressed on immature DCs (iDCs), compared to mature DCs (mDCs), and mediates the capture, destruction and presentation of microbial pathogens to induce successful immune responses [19].

TLRs interact with a wide range of microbial compounds and trigger strong innate immune responses. Even though TLRs are an essential warning system that alerts host immune cells to the presence of invading microbes, it remains unclear whether they also facilitate antigen uptake, as it seems this process is mediated majorly by scavenger receptors and CLRs (e.g., DC-SIGN). TLR family members are expressed on innate immune cells and respond to different stimuli. While TLR-4 recognises lipopolysaccharide (LPS), TLR-2 binds lipoproteins and glycoproteins. In addition, TLR-2 mediates cellular responses to a variety of infectious pathogens and their products (e.g. yeast walls, whole mycobacteria, mycobacterial lipoarabinomannan) [6]. Bacterial DNA with unmethylated CpG motifs is meanwhile recognised by TLR-9 (Figure 1-2).

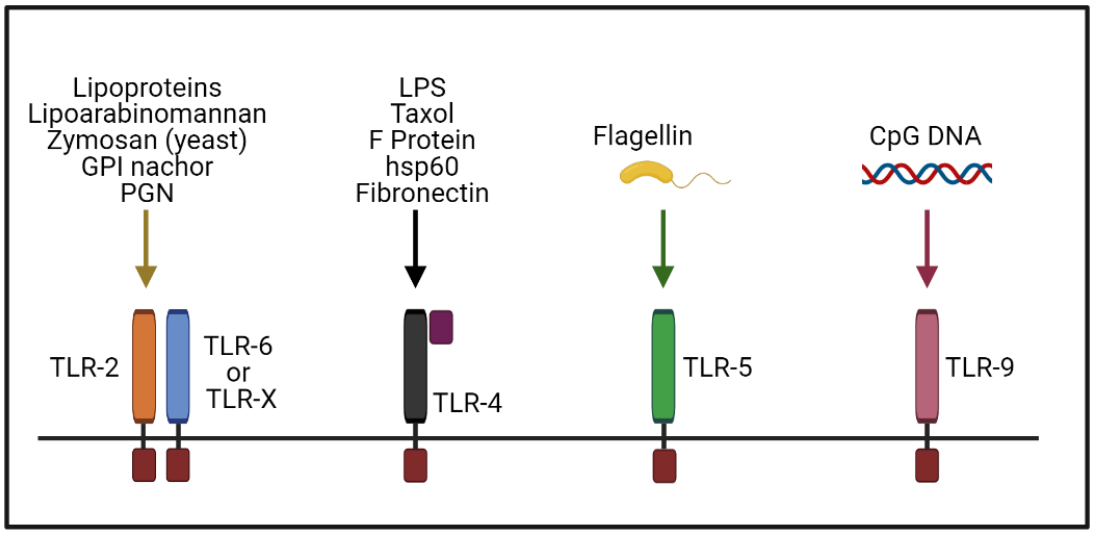


Figure 1-2: TLRs and their ligands

TLR family members can recognise certain PAMPs and host-derived products. TLR-2 recognises a variety of microbial products, while TLR-4 is essential for signalling via LPS from Gram-negative bacteria. TLR-4 binds not only viral and plant products but also endogenous host-derived products, such as hsp60 and fibronectin fragments. Compared with TLR-2 and

TLR-4, recognition by TLR-5 and TLR-9 is more restricted and essential for flagellin- and CpG DNA–mediated signalling, respectively. Figure generated in Biorender.

1.1.1.1 The role of dendritic cells in the immune system

DCs are mononuclear phagocytes, specialised in antigen presentation. They have distinct micro-sized protrusions (so-called lamellipodia) on their surfaces, and due to this morphology DCs are also described as “star”-like cells [20]. DCs are quintessential in the facilitation and regulation of an immune response, due to their capability to prime naïve T cells [21]. During their immature state, DCs patrol different tissues especially in regions where invasion of pathogens is likely, e.g. the digestive tract, respiratory epithelium or the skin [22]. After encountering a stimulus, DCs can enter a semi or fully mature state and migrate to draining lymph nodes where they interact with their cognate naïve T cells leading to T cell polarisation to distinct functional phenotypes (Figure 1-3). When encountering pathogens DC uptake and process antigens, and if the antigens are from an extracellular source they will be presented via the major histocompatibility complex class II (MHC II) on DC surface to naïve CD4+ T cells, or via MHC class I to CD8+ T cells if they are from intracellular sources [23]. DCs have the ability to efficiently present internalised antigens on MHC I molecules, a process termed crosspresentation. This allows immunity against tumours and pathogens that normally wouldn’t infect APCs [24]. Internalised antigens can be presented via i) the vacuolar pathway or ii) the endosome to lysosome pathway [25]. In i) Cathepsin S degrade antigens in endosomes and antigens are then loaded onto MHC I in the endosomes. In the ii) endosome to lysosome pathway, antigens are transported into the

cytosol for proteosomal degradation. Afterward, antigen-derived peptides are transported back into the endosomes (soluble antigens) or into the endoplasmic reticulum (ER) (particular antigens) via transporter-associated with antigen processing (TAP). Insulin-regulated aminopeptidase (IRAP) or endoplasmic reticulum aminopeptidase (ERAP) then trims the antigen, which is then loaded onto MHC I. Under normal conditions, when no inflammation is present, DCs migrate rapidly between tissues sites and lymphoid organs presenting 'self-proteins' to T cells, an important process for maintaining peripheral tolerance.

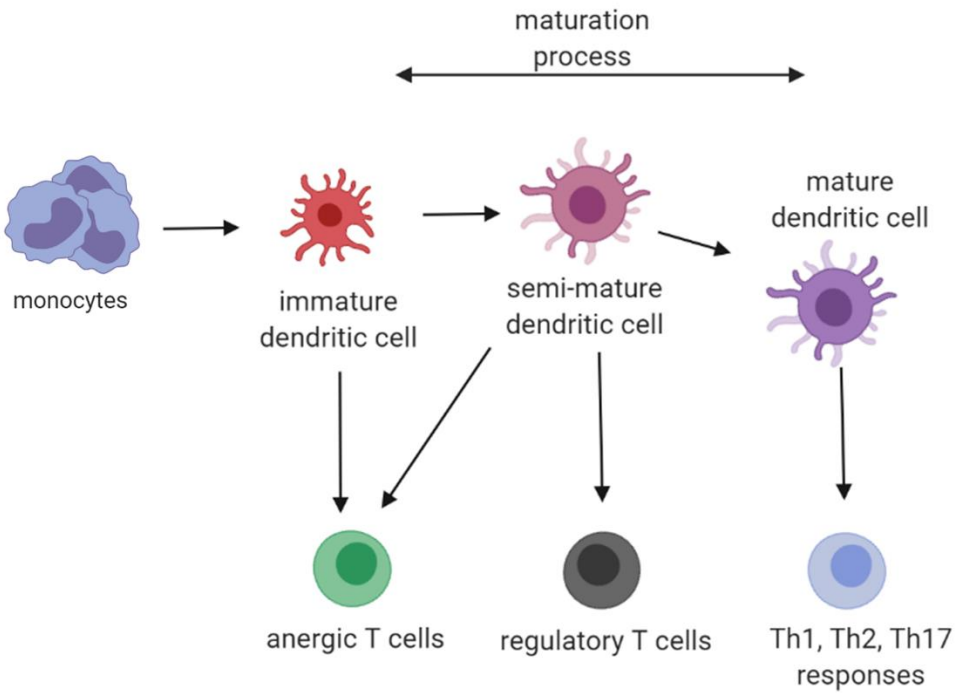


Figure 1-3: Overview of monocyte to DC differentiation, maturation and the polarisation of T lymphocytes.

Monocytes can differentiate to iDCs. iDCs induce anergy in T cells or can mature into either semi-mature or fully mature DCs. Semi-mature DCs do not possess all costimulatory molecules and lead to regulatory T cells or anergic T cells inducing tolerance against pathogens or self-

antigens. A fully matured DC initiates cognate T cell responses and polarisation of naïve T cells into Th1, Th2, or Th17 subsets. Figure made in Biorender.

iDCs accumulate MHC II in the late endosome-lysosome compartment, express low levels of co-stimulatory molecules and have only limited cytokine secretion capacity [26], [27]. When iDCs encounter a stimulus, e.g. bacterial or viral components, they recognise these harmful pathogens through PRRs and differentiate to so-called mDCs [2], [3], [15]–[18], [28]. The balance of DC function and their role in the immune system is dependent on the maturation state as is summarized in Figure 1-4.

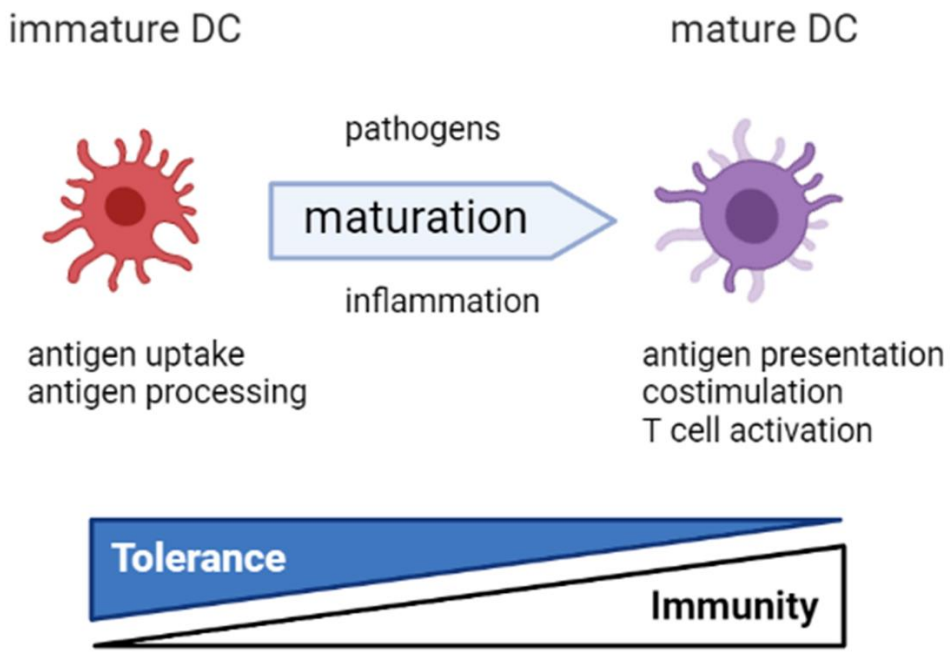


Figure 1-4: Brief overview of immature and mature DC functions and the role they play in the tolerance-immunity spectra.

The main function of iDCs are the search, uptake and processing of antigens in the host body. Upon maturation DCs upregulate activation markers, such as costimulatory molecules and MHCs that present antigens in order to communicate with T cells. At the same time DCs

downregulate the ability to uptake and process antigens in favour of the new functions. This DC maturation process tips the balance from tolerance to immunity induction in the host body. Figure made in Biorender.

The binding of ligands to TLRs or CLRs leads to maturation of DCs; thus mDCs downregulate their antigen-capturing ability, upregulate the surface expression of MHC I and II and co-stimulatory molecules (such as CD83 and CD86), secrete pro-inflammatory or regulatory cytokines and express *C*-C chemokine receptor type 7 (CCR7) [26], [27]. CCR7 is a homing receptor of the G-protein coupled receptor family. Its ligands chemokine (C-C motif) ligand 19 (CCL19) and CCL21 are expressed on reticular fibroblastic cells in the lymph nodes, therefore allowing the homing of mDCs into the draining lymph nodes [26], [27], [29]. Naïve T cells enter draining lymph nodes via high endothelial venules (HEV) and interact with DCs that are presenting antigens on their MHCs [30].

CD83 and CD86 are widely used markers for investigating DC activation/maturation: CD86, also known under the name of B7-2, binds CD28 and CTLA4 on T cells in order to provide a co-stimulatory signal to T cells and is essential in evoking an effector T cell response [31]. CD83 is widely used as a DC maturation marker. It has also been shown that downregulation of CD83 leads to less potent induction of allogeneic T cell proliferation and less priming potential of DCs in general, however its exact function is yet to be fully understood [32].

In response to stimulation, DCs can acquire different phenotypes. Danger signals and PAMPs can activate iDCs into classical mDCs as noted above. Tolerogenic DCs are naturally induced by anti-inflammatory cytokines IL-10 or

transforming growth factor-β (TGF-β) in the tumour microenvironment or other tolerogenic environments. Under steady-state conditions immature and semi-mature DCs remain tolerogenic until exposed to a pro-inflammatory milieu which induces them to become immunogenic. Tolerogenic DCs can also be induced by chemicals, pathological conditions and molecular modifications. Both naturally occurring and induced tolerogenic DCs release anti-inflammatory cytokines such as IL-10 and induce T cell anergy, T cell apoptosis and/or T_{reg} expansion [33]–[36].

1.1.1.2 DC origin and subsets

Human DCs can be found in a variety of subsets, depending on their phenotype, function and location. DCs originate from a common progenitor: CD34+ haematopoietic stem cells (HSC) which give rise to progenitors of granulocytes, monocytes and human DCs (GMDPs), the progenitors of monocytes and human DCs (MDPs) and the progenitors of monocytes and the common progenitor of human DCs (PDCs) [37]. The progenitor of human DCs can be found in umbilical cord blood, bone marrow and peripheral blood and lymphoid tissues. The PDCs are then used to generate different types of DCs [38]. These types can be characterised by elevated MHC-II expression while lacking common lineage markers, such as CD3 (T cells), CD19/20 (B cells),

and CD56 (NK cells). Traditionally DCs have been referred to as HLA-DR^{+} lineage^{-} cells.

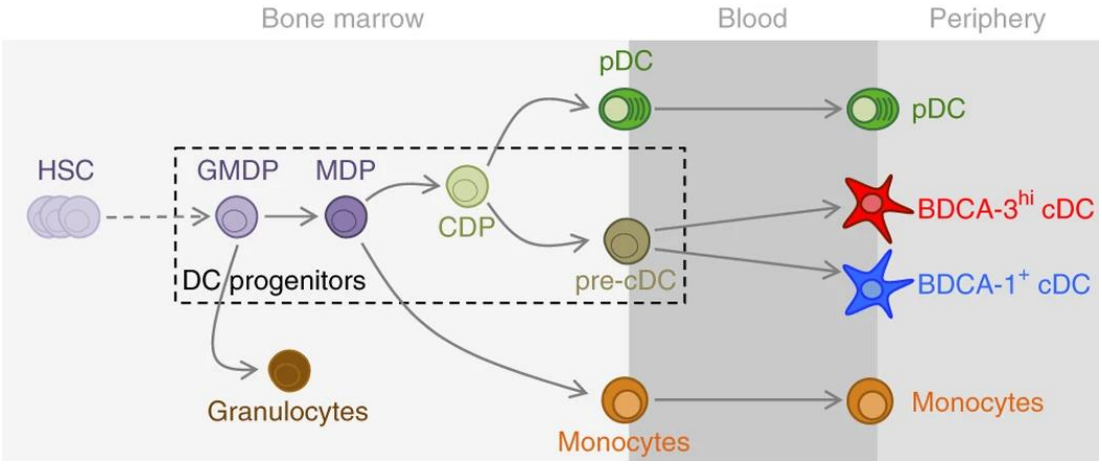


Figure 1-5: Schematic overview of human DC hematopoiesis

DC hematopoiesis is initiated in the bone marrow. A granulocyte, monocyte and DC progenitor (GMDP) develops into a monocyte and DC progenitor (MDP). MDPs give rise to monocytes and a common DC progenitor (CDP), which loses the potential to produce monocytes. CDPs give rise to plasmacytoid DCs (pDCs), as well as circulating cDC precursor (pre-cDC). Pre-cDCs migrate from the bone marrow through the blood to the periphery to produce the two major subsets of conventional (cDCs). Taken from [39].

Conventional DCs (cDCs) are highly migratory cells that can switch between tissues and towards lymphoid organs and are also present in the peripheral blood. Migration through the blood to lymphoid tissues occurs by entering into lymph nodes through HEVs from where they distribute themselves and become differentiated cDCs [40]. Another subtype of DCs are plasmacytoid DCs (pDCs), which are characterised by the expression of CD11c and CD123^{high} [41], [42]. They circulate through the blood stream and infiltrate the bone marrow, spleen, thymus, lymph nodes, and the liver. One of their functions is to sense viral nucleic acids and produce large amounts of type I IFN, as well as present antigens and initiate T cell responses [43], [44]. These

two DC subtypes are short-lived and are continuously regenerated from HSCs in the bone marrow.

LCs are the first immunological barrier against pathogens and environmental insults in the skin [45]. Precursors of LCs enter the skin before birth as a single wave of recruitment. There they evenly distribute themselves and differentiate into LCs expressing langerin, MHC II and CD11c [46]. LCs are of myeloid origin and are shown to renew in tissues independently from the bone marrow, suggesting the existence of a dermal or epidermal progenitor [46]. Recent studies have thereafter identified that LCs renew from the proliferation of resident, differentiated LCs. This process has shown to become enhanced through inflammation [46]. Similar to circulating DCs, LCs are able to ingest antigens present in the skin and to migrate to the regional lymph node in both steady-state and inflammatory conditions [47], [48].

1.1.1.3 Monocyte-derived DCs as an experimental model

Circulating DCs have low frequency and comprise approximately less than 1 % of circulating peripheral blood mononuclear cells (PBMCs). Due to the difficulty of isolating sufficient numbers for *in vitro* studies, many such studies use monocyte-derived dendritic cells (moDCs). As their name suggest moDCs are derived from peripheral blood monocytes, which *in vivo* could infiltrate inflammatory tissues to differentiate into DCs. Human monocytes isolated from peripheral blood are cultured in the presence of Interleukin 4 (IL-4) and granulocyte macrophage colony-stimulating factor (GM-CSF) and differentiate into DCs over the course of 6 days [49], [50]. The moDCs have many features of primary myeloid DCs, including their potent antigen-presentation [49], [50].

During differentiation from monocytes, these cells lose the expression of typical monocyte markers such as CD14 and FcγRI and acquire DC morphology and surface phenotype. Like iDCs they start to express CD1 molecules, FcγRII, CD11c and DC-SIGN, as well as low to moderate levels of MHC class I and II and co-stimulatory molecules CD40, CD80 and CD86, and inter-cellular adhesion molecule-1 (ICAM-1) [15], [49]. Following stimulation the moDCs mature (just like primary DCs), which leads to a loss of FcγRII expression and reduced antigen-uptake capacity (reduction of antigen capturing markers), but highly upregulated expression of MHC and costimulatory molecules, ICAM-1 and of the so-called maturation DC marker CD83 and CD86 [49], [51]. Same as primary DCs, moDCs are potent inducers of allogeneic and autologous T cell responses and are able to prime naïve T cells [49]. Overall, these functional properties make them a suitable experimental model for DC research.

1.2 Adaptive immune system

Cells of the adaptive arm (e.g., T lymphocytes, B lymphocytes) can recognise all kinds of molecular patterns (so-called antigens). In principle, they can recognise not only antigens from pathogens, but also from human tissues (so-called self-antigens). The discrimination between pathogenic and self-antigens, and thus the switch from immune activity to immune tolerance is based on a finely regulated and complex interplay between activating and suppressive mechanisms. T lymphocytes as part of the adaptive immune system have to be educated in lymphoid organs by APCs before they can expand and act. They are selected by their affinity to a particular antigen and can mount a highly

specific response against foreign antigens. In other words, this part of the immune system can ‘adapt’ to the circumstances and the kind of molecular target it shall engage, hence the name adaptive immune system [1]. As soon as the body is infected with a specific pathogen and the innate immune cells have encountered it, adaptive cells, such as T and B cells, start to develop an immunological memory [1].

1.2.1.1 T cells: origin and selection

T cells are important for triggering an immune response. When naïve T cells are activated, they proliferate and differentiate into effector T cells and eventually memory T cells which are important for potential re-infections. Memory T cells are an important part of the immunological memory and will go through quick expansion when encountering the antigen, they have been primed against.

T lymphocytes derive from the bone marrow and T cell precursors differentiate into CD4+ or CD8+ T cells in the cortex of the thymus. Within the thymus, T cells undergo selection processes: First the cortical epithelial cells check which of the T lymphocytes are able to bind MHC molecules and select these in the manner of a positive selection giving the selected ones critical survival signals [1], [52]. The T lymphocytes that are unable to bind MHC molecules do not receive a survival signal and die. In a next step, the negative selection, the medullary thymic epithelial cells (mTECs) present self-antigens and thus inspect the previously positively selected T cells for their ability to recognise self-antigens [52]. T cells that strongly react to self-antigens get a death-signal via programmed cell death receptors (leading to apoptosis). This deletion of

hyper-reactive T cells prevents a later possible unfavourable induction of autoimmune reaction against self-antigens. The T cells which are still alive leave the thymus via the blood stream as naïve T cells [1], [52], [53].

Not all self-antigens are presented by mTECS in the thymus, therefore a peripheral tolerance is also required in order to prevent harmful autoimmune responses [54]. Induction of peripheral tolerance is possible via three main mechanisms: anergy, deletion or suppression via T_{regs} [52]. Anergy is the result of antigen presentation without a co-stimulatory signal. If a T cell does not receive a co-stimulatory signal, it goes into anergy and cannot be activated anymore. This interaction would be induced by tolerogenic or semi-mature DCs. The second mechanism, deletion, occurs after the T cell continuously get presented the same antigen in a high concentration which results in its deletion – as this indicates a self-antigen. The last mechanism is via the suppressive T_{regs}, which secrete TGF-ß and IL-10, thereby inhibiting the function of surrounding T cells [1], [53].

In summary, immature T cells that recognise MHC receive signals for survival, out of which, those that interact strongly with self-antigen are removed from the repertoire first in the thymus (central tolerance) and afterwards in the periphery (peripheral tolerance) [52], [53].

1.2.1.2 T cell subsets and their function in health and disease

Two main subsets of T lymphocytes have been found in the human body: CD4+T cells and CD8+ T cells. CD4+ T cells can be further divided into Th1, Th2, Th17 or T_{regs} depending on their phenotype and function. The

development of CD4+T cells into different subsets is induced by various polarising factors: cytokines, specific TLR engagement, the combination of co-stimulatory markers expressed on DCs [55]. Th1 T cells are induced via the secretion of the cytokine IL-12 from DCs, Th2 T cells via IL-4 secretion, Th17 via IL-6 secretion and T_{regs} via IL-10 and TGF-ß secretion (see Figure 1-6) [1].

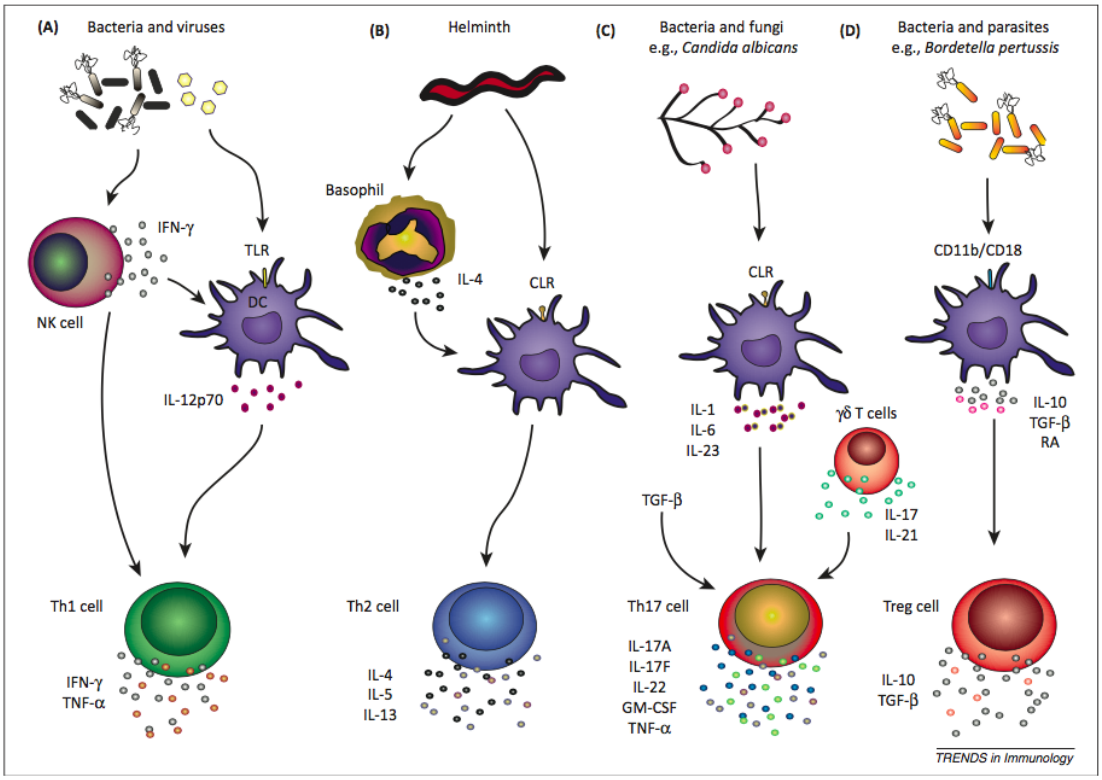


Figure 1-6: Overview of T cell polarisation dependant from perpetrators.

(A) Bacterial and viral antigens are recognized via TLRs on DCs and via IL-12p70 ensue a Th1 cell response. (B) Helminths interact with DCs via CLRs and effect a TH2 polarisation. (C) Fungi also signalize via CLR but lead to a Th17 polarisation. (D) Parasites interact via CD11b/CD18 with DCs, which secrete IL-10, TGF-ß to polarize naïve T cells into Tregs. Taken from [56].

Th1 cells secrete cytokines that are essentially pro-inflammatory and promote cytotoxicity against intracellular parasites such as bacterial and viral pathogens or cancerous tissues (e.g. IFN-γ, tumour necrosis factor α (TNFα))

[1]. Th1 cells also appear to be involved as the pro-inflammatory drivers of autoimmune disorders.

The main cytokines secreted by CD4+ Th2 cells are IL-4, IL-5, and IL-13 and play a defensive role against extracellular parasites. Th2 cytokines are also main players in allergic reactions [1], [57]. A relatively recently discovered subset is Th9 cells, that primarily produces IL-9 and is involved in the survival and expansion of CD4+ T cells, as well as the recruitment of mast cells. Th17 cells secrete the cytokines IL-17, IL-21, IL-22, IL-25 and IL-26. Especially, IL-17 is necessary for the protection against extracellular pathogens by mediating the recruitment of neutrophils and macrophages to the infected tissue. Dysregulation of Th17 cells may play an important role in the pathogenesis of several inflammatory autoimmune disorders, such as systemic lupus erythematosus, rheumatoid arthritis, Sjogren syndrome, but also type 1 diabetes, multiple sclerosis and other diseases [58]–[60]. T_{regs} play a pivotal role in regulating or suppressing other cells in the immune system via secretion of IL-10 and TGF-ß. They control immune responses to self and foreign antigens and help to prevent excessive inflammation and autoimmune diseases. A mutation in the master regulator of T_{regs} development FOXP3 has been demonstrated to play a role in the autoimmune disorder systemic lupus erythematosus (SLE) and the X-linked syndrome IPEX (self-reactive lymphocytes) [56].

Naïve CD8+ T cells are primed by MHC I cross-presented antigens on DCs to induce the generation of effector CD8+ T cells with cytolytic capacity, also referred to as cytotoxic T lymphocytes (CTLs) [61]. CTLs are the key immune

cells for killing cancer cells presenting MHC I molecules. To do this, CTLs must be primed by DCs, and utilise two main pathways to kill cancer cells. These two pathways are granule exocytosis and Fas ligand (FasL)-mediated apoptosis induction. Granule exocytosis is mediated by the release of granzymes A and B from CTLs. Additionally, when CTLs encounter cancer cells they produce perforin to make pores in the plasma membranes. The released granzymes then enter cancer cells and cleave their intracellular substrates. Secondly, the FasL-mediated apoptosis pathway activates caspases through activation of FasL and the subsequent cytochrome c release in the target cells. CTLs also release IFNγ and TNFα to induce cytotoxicity in the cancer cells [62]. The number of CTLs in the tumour microenvironment is a pivotal prognostic marker for cancer [63].

1.2.1.3 Dendritic cells and their interaction with T cells

For the DC-T cell-interaction leading to an activation of a naïve T-cell, different signals are needed which include (summarised in Figure 1-7) the presentation of antigens via MHCs (signal 1), a co-stimulatory molecule (signal 2), and polarising cytokines (signal 3) [64]. The first signal is the upregulation of MHC I and MHC II for presenting antigens. For signal 2, the co-stimulatory molecules such as CD40, CD80, CD86 are upregulated, while the endocytic activity of the DCs is downregulated [65]. Without signal 2, the interaction between DC and T lymphocyte is disturbed and the T lymphocyte goes into anergy, a mechanism involved in peripheral tolerance when T cells are presented with self-antigens. For signal 3, secreted cytokines such as IL-10, IL-12 or IL-23

may polarise the respective naïve T cell to Th1, Th2, Th17 or T_{regs} (summarised in Figure 1-6) [64], [66].

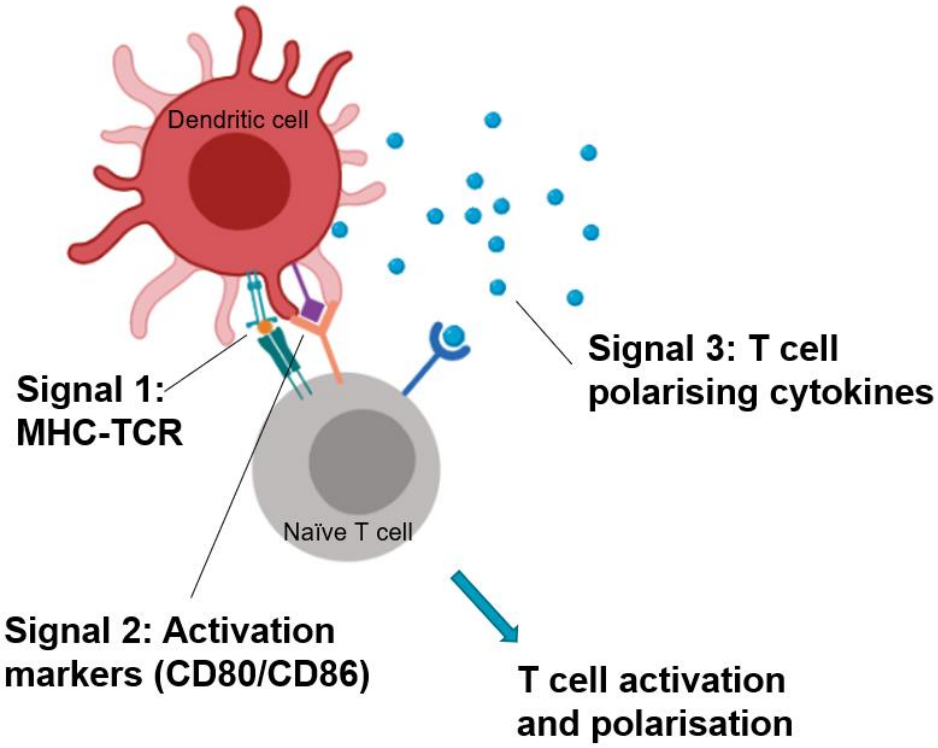


Figure 1-7: The costimulatory signals between DCs and T lymphocytes**.**

Dendritic cells from the innate immune system present their antigen to naïve T cells in the local draining lymph nodes. As signal 1 the T cell receptor ligates to MHC I/II associated peptides processed from pathogens, for signal 2 binding of CD28 on T lymphocytes to CD80 and CD86 expressed by DCs leads to T cell lineage differentiation. Signal 3 is the polarizing cytokine signal from the innate immune cells. Depending on the type of antigen presented and nature of the cytokines in the microenvironment, DCs direct the development of Th1, Th2 or Th17 lymphocyte lineages. Figure generated in Biorender.

1.3 Biomaterials in immunomodulation

Biomaterials have been used in implantable devices for many years with the oldest evidence of the introduction of non-biological materials into the human

body dating back 9000 years (human remains referred to as the ”Kennewick Man”) [67]. Sutures and dental implants have also been used for thousands of years. Prior to 1950 most of the biomaterial usage was unsuccessful, due to poor understanding of biocompatibility of materials. With the development of nylons, high performance metals, ceramic, and polymeric materials during the 1940/50s, the peace time applications for these materials became a focus of medical doctors and surgeons with the wish to replace and replenish organs and tissues. Nowadays, biomaterials are commonly used as implants and other medical devices over a wide range of applications [68], [69].

Biomaterial usage is always intended towards either improving an organ function or as a diagnostic/therapeutic tool; however, one common disadvantage of many biomaterials is the induction of adverse immune reactions resulting in excessive inflammation, impairment of healing, fibrotic encapsulation, tissue destruction, or even isolation and rejection of medical devices.

Such adverse immune responses are generally known as the foreign body response (FBR) to implants. During the FBR macrophages unsuccessfully attempt to phagocytose the implanted material, which leads to the formation of a foreign body giant cells ending with fibrotic encapsulation and ultimately device failure as any further interplay between the biomaterial and host tissue has become impossible [70], [71]. The first cells arriving at the implantation site are macrophages together with neutrophils. Following implantation, protein adsorption on the surface of the biomaterial results in the initiation of the coagulation cascade, complement (which can polarise immune cells

towards an inflammatory response) and the formation of a provisional matrix. Following matrix formation APCs including macrophages and DCs can be recruited to the implant site by immune cell attracting chemokines released from the matrix as well as surrounding cells. Macrophages persist at the implantation site, adhering to the implant surface and coalescing with neighbouring macrophages to form a giant cell body, which attempts to engulf the material. Within this encapsulation, macrophages secrete several inflammatory mediators, including reactive oxygen species (ROS) and degradative enzymes that are supposed to break down the material. Inflammatory signals, such as foreign cell – associated antigen release or some material degradation products only exacerbate the inflammatory response around the material, prompting T cells to induce chronic inflammation. DCs play a critical role in enabling the chronic adaptive response against engineered constructs or implant-associated antigens (e.g., from co-delivered cells, proteins, or drugs). It has previously been found that DCs also infiltrate the implant area and potentially play a role in the development and resolution of the foreign body response.

Another negative outcome of biomaterial implantation is acute to chronic inflammation surrounding the biomaterial environment due to degradation products. For example, polymethylmethacrylate (PMMA), cobalt chromium (CoCr), titanium, alumina ceramics and ultra-high-molecular-weight polyethylene (UHMWPE) are commonly used in hip replacements and other prosthetics but have shown to wear, leading to formation of wear or particle

debris. Wear and tear of implants therefore often leads to a highly inflamed environment [72]–[75].

Immune inert biomaterials have been developed in the attempt to avert negative outcomes of material-host interactions, though to only limited success. However, in the last decades a shift towards materials that can interact with the host immune system in a favourable way, rather than avoiding it, has been made. Immune-instructive materials have a clear application in the medical device field and can be used to reduce FBR, promote healing and device integration. In addition, immune-instructive materials, by virtue of being able to modulate immune responses, can also be used in immunotherapies designed for (auto) inflammatory diseases and/or vaccination. In these cases, materials are designed to direct the response of interacting immune cells towards a desired outcome, e.g., inducing tolerance in the treatment of autoimmune diseases or inducing potent adaptive immune responses for vaccinations or cancer. This new focus offers an alternative to cytokine-based immunotherapies which has previously shown to have low response rates and high toxicities [76], [77]. In the following section I discuss different approaches for developing materials with bio-instructive properties.

1.4 Surface chemistry

One way to alter biomaterials is to modify the surface chemistry, leading to differential protein adsorption and, subsequently cell behaviour. Surface chemistry has been shown to be a key factor which affects protein adsorption to implant surfaces [78], [79]. Instantly after insertion of a biomaterial in the body, adsorption of plasma and interstitial fluid proteins onto the material

surface occurs. Proteins such as fibronectin, vitronectin, fibrinogen and IgG have been reported to adsorb onto material surfaces [80]. These adsorbed proteins possess binding domains which are recognisable by several cell types; hence surrounding cells utilise them as adhesion sites [70], [81]. The composition of the adsorbed proteins, as well as their conformation on the material surface has been identified as one of multiple factors that influence cell responses [82], [83]. The modification of surface wettability, hydrophobicity and surface charge have also been found to modulate the amount and composition of protein adsorption. Therefore, modification of material surface chemistry presents a way of controlling protein adsorption and eventually cell response. Generally, higher surface hydrophilicity improves biocompatibility of medical devices *in vitro* [82], [84].

Modified surfaces with varying functional groups such as methyl, hydroxyl, amino and carboxyl have been shown to influence cell adhesion [82], [85]. Methyl and hydroxyl surfaces are hydrophobic and neutral hydrophilic functional groups respectively, while amino and carboxyl surfaces show positively and negatively charged characteristics respectively [86]. Cell adhesion on surfaces containing amine functional groups have been shown to increase when compared with functionalities such as carboxyl, methyl and hydroxyl groups [82]. As the surface of cells is typically negatively charged, the presence of positive surface charges can often promote cell adhesion.

Polymeric materials are composed of regularly repeating monomeric units. This allows architectures with a controllable degradation rate. Polymers are widely used in many tissue engineering applications, particularly due to their

biomechanical and biodegradability properties. Widely used synthetic polymers include poly(caprolactone) (PCL), poly(lactic acid) (PLA), poly(glycolic acid) (PGA), and poly(lactic-co-glycolic acid) (PLGA). PLGA has shown both regulatory as well as stimulatory effects depending on the composition it was fabricated (differing lactic:glycolic ratios) [87]–[90]. Natural polymers such as collagen and fibrin are also susceptible to enzymatic degradation and by this way, they can release immune modulating molecules. Silk as a natural polymer has also been shown to induce a macrophage response, and a controlled release of cytokines from coated silk polymer can induce and reverse M1/M2 macrophage polarisation.

1.5 Surface topography

Usually, *in vitro* cell culture is carried out on flat surfaces. In reality, this is completely different than the physiological environment cells encounter in their host tissue. To portray a more physiological relevant environment, surface structure must be kept in mind. The extracellular matrix (ECM) in which many cell types reside, is a complex consisting of glycoproteins, polysaccharides, proteins, low molecular weight compounds, electrolytes and water. Through this, the ECM interacts with surrounding cells and tissues and therefore plays a critical role in tissue homeostasis, mechanics and functionality. The proteins and collagens within the ECM provide structural support and binding sites for cells and tissues *in vivo*, as well as biophysical cues that are essential in modulating cell behaviours [91]–[93]. These binding sites consist of geometrically defined shapes (ranging from nano to micro scale) and are known to have an effect on cell migration, function, adhesion, proliferation and

differentiation via mechanotransduction [91], [94]. In mechanotransduction, cells are guided by interpreting biophysical signals from the encountered ECM components. In order to mimic ECM structures, researchers have employed various nano- and micro-fabrication techniques [91], [95]. Surface structure can be modulated by engineering the physical properties, such as surface roughness, curvature, geometry or even via the introduction of more complex topographies.

Grooves (nano or microscale) are continuous lines, similar to channels, with varying dimensions across the material surface and have been found to influence cell orientation and cell area [96], [97]. Microgrooves influence cell behaviour in very distinct ways, such as improvement of phenotypical characteristics of primary cells [98]. Changes of topographical geometry have also been shown to influence the adsorption of proteins down to the nanoscale [86]. In a recent study natural (plant and insects) surfaces were replicated in polystyrene (PS), to culture mesenchymal stem cells on these topographies and to incorporate natural design into topography research [99]. For metal implants, an increase in surface roughness can increase the surface area leading to osteoblast differentiation with higher expression of alkaline phosphatase (ALP) and osteocalcin expression compared to smooth surfaces [100].

Other novel micro- and nano-fabrication approaches and technologies enable the development of complex surface features with controlled pattern, periodicity, shape, and dimensional properties [101]–[106]. Various platforms have been able to give a screening overview of the gradients of different

structures or the complex design of topographies [107], [108]. Gradients of topographies or surface roughness have been studied with mesenchymal stem cells (MSCs) and fibroblasts, with different morphologies and migration being observed [107], [108].

One of these platforms is the TopoChip, a 2 by 2 cm chip made from polystyrene, that is divided in areas of 290 by 290 μm^2, designated as 'TopoUnits'. The TopoChip holds 2176 distinct, randomly designed surface topographies as TopoUnits using a mathematical algorithm as a design tool. Topographic features are built up using three types or microscale primitive shapes: circles, isosceles triangles (with one angle of 36° and two angles of 72°), and thin rectangles (3 µm width) [109]. With this approach several cell types have been successfully investigated in how they react to these TopoUnits. Specific micro-topographies that are able to promote enhanced clonogenicity of induced pluripotent stem cells (iPSCs), augment differentiation of tonsil-derived MSCs towards fibroblastic reticular cells, improve the osteogenic potential of MSCs, improve phenotypic maintenance of tenocytes and polarize macrophage phenotype have been identified [110]–[113]. Additionally, a 96-well platform –TopoWellPlate- has been developed with each well representing a unique micro-topographical design, enabling the screening and use of non-adherent cell types as well as non-microscopic experimental techniques, such as ELISA, flow cytometry, qPCR or western blots [114].

1.6 Modulating macrophage cell responses using biomaterials

Modulation of macrophage phenotype using different biomaterials or surface topographies has been extensively investigated. Brodbeck *et al*. demonstrated that adhered macrophages undergo increased levels of spontaneous apoptosis on anionic and hydrophilic surfaces *in vivo*, due to low integrin attachment sites [115]. This results in a reduced level of foreign body giant cells (FBGCs) formation. Hence, there was a thinner FBR around the inserted implants compared to ones formed around implants with hydrophobic and cationic surfaces. Wettability properties of materials also have an impact on macrophage polarisation. An *in vitro* study by Rostam *et al.* revealed that human monocytes cultured for 6 days on untreated hydrophobic polystyrene surfaces exhibited an M2-like phenotype, expressing higher level of mannose receptor (MR), IL-10 and CCL-18 compared to cells cultured on hydrophilic oxygen plasma-etched polystyrene surfaces [116].

Topographical gratings of 500 nm on PCL, PLA and polydimethylsiloxane (PDMS) induce increased RAW 264.7 macrophage cell line adhesion and elongation compared to planar controls, where the native round morphology is maintained [117]. While no distinctive patterns were revealed, all gratings (250 nm to 2 µm line width) affect cell morphology and cytokine secretion *in vitro*, and cell adhesion *in vivo* [117]. In another study, micro and nano-patterned grooves influenced macrophage elongation, which peaked on substrates with 400-500 nm wide grooves, while not affecting inflammatory activated macrophages which were driven towards pro-healing M2 phenotype [118]. Studies using nano and micro grooves and ridges have shown that

macrophages are sensitive to up to 25 μm groove depth, down to as shallow as 44 nm depth. A study by McWhorter *et al*. reported that 20 μm fibronectin lines printed on PDMS surfaces induced elongation of bone marrow derived macrophages (BMDMS) and polarised them towards M2 phenotype, independent of exogenous cytokines [119]. Non fouling polymeric biomaterials for coatings aim to prevent protein adsorption and therefore attenuate the host inflammatory response. Furthermore, Rostam *et al*., discovered a selection of acrylates and methacrylates which promoted macrophage attachment and differentiation towards pro- or anti-inflammatory phenotypes *in vitro* and which was successfully translated into a murine *in vivo* model with polymer-coated catheters [120]. While the molecular basis of macrophage polarisation in these studies is yet to be fully understood, it is likely to be driven by differential adsorption of biomolecules in biological fluids (e.g., serum) on different polymer surfaces [120].

1.7 Biomaterial-based DC modulation

With a growing understanding of material-cell relationships in immune responses, biomaterial scientists aim to develop strategies to engineer appropriate interactions within the adaptive immune system. These strategies can be based on biomaterial design, biomaterial-controlled drug or cytokine release and take aim for usage in vaccines for infectious disease or cancer, tissue engineered constructs, cell/tissue transplants, and autoimmune disorders. The adaptive immune response in any given scenario is vastly influenced by the phenotypic state of DCs. Therefore, a strategy to modulate adaptive immune responses is to utilise biomaterials to control DC phenotype.

Studies on DC responses to biomaterials have been sparse, though in recent years, the focus has turned to DCs [121]. A DC biomaterial interaction study by Vasilijic *et al*. investigated DC response to implanted biomaterials *in vivo* [122]. In their study, polyvinyl sponges (two per animal) were implanted at dorsal sites of the skin in rats. The sponges were left in place for different time periods (3-14 days), and after extraction resident inflammatory immune cells were isolated. It was shown that DCs progressively infiltrated into the sponges, reaching a peak at day 10 after implantation, and decreasing afterwards again. In a second step, the phenotype of infiltrated DCs was investigated. During the early phase of inflammation (day 6), DCs showed higher capability to stimulate the proliferation of allogeneic lymphocytes and CD4+ T cells than late-stage inflammation DCs (day 14). Accordingly, DCs in the late phase of inflammation downregulated the expression of CD80, CD86 and CD54 from higher levels during the early phase. One remarkable observation from this study was that the number of DCs staining for His 24 or His 48 (putative pDC markers) was higher at the day 14 time point than that at day 6. These observations indicated a switch in the functionality and phenotype of sponge infiltrated DCs from the early to late stages of inflammation. Increased amounts of IL-10 and TGF-β1 in culture supernatants and sponge exudate confirmed this functional change in DCs to that of a regulatory type. Overall, this study demonstrated that a significant number of DCs infiltrated/migrated to the implementation site following subcutaneous implantation. Moreover, DCs that were found in close vicinity to the biomaterials acquired a tolerogenic phenotype as the acute inflammation resolved, and these observations may be applied toward the

suppression of chronic inflammation and prevention of unsolicited autoimmune responses [122].

It has been observed, that DCs respond differentially to materials with different chemistries (summarized in Table 1): iDCs cultured with agarose showed no activation or maturation, while PLGA culture induced iDCs to undergo activation and express a mature phenotype [89]. PLGA -treated DCs expressed enhanced levels of co-stimulatory molecules (CD40, CD80 and CD86), MHC II (HLA-DQ and HLA-DR) and DC maturation marker (CD83) in comparison to untreated iDC controls [89]. Altogether a list of widely used materials were tested and in summary it was found, that PLGA or chitosan films induced DC maturation, while alginate and agarose did not, with hyaluronic acid films even suppressing DC maturation [123]. Mixed lymphocyte reactions showed that DCs treated with PLGA and chitosan films supported higher T cell proliferation compared to iDCs, DC treated with hyaluronic acid films induced less T cell proliferation, and DCs treated with agarose and alginate films did not differ from iDCs in allo-stimulatory capacity [124]. Surprisingly, both PLGA and agarose induced higher NFκB activation in iDCs, and the activation level was much higher in the DCs treated with agarose [89], [125]. Interestingly, in other studies chitosan and high molecular weight HA are reported to have intrinsic anti-inflammatory properties due to their oxygen species-scavenging properties [126]. Specifically, chitosan has been widely used in wound healing, tissue engineering and regenerative medicine [127]. In several studies, synthetic polymers were investigated for their ability to modulate DC phenotype. A number of polymethacrylates –

polyhydroxyethylmethacrylate (pHEMA) and poly (isobutyl-co-benzyl-co-terahydrofurfuryl) methacrylate (pIBTMA) were shown to induce the least and most mature DC phenotype, respectively [128]. Surprisingly, in the presence of pHEMA, the effect of LPS was completely eliminated, suggesting that polymers can override the effect of soluble stimulatory factors. It can be concluded that DCs show different reactions when cultured on synthetic polymers.

Table 1: Literature known surface coating effects on DCs

Material	Effect on DCs	Modulation of DC function	Ref
pHEMA	Maintenance of iDC function	• CD83, CCR7 and DC-SIGN same as iDC • high secretion of IL-16 • Maintain iDC phenotype in presence of LPS (through activation of ISRE, E2F-1, GR-PR, NFAT, HSF). • Suppression of NF-κB	[129]
pIBTMA	Activation of DCs	• activation of NF-κB • induction of pro-inflammatory cytokines (TNFα, IL-8, IL-1β, IL-18, MIP-1a) and IL-10 • increased CD86 • CD83, CCR7, DC-SIGN same as iDC • mDC Morphology	[129]
Chitosan	Activation of DCs	• Higher T cell proliferation • higher levels of co-stimulatory (CD80, CD83, CD86) and HLA-DQ than iDCs • more pro-inflammatory cytokines	[123], [126], [127], [129]

		• reduced endocytic ability to iDC	
HA	Suppresses DCs	• Less T cell proliferation than iDC	[126], [129], [130]
Agarose	Maintenance of iDC function	• Same T cell proliferation as iDCs	[125], [130]
PLGA	Activation of DCs	• CD40, CD80, CD83, CD86, MHC II upregulation • higher T cell proliferation • higher levels of co-stimulatory (CD40, CD80, CD83, CD86) and HLA-DQ than iDCs • more pro-inflammatory cytokines • reduced endocytic ability to iDC	[90], [125]
Alginate	Maintenance of iDCs	• Same T cell proliferation as iDCs	[130], [131]

Not only the composition of the material itself, but also the material architecture – such as films, scaffolds, (nano/micro) particulates – has been indicated to influence DC response. Recent work suggests that polymeric microparticles endocytosed by DCs can trigger the inflammasome via NALP3, inducing both humoral and cellular immunity [132]. This was found to be size- dependent, with particles between 400 nm and 1 µm inducing the highest secretion of IL-1β (when LPS was additionally administered) [132]. Similarly, the size of particles can affect the biodistribution of particles in the host and subsequent protein adsorption. It is already known that small particles <100 nm size are transported interstitially towards the lymph nodes, where they encounter larger

numbers of DCs, whereas larger particles distribute into the tissue [133]. The particle distribution has an impact on which cell types will be targeted/modulated by the particles.

Lewis and colleagues have extensively investigated the targeted delivery of DC modulatory microparticles in an easily injectable size of 1 µm [134]–[136]. With this they accomplished DC-targeted delivery of regulatory vaccine components that are both modular and multifunctional (e.g., PLGA). Fabricated PLGA microparticles were designed to passively target DCs and were loaded with DC recruitment agents, tolerogenic factors (e.g. IL-10 or TGF-β), and denaturated insulin peptides, which prevented hyperglycemia in a type 1 diabetes murine model [136]. After successfully treating diabetes, the same model was successfully translated to autoimmune encephalomyelitis (EAE) and rheumatoid arthritis (RA). Changing the autoantigen enabled the successful treatment of both EAE and RA, which further highlights the versatility and adaptability of the system [135], [137].

Clearly, biomaterials can affect DC phenotype and activation status, which can be used to modulate immune responses. However, the diversity of materials used in these studies makes it very difficult to deduce which properties are the most important to modulate DC phenotype. A study by Shokouhi *et al*., proposed that DC function altered by biomaterials can directly affect the immune response at the implantation site [138]. They hypothesised that the effect of biomaterials on DC phenotype may influence the adaptive immunity against a co-delivered antigen. The knowledge of DC-biomaterial interactions, mechanisms and their consequences is still in its infancy, making rationale

design of materials with the ability to influence different aspects of DC function rather challenging. Nevertheless, the concept of developing immune-instructive materials with the ability to promote DCs to distinct pro- or anti-inflammatory responses is very attractive, with potential applications as vaccine adjuvants to enhance or maximize a protective immunity or suppress deleterious immune response in inflammatory diseases. As the role of DCs in the FBR to medical devices is only researched sparsely so far, a desired application in that area could also be known in the future.

Recent research on MyD88 and TLR knock out mice demonstrated that DCs use TLR-2, -4 and -6 for the response to a group of chemically and physically diverse biomaterials. Knock out mices for any of these TLRs or MyD88 showed impaired expression of activation markers and reduced production of pro-inflammatory cytokines relative to the wild-type controls [139]. A possible explanation for the modulatory ability of polymers would be that their surface presents itself as ligands to either one of the TLRs identified, although this is not proven yet. ECM proteins adsorbed on tissue-culture polystyrene plates have been shown to affect DC morphology, cytokine production, and their allo-stimulatory capacity. For example, DCs cultured on collagen and vitronectin substrates released higher levels of IL-12p40, whereas DCs treated on albumin and serum-coated substrates generated higher amounts of IL-10 compared to other substrates [138]. A number of non-PRR receptors including Fc receptors and integrins have also been implicated to play a role in the DC responses to biomaterial surfaces in an adhesion-dependent manner. For instance, Acharya *et al.* demonstrated that different adsorbed, adhesive

protein (fibronectin, laminin, collagen type I, vitronectin, fibrinogen, bovine serum albumin, and fetal bovine serum (control)) layers on biomaterials could influence DC morphology, co-stimulatory marker expression, cytokine production, and allo-stimulatory capacity. They reported that adhesive substrates supported similar levels of DC adhesion and expression of positively stimulatory molecules. DC morphology and production of pro- and anti-inflammatory cytokines (IL-12p40 and IL-10, respectively) varied in an adhesive substrate-dependent manner. For example, DCs cultured on collagen and vitronectin substrates generated higher levels of IL-12p40, whereas DCs cultured on albumin and serum-coated tissue culture-treated substrates produce the higher levels of IL-10 compared to other substrates. Further, substrate-dependent modulation of IL-12p40 cytokine production correlated well with CD4+ T-cell proliferation and Th1 type response in terms of IFN-γ producing Th cells [139]. This indicates that rational biomaterial design can direct the adsorption of proteins layers which may serve to influence DC phenotype and function.

In summary, there is evidence suggesting that DCs are able to detect and interact with biomaterials specifically via TLR-2, -4 and -6, β-integrins or “biomaterial–associated molecular patterns” (BAMPs) [121], [140], [141], however the exact mechanisms and pathways underpinning DCs interaction with different biomaterials are yet to be elucidated.

In addition to the treatment of DCs with planar biomaterial or particulates, studies have also been carried out to investigate the interactions of DCs with porous scaffolds. The phenotype of DCs upon seeding the cells on PLGA or

agarose scaffolds was examined. It was found that, similar to treatment of DCs with the film versions of these polymers, DCs treated with PLGA scaffolds displayed a moderately mature phenotype with dendritic processes, elevated expression of maturation markers and increased secretion of pro-inflammatory cytokines to the level similar to cells treated with PLGA films, while agarose scaffold did not induce DC maturation [128]. It was also found that biomaterial scaffolds engineered with a proper lymphoid microenvironment in mind allow DC migration and interaction with T-cells, which represents a promising strategy to create ectopic lymphoid tissue [142].

Furthermore, Kim *et al* developed PLG scaffolds loaded with GM-CSF and tumour antigens, in order to recruit and activate DCs [143]. In another study they prepared crosslinked methacrylated PEG and methacrylated alginate into macroporous scaffolds, which were then loaded with GM-CSF, CpG-ODN (a TLR ligand), and tumour antigens [144]. There, a biomaterial-based acute myeloid leukaemia (AML) vaccine was developed, which demonstrated to induce robust immune responses against AML [144]. It was shown to even prevent AML engraftment in a prophylactic vaccination strategy.

This approach of *in vivo* DC modulation is thought to improve poor functionality and the low persistence of DCs. In DC-based immunotherapies against cancer, DCs are usually isolated from the patient and are treated with tumour antigen and other activating agents *ex vivo* to be later transferred back into the patient, with the goal of inducing strong antigen-specific anti-tumour immune responses. In the past, this has proven to be successful, albeit the clinical

efficacy is low due to decreased DC persistence and their poor functionality [145]–[147].

1.8 Screening strategies for biomaterial discovery

In traditional biomaterial research only a limited number of materials are evaluated simultaneously, leading to slow progress. High throughput screening (HTS) has previously shown to be effective in the identification of new bio-instructive materials, especially synthetic polymers [120], [148]–[150]. In the past ten years, established libraries of combinatorial polymers and topographies have created opportunities to quickly identify simple polymers and topographical cues with bio-instructive properties with great success [109], [148]–[153]. For instance, several acrylate polymers that modulate stem cell renewal, stop bacterial biofilm formation or instruct macrophage polarization have been identified using polymer screening platforms [120], [148], [127], [129]. A number of these polymers are currently being translated into clinical applications [120].

A combination of both chemical and structural aspects into a novel screening platform called the ChemoTopoChip was developed recently [120], [154]. It was utilised to identify materials suitable for bone regeneration by screening with human immortalized mesenchymal stem cells and human macrophages. Specific topographies were identified that exhibited immunomodulatory effects, concurrently polarising macrophages towards a pro-healing phenotype and inducing bone regeneration. The same screening platforms could potentially be utilised to assess biomaterial impact on DC phenotype and function.

1.9 Hypothesis and aims

It is hypothesised that DC phenotype can be modulated by synthetic polymers and surface topography to elicit either pro-inflammatory or regulatory/tolerogenic phenotypes, with downstream functional changes in the adaptive immune response. Pro-inflammatory materials that activate DCs could be utilised as vaccine adjuvants or in DC based cancer treatment, while materials that suppress DC activation could find application in the treatment of autoimmune diseases.

Therefore, in this project I used a screening platform to investigate the effect of simple homo polymers on human moDCs phenotype, function, and ability to prime T cell activation. A polymer library previously used to identify materials with the ability to instruct stem cell differentiation or stop bacterial biofilm formation was utilised in this project [148], [149], [151]. In addition, I investigated the impact of different topographies on DC motility, migratory behaviour, and phenotype.

Chapter 2: General Methods

Chapter 2 General Methods

2.1 Cellular and molecular techniques

2.2 Monocyte isolation

Buffy coats were obtained from healthy donors (National Blood Service, Sheffield, UK) after obtaining informed written consent and following ethics committee approval (Research Ethics Committee, Faculty of Medicine and Health Sciences, University of Nottingham). All methods were performed in accordance with the relevant guidelines and regulations. PBMCs were isolated from the buffy coat by density gradient centrifugation of blood on Histopaque - 1077g/mL. $CD14^+$ monocytes were isolated from PBMCs by positive selection, using a magnetic activated cell sorting (MACS) method by Miltenyi Biotec, UK. This monocyte isolation approach routinely yielded a purity of over 95% purity for $CD14^+$ cells.

2.2.1 Dendritic cell generation

Purified monocytes were suspended in RPMI-1640 medium supplemented with 10% heat inactivated fetal bovine serum (FBS), 2 mM L-glutamine and 100 U/mL penicillin and 100 µg/mL streptomycin (all from Sigma-Aldrich) (later referred to as “complete RPMI medium”). Cells were seeded in a density of 1 x 10^6 cells/ml. Cells were supplemented with a differentiation cocktail consisting of the cytokines 50 ng/mL GM-CSF and 20 ng/mL IL-4 and incubated at 37˚C, 5% CO_2 in a humidified incubator for six days. After three

days, cells were supplemented with additional GM-CSF and IL-4. MoDCs can be harvested and used as iDCs for experiments on day 6 of culture.

2.2.2 **Enzyme linked immunoglobulin linked assay (ELISA)**

A sandwich ELISA was used to quantify cytokine secretion and manufacturer's instructions were followed. Slight adaptations to volume used were done to use the system in a 384-WP format due to low sample volumes. Optical densities were read on a GlowMaxPro plate reader.

2.2.3 **Flow cytometry**

Purity of monocytes was confirmed via flow cytometry on a Canto II using the Kaluza Software. Monocytes were stained with anti-CD14 antibody. 10 000 events were acquired, and the live population was gated upon by SSC/FSC gating.

Unstained controls and isotype-matched antibodies were used to determine the level of unspecific binding. Correct differentiation of monocytes to DCs was confirmed by CD11c staining and maturation status of DCs after treatment was confirmed, by staining with anti-CD86, CD80, CD83 and HLA-DR, CD206 and CD209. A list of all used flow cytometry antibodies can be found in Table 2.

Table 2: List of used flow cytometry antibodies

Antibody	Clone	Catalogue number	Company
CCR7 PeCy7	G043H7	353226	BioLegend
CD14 Fitc	REA599	130-110-518	Miltenyi
CD206 PerCP	DCN228	130-104-129	Miltenyi
CD209-APC	DCN46	551545	BD Pharmingen
CD80 Fitc	2D10.4	LS-C105944	LSBio (Lifespan)
CD83 Fitc	HB15e	305306	BioLegend
CD83 Fitc	REA714	130-110-507	Miltenyi
CD86 PE	REA968	130-116-160	Miltenyi
CD86-PE	IT2.2	305406	BioLegend
DEC-205 APC	HD30	342207	BioLegend
HLA-ABC Fitc	B9.12.1	IM1838U	IOTest
HLA-DR PerCP	REA805	130-111-793	Miltenyi
HLA-DR PerCP	AC122	130-113-966	Miltenyi
ICAM	HA58	353106	BioLegend
PD-L1 APC	29E2A3	329708	BioLegend
PD-L2 APC	MIH18	345508	BioLegend

2.3 Surface characterisation methods

2.3.1 X-ray photoelectron spectrophotometry (XPS)

XPS is a surface characterisation technique that analyses the surface elemental composition of substrates. The energy spectrum of electrons emitted from material surfaces following excitation of electron by x-rays are measured in this technology [155], [156]. XPS involves irradiating materials by X-rays in ultra-high vacuum conditions [157]. Absorption of X-rays energy by atoms in the materials cause ejection of electrons from the core levels or valence levels. Several of the ejected photoelectrons escape into the vacuum system and reach a detector that analyses their energies and intensities. An equation calculates the relationship between kinetic energy (KE) of the ejected photoelectrons and electron binding energy (BE) and the energy of the exciting X-ray (hv) [155], [157]:

$$KE = hv - BE - \varphi$$

φ is the spectrometer work function [157]. Depending on the element from which the photoelectron originates a specific binding energy of the photo electron is measured [156], [158]. Hence, an XPS spectrum is generated by plotting the photo-electron intensity against the binding energy. There is a direct proportion between intensities of detected photoelectrons and the concentration of elements they originated from [155], [159]. As XPS samples up to 10nm depth into the material, the relative amount of elements present on and just below the surface of a material can be calculated using information from the XPS spectrum. Due to its sensitivity, XPS is increasingly being used

to gain quantitative information about organic and inorganic components of samples [151], [157]. XPS can also be used to quantify protein adsorption by measuring the amount of proteins adsorbed to biomaterials [160]–[162]. This is specifically done by quantifying the elements emitted from the substrates or the introduction of protein specific elements (usually nitrogen) onto the substrate [159], [160].

2.3.2 **Time of flight – secondary ion mass spectrometry (ToF-SIMS)**

ToF-SIMS is a surface-sensitive analytical method that uses a pulsed ion beam (Cs or microfocused Ga) to remove molecules from the very outmost surface of the sample. Secondary particles (secondary ions) generated farther from the impact site tend to be molecular compounds, typically fragments of much larger organic macromolecules. These particles are then accelerated into a ‘flight tube’ and their mass is determined by measuring the exact time at which they reach the detector (i.e. time-of-flight). This is measured in nanoseconds, giving the possibility to produce a mass resolution as small as 0.00X atomic mass units. ToF-SIMS can be used for surface spectroscopy, surface imaging and depth profiling. ToF-SIMS provides information about the molecular mass and structure of the top 2nm of a surface material [151], [163]. ToF-SIMS is very sensitive and is able to distinguish between very similar chemical species. Due to its sensitivity this technique can also be applied to identify the distribution of amino acids in protein adsorption studies [161].

Chapter 3: Screening of an acrylate and methacrylate library for immunomodulation of DCs

Chapter 3 Screening of an acrylate and methacrylate library for immunomodulation of DCs

3.1 Introduction

DCs are key players of the immune system; as the bridge between the innate and the adaptive arm of the immune system, they play an integral role in the regulation of an immune response. The direction and magnitude of immune responses is influenced in part by the level of DC activation status, determined by their surface phenotype and cytokine profiles, and can be used to predict their either stimulatory or regulator/inhibitory function.

In recent years, the research on biocompatible biomaterials has seen a 'paradigm shift' in the design and engineering of such materials. This new direction of biomaterial design is driven by the quest to find immune-instructive materials that are able to modulate the host's immune responses in order to instruct the immune system in a desired direction and clinical outcome [20]. There is a substantial interest in modulating the function of the immune system for treating inflammatory and autoimmune diseases, increase vaccination efficacy with better adjuvants and enhance materials designed for implanted medical devices to prevent inflammation and rejection. Recent research has shown that a number of biomaterial characteristics - such as surface chemistry or topography - influence various cell types including a number of immune cells [116], [121], [164]. A study by Shokouhi *et al*., proposed that DC function that has been altered by biomaterials can directly affect the immune response at the implantation site [138]. This information makes immune-instructive

biomaterials very interesting for enhancing adjuvant efficacy, as vaccine delivery seeks to enhance or maximize a protective immunity.

Our understanding of DC-biomaterial interactions, mechanisms and their consequences is still in its infancy. Recent *in vitro* studies have shown that some biomedical polymers have been able to induce upregulation of surface molecules and the secretion of pro-inflammatory cytokines in murine and human DCs [89], [165]. As mentioned previously, the current assumption is, that DCs are able to detect and interact with biomaterials specifically via TLR-2, 4 and 6, β-integrin or “biomaterial–associated molecular patterns” (BAMPs) [121], [140], [141].

As one specific subgroup of biomaterials, polymers have been found to be tuneable in their physical, chemical and biological properties [166]. With the increasing importance of immune cell-biomaterial interactions and their significant involvement in clinical outcome, a new focus on identifying new simple synthetic polymeric biomaterials with the ability to modulate human DC phenotype and function is necessary. These polymers can then be characterized as immune-modulatory - driving immune responses in a specific direction. In the past ten years, established libraries of combinatorial polymers in high throughput-screening formats have already created opportunities to identify simple polymers with bio-instructive interactions with great success [148]–[153].

To discover new synthetic materials, high throughput methodologies have been employed to screen a large chemical combinatorial space. A variety of acrylate-based polymers have been used for tissue engineering, surgical glues

and drug delivery [151]. Polymer library and microarrays are a powerful approach by which thousands of materials can be investigated. Our library consists of (meth)acrylate and (meth)acrylamide monomer library was explored as the most chemically diverse polymer microarray to date, utilising >90% of photo curable monomers that are readily commercially available. To maximise the chemical diversity that can be explored, monomers comprising a variety of nitrogen, fluorine, oxygen, aromatic and aliphatic side chain functionalities were included. Monomers were selected based on their ability to be polymerised in situ initiated by UV irradiation, low volatility and wide diversity in side-chain and main-chain chemistry to achieve the largest chemical combinatorial space yet published using a polymer microarray. Overall, there are a number of commercially available monomers, and these can be polymerized quickly using a light-activated radical initiator. Monomers were purchased from Sigma-Aldrich, Scientific Polymers, Acros Organics, or Polysciences and were used as received.

In this chapter a previously established (meth)acrylate library was fabricated in a well plate format to screen for polymer effect on DCs [148], [149]. Due to the non-adherent nature of DC, I chose to fabricate the library in a well plate format in order to investigate soluble factors of cellular response to polymers. Additionally, a well plate format allows the harvest of DCs and utilisation in cell-based assays which is impossible from an array format. Initially a 96-wellplate format was chosen to enable the investigation of larger numbers of polymers, followed by 24-wellplate format for in-depth characterisation studies.

3.2 Methods

3.2.1 Monocyte isolation

Monocytes were isolated from buffy coat as described in section 2.2 and differentiated into DCs as described in section 2.2.1.

3.2.2 Monomer to polymer polymerisation by UV

96- well polypropylene plates were chosen due to their wide solvent-suitability and were etched using oxygen plasma, ran at 100 watts for 10 minutes, at a pressure of 0.09 mbar. Polymerisation solution for polymers from the library consisted of monomers (50% v/v) in isopropylalcohol (IPA) with photo-initiator (PI) (2,2-diemethoxy-2-phenylacetophenon; DMPA) (1% w/v). 10 µl of polymerisation solutions were dispensed into oxygen etched 96-well polypropylene plates and polymerised under ultraviolet (UV) light at a wavelength of 365 nm for 1 hour, in an argon (Ar) environment (O2 <<2000 ppm).

3.2.3 Polymer plate washes for cell culture

The resulting polymers were rinsed with 100% IPA twice and incubated in distilled water for 72 hours at 37°C. This was done to remove any non-polymerized monomer residues. Polymers were subsequently dried, and UV sterilised at a wavelength of 245 nm for 20 minutes. Polymers were further incubated overnight in complete cell culture medium before being used for cell culture.

3.2.4 **Determination of cell viability**

DCs were seeded in a concentration of 5 x 10^5 cells/well in duplicate onto polymers and incubated at 37ºC and 5% CO_2 for 6 hours. Cell viability was measured using CytoToxGlo (Promega) following the manufacturer's instructions. CytoToxGlo uses a luminogenic peptide substrate, the AAF-Glo™ substrate to measure dead-cell protease activity, which is released from cells that have lost membrane integrity. The AAF- Glo™ substrate cannot cross the intact membrane of live cells and does not generate any appreciable signal from the live-cell population. The assay relies on the properties of Ultra-Glo™ Recombinant Luciferase, which uses aminoluciferin as a substrate to generate a stable "glow-type" luminescent signal and is formulated to improve performance across a wide range of assay conditions. After reading the initial dead-cell protease activity, each well population is lysed with Digitonin to read the total cell protease activity in order to amount for varying cell numbers per well. Briefly, 25 µl of cell suspension was transferred to a 384- well plate, 12.5 µl of the assay substrate was added and the plate was briefly placed on an orbital shaker to be mixed. The assay plate was incubated for 15 minutes at room temperature before the dead cell luminescence was read on a GloMax Discover (Promega). Following this, the lysis reagent was added for 15 minutes, and total cell luminescence was read, therefore all cytotoxicity data is normalised to respective cell number per well. In order to present viability data, for each cytotoxicity data point the corresponding viability was calculated.

3.2.5 **DC culture on polymer coated surfaces**

After preparing the polymer plates for cell culture, as described in 3.3.1, immature DC were harvested, washed once, re-suspended in fresh complete media and transferred to the coated wells. For investigating the effect of the polymers on iDCs, cells were cultured on polymers for 24 hours. For investigation of polymer effect on DC maturation, DCs were conditioned for 6 hours on the polymers and then stimulated with 0.1 µg/mL lipopolysaccharide (LPS from *E. coli*, Sigma-Aldrich) and cultured for a further 18 hours. Cells were then used for the assays described below.

3.2.6 **Flow cytometry staining**

Polymer-treated and control DC were harvested, washed twice with PBS (supplemented with 0.5% BSA and 0.1% NaN_3, later mentioned as PBA) and then stained for CD83 (FITC, clone REA714, IgG1, Miltenyi Biotec) and CD86 (PE, clone REA968, IgG1, Miltenyi Biotec) for 20 minutes at 4ºC. The cells were then washed with PBA and fixed in 1% paraformaldehyde (PFA) in PBS. Cells were usually analysed within 24 hours.

3.2.7 **Cytokine analysis**

Culture supernatants from 3 independent experiments were collected after 24 hours culture. IL-6, IL-10, IL-12 and IFN-γ were measured by DuoSet ELISA kit (R&D Systems) as per the manufacturer's instructions. Modifications of the protocol allowed analysis of cytokines in a 384-well plate format, giving the opportunity to read duplicates from each donor.

3.2.8 **Endocytosis assay**

DCs were cultured on scaled up polymers in 24- well plates and appropriate controls for 24 hours. DC were washed once with PBS, re-suspended in complete media with human AB serum and transferred into FACS tubes (4 x 10^5 cells in 400 µl). Dextran-FITC (40,000 kDa, Sigma) was added to a final concentration of 1 mg/mL and the tubes were incubated for 90 minutes at 37ºC or 4ºC. Cells were harvested, washed twice with ice-cold PBS, then fixed in 1% PFA in PBS to be immediately analysed by flow cytometry.

3.2.9 **Statistical analysis**

All graphical presentation and statistical analysis were carried out using Prism 8 (GraphPad software, Inc., USA). Student T-test or one-way-ANOVA and a multiple comparisons post-test was performed and is stated below each graph.

A value $p<0.05$ was considered statistically significant. For significance: *<0.05; **<0.01; ***<0.001; ****<0.0001.

3.3 Results

Due to DC being non-adherent cells, an established library mentioned previously was used and prepared in a well plate format [151]. In this format it was possible to evaluate the effect of polymer modulation on non-adherent cells and soluble mediators. Polymer names and acronyms are stated in Appendix 1.

3.3.1 Evaluation of DC viability on polymer surface

Initially, DC viability was assessed in the well plate format to determine whether manual fabrication was able to produce viable surfaces. Manual UV polymerisation can leave some monomer residents or solvents which are detrimental to cell viability. A comparison of viability pre and post washing procedure (Table 3) showed that extensive washing removes potential remnants of monomers and solvent from the polymerised system in Figure 3-1.

Table 3: Polymer plates preparation for cell culture

Washing method	Time/amount
Isopropanol	2x rinse and discard
Distilled H_2O	72 hrs in incubator
Dry	Until dry

UV sterilisation at 245 nm	20 minutes
Complete media	Overnight in incubator media priming
Cells seeding	-

The cytotoxicity was significantly reduced after the procedure described in Table 3 (Figure 3-1).

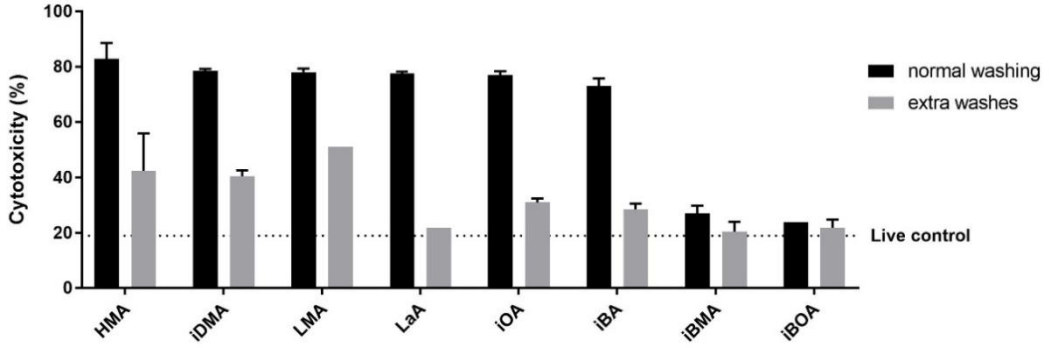


Figure 3-1: Viability comparison of pre-culture procedure

Polymers were fabricated as described before, and plates prepared either with vacuum oven for 7 days followed by UV sterilization and media prime overnight (normal washing) or according to washing procedure stated in Table 3. iDCs were seeded on the polymers for 6hrs and cytotoxicity assessed by CytoToxGlo with 1 donor and 2 wells per polymer for selected polymers.

Analysis of the media used during the priming step also revealed that following the cell culture preparation procedure only femtogram levels or non-detectable levels of monomers were found (Table 4). Analysis of the exact monomer concentration found (and concentrations up to 1500 times the found concentration) and its effect on DC viability and DC phenotype was also

assessed and showed no detrimental effect on cell viability and additionally, no modulatory effect on DC phenotype (Appendix 2 and Appendix 3).

Table 4: Liquid extraction surface analysis – mass spectrometry of monomer remnants in priming media from 5 selected polymers, by Joris Meurs

Monomer	Actual amount (g/mL)
ZnA	2.24765×10^{-11}
pEGMEMA	1.70514×10^{-14}
DEAEA	2.41313×10^{-14}
PhMA	-
THFuA	-

DC viability was measured after 6 hours of polymer treatment, for this, cells were subjected to a viability assay (CytoToxGlo, Promega). CytoToxGlo uses a luminogenic peptide substrate, the AAF-Glo^{TM} substrate to measure dead-cell protease activity, which is released from cells that have lost membrane integrity. For better comparison, all data points were normalised against the tissue culture plastic control (TCP) which was set as 100%, and the overall ranked order of viability was graphed (see Figure 3-2). The ranked order portrays a form of a slope that flattens out shortly before the TCP control. The top 55% (120 polymers) of viable polymers weretaken forward to the next

screening steps. The lowest DC viability of selected polymers is therefore 93% and the highest 116% - compared to TCP. Interestingly, 33% of the investigated polymers supported DC survival more efficiently than TCP, which could be an interesting aspect to keep in mind for (*ex vivo*) DC cultures. A full data list of DC viability on polymers are stated in Appendix 1.

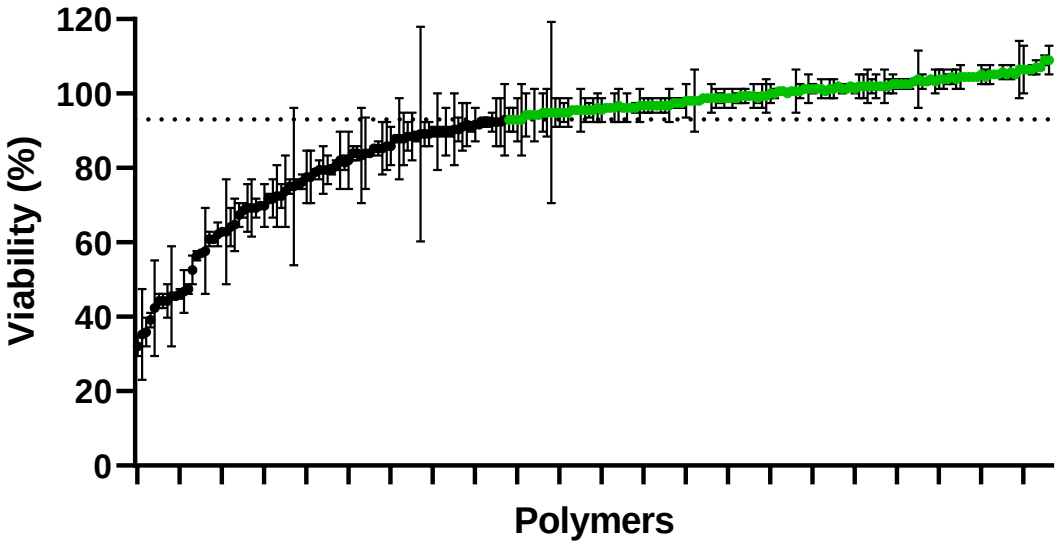


Figure 3-2: Viability assay of DCs cultured on polymer coatings in 96 well-plates with plates prepared as described in Table 3.

50 000 immature DCs were seeded in each well of polymer coated 96 well-plates in duplicate; data has been normalised to the tissue culture plastic control of immature DCs (100% viability) and is presented as mean ± range (n=2). Viability was assessed by CytoToxGlo (Promega). The dotted line represents the threshold chosen to select polymers (further indicated with green) for phenotyping.

3.3.2 Identification of polymers that induce DC activation

Assessment of DC maturation in response to biomaterials typically involves the treatment of iDCs with biomaterials pre-placed in wells using

immunological assays such as flow cytometry for the expression of DC-specific or maturation-specific surface markers. A total of 120 polymers were shown to support DC viability comparable to or above tissue culture plastic, which were then investigated on their ability to induce DC maturation. For this, 2 markers were chosen to determine the activation levels of treated DCs. CD83 as a marker molecule for mDCs, as well as co-stimulatory marker CD86 were selected based on their high level of upregulation following DC stimulation. CD86 binds to surface markers on T cells and the role of CD83 is still unclear but the marker is upregulated highly after DC stimulation with a pathogen. As such, they are essential for evoking a T cell effector response and have been chosen to be good markers to assess DC activation level.

The majority of investigated polymers induced upregulations of CD83, while a limited number of them actually kept CD83 levels below the iDC control (Figure 3-3). 3 polymers upregulated the expression levels of CD83 close to the LPS stimulated DC control (DEAEA upregulated to 73%). Several polymers were able to significantly increase CD83 levels - namely, MTEMA, MAPtMA, F7BA, HEAm, pEGDA, Mam, EaNia, PhEA, COEA, pEGMEMA and DEAEA.

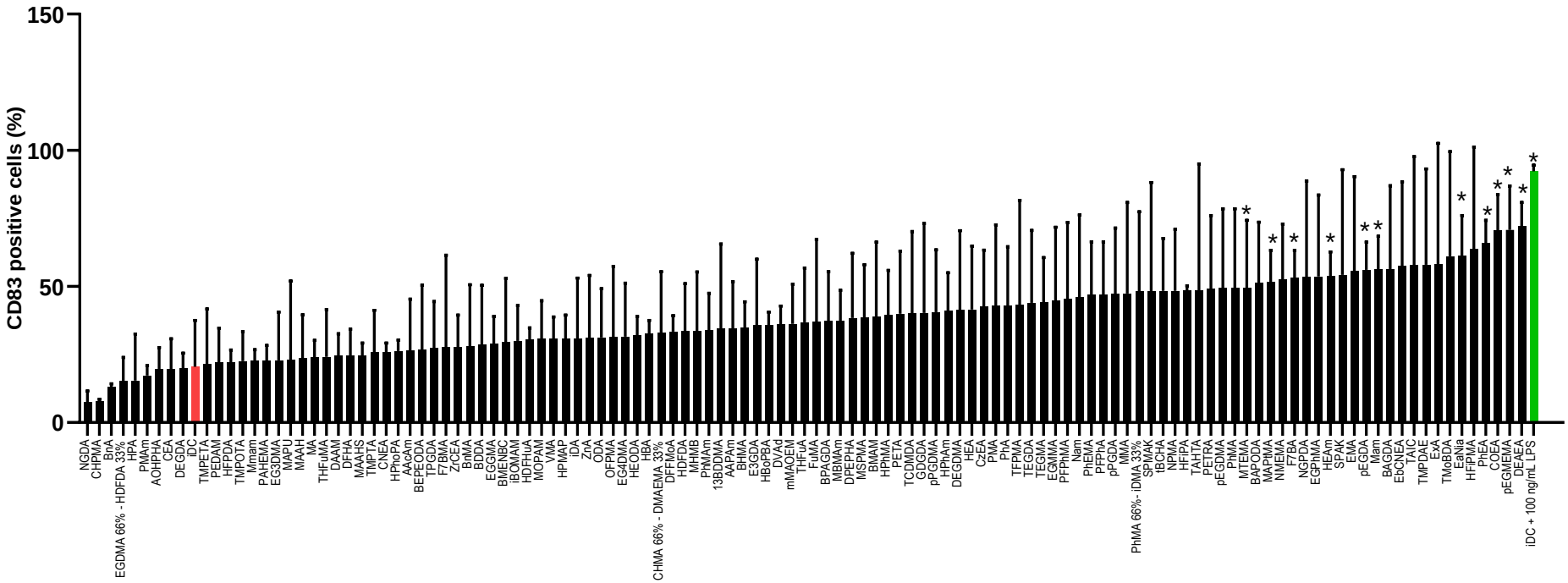


Figure 3-3: Polymers increase CD83 expression on DCs

iDCs were seeded on polymer coatings for 24 hours, stained with anti-CD83 flow cytometry antibody and acquired via flow cytometry. Data is from 3 independent experiments and shows percentage of positive cells as mean ± SD. Experimental conditions are compared to the negative iDC control (red bar). The green bar represents iDC + 100 ng/mL LPS and acts as a positive control. For significance t-tests were performed and shown as *<0.05; **<0.01; ***<0.001; ****<0.0001.

A majority of polymers had a slight upregulating effect on CD86 expression, with 3 keeping levels lower than the iDC control. A few of them induced CD86 expression levels close to the LPS control, with DEAEA just being 6% off. Several of the polymers were able to significantly upregulate CD86 expression on DCs: HBoPBA, pEGDA, F7BA, HEAm, NPMA, Mam, pEGMEMA and DEAEA.

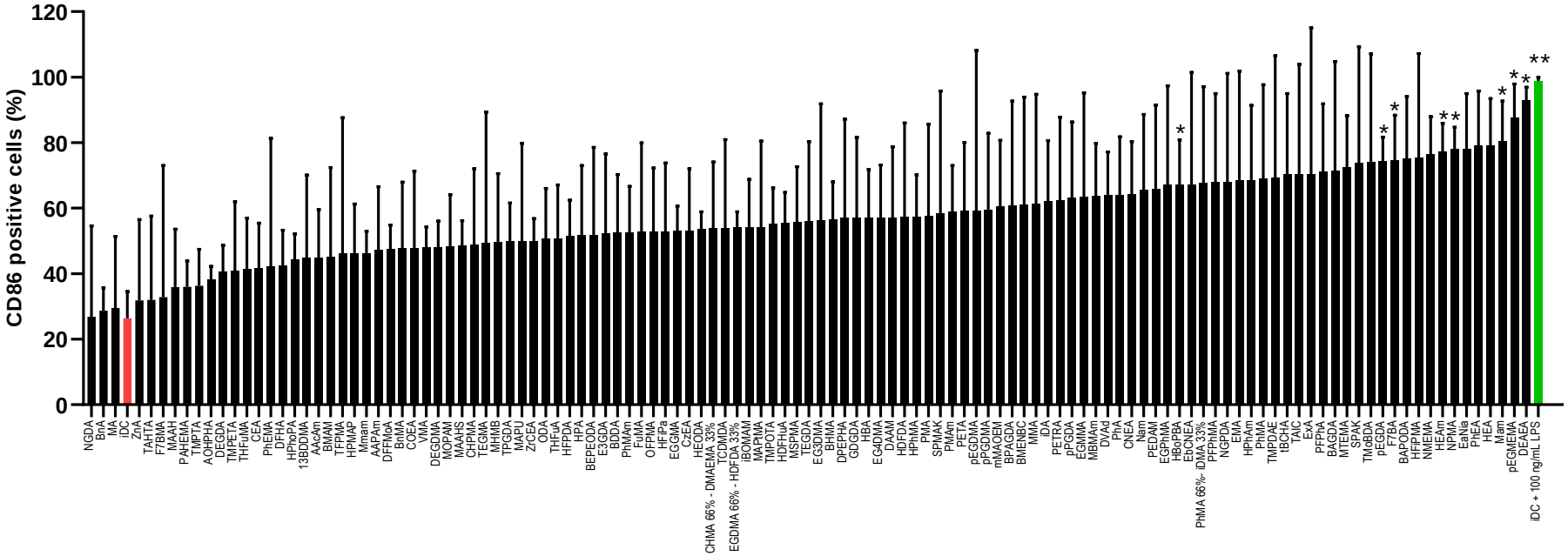


Figure 3-4: Polymers increase CD86 expression on DCs

iDCs were seeded on polymer coatings for 24 hours, stained with anti-CD86 flow cytometry antibody and acquired via flow cytometry. Data is from 3 independent experiments and shows percentage of positive cells as mean ± SD. Experimental conditions are compared to the negative iDC control (red bar). The green bar represents iDC + 100 ng/mL LPS and acts as a positive control. For significance t-tests were performed and shown as *<0.05; **<0.01; ***<0.001; ****<0.0001.

In a correlation graph, the spread between the negative control (red dot) and the positive LPS stimulated control (green dot) are visualised. Polymers able to upregulate both CD83 and CD86, with limited variance between donors were chosen to take into the next round of analysis. Overall, these polymers elevated the expression levels of CD86 more than of CD83, but a correlation between both calculates a good fit of the two expression levels (R^2= 0.931).

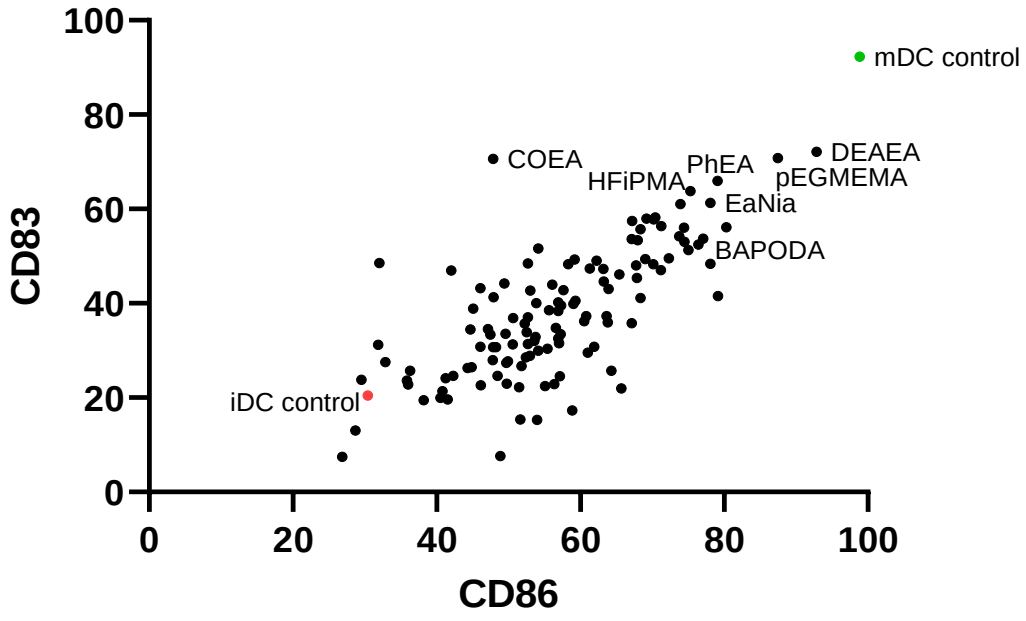


Figure 3-5: Correlation of CD83 and CD86 expression on polymer cultured DCs

Mean of surface marker expression gained from donor averages were used to correlate CD83 and CD86**.** 7 representative points are labelled with their respective polymer names.

3.3.3 Identification of polymers that suppress surface marker upregulation

Considering the possibility that the effect of polymer treatment could render DCs less responsive to further stimulation, the maturation state of these cells

was studied after first conditioning them on the polymers and followed by LPS stimulation. Afterwards, maturation levels established by CD83 and CD86 expression were determined by flow cytometry. However, DCs conditioned with the majority of investigated polymers were still able to fully mature in response to LPS stimulation. A minority of polymers were able to prevent the development of a mature phenotype and showed significantly lower expression levels of CD83 than the iDC + LPS condition. 6 polymers were able to make DCs significantly less responsive to LPS in upregulating CD83 (* for ZnA, HDFHuA, EGDMA-66%-HDFDA-33%, PhMAm, MTEMA and ** for PEDAM).

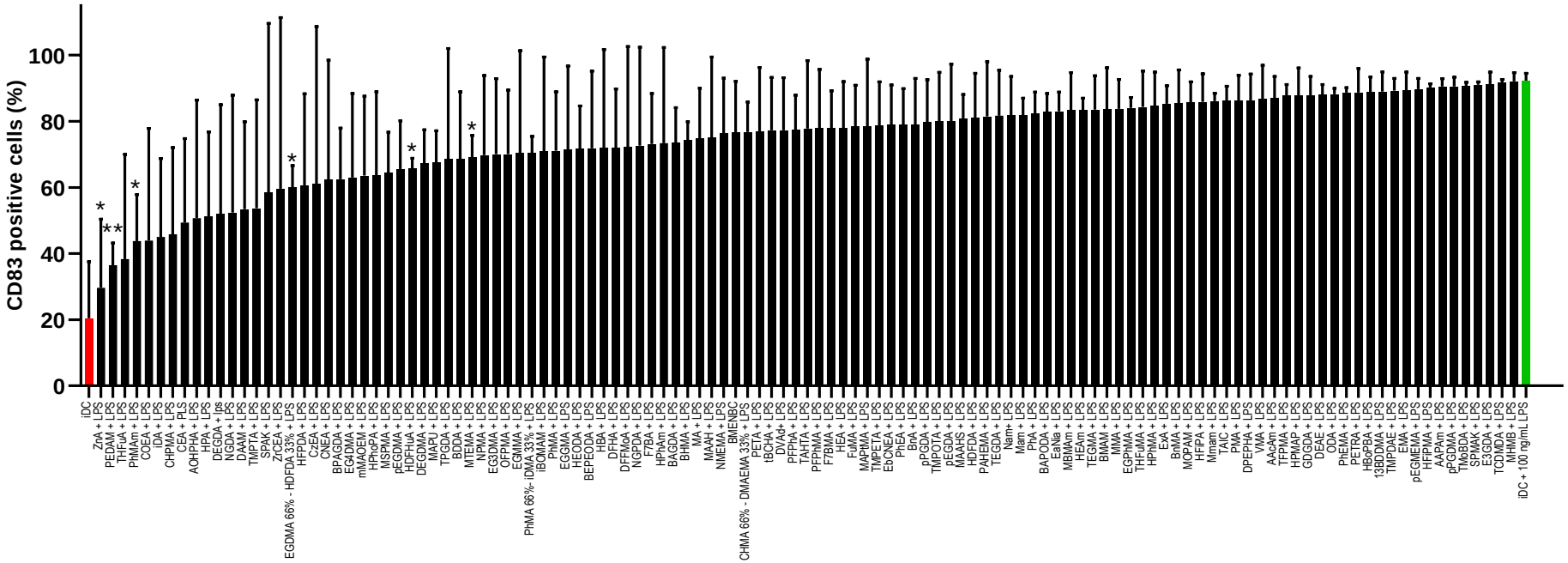


Figure 3-6: Polymers render DCs less susceptible to CD83 upregulation upon LPS stimulaton

iDCs were seeded on polymer coatings for 6 hours, then stimulated with 100 ng/mL LPS and cultured for further 18 hours and stained with anti-CD83 flow cytometry antibody and acquired via flow cytometry. Data is from 3 independent experiments and shows percentage of positive cells as mean ± SD. Polymer conditions are compared via t-test to the iDC + LPS control (green bar). For significance t-tests were performed and shown as *<0.05; **<0.01; ***<0.001; ****<0.0001.

DC conditioned on most polymers and then stimulated by LPS were still able to upregulate their CD86 expression. Only 3 polymers prevented the upregulation of CD86 expression in the presence of LPS significantly (ZnA**, COEA* and EGDMA-66%-HDFDA-33%*).

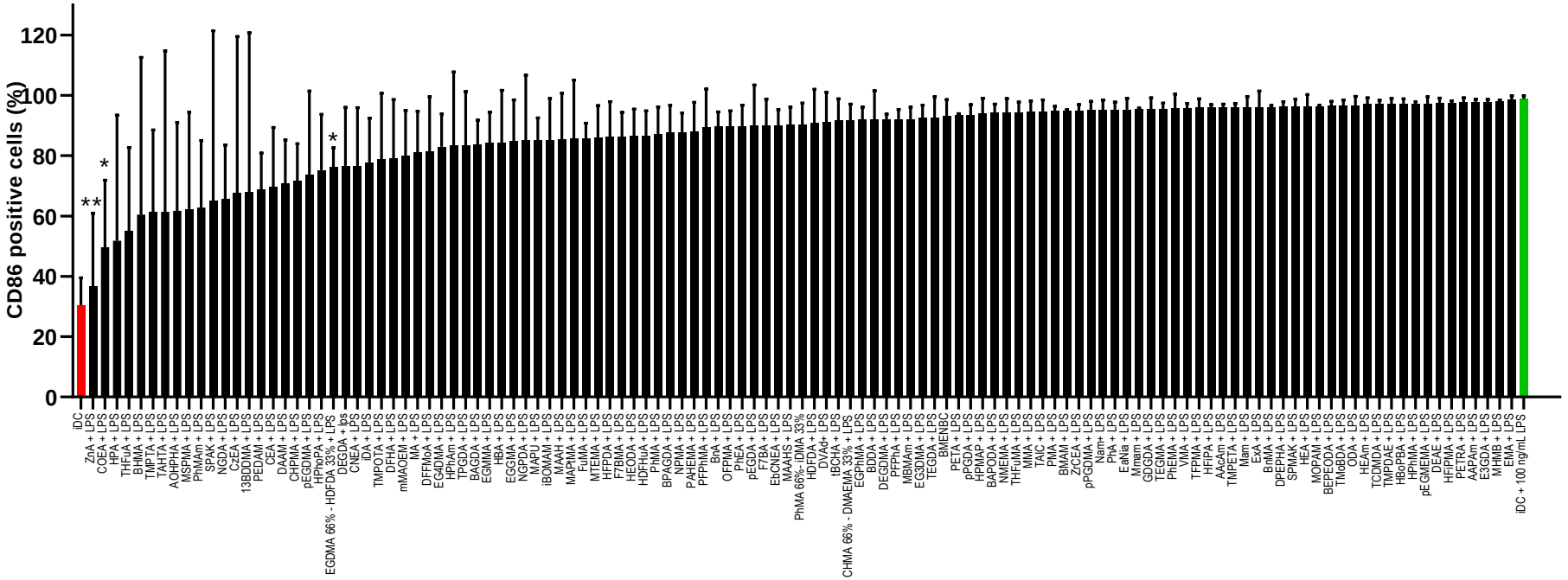


Figure 3-7: Polymers render DCs less susceptible to CD86 upregulation upon LPS stimulation

iDCs were seeded on polymer coatings for 6 hours, then stimulated with 100 ng/mL LPS and cultured for further 18 hours and stained with anti-CD86 flow cytometry antibody and acquired via flow cytometry. Data is from 3 independent experiments and shows percentage of positive cells as mean ± SD. Polymer conditions are compared via t-test to the iDC + LPS control (green bar). For significance t-tests were performed and shown as *<0.05; **<0.01; ***<0.001; ****<0.0001.

In a correlation graph, the spread between the non-stimulated (red dot) and the positive LPS stimulated control (green dot) are visualised. Polymers able to render DCs less responsive to LPS stimulation after polymer culture are polymers close to the red dot. 9 polymers that induced lower levels of both surface markers, as well as low biological variation between donors were chosen to take forward into the next stage of the screening.

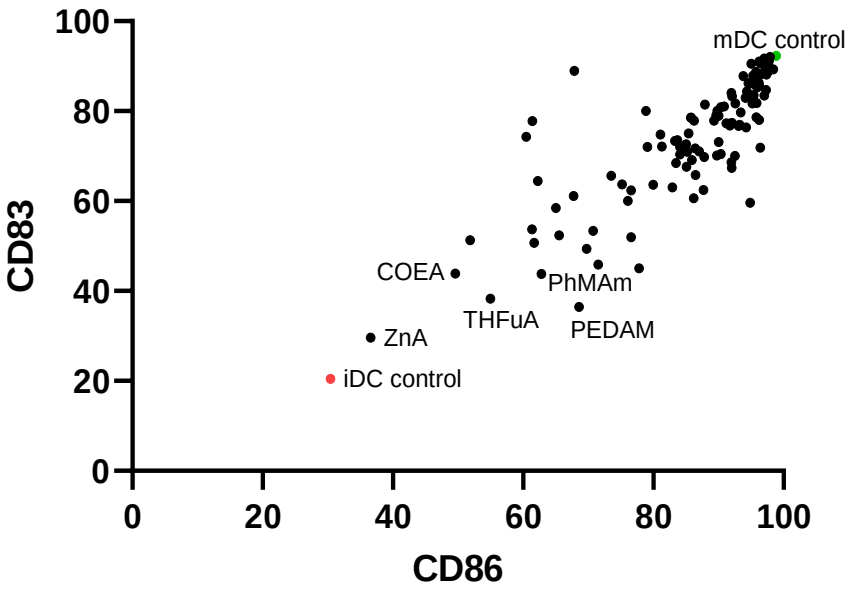


Figure 3-8: Correlation of polymer CD83 and CD86 expression in LPS presence

Mean of surface marker expression gained from above figures are used to correlate CD83 and CD86. 5 representative points are labelled with their respective polymer names.

3.3.4 Cytokine production in response to polymers

To determine the influence of polymers on cytokine production by DCs, DCs were cultured on polymers and TCP for 24 hours (for LPS conditions, cells were conditioned for 6 hours followed by LPS stimulation). 17 polymers that

are categorised as stimulatory polymers and 9 polymers, that are categorised as DC activation suppressing polymers were used for this study.

Generally, there was a considerable variation in the levels of cytokine production between different donors in response to investigated polymers.

Except for polymers HFiPMA, BAPODA, pEGMEMA and CNEA, DCs cultured on polymer surfaces did not induce any changes to IL-10 and IL-12 levels compared to TCP. Upon culture on polymer surfaces, DCs from donor 2 produced higher levels of IL-10 and IL-12, while many conditions had cytokine secretion below the detection level. Overall, IL-10 secretion was slightly elevated when DCs were cultured on polymers, whereas only one polymer increased IL-12 secretion (Figure 3-9).

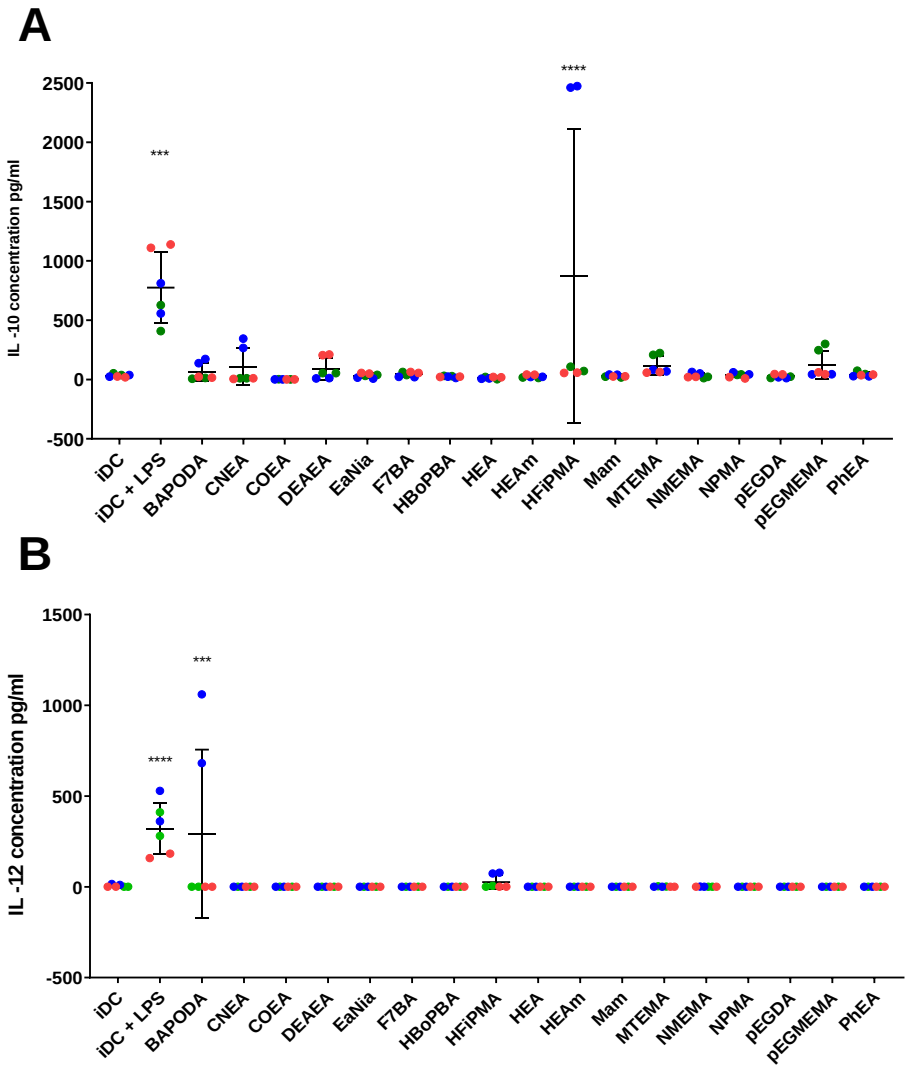


Figure 3-9: Cytokine secretion by DCs after polymer culture

Immature DCs were cultured for 24 hours on polymer coatings. Polymers are investigated for their ability to modulate IL-10 (A) and IL-12 (B) secretion by DCs. Experimental conditions are compared to the TCP iDC control. Data is from 3 independent experiments with 2 technical repeats each and represented as mean ± SD. All data points have been normalised according to the viability these polymers effected from the viability screening. For significance a ONE-way ANOVA with Bonferroni multiple comparisons test was performed and shown as *<0.05; **<0.01; ***<0.001; ****<0.0001. Data points are colour-based on donors.

IL-12p70 and IL-10 secretion levels were significantly decreased when DC where initially conditioned on the polymers, and then stimulated with LPS (Figure 3-10).

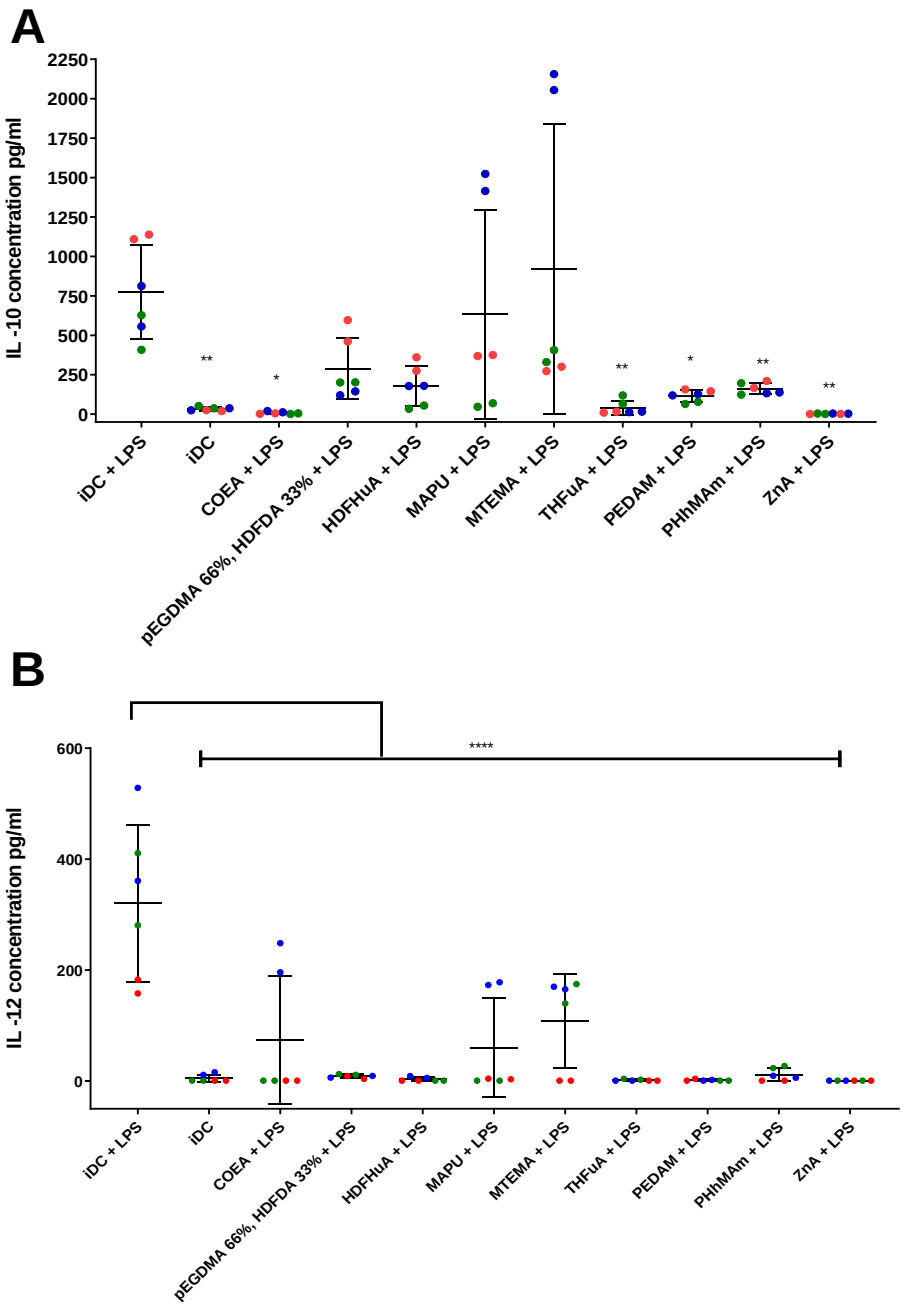


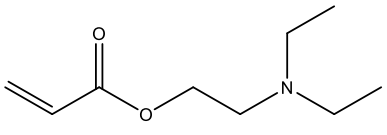
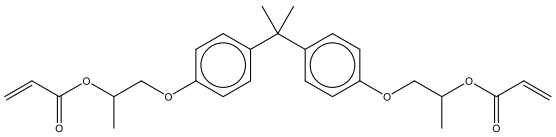
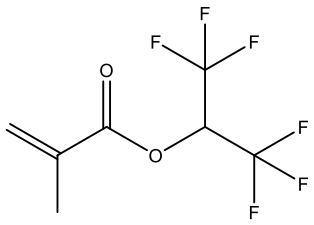
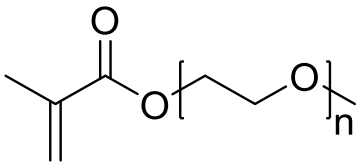
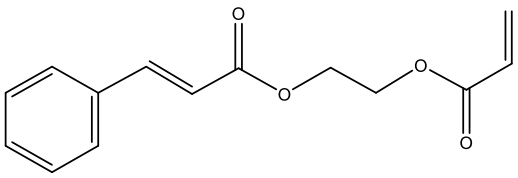
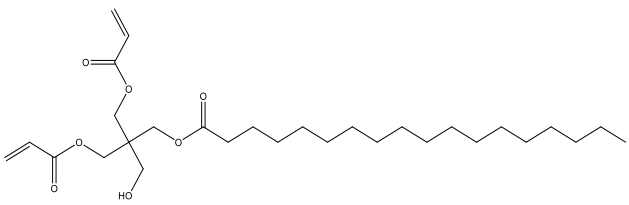
Figure 3-10: Polymers suppress cytokine secretion in presence of stimulus

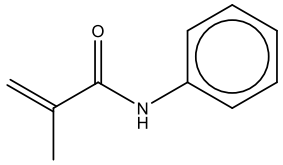
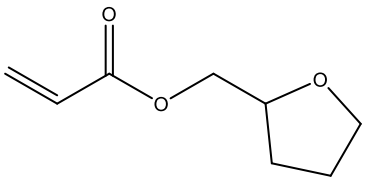
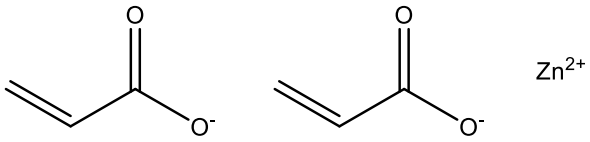
For assessing whether polymer coatings can modulate IL-10 (A) and IL-12 (B) secretion in presence of a stimulus, DCs were conditioned on the different polymers for 6 hours, then stimulated with 100 ng/mL LPS and cultured for a further 18 hours. Data is from 3 independent experiments with 2 technical repeats each and represented as mean ± SD. Experimental conditions are compared to the TCP stimulated DC (iDC + LPS) control. All data points have been normalised according to the viability these polymers effected from the viability screening.

For significance a ONE-way ANOVA with Bonferroni multiple comparisons test was performed and shown as *<0.05; **<0.01; ***<0.001; ****<0.0001Data points are colour-based on donors.

On this basis from the stimulatory polymers BAPODA, DEAEA, HFiPMA, and pEGMEMA were chosen to take forward as these polymers were able to increase the secretion of IL-10 and/or IL-12 above the levels of TCP control. From the regulatory polymers PEDAM, PhMAm, THFuA and ZnA were chosen. COEA is an interesting polymer, as it presented itself in both the stimulatory and regulatory polymer groups and was therefore included in further studies. CNEA was excluded due to its low upregulation of CD83 and MTEMA due to its high biological variation (lower variation than HPA), but for both polymers the medium performance in both surface marker expression and cytokine secretion did mean they were not chosen for further studies. The 9 selected polymers and their chemical structures can be found in Table 5.

Table 5: Polymer structures

Polymer name	Polymer structure
DEAEA	
BAPODA	
HFiPMA	
pEGMEMA	
COEA	
PEDAM	

PhMAm	
THFuA	
ZnA	

3.3.5 **Endocytosis**

One of the characteristic features of iDCs is their high endocytic ability. After maturation, this capacity decreases, allowing DCs to present the antigens they have captured to T cells. To simulate uptake of soluble antigens, the dextran-FITC uptake by DCs after treatment with selected polymers was investigated. Three of the stimulatory polymers showed a decrease of uptake ability compared to iDC.

Interestingly, when investigating the endocytic ability for the DC regulatory polymers that suggested a ‘more immature’ profile, three of the five polymers actually decreased endocytic ability – taking up only the bare minimum of dextran. The only polymer that maintained a high endocytic ability, even in presence of a strong LPS stimulation, was ZnA - whose endocytic ability level

are around the ones from iDCs. This result clearly underlines the previously presented ‘more immature’ profile of ZnA treated DCs.

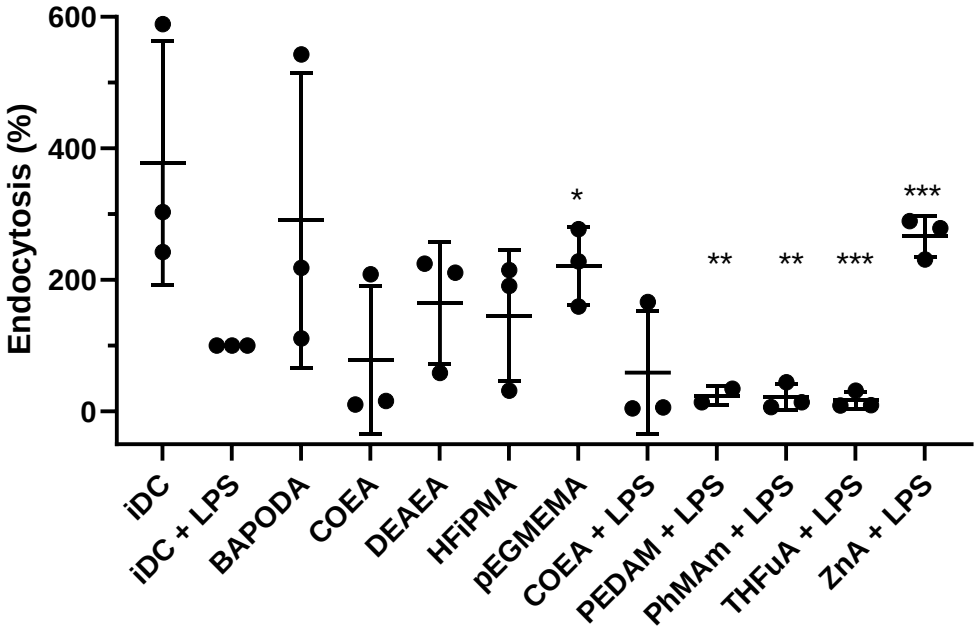


Figure 3-11: DCs modulate uptake ability after polymer culture

iDCs were cultured on polymers for 24hrs, followed by feeding with FITC-Dextran to assess the uptake of a model soluble antigen. Data is from 3 independent experiments and % of uptake is presented as mean ± SD. For donor-to-donor comparison, iDC + LPS was set as 100% per donor and samples are compared to iDC + LPS. ONE-way ANOVA with Bonferroni multiple comparisons test was performed to assess significance (*<0.05; **<0.01; ***<0.001; ****<0.0001).

3.4 Discussion

DCs are crucial immune cells linking the innate and adaptive immunity, playing an important role in the orchestration of the adaptive immune response. Notably, DC phenotype is a powerful indicator of their downstream effector functions. The discovery of the ability to modulate these functions has opened up a new direction of immune targeted therapies. In the past ten years, established libraries of combinatorial polymers in high throughput-screening formats have created opportunities to identify simple polymers with bio-instructive interactions with great success [148]–[153]. A polymer library previously used to identify materials with the ability to instruct stem cell differentiation or stop bacterial biofilm formation [148], [149], [151] was used as the material source here. Materials, that have been found to be modulatory of the innate arm of the immune system – specifically cell types such as macrophages - have been reported intensively, however modulations of cells that translate into the adaptive arm have been less thoroughly investigated [116]. Biomaterials have in the past been found to modulate host immune responses, as well as the phenotypic state of DCs. Various polymers (alginate, agarose, chitosan, HA and PLGA) have been shown to exert differential effects on DC activation levels [89], [123], [167]. While some routinely used biomaterials such as chitosan, agarose, titanium have been shown to affect DC phenotype activation levels [129], [167], to my knowledge there has been no attempt yet to undertake an unbiased screen of wider chemical space to identify new materials that are able to instruct DCs activation towards distinct stimulatory or regulatory functional phenotypes.

None of the polymers from the source library used here, have previously been investigated for their potential on modulating DC phenotype and function. This study set out with the aim of assessing a library of polymers on their ability to modulate DC phenotype and function.

Cell viability on synthetic surfaces is critical for downstream functions. Hence, in the first instance I investigated DC viability on different polymers. Out of 222 polymers investigated in this study, 110 supported DC viability in levels comparable with TCP whereas cells cultured on 83 polymers showed lower viability and 29 polymers supported DC viability greater than TCP. The low viability on these polymers could be due to trapped solvent in the polymers which is detrimental to cell survival, or due to some non-polymerised monomer residue inside the well or even some non-reacted photo initiator (both are known to be toxic in non-reacted form) [168], [169]. Earlier studies have shown that residual monomers are toxic to PBMCs, as well to fibroblasts in a dose-dependent manner, which can be seen in agreement to data presented here. Extra washing steps were expected to remove all residual monomer and photo initiator, but the low cell viability for some of the polymers suggests otherwise. There might still be significant doses of harmful residues within the system that have detrimental effects on DC viability. Additional studies will be needed to ‘clean’ out fabrication residues and remove the introduction of methodological error and to find new fabrication approaches that prevent a build-up of possible harmful residues. For the polymers taken forward (and specifically for the hit polymer characterised in the next chapter) analysis of the last media washing step revealed low concentrations of monomer to be present (femtogram range).

As even low amounts of monomer can have a detrimental or even modulatory effect on cells, raw monomer in the range of the concentration found in cell culture supernatant were added to DC cultures with no significant subsequent cytotoxicity or phenotype modulation observed (Appendix 2 and 3).

The greater viability than TCP is interesting and could be due to protein adsorption onto these polymers that support cell viability. The reason why these polymers supported higher viability was not further investigated in this study but could prove to be relevant for *ex vivo* DC cultures as an alternative culture surface (such as Polyolefin bags) to TCP. Previously, gas permeable hydrophobic culture bags have been found to be superior for viability, yield and function of DCs cultured in TCP flasks or well plates. Comparing various well plate formats and plate materials, a study concluded that DCs cultured and assayed under conditions that minimise cell adherence are functionally better, as well as support more viability [170].

For the second screening step, phenotype modulation, my results demonstrate that upon culture of DCs on synthetic polymers, DCs react differently to polymer chemistry. Of the polymers that were seen as supporting DC survival, a group was identified as inducer of a mature phenotype (in terms of key surface markers CD83 and CD86) – stimulatory polymers - and another group suppressed the development of a mature phenotype even when stimulated with 100 ng/mL LPS – regulatory polymers. In several earlier studies, polymers were investigated for their ability to modulate DC phenotype. Although none of the polymers identified here were used in previous studies, a number of polymethacrylates – pHEMA and pIBTMA were shown to induce the least and

most mature DC phenotype, respectively [128] – supporting the data here about the ability of synthetic polymers to modulate DCs.

The upregulation of CD83 and CD86 by several of the polymers analysed here, indicate first assumptions of potential improved DC-T cell interactions. Conversely, specific polymers that were able to suppress the development of a mature phenotype (even in presence of the very potent stimulant LPS), should therefore be less capable of effecting a functional T cell response and more probable to induce tolerance/anergy in T cells or regulatory T cells. For a proper T cell effector response, there have to be 3 signals exchanged between DC and T cells:

1. Antigen needs to be presented via MHC I or II on DCs.

2. Co- stimulation via CD83, CD86 and others.

3. Polarizing cytokines need to be secreted by DCs.

Contrary to expectations, the next screening step, cytokine secretion, did not produce the results that were anticipated: The majority of stimulatory polymers investigated did not show any effect on the production of IL-10 and IL-12p70, and the ones, that showed some modulation, did so in a statistically non-significant manner. Only HFiPMA showed a significant upregulation of IL-10 in the cell culture media, this however has to be attributed to the biological donor variation between low and high responders.

DCs can skew the differentiation of naïve T cells towards Th1, Th2, Th17 and also regulatory T cells. Therefore, the cytokine balance is specifically important

to assume the direction of the evoked immune response. To ensure that potentially different number of viable cells in each culture condition did not contribute to different levels of cytokines, cytokine secretion levels were normalised according to the viability results. Most stimulatory polymers induced slightly elevated secretion levels of IL-10 and IL-12p70, although two did so in a statistically significant manner. Other studies looking at pMAs (polymer methacrylates) showed IL-10 to also only be slightly modulated to above TCP levels, which is the same as observed here – indicating that surface polymer coatings might not be able to induce heavy cytokine secretion [128]. These findings agree with data presented in this chapter. As only two cytokines were investigated here, additional investigations, that look at additional cytokines (e.g. IL-6, IL-1β or TNFα) will be needed to determine the polymer-cultured DCs cytokine secretion pattern more in detail [54]. IL-6 is connected to B cell differentiation into plasma cells, T cell proliferation, differentiation of CTLs and IL-2 production [54]. Specifically IL-6 has been described to participate in the differentiation of Th2 and Th17 cells, which displays pro-inflammatory functions [54].

DCs ability to uptake antigens determines their ability to process and present antigens to induce adaptive immune responses. Therefore, I investigated the ability of polymer cultured DCs to uptake soluble antigens as a critical factor for deciding which polymers to take forward. The results of the uptake study agree with the phenotype data obtained earlier, which suggest a ‘more mature’ profile exhibited by stimulatory polymer-treated iDCs as uptake is decreased in comparison to TCP cultured iDCs. Similar DC phenotype and endocytosis

levels were previously observed on laminin and fibronectin coatings, and agree to my observations here [171]. Stimulatory polymer cultured DCs are however still able to uptake antigens, which is useful in therapeutic settings. Regulatory polymers were mostly shown to completely suppress antigen uptake, although ZnA cultured DCs were still able to uptake antigens at a level similar to TCP cultured iDCs. This supports earlier results describing ZnA as a regulatory polymer for inducing tolerogenic DCs. ZnA ability to additionally suppress IL-12 secretion proves interesting when looking for a potential therapeutic for Crohn's disease. Abnormal high IL-12 levels have been described in animal models of autoimmune diseases, in related studies it was found that IL-12 blocking leads to a stable remission of patients of active Crohn's disease [172]. As the here described regulatory polymers were able to suppress secretion of IL-12, they could be used as an alternative for IL-12 blocking or similar applications.

Here, I have screened a library of polymers for their immune modulatory properties on DCs and show that the initial phenotype-based screen has translated into functional DC modulation. Future studies should focus on elucidating the connection between material properties and biological effect. Understanding how biomaterials affect the DC response will facilitate the selection and design of biomaterials that direct a desired immune response for tissue engineering or vaccine delivery application. Following results from this chapter it was decided to choose DEAEA and HFiPMA as candidates for functional studies of stimulatory polymers and ZnA as a candidate for regulatory functional studies.

Chapter 4: Surface characterisation of selected hit polymers and its functional effect on DCs

Chapter 4 Surface characterisation of selected hit polymers and their functional effect on DCs

4.1 Introduction

In chapter 3 the screening of a polymer library including 222 Acrylates and methacrylates was used to select 2 polymers as stimulatory polymers – able to active DC phenotype, modulate cytokine secretion and endocytic uptake, while supporting DC viability. Another polymer was chosen to investigate further as regulatory polymers – rendering DCs less responsive to LPS stimulation via TLR-4. These selections were made based on certain criteria, that indicated that these 3 polymers are good candidates for further analysis.

Previously, biomaterial surfaces have been found to modulate cell behaviour through either surface stiffness (targeting cellular mechano-sensing) or protein adsorption of serum proteins. Various surface characterisation techniques have been developed to study biomaterial surface characteristics, such as Young's modulus for material stiffness and XPS to measure thickness of bio-adsorbate layer. Increased biomaterial stiffness has previously been found to increase pro-inflammatory responses activation [173], [174]. XPS is a surface sensitive technique used for quantitative measurement of elemental composition of substrates. For biomaterial surfaces, XPS can help to estimate the thickness of adsorbed proteins on surfaces by measuring elemental nitrogen present in adsorbed layers.

The polymer candidates investigated in this chapter could potentially find application in clinical settings. Therefore, further characterisations are necessary to evaluate the downstream functional effects of polymer modulated DCs. Activated DCs form an immunological synapse with T cells, presenting antigen and priming T cells. Primed T cells get activated and proliferate to act upon the antigen. Induction of T cell responses is dependent on costimulatory marker molecules on DCs, as well as the secretion of polarising cytokines by DCs.

Stimulatory polymers that prove their ability in inducing increased antigen-specific T cell responses can find utilisation in vaccination adjuvants, drug delivery systems or immune stimulants in cancer therapy. The ability of DCs to induce CTLs is essential to fight cancer and determines their utility in cancer immunotherapies. Regulatory polymers could find application in autoimmune disease if the induced immune response warrants this.

Microarray technique provides an easy way to screen many thousands of genes or proteins in one assay and is widely used to detect expression change patterns under various physiological and pathological conditions. Earlier studies have used microarrays to investigate the expression profiles of DCs, tolerogenic DCs and DC-hybrids [175], [176]. Various statistical and bioinformatics tools can be applied to determine key molecules, signalling pathways and biological processes of cells. Recent progress in bioinformatics analysis allows to better interpret the gene expression profiles as revealed by microarray studies. One advanced bioinformatics tool is the Ingenuity pathway analysis (IPA) software program, which can analyse the gene expression

patterns using a build-in scientific literature-based database (according to IPA Ingenuity Web site).

In the previous chapter, the initial screening of an acrylate and methacrylate and acrylamide library for DC modulation revealed 3 homopolymers that supported cell viability and modulated surface marker expression, cytokine secretion as well as endocytosis ability. This chapter discusses some basic material characterisation and the description of the functional modulations by DCs and forms the basis of deciding whether polymers are suited for clinical applications. Additionally, the best two performing stimulatory polymers are investigated for their ability to induce tumour-killing T cells, as well as their gene expression levels in a gene microarray.

4.2 Methods

4.2.1 Monocyte isolation

Monocytes were isolated from buffy coat as described in general methods section 2.2 and differentiated into DCs as described in section 2.2.1.

4.2.2 Monomer to polymer polymerisation by UV

24- well polypropylene plates were prepared as described in section 3.2.2. The volume used for the 24 – well plates was 100 µl, everything else remained the same.

4.2.3 Polymer plate washes for cell culture

Polymer plates were prepared as described in section 3.2.3.

4.2.4 Cell culture

Monocytes were isolated from buffy coats as described in 2.2 and differentiated into DCs as described in 2.2.1.

4.2.5 XPS analysis

Coverslips were first silanized and then used for polymer coating purposes. Per coverslip 20 µL of monomer-photo initiator solution was used, this was then polymerized via UV for 60mins. For XPS analysis, coverslips were washed as previously described. Serum-positive samples were produced by incubating the coverslips overnight with complete RPMI cell culture media. Serum-negative samples were left as is. All samples were washed with MilliQ

water 10 times for 10 minutes to remove unbound and loosely bound proteins and dried prior to sample acquisition. Data was analysed with the CasaXPS software.

XPS analysis was carried out using the Kratos AXIS ULTRA with a mono-chromated aluminium Kα X-ray source (1486.6 eV) as previously described [177]. Spectra were acquired with the Kratos VISION II software. A wide scan (binding energy range – 1400 eV to -5 eV, with pass energy 80 eV and sweep time of 20 minutes) was used to identify elements present on the surface of polymer samples. For each polymer condition, two separate areas (300 x 700 μm) were analysed. CasaXPS software (Version 2.3.19 PR1.0) was used to analyse spectra generated from wide scans. Elemental compositions (in atomic percentage) were determined by quantifying elemental peak areas on survey spectra, after subtraction of tougaard background. Proportions of carbon (C), oxygen (O) and nitrogen (N) on untreated and FBS/RPMI treated polymers were calculated by averaging total atomic percentages obtained for each element from analysed areas.

Following quantification of nitrogen atomic percentage on untreated and FBS/RPMI treated polymer samples, values obtained were applied in estimating the thickness of protein over-layers using the equation:

$$d_{N(1s)} = -L_{N(1s)}\, cos\theta\, ln\left(1 - \frac{[N] - [N]_0}{[N]_\infty - [N]_0}\right)$$

Where L = electron attenuation length (3.02nm), cos (θ) =1, [N] = measured nitrogen fraction on FBS/RPMI treated polymer substrate, $[N]_\infty$ = atomic

fraction of nitrogen in the pure protein (15%) and $[N]_0$ = nitrogen fraction on untreated polymer substrate (0%).

4.2.6 **ToF-SIMS**

ToF-SIMS is a surface-sensitive analytical method that uses a pulsed ion beam (Cs or microfocused Ga) to remove molecules from the very outmost surface of the sample. Secondary particles (secondary ions) generated farther from the impact site tend to be molecular compounds, typically fragments of much larger organic macromolecules. These particles are then accelerated into a 'flight tube' and their mass is determined by measuring the exact time at which they reach the detector (i.e. time-of-flight). This is measured in nanoseconds, giving the possibility to produce a mass resolution as small as 0.00X atomic mass units. ToF-SIMS can be used for surface spectroscopy, surface imaging and depth profiling. ToF-SIMS provides information about the molecular mass and structure of the top 2nm of a surface material [151], [163]. ToF-SIMS is very sensitive and is able to distinguish between very similar chemical species. Due to its sensitivity this technique can also be applied to identify the distribution of amino acids in protein adsorption studies [161].

4.2.7 **AFM**

The stiffness measurements using the Atomic Force Microscope (AFM) was measured by collaborator Dr Francesco Pappalardo at the School of Pharmacy. The MFP-3D Standalone AFM (Oxford Instruments, Asylum Research Inc., CA) was used to obtain force displacement curves of the polymer samples in water for Young's modulus calculation. Following data collection, the Derjaguin-Muller-Toporov mathematical model was used to fit the slope of the retracting curve using least squares regression line for calculation of Young's modulus.

4.2.8 **DC culture on polymer coated surfaces**

After preparing the polymer plates for cell culture as previously described, immature DC were harvested, washed once, re-suspended in fresh complete media and transferred to the coated wells. For investigating the effect of the polymers on iDC, cells were cultured on polymers for 24 hours. For investigation of polymer effect on DC maturation, DCs were conditioned for 6 hours on the polymers and then stimulated with 0.1 µg/mL lipopolysaccharide (LPS from *E. coli*, Sigma-Aldrich) and cultured for a further 18 hours. Cells were then used for the assays described below or analysed for expression of surface markers.

4.2.9 **Flow cytometry staining**

Polymer-treated and control DC were harvested, washed twice with PBS (supplemented with 0.5% BSA and 0.1% NaN_3, later mentioned as PBA) and then stained for CD83 (FITC, clone REA714, IgG1, Miltenyi Biotec) and CD86

(PE, clone REA968, IgG1, Miltenyi Biotec) for 20 minutes at 4ºC. The cells were then washed with PBA and fixed in 1% PFA in PBS. Cells were usually analysed within 24 hours.

4.2.10 **Cytokine analysis**

Culture supernatants from 3 independent experiments were collected after 24 hours culture. IL-6, TNF-α and IFN-γ were measured by DuoSet ELISA kit (R&D Systems) as per the manufacturer's instructions. Modifications of the protocol allowed analysis of cytokines in a 384-well plate format, giving the opportunity to read duplicates from each donor.

4.2.11 **Sample preparation for Microarrays**

DCs were cultured on the polymers as described in section 4.2.8. Total RNA was isolated from cells using RNeasy plus kit (Qiagen). For microarray experiments, total RNA was first reverse transcribed into single-stranded cDNA with T7 promoter sequence at the 5'end and then converted to double-stranded cDNA, which acts as a template for in vitro transcription. In a next step, antisense RNA is synthesised and amplified by in vitro transcription of the second-stranded cDNA template using T7 RNA polymerase. Enzymes, salts and inorganic phosphates as well as unincorporated nucleotides were removed to prepare the cRNA for 2nd cycle single-stranded cDNA synthesis. Single-stranded cDNA was then fragmented, labelled, and hybridized onto the Clariom S arrays.

4.2.12 **Microarray data analysis**

Whole-genome transcriptome analysis was conducted by hybridizing 4 biological samples of total RNA per treatment to the Clariom S arrays (#902926, Affymetrix, High Wycombe, Bucks, UK). All steps of sense cDNA synthesis, fragmentation and hybridization were performed according to the manufacturer's protocol (GeneChip® 3000 System, Affymetrix).

4.2.13 **Bioinformatics analysis**

Gene expression profile data was generated as CEL files and subjected to analysis by the Partek Genomics Suite 6.6 software. Quality Control (QC) metrics were checked by examining surface defects, hybridization, labelling, and a ratio of the 3′ probe set to the 5′ probe set (3′/5′ ratio) to provide the quality of the microarray data. The values were log2 transformed and quantile normalisation using the Robust Multi-array Average (RMA). The list of genes of interest comprised genes upregulated or downregulated by at least 1.5-fold with adjusted p-value <0.05.

Briefly, outcomes from microarray analysis were first uploaded into Qiagen's IPA system for core analysis and then overlaid with the global molecular network in the Ingenuity pathway knowledge base (IPKB). IPA was performed to identify canonical pathways that are most significant to microarray outcomes and to categorize differentially expressed genes in specific functions.

4.2.14 **T cell co-cultures**

Autologous CD3+ T cells were separated by negative selection from the whole T cell fraction of PBMCs using a CD3+ T cell kit and naïve/memory T cells were further separated by using CD45RO beads (Miltenyi Biotec) [178]. They were then co-cultured with Polymer-conditioned DCs in a 10:1 ratio and kept for 8 days in culture. Half of the media was exchanged on day 3 with fresh media containing IL-2. T cells stimulated with anti-CD3 and anti-CD28 on day 7 were used as positive control. BrdU colorimetric assay (Roche) was used to determine the proliferation rate of T cell, and the supernatants were analysed in ELISAs to determine IFN-γ production/T cell activation.

4.2.15 **IDO activity**

IDO activity was determined as described before [179]. Briefly, DCs were seeded in a 24-well plate with complete RPMI media supplemented with 100 mM L-tryptophan (Sigma- Aldrich). A colorimetric assay for IDO activity was determined after 24 hrs of culture by measuring the levels of L-kynurenine (KYN) produced in culture supernatants. The concentration of L-KYN was then calculated from a standard curve of defined concentrations from 0 to 200 mM.

4.2.16 **Tumour killing assay**

For the tumour killing assays a adapted version of a previously described method was performed [180]. Autologous naïve CD8 T cells and monocytes were isolated from commercially sourced haplo-matched PBMC vials. For this, DCs were cultured on flat polymer coatings for 24 hours, followed by addition of MCF7 (a breast cancer cell line) cells that had been rendered non-

proliferative by mitomycin c (MMC) for another 24 hours. These DCs were then co-cultured with autologous naïve CD8 T lymphocytes for 8 days in a 1:10 ratios (DC: T cells). Every 3 days, 100 µl of cell culture media was removed and substituted with fresh media containing 200 IU/mL IL-2. Proliferated tumour specific CTLs were then seeded on MCF7 monolayers for 6 hours in differing ratios (1:5 to 1:20). Cells were then stained with LIVE/DEAD Viability/Cytotoxicity Kit (Thermo Fisher, calcein-AM and ethidium homodimer-1) and imaged to calculate % of specific lysis.

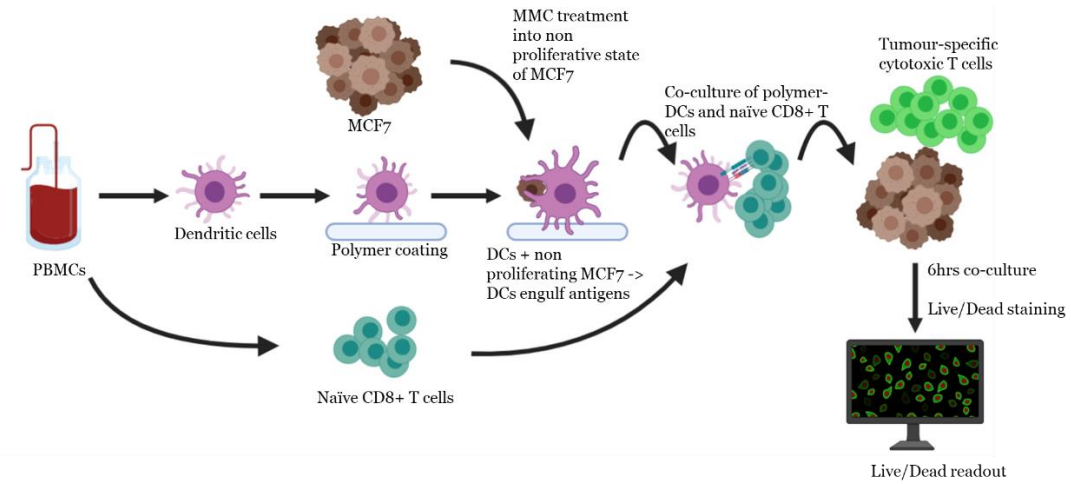


Figure 4-1: Schematic overview of tumour killing experiment

DCs were first generated from monocytes, cultured on the polymer coatings and fed MMC-treated MCF7 cells. DCs were then co-cultured with naïve CD8+ T cells and proliferated CTLs were added to MCF7 monolayers to determine CTL ability to kill MCF7 cells in an imaging-based assay. Figure generated in Biorender.

4.2.17 **Statistical analysis**

All graphs were prepared, and all statistical analysis was carried out using Prism 8 (GraphPad software, Inc., USA). Student T-test or one-way-ANOVA

and multiple comparison post-tests were performed and are stated below each graph.

A p value $p<0.05$ was considered statistically significant and portrayed as *<0.05; **<0.01; ***<0.001; ****<0.0001.

4.3 Results

4.3.1 Material characterisation

In order to find out more about the polymeric coatings and their adsorption of proteins from media, several surface analysis techniques (XPS and AFM) were applied.

4.3.1.1 Bio-adsorbate layer thickness on polymers

XPS is a surface chemical analysis technique that can be used to analyse the surface chemistry of a material by virtue of its shallow (ca. 10 nm analysis depth). It was used here to primarily determine the composition of the surface chemistry of the polymer coatings and from this to calculate the protein layer adsorption. To investigate the influence of polymers on the adsorption of proteins, polymers were treated with serum containing culture medium and gently rinsed 10 times with distilled water in order to remove any loosely bound proteins [181].

Following removal from the well plate, the samples were washed ten times in MilliQ water to remove any loosely bound proteins and excess buffer salts. Proteins left on polymer surfaces were considered to be strongly bound. Afterwards, untreated polymers (used as controls) and FBS/RPMI treated polymers were examined using XPS and the atomic fraction of nitrogen present on untreated and FBS treated coatings measured. The measured nitrogen fraction was indicative of the adsorbed protein layer. The compositions of the different polymer coatings can be found in Table 6. All

polymer surfaces treated with FBS exhibited varying levels of adsorbed proteins as was shown by the measured nitrogen fractions.

HFiPMA showed a 23% elemental concentration of fluorine, which was attributed to the fluor in the polymer structure. Zinc was found in low percentages in ZnA, which also corresponds to its chemical structure. Silica (and therefore the glass coverslip) was measured in DEAEA coatings, indicating either gaps in the coating or a very thin coating as the XPS probes to a depth of 10 nm. Subsequent TOF-SIMS measurements revealed no holes in the coating (with a depth sensitivity of circa 2 nm), hence explaining the measurements as DEAEA coating to be deeper than 2 nm but less than 10 nm (Figure 4-2). Additionally, some areas of less ion intensity were observed in the total ion overview images; however, no Si or SiO_2 were measured within these areas.

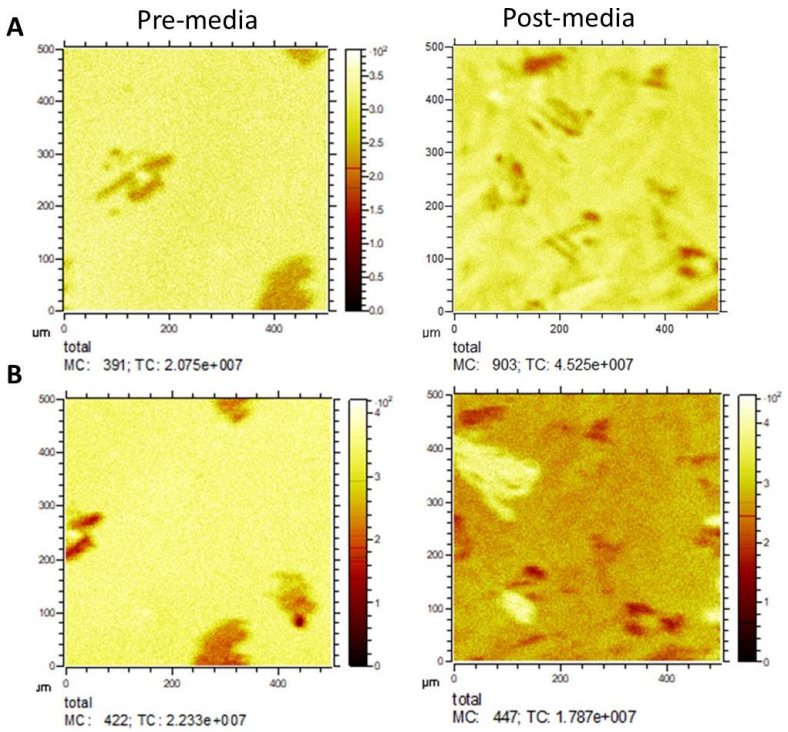


Figure 4-2: DEAEA TOF-SIMS overview

Coverslips were coated with DEAEA, incubated with complete media overnight and measured by TOF-SIMS before and after media treatment. (A) is an overview of total ions of the negative spectrum and (B) is a total ion overview of the positive spectrum. Left panels are pre-media treatment, right panels are after media treatment.

Table 6: Atomic percentages of polymers films after media incubation (by XPS), acquired by Craig Stoppiello

Elemental concentration (atomic %)	DEAEA		HFiPMA		ZnA	
	pre	post	pre	post	pre	post
C 1s	36.55	54.65	33.59	57.81	56.43	63.63
F 1s	2.37	1.435	15.95	22.87	0.29	0.05

K 2s	0.995	0.295	0.43	0	0.25	0
N 1s	2.25	2.49	1.09	4.52	0.93	12.1
Na KLL	1.11	0.84	0.65	0.04	9.46	3.33
O 1s	40.85	29.32	34.5	14.18	26.54	19.36
Si 2p	15.14	10.64	11.2	0.535	0.01	0.09
Ti 2p	0.39	0.21	0.34	0	0	0
Zn 2p	0.16	0.13	0.08	0.04	6.7	1.37

The nitrogen atomic percentage was highest for ZnA and lowest for DEAEA. The measured nitrogen fractions on the polymers were used to calculate the thickness of adsorbed proteins after FBS treatment (Figure 4-3). The thickest protein over-layer on the polymers was observed on ZnA with 4.53nm, which is significantly higher than the protein layers on DEAEA and HFiPMA coatings. The DEAEA coating had a roughly 2.006nm nm thick protein layer, while HFiPMA coating produced thickness of 0.892nm. These results suggest that stimulatory polymers (DEAEA and HFiPMA) impeded adsorption of serum proteins while the regulatory polymer ZnA promot protein adsorption.

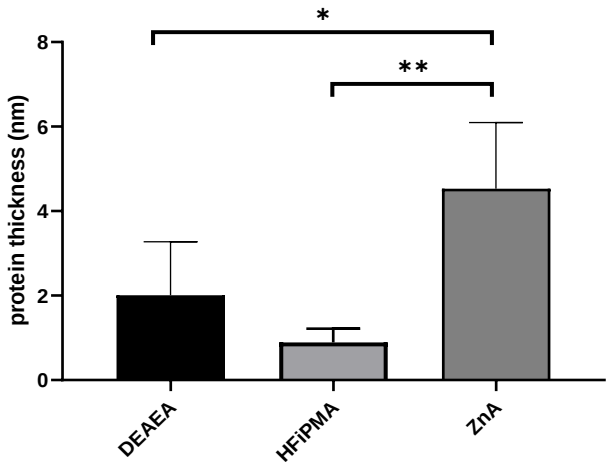


Figure 4-3: Bio-adsorbate layers on polymer coatings

The thickness of serum proteins adsorbed to polymer coatings were calculated by an equation and taking the amount of elemental nitrogen fractions (analysed by XPS) into account. Data are from 2 separate coverslips with 2-3 areas measured per chip. For significance, a ONE-way ANOVA was performed with Tukey multiple comparisons test. * p< 0.05, ** p<0.01, *** p < 0.001 and **** p < 0.0001.

4.3.1.2 Atomic force microscopy (AFM)

AFM is well suited to quantify stiffness of materials. In order to measure the modulus of polymer coatings the three polymer coatings were analysed by AFM. Figure 4-4 shows the Force-Displacement curve of the three polymers investigated in their dry and wet state. The curves imply how far the AFM probe indented into the sample, conversely giving a measure of their stiffness. The greater the distance the probe travelled, the softer the sample. The regulatory polymer ZnA (wet state) had a significantly higher indention of the probe, compared to the other polymers in wet and dry conditions and ZnA in dry condition.

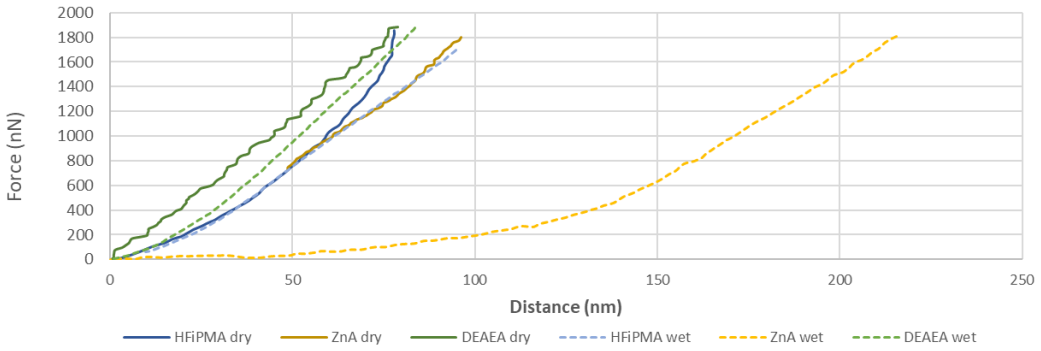


Figure 4-4 AFM Force-Displacement curve of representative force curves extracted from polymer films, acquired by Francesco Pappalardo.

The force-displacement curve measurements translate directly into the Young's modulus of stiffness and show significant differences between the stimulatory polymers and the regulatory polymer (Figure 4-5). While all coatings were generally quite stiff (GPa range), DEAEA and HFiPMA coatings had a modulus of circa 2 GPa and are therefore stiffer than the ZnA coating with a modulus of around 0.2 GPa. Physiological tissue stiffness generally ranges from ~0.2 kPA in the lungs to ~15 kPa in skeletal muscle or cartilage, which is significantly softer than the polymers measured here [182], [183].

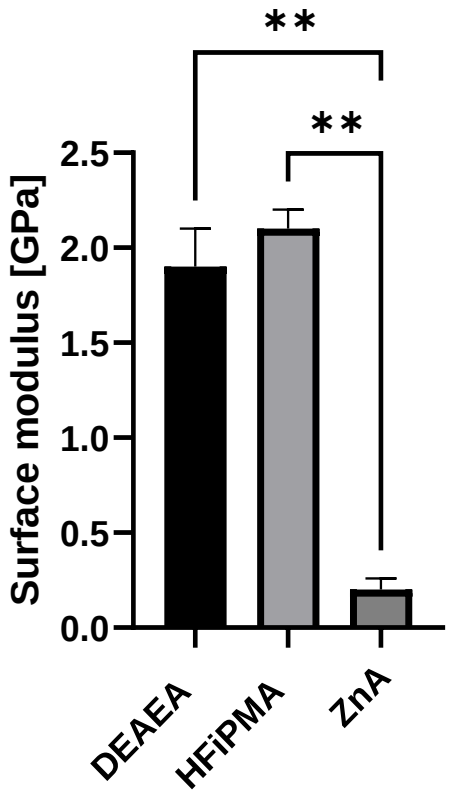


Figure 4-5 Young's modulus of wet polymer films

Stimulatory polymers are coloured green, while the regulatory polymer is coloured orange. Each sample was measured with 4 Force Maps of 2µm consisting of 65 Force points. n=2. One-way ANOVA with Tukey multiple comparisons test was applied. * p< 0.05, ** p<0.01, *** p < 0.001 and **** p < 0.0001.

4.3.2 Cytokine secretion on scaled up polymer coatings

To determine the influence of polymer coatings on cytokine production by DCs, iDCs were cultured for 24 hours on the polymer coatings and the levels of pro-inflammatory cytokines (TNFα, IL-6) and anti-inflammatory cytokine IL-10 secreted into the cell culture media over the course of incubation was quantified by ELISA. The three hit materials chosen in the previous chapter were used for this study. These included two stimulatory polymers (DEAEA

and HFiPMA) and one regulatory polymer (ZnA). The stimulatory polymers induced higher secretion levels of pro-inflammatory cytokines (TNFα and IL-6), as well as anti-inflammatory cytokine IL-10 when compared to the TCP iDC control.

Stimulatory polymer cultured DCs (DEAEA and HFiPMA) showed increased secretion of TNFα compared to TCP. While in the TCP condition TNFα levels were not detectable, DEAEA conditions increased to 200 pg/mL and HFiPMA increased up to 2140 pg/mL which is even higher than TCP + LPS (the positive stimulation control, 1965 pg/mL) and is highly significant ($p<0.0001$). ZnA coatings did not induce any detectable TNFα secretion levels, in both the base condition and the LPS stimulation condition which is significantly lower TCP + LPS ($p<0.0001$).

In the control condition TCP the pro-inflammatory cytokine IL-6 was secreted at 200 pg/mL with the stimulatory polymer coatings showing varying effects: DEAEA conditions had IL-6 of 60 pg/mL and HFiPMA 340 pg/mL. HFiPMA IL-6 levels are increased compared to TCP condition, albeit not significantly and, being lower than TCP + LPS (420 pg/mL). ZnA coatings induced IL-6 secretion of 120 pg/mL, with the ZnA + LPS condition showing significantly reduced secretion at 10 pg/mL ($p<0.0001$).

The anti-inflammatory cytokine IL-10 was close to not detectable at TCP base condition, with stimulatory coatings DEAEA and HFiPMA showing increased levels at 1850 and 1350 pg/mL respectively. Both the stimulatory polymers showed a combinatory effect with LPS with DEAEA + LPS (8000 pg/mL) and HFiPMA + LPS (7000 pg/mL). The regulatory coating ZnA showed close to no

detectable levels of IL-10 secretion in both the base condition and the LPS stimulation condition (comparable to TCP condition).

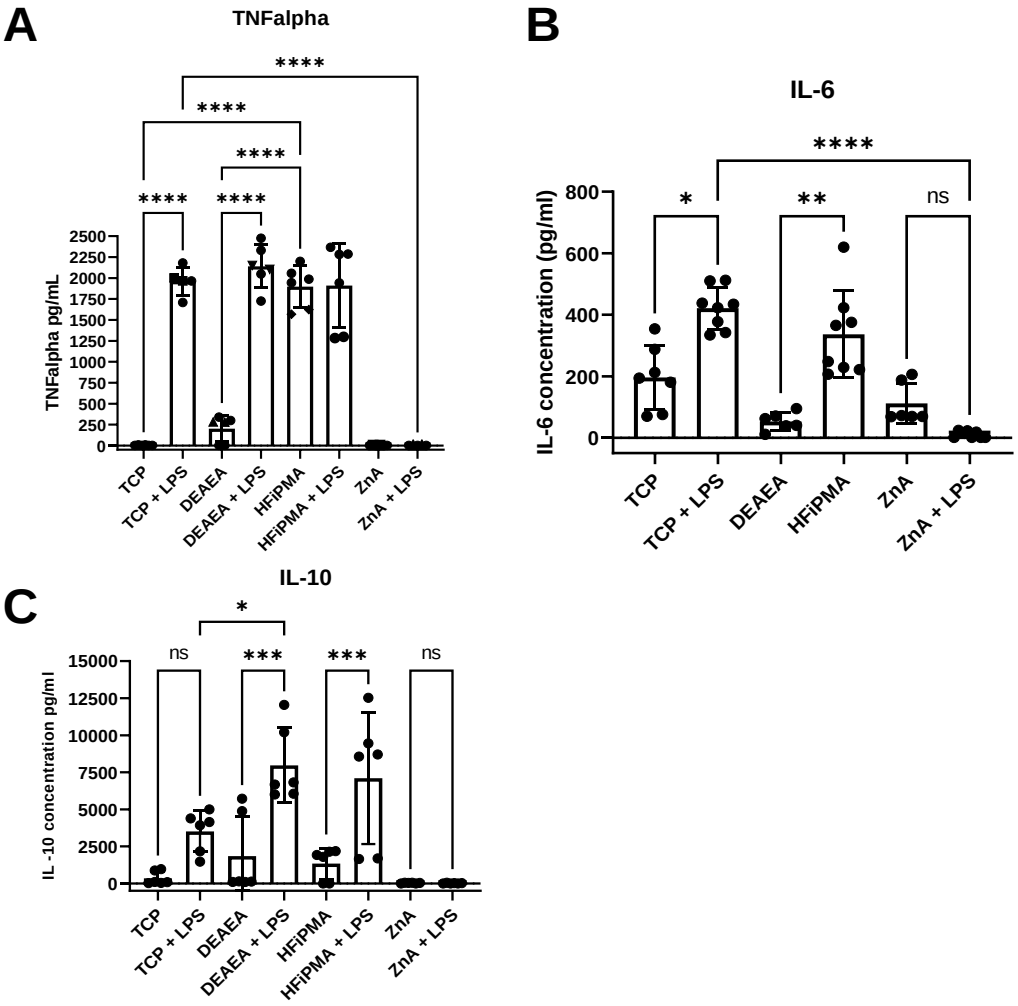


Figure 4-6: Polymer treatment modulates DCs cytokine secretion

DCs were cultured on polymer coatings for 24 hours. Levels of pro-inflammatory (TNF-α, IL-6) and anti-inflammatory (IL-10) cytokines in culture supernatants were determined by ELISA. (A) TNF-α, (B) IL-6 and (C) IL-10. Data is from 3 independent experiments with 2 technical repeats each. TCP – tissue culture polystyrene, and data is presented as mean + SD. Statistical analysis was performed using one-way ANOVA with Dunnett's post hoc multiple comparison tests. * $p < 0.05$, ** $p<0.01$, *** $p < 0.001$ and **** $p < 0.0001$.

4.3.3 Surface marker expression on scaled up polymer coatings

To determine the influence of polymers on the expression levels of surface markers of DCs, DCs were cultured for 24 hours on polymer coatings. Afterwards DCs were harvested, stained for surface markers and samples acquired on flow cytometry. The investigated surface markers were chosen due to their role in DC activation and antigen processing/presentation.

The activation marker CD80 is shown to be upregulated after DC culture on stimulatory polymers, although not significantly when compared to TCP control. DC culture on regulatory polymer ZnA maintained CD80 expression at TCP levels. HLA-ABC, a part of the MHC-I complex showed general high variation between blood donors. Stimulatory polymers DEAEA and HFiPMA maintained HLA-ABC levels similar to TCP, while regulatory polymer ZnA slightly decreased HLA-ABC levels compared to TCP. Adding LPS stimulation drastically increased the HLA-ABC levels in the DEAEA + LPS condition above TCP + LPS levels, while HFiPMA and ZnA + LPS both produced lower HLA-ABC levels than the TCP + LPS control.

DEC-205 expression was also widely irregular between blood donors. Stimulatory polymer DEAEA increased DEC-205 expression level, while HFiPMA maintained similar levels to TCP control and ZnA showed a decrease in DEC-205 expression. Stimulatory polymers + LPS had a combinatory effect in the DEAEA condition, increasing DEC-205 levels to 70% (above TCP + LPS), while HFiPMA + LPS maintained same levels than without LPS. ZnA + LPS DEC-205 expression was significantly downregulated to nearly 0% positive cells.

ICAM (CD54) an intracellular adhesion glycoprotein had a tight variation between blood donors. DEAEA coatings upregulated ICAM expression 22% compared to TCP, HFiPMA induced upregulation of 10% with a higher variation between blood donors. ZnA coatings significantly downregulated ICAM expression on DC to 13% positive cells. Stimulatory polymer coatings did not show any effect on conditions that had been stimulated with LPS. ZnA coatings did suppress ICAM expression down to 5% positive cells.

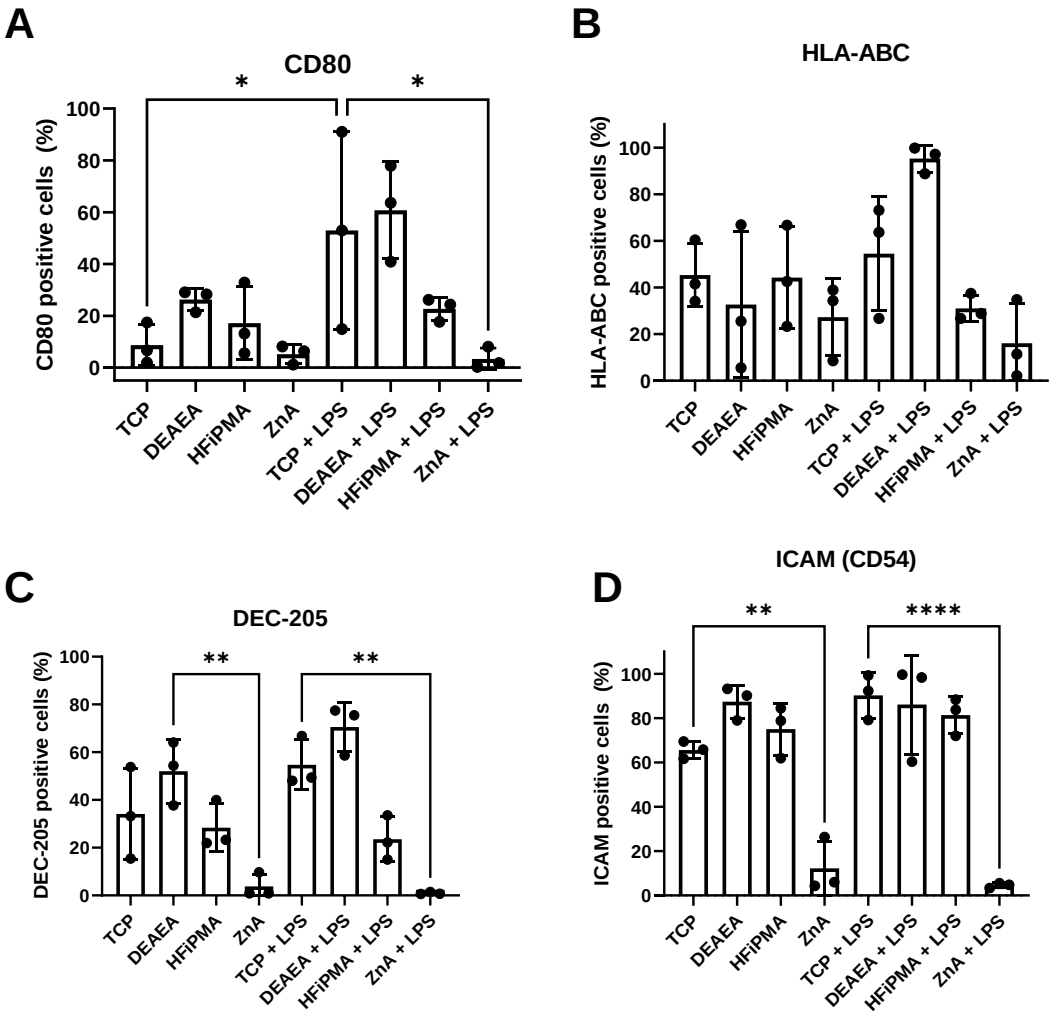


Figure 4-7: Polymer treatment modulates surface marker expression on DCs

DCs were cultured in polymer coated well plates for 24 hours (without and with LPS stimulation) before being stained for flow cytometry acquisition. Data is from 3 independent experiments with 10,000 events routinely acquired in each sample. TCP – tissue culture polystyrene, and data is presented as mean + SD. Statistical analysis was performed using one-way ANOVA with Dunnett's multiple comparison tests. * $p< 0.05$, ** $p<0.01$, *** $p < 0.001$ and **** $p < 0.0001$.

4.3.4 Gene microarray analysis supports relevance of stimulatory polymers for cancer immunotherapy

To investigate molecular changes of DCs cultured on stimulatory polymers, microarray analysis was performed to detect the expression levels of more than 21,000 genes after 24 hours of polymer culture. Compared with TCP cultured iDCs both DEAEA and HFiPMA treated DCs resulted in a number of differentially expressed genes (Figure 4-8). HFiPMA treated DCs have more significantly differentially expressed genes to TCP DCs than DEAEA cultured DCs, while also having more genes in common to TCP + LPS than DEAEA cultured DCs.

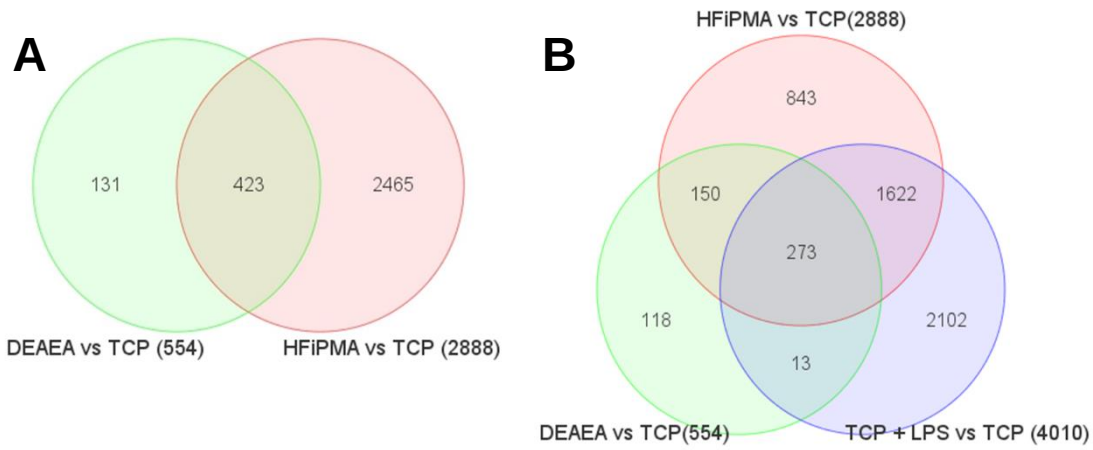


Figure 4-8: Differentially expressed genes of DEAEA, HFiPMA and TCP + LPS vs TCP

Venn diagram visualising the differentially expressed genes of polymer and LPS stimulated conditions compared to TCP cultured DCs.

To obtain an elementary investigation of the molecular mechanisms happening upon DC polymer culture, microarray data were submitted to IPA core analysis. The differentially expressed genes were categorized to related canonical pathways based on IPKB. The top enriched categories of canonical pathways

with a p-value less than 10^{-3} are listed for each polymer condition in Table 7. Generally, canonical pathways related with DC maturation, T cell signalling, and other inflammation and immune responses seem to be activated. A list of all canonical pathway with z-scores available is listed in Appendix 6. For each biological function a statistical quantity is computed, called the activation z-score. The activation z-score is used to infer likely activation states of biological functions based on comparison with a model that assigns random regulation directions. Under ideal circumstances the activation z-score can also be used to predict implicated biological functions independently from their associated p-value, based on significant pattern match of up/down regulation.

Table 7: Top canonical pathways for DEAEA and HFiPMA cultured DCs

DEAEA		HFiPMA	
Pathway	**Z-score**	**Pathway**	**Z-score**
Th2 pathway	0	**DC maturation**	positive
Th1 and Th2 activation pathway	No pattern available	**B cell receptor signalling**	negative
Role of Pattern recognition receptors in recognition of bacteria and virus	Negative	**Neuroinflammation signalling pathway**	positive
Communication between innate and adaptive immune cells	No pattern available	**Systemic lupus in B cell signalling pathway**	positive
TLR signalling	0	**Phagosome formation**	No pattern available
Crosstalk between DCs and natural killer cells	0	**Th1 and Th2 activation pathway**	No pattern available

OX40 signalling pathway	0	**Crosstalk between DCs and natural killer cells**	positive

Investigating top analysis ready molecules of up and down regulated genes for each condition can reveal more details about what is happening on a transcription basis. A full analysis of TCP+LPS vs TCP DCs and their gene expression are shown in Appendix 7.

4.3.4.1 DEAEA treated DCs upregulate genes involved in antigen presentation and DC maturation

DEAEA cultured DCs were found to have several genes upregulated that are involved in the development of the adaptive immune response and anti-tumour responses (CRLF2, MYO1G, TNFSF4 (also known as OX40L), CCR7, IL12B and NCF1). The top 10 of up and downregulated genes are shown in Table 8 and Table 9.

Table 8: DEAEA vs TCP – Top 10 upregulated genes

Gene	Expression Foldchange	Function	Ref
CRLF2	+5.143	TSLPR (other name), involved in T, B and NK cell responses; overexpression associated with activation of the JAK-STAT pathway.	[184]
GPR157	+4.416	Unknown function	
NCCRP1	+3.898	Unknown function (non-specific cytotoxic cell receptor protein 1 homolog (zebrafish)), epigenetical regulated tumour suppressor	[185]

STRIP2	+3.790	Striatin-interacting protein 2, implicated in migration, Part of striatin-interacting phosphatase and kinase complex (STRIPAK) complex which has critical role in protein (de)phosphorylation.	[186], [187]
MYO1G	+3.712	Enhances DC-T cell interactions during LN surveillance, due to increased turning and meandering motility of DCs	[188]
TNFSF4	+3.589	OX40L (other name), member of TNF family, co-stimulatory molecule that primes naïve CD4+ towards Th2 and memory T cells.	[189] – [191]
CCR7	+3.536	Chemokine receptor, that is responsible to chemotaxis and regulates migratory speed of DCs. Makes DCs migrate to secondary lymph nodes to its ligands CCL19 and CCL21 (both expressed by fibroblastic reticular cells in the paracortical regions of the lymph nodes where T cells are found).	[192] – [194]
TMEM176A	+3.538	Candidate regulators of inhibition of DC maturation and function, associated with iDCs, tmem176a+b bind multimers and restrain DC maturation. Required for optimal MHCII antigen presentation to CD4+T cells	[195], [196]
IL12B	+3.349	Encodes p40 subunit, forms with p35 IL-12, and is also a subunit for IL-23. IL-12 mediates Th1 development.	[197]
NCF1	+3.271	Promotes autoreactive CD8+ T cells activation via cross-presentation	[198]

Molecule adaptor predictor (MAP) enables interrogation of sub-networks and canonical pathways and hypothesis generation by selecting a molecule of interest, indicating up or down regulation, simulating directional consequences

of downstream molecules and the inferred activity upstream in the network or pathway. One of the main upregulated genes, TNFSF4/OX40L was upregulated by 3.5-fold change and using MAP is predicted to upregulate downstream effects of T cell expansion (see Figure 4-10).

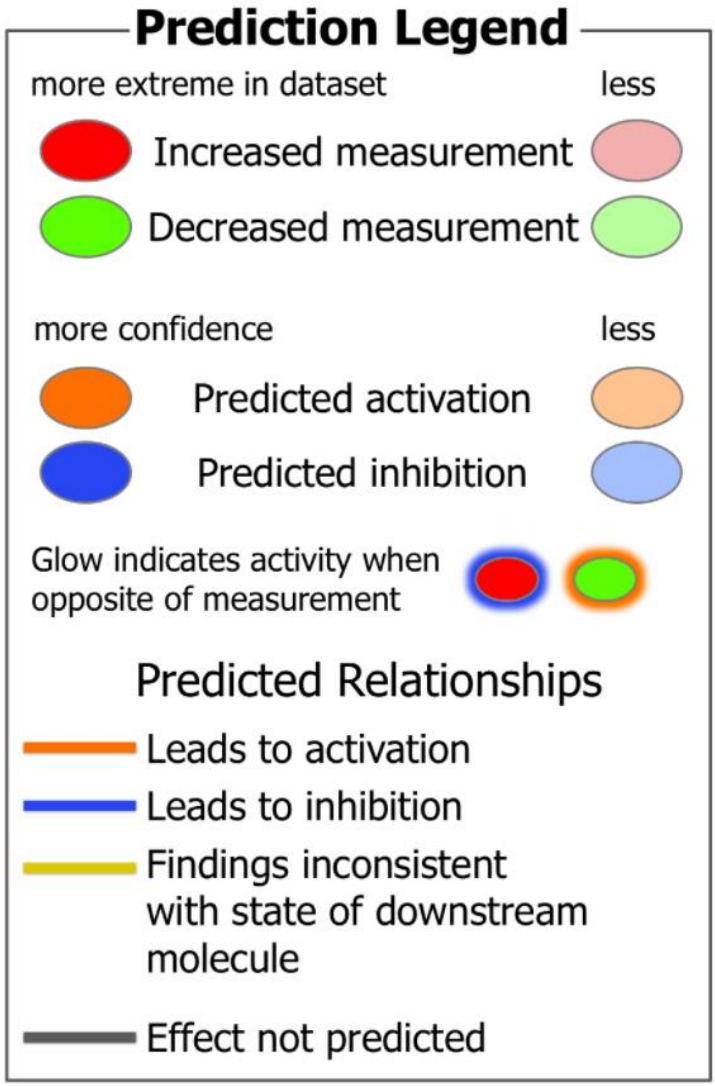


Figure 4-9: MAP Prediction legend

Legend for pathways with MAP to explain gene relationship, their measurement, and their predicted activation/inhibition. Red symbolises increases measurement; green symbolises decreased measurement. Orange indicates predicted activation, while blue predicts inhibition of gene. Colour intensity indicates the extremity of measurement or confidence in prediction. Following on from the prediction of gene expression, orange relationship lines indicate that the

relationship leads to activation, while blue connection leads to inhibition. The yellow connection indicates findings that are inconsistent with state of downstream molecule. Black connections mean that effects cannot be predicted based on data provided.

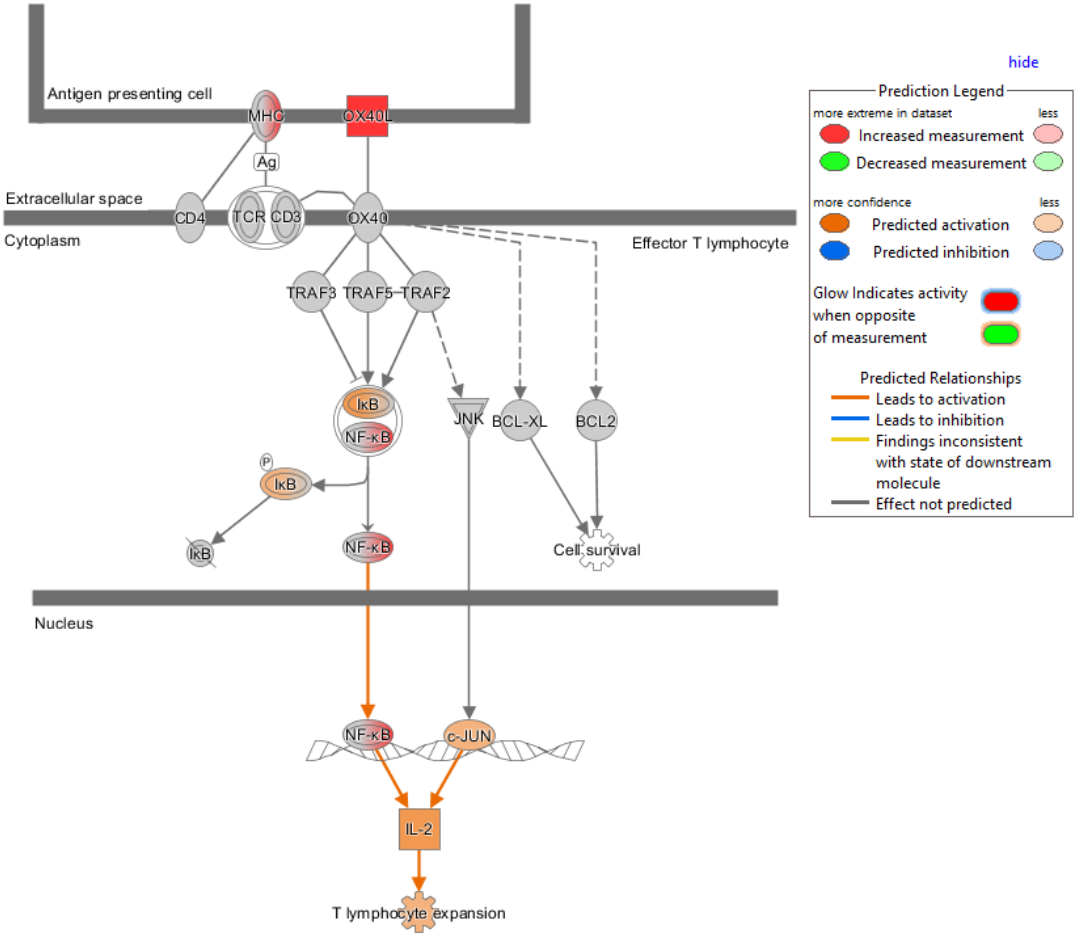


Figure 4-10: DEAEA - OX40L signalling pathway

Molecule adaptor prediction (MAP) utilised to predict downstream effects of OX40L expression on DCs. Red symbolises increases measurement; green symbolises decreased measurement. Orange indicates predicted activation, while blue predicts inhibition of gene. Colour intensity indicates the extremity of measurement or confidence in prediction. Following on from the prediction of gene expression, orange relationship lines indicate that the relationship leads to activation, while blue connection leads to inhibition. The yellow connection indicates findings that are inconsistent with state of downstream molecule. Black connections mean that effects cannot be predicted based on data provided.

Another canonical pathway that has been shown to be upregulated was the antigen presentation pathway in DEAEA cultured DCs, specifically cross-presentation to CD8+ T cells was measured, and by MAP tool predicted to be upregulated (Figure 4-11).

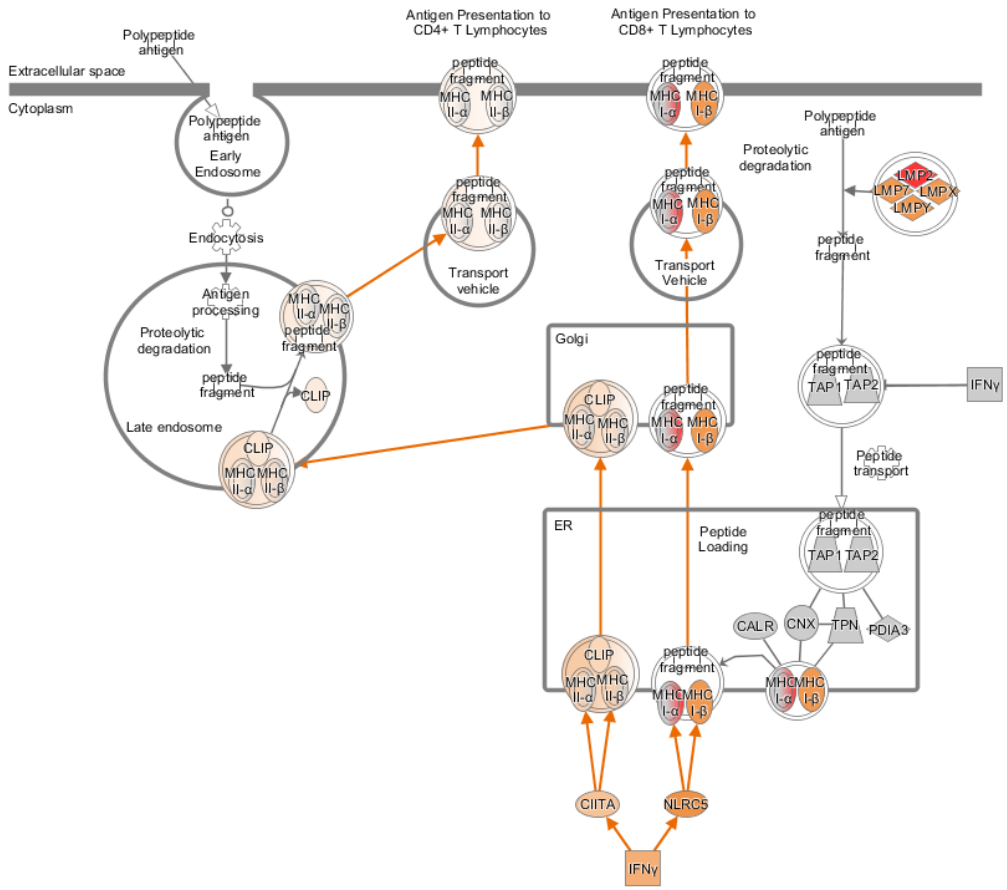


Figure 4-11: DEAEA- Antigen presentation Pathway

Molecule adaptor prediction (MAP) utilised to predict downstream effects of antigen presentation pathway molecule expression on DCs. Red symbolises increases measurement; green symbolises decreased measurement. Orange indicates predicted activation, while blue predicts inhibition of gene. Colour intensity indicates the extremity of measurement or confidence in prediction. Following on from the prediction of gene expression, orange relationship lines indicate that the relationship leads to activation, while blue connection leads to inhibition. The yellow connection indicates findings that are inconsistent with state of downstream molecule. Black connections mean that effects cannot be predicted based on data provided.

An interesting canonical pathway to investigate was the DC maturation pathway. Several internal DC markers indicated that upstream TLR2/4, FcγR, TLR2/3/4/9 and CD40 were predicted to be activated (Figure 4-12). Downstream signalling leading to DC maturation, migration, antigen presentation, and cross presentation as well as Th1, Th17 were measured and predicted to be upregulated. Conforming to other results the antigen uptake is downregulated after DEAEA culture. NFκB, costimulatory molecules and pro-inflammatory cytokines are significantly upregulated (Figure 4-12 to Figure 4-15).

Most of these observations confirm phenotype and functional results, from this and earlier chapters, such as the phenotype study.

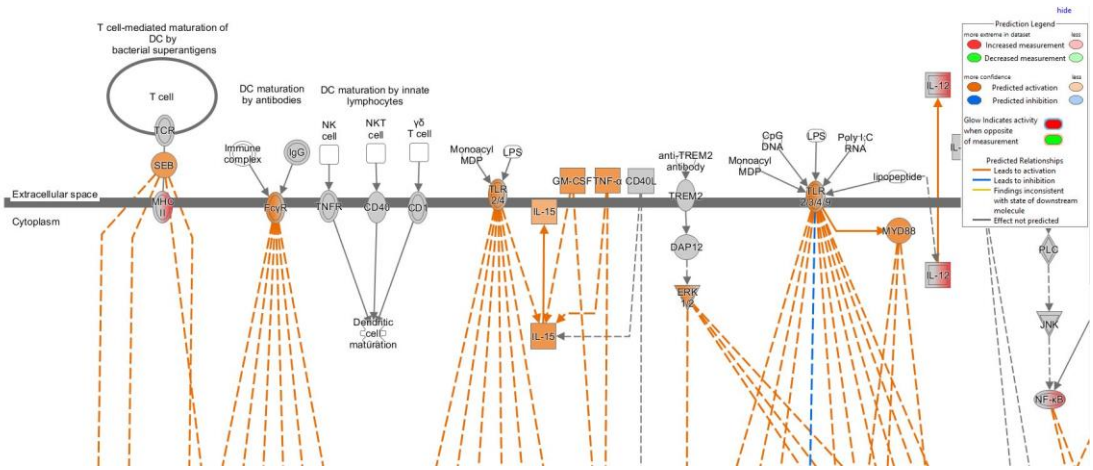


Figure 4-12: DEAEA- DC maturation part1

Molecule adaptor prediction (MAP) utilised to predict up and downstream effects of DC maturation canonical pathway in DEAEA cultured DCs. Red symbolises increases measurement; green symbolises decreased measurement. Orange indicates predicted activation, while blue predicts inhibition of gene. Colour intensity indicates the extremity of measurement or confidence in prediction. Following on from the prediction of gene expression, orange relationship lines indicate that the relationship leads to activation, while blue connection leads to inhibition. The yellow connection indicates findings that are inconsistent with state of

downstream molecule. Black connections mean that effects cannot be predicted based on data provided.

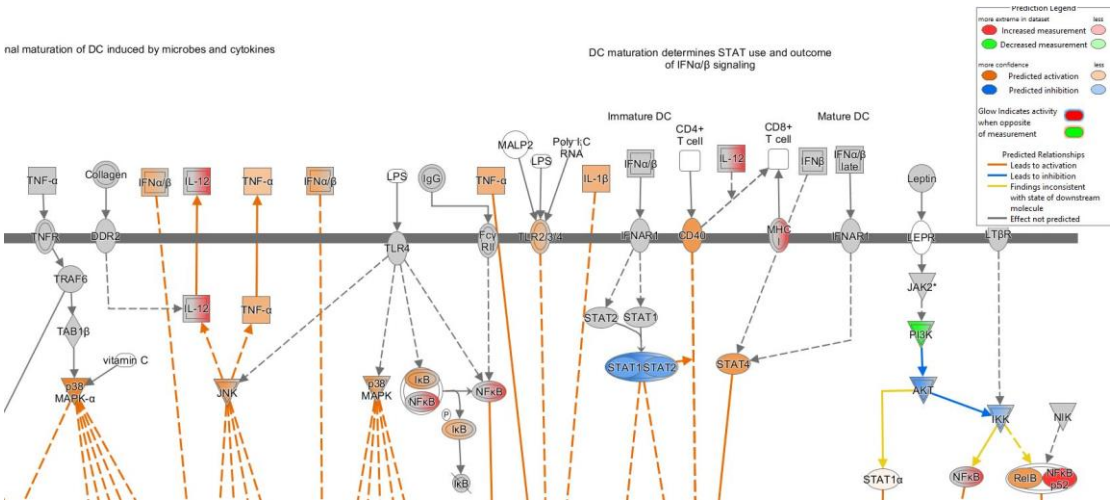


Figure 4-13: DEAEA- DC maturation part2

Molecule adaptor prediction (MAP) utilised to predict up and downstream effects of DC maturation canonical pathway in DEAEA cultured DCs. Red symbolises increases measurement; green symbolises decreased measurement. Orange indicates predicted activation, while blue predicts inhibition of gene. Colour intensity indicates the extremity of measurement or confidence in prediction. Following on from the prediction of gene expression, orange relationship lines indicate that the relationship leads to activation, while blue connection leads to inhibition. The yellow connection indicates findings that are inconsistent with state of downstream molecule. Black connections mean that effects cannot be predicted based on data provided.

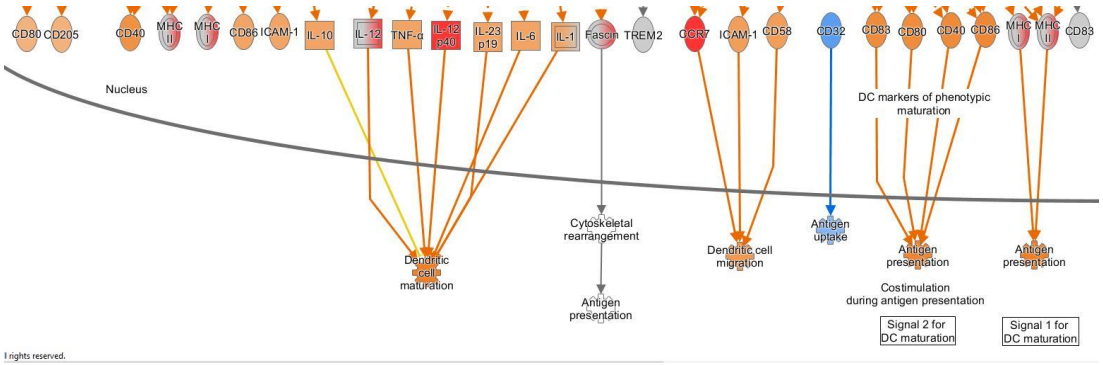


Figure 4-14: DEAEA -DC maturation part3

Molecule adaptor prediction (MAP) utilised to predict up and downstream effects of DC maturation canonical pathway in DEAEA cultured DCs. Red symbolises increases measurement; green symbolises decreased measurement. Orange indicates predicted activation, while blue predicts inhibition of gene. Colour intensity indicates the extremity of measurement or confidence in prediction. Following on from the prediction of gene expression, orange relationship lines indicate that the relationship leads to activation, while blue connection leads to inhibition. The yellow connection indicates findings that are inconsistent with state of downstream molecule. Black connections mean that effects cannot be predicted based on data provided.

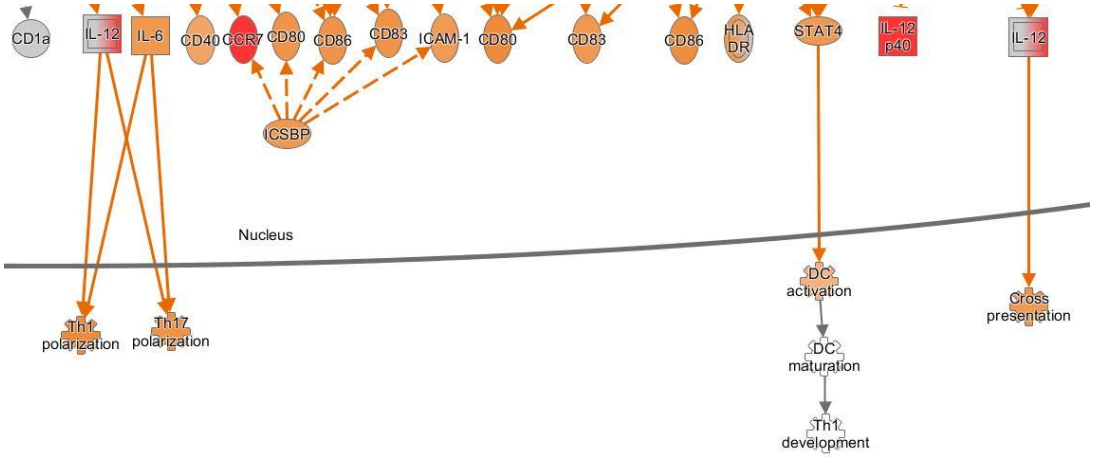


Figure 4-15: DEAEA-DC maturation part 4

Molecule adaptor prediction (MAP) utilised to predict up and downstream effects of DC maturation canonical pathway in DEAEA cultured DCs. Red symbolises increases measurement; green symbolises decreased measurement. Orange indicates predicted activation, while blue predicts inhibition of gene. Colour intensity indicates the extremity of measurement or confidence in prediction. Following on from the prediction of gene expression, orange relationship lines indicate that the relationship leads to activation, while blue connection leads to inhibition. The yellow connection indicates findings that are inconsistent with state of downstream molecule. Black connections mean that effects cannot be predicted based on data provided.

Downregulated genes for DEAEA cultured DCs involve genes with unknown functions, but also some genes involved in DC motility and DNA replication and synthesis.

Table 9: DEAEA vs TCP - Top 10 downregulated genes

Gene	Expression Foldchange	Function	Ref
FAM111B	-4.270	Unknown function, but may be related to DNA replication as predicted by its pattern of expression	[199]
F13A1	-4.149	May be responsible for DC motility	[200]
SELENOP	-3.969	Plasma Se transport protein, also exhibits SELENOP lipid hydroperoxide reductase activity	[201]
PCLAF	-3.732	Proliferating cell nuclear antigen clamp, binds proliferating cell nuclear antigen (PCNA) to form functional complex involved in DNA repair	[202]
CCNE2	-3.654	CDK2 partner in late G1 and S phases of mammalian cell cycle	[203]
CIBAR1	-3.610	Positive regulator of ciliary hedgehog signalling.	
TYMS	-3.418	Involved in dNTP synthesis	[204]
DDIAS	-3.129	Associated with cisplatin resistance in lung cancer cells	[205]
MCM8	-3.036	Involved in repair of ds DNA breaks	[206]

TPM1	-3.004	T cell phenotype modifier, controls IL-12 responsiveness, noncytokine gene that influences early IL-12 receptor expression	[207]

TLR-1 and TLR-6 were measured to be downregulated and several other TLRs were predicted to be inhibited with subsequent downstream inhibition (Figure 4-16). Due to high NFκB upregulation the ensuing adaptive immune response was however activated.

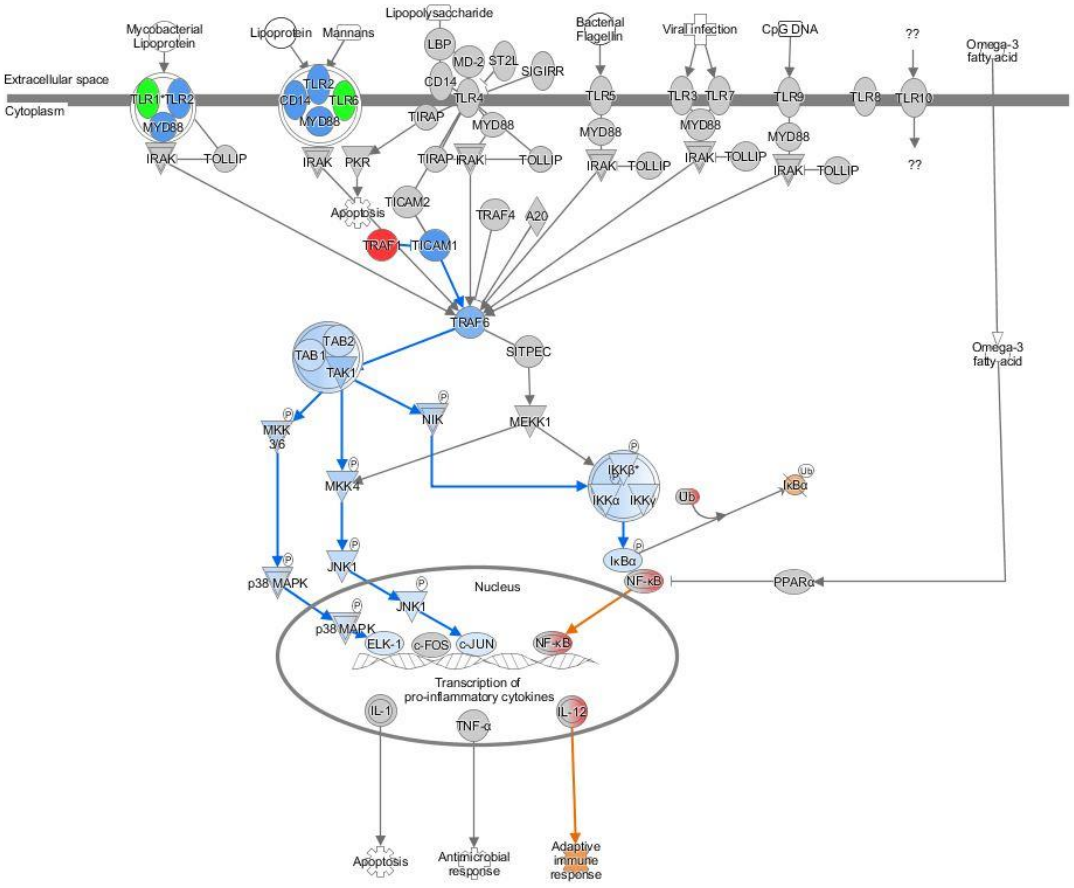


Figure 4-16: DEAEA - TLR signalling

Molecule adaptor prediction (MAP) utilised to predict up and downstream effects of DC maturation canonical pathway in DEAEA cultured DCs. Red symbolises increases measurement; green symbolises decreased measurement. Orange indicates predicted activation, while blue predicts inhibition of gene. Colour intensity indicates the extremity of measurement or confidence in prediction. Following on from the prediction of gene expression, orange relationship lines indicate that the relationship leads to activation, while blue connection leads to inhibition. The yellow connection indicates findings that are inconsistent with state of downstream molecule. Black connections mean that effects cannot be predicted based on data provided.

4.3.4.2 HFiPMA culture activates genes and canonical pathways involved in adaptive immune responses and induction of anti-tumour responses

For HFiPMA cultured DCs genes of DC maturation, as well as genes favouring anti-tumour responses, immune cell recruitment/activation and DC migration are upregulated (CXCL8, IL2RA, CRLF2, TNFAIP6). Several genes involved in the induction of tolerance are also upregulated (ITGB8, INHBA) as can be found in Table 10.

Table 10: HFiPMA- Top 10 upregulated genes

Gene	Expression Foldchange	Function	Ref
CXCL8	+30.699	Associated DC activation marker, as well as chemotactic factor for neutrophils. Anti-tumour immune response as well as DC migration and immune cell recruitment	[208]
IL2RA	+26.535	Encodes CD25, mDCs can lend their CD25 to primed T cells to facilitate early high-affinity IL-2 signalling, which is crucial for subsequent T cell expansion and antigen specific effectors	[209]
ITGB8	+23.423	Encodes Integrin β8-subunit, regulates Th17 cell development and is involved in inducing tolerogenic function and T_{regs}	[210]

IL12B	+20.538	Encodes p40 subunit, forms with p35 IL-12, and is also a subunit for IL-23. IL-12 mediates Th1 development	[197]
CRLF2	+17.389	TSLPR (other name), involved in T, B and NK cell responses; overexpression associated with activation of the JAK-STAT pathway.	[184]
SPECC1L-ADORA2A	+15.163	Nonsense-mediated RNA decay	
FERMT2	+14.207	Links cortical actin structures, plasma membrane tension and focal adhesion function to stabilize podocyte morphology.	[211]
INHBA	+14.102	Key regulator of peripheral T cell tolerance	[212]
SGPP2	+13.327	Involved in IBD	[213]
TNFAIP6	+13.156	Key regulator of inflammation and downregulates IFN-α and TNF-α by suppressing IRF7 phosphorylation	[214]

For HFiPMA cultured DCs, the cross-presentation pathway to CD8+ T cells is upregulated while antigen presentation to CD4+ T cells is diminished (Figure 4-17).

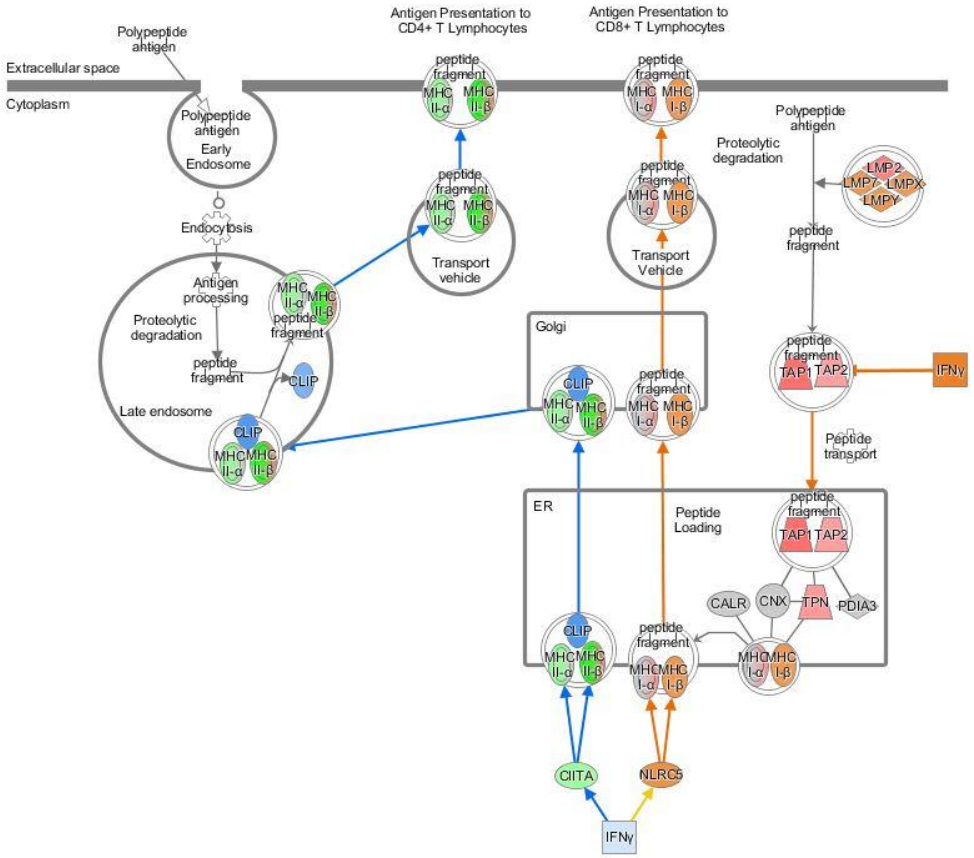


Figure 4-17: HFiPMA – Antigen presentation pathway

Molecule adaptor prediction (MAP) utilised to predict downstream effects of OX40L expression on HFiPMA cultured DCs. Red symbolises increases measurement; green symbolises decreased measurement. Orange indicates predicted activation, while blue predicts inhibition of gene. Colour intensity indicates the extremity of measurement or confidence in prediction. Following on from the prediction of gene expression, orange relationship lines indicate that the relationship leads to activation, while blue connection leads to inhibition. The yellow connection indicates findings that are inconsistent with state of downstream molecule. Black connections mean that effects cannot be predicted based on data provided.

Interestingly, MPEG1, a genethat encodes perforin-2, is one of the top 10 genes that are downregulated in HFiPMA cultured DCs (Table 11). AIF1 is a scaffold protein that shifts the immune microenvironment towards tolerance when suppressed. RGS18 and F13A1 are two genes that are supposedly,

reducing and increasing DC motility, respectively. CD200R1 inhibition increases Th17 polarisation of T cells, while inhibiting T_{regs}.

Table 11: HFiPMA- Top 10 downregulated genes

Gene	Expression Foldchange	Function	Ref
MS4A6A	-69.560	Signal transduction, unknown	
F13A1	-33.897	May be responsible for DC motility	[200]
AIF1	-20.691	Calcium-responsive cytoplasmic scaffold protein that directs haematopoiesis and immune responses within DCs and macrophages, AIF1 suppression restrains insulitis by shifting immune microenvironment towards tolerance	[215], [216]
MPEG1	-19.446	Encodes Perforin-2	[217]
C1orf162	-19.424	High expression in tolDCs	[218]
RGS18	-17.956	Engagement of TLR3 or TLR4 reduces RGS18 without modifying other RGS proteins, RGS18 inhibits Gα signalling, and this reduces CXCL12-,19,21-Ligand mediated DC migration	[219]
TMEM236	-17.095	Unknown function	
P2RY14	-16.196	Implicated in extending the known immune system functions of P2Y receptors by participating in the regulation of the stem cell compartment, upregulated after allergen challenge, activated by UDP-sugars, on iDCs	[220]
CD200R1	-15.107	Expression positively correlated with T_{regs} and negatively with Th17; CD200R1 decrease therefore increases Th17 and decreases T_{regs}	[221]
FCER1A	-15.006	Normal downregulation of FCER1A in monocyte derived DCs, classifier of non-inflammatory DCs when FCER1A expression	[222]

TLR-1, -3, -4, and -6 are measured to be downregulated while Myd88 is predicted to be inhibited (Figure 4-18). An increased NFκB and TRAF6 downstream signalling however induces an increased adaptive immune response.

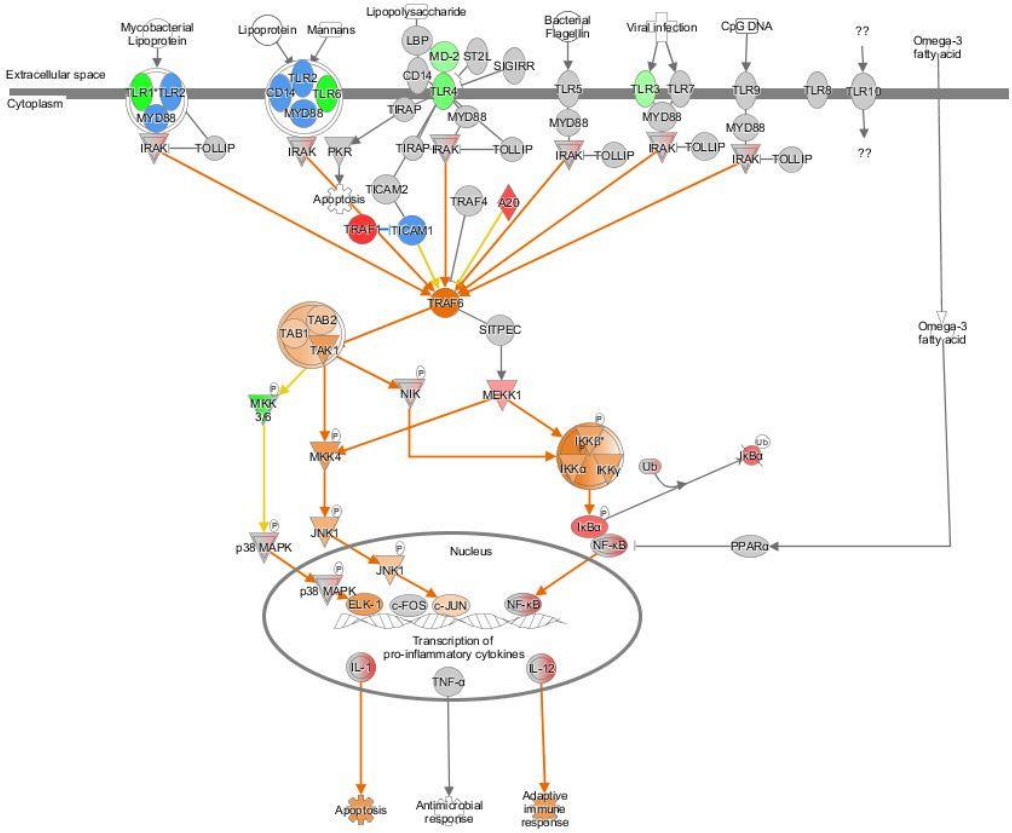


Figure 4-18: HFiPMA - TLR signalling

Molecule adaptor prediction (MAP) utilised to predict downstream effects of TLR signalling on HFiPMA cultured DCs. Red symbolises increases measurement; green symbolises decreased measurement. Orange indicates predicted activation, while blue predicts inhibition of gene. Colour intensity indicates the extremity of measurement or confidence in prediction. Following on from the prediction of gene expression, orange relationship lines indicate that the relationship leads to activation, while blue connection leads to inhibition. The yellow connection indicates findings that are inconsistent with state of downstream molecule. Black connections mean that effects cannot be predicted based on data provided.

In the integrin signalling pathway, the α and β integrin subunits show mixed expression patterns, with several downstream components being downregulated, which functionally is predicted to lead to several inhibited cellular functions (e.g., ERK/MAPK-mediated transcription, cytoskeletal remodulation, Wnt signalling and tumour invasion) (Figure 4-19).

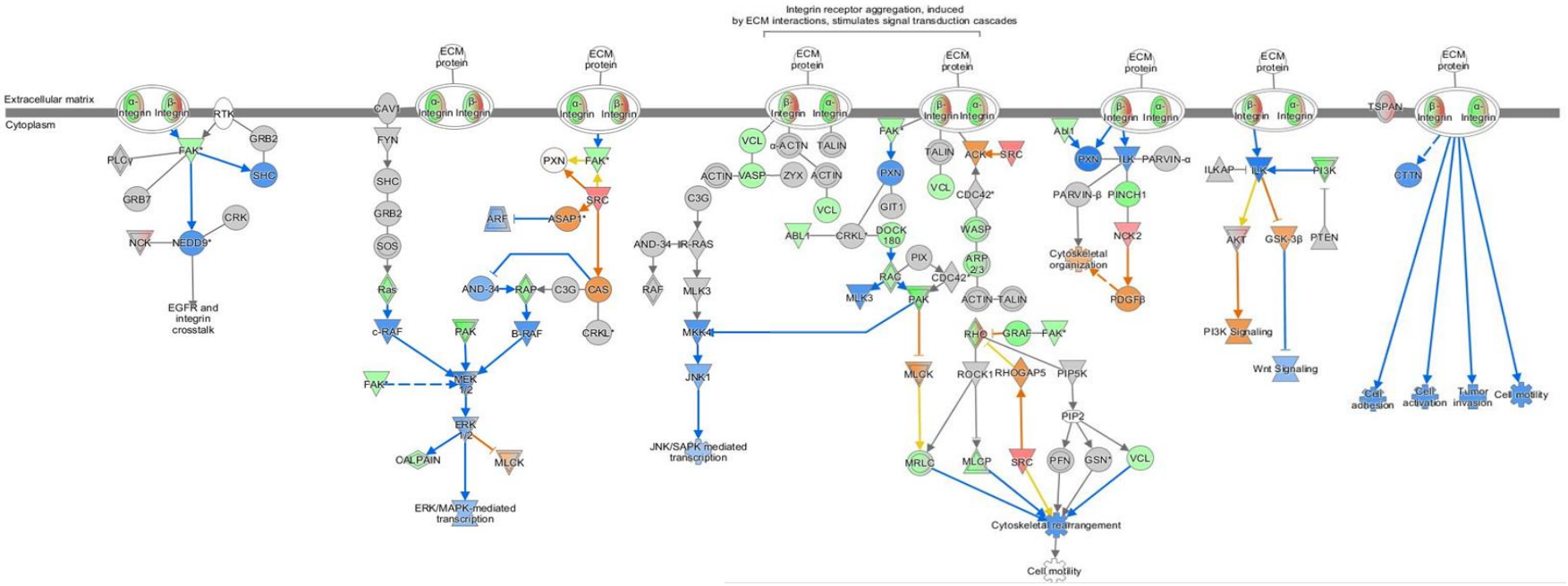


Figure 4-19: HFiPMA - Integrin signalling

Molecule adaptor prediction (MAP) utilised to predict downstream effects of integrin signalling on HFiPMA cultured DC. Red symbolises increases measurement; green symbolises decreased measurement. Orange indicates predicted activation, while blue predicts inhibition of gene. Colour intensity indicates the extremity of measurement or confidence in prediction. Following on from the prediction of gene expression, orange relationship lines indicate that the relationship leads to activation, while blue connection leads to inhibition. The yellow connection indicates findings that are inconsistent with state of downstream molecule. Black connections mean that effects cannot be predicted based on data provided.

The NFκB pathway is upregulated with both the normal and the alternative NFκB pathway significantly upregulated for HFiPMA cultured DCs, leading to pro-inflammatory responses and lymphogenesis (Figure 4-20).

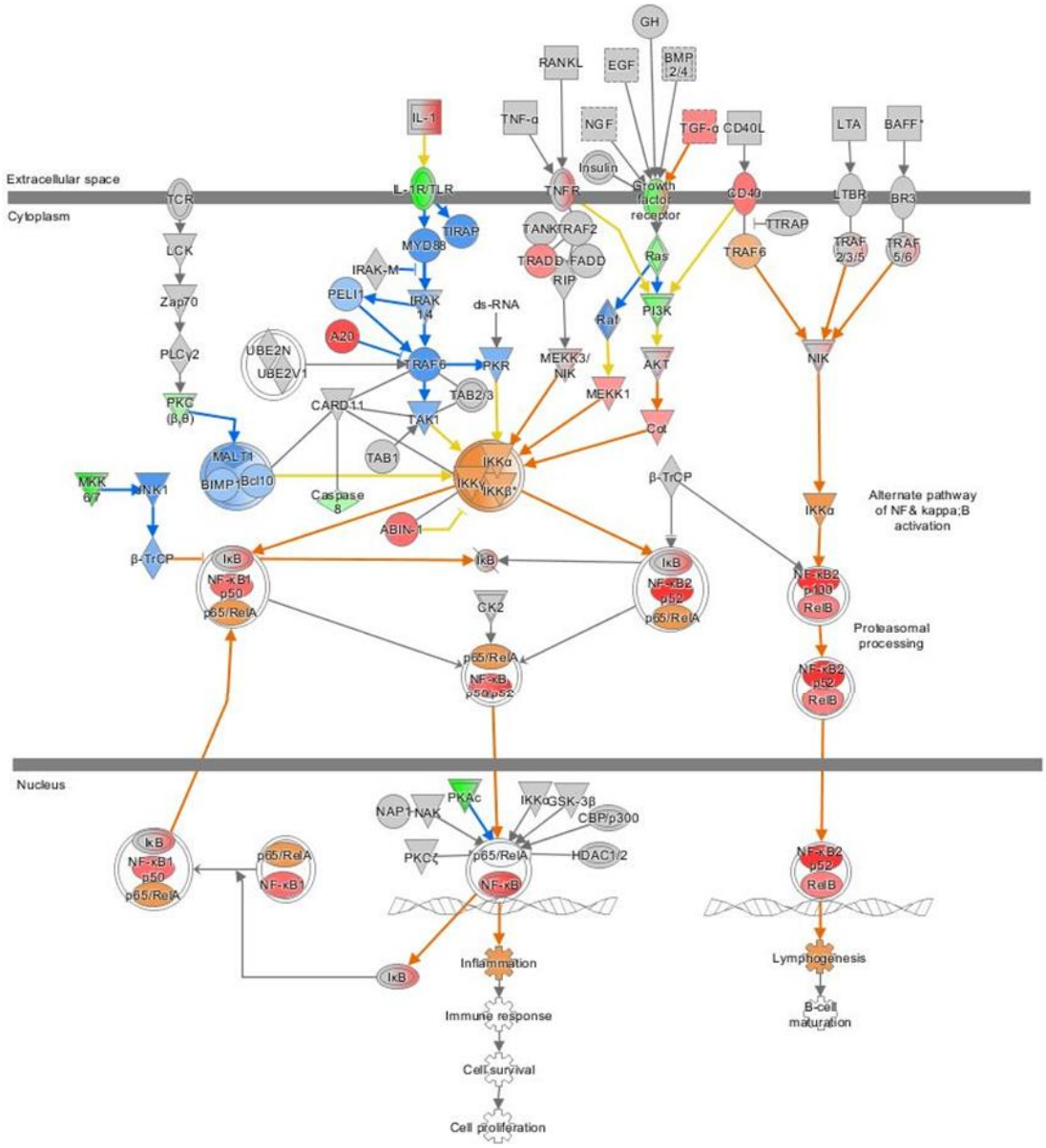


Figure 4-20: HFiPMA - NFκB signalling

Molecule adaptor prediction (MAP) utilised to predict downstream effects of NFκB signalling on HFiPMA cultured DCs. Red symbolises increases measurement; green symbolises decreased measurement. Orange indicates predicted activation, while blue predicts inhibition of gene. Colour intensity indicates the extremity of measurement or confidence in prediction. Following

on from the prediction of gene expression, orange relationship lines indicate that the relationship leads to activation, while blue connection leads to inhibition. The yellow connection indicates findings that are inconsistent with state of downstream molecule. Black connections mean that effects cannot be predicted based on data provided.

Many markers involved in DC maturation are measured to be significantly upregulated in HFiPMA cultured DCs (Figure 4-21 and Figure 4-22).

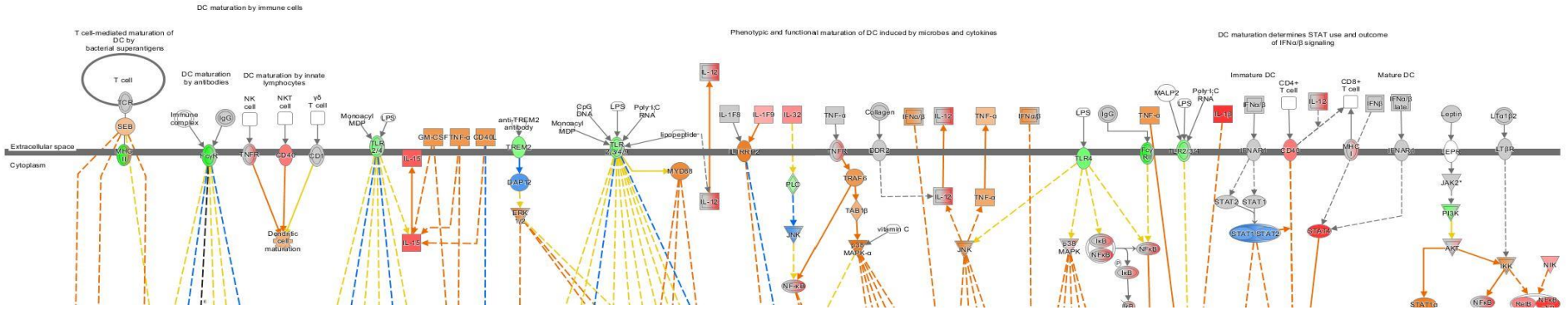


Figure 4-21: HFiPMA – DC maturation part 1

Molecule adaptor prediction (MAP) utilised to predict up and downstream effects of DC maturation on HFiPMA cultured DCs. Red symbolises increases measurement; green symbolises decreased measurement. Orange indicates predicted activation, while blue predicts inhibition of gene. Colour intensity indicates the extremity of measurement or confidence in prediction. Following on from the prediction of gene expression, orange relationship lines indicate that the relationship leads to activation, while blue connection leads to inhibition. The yellow connection indicates findings that are inconsistent with state of downstream molecule. Black connections mean that effects cannot be predicted based on data provided.

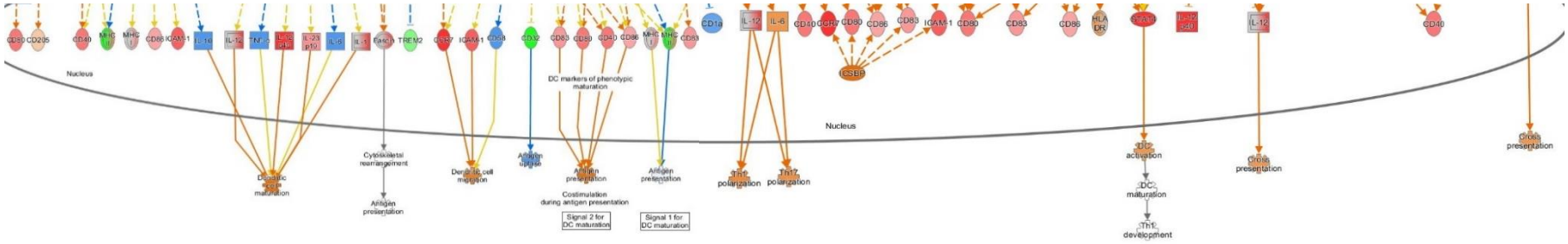


Figure 4-22: HFiPMA- DC maturation part 2

Molecule adaptor prediction (MAP) utilised to predict up and downstream effects of DC maturation on HFiPMA cultured DCs. Red symbolises increases measurement; green symbolises decreased measurement. Orange indicates predicted activation, while blue predicts inhibition of gene. Colour intensity indicates the extremity of measurement or confidence in prediction. Following on from the prediction of gene expression, orange relationship lines indicate that the relationship leads to activation, while blue connection leads to inhibition. The yellow connection indicates findings that are inconsistent with state of downstream molecule. Black connections mean that effects cannot be predicted based on data provided.

HFiPMA treated DCs showed increased Th1 signalling due to high transcription levels of costimulatory molecules such as ICAM1, CD40, CD80 and CD86 as well as pro-inflammatory cytokines such as IL-12 (Figure 4-23). Th2 signalling as well was shown to be heavily induced due to high costimulatory molecule transcription, with OX40L promoting T cell expansion and survival, while limiting the development of regulatory T cells.

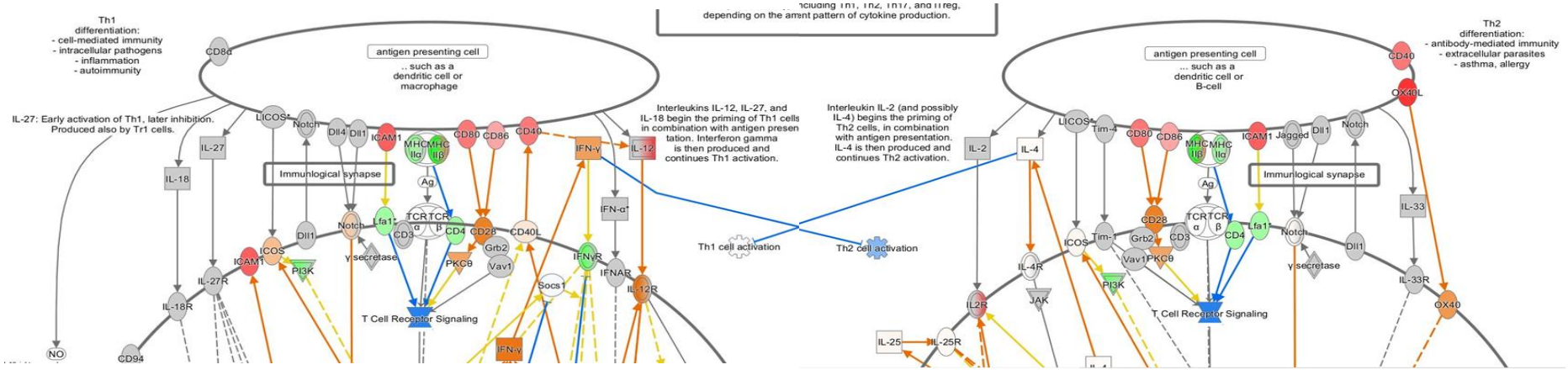


Figure 4-23: HFiPMA – Th1 and Th2 activation pathway

Molecule adaptor prediction (MAP) utilised to predict downstream effects of Th1 and Th2 activation by HFiPMA cultured DCs. Red symbolises increases measurement; green symbolises decreased measurement. Orange indicates predicted activation, while blue predicts inhibition of gene. Colour intensity indicates the extremity of measurement or confidence in prediction. Following on from the prediction of gene expression, orange relationship lines indicate that the relationship leads to activation, while blue connection leads to inhibition. The yellow connection indicates findings that are inconsistent with state of downstream molecule. Black connections mean that effects cannot be predicted based on data provided.

Dectin-1, C3aR, TLR-1, -3, -4, -6 are PRRs that were measured to show lower transcription levels on HFiPMA cultured DCs, with several other PRRs predicted to be downregulated (Figure 4-24).

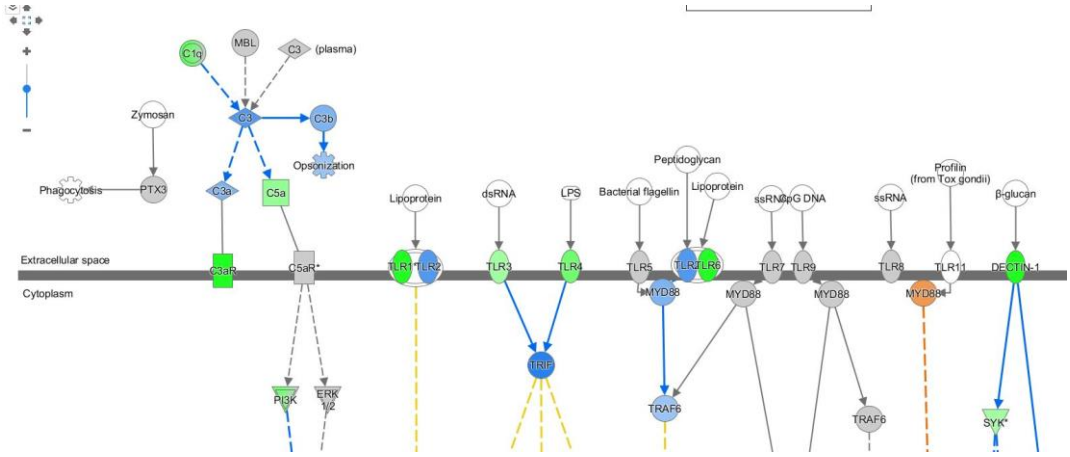


Figure 4-24: HFiPMA - Pattern recognition receptors

Molecule adaptor prediction (MAP) utilised to predict downstream effects of Pattern recognition receptors on HFiPMA cultured DCs. Red symbolises increases measurement; green symbolises decreased measurement. Orange indicates predicted activation, while blue predicts inhibition of gene. Colour intensity indicates the extremity of measurement or confidence in prediction. Following on from the prediction of gene expression, orange relationship lines indicate that the relationship leads to activation, while blue connection leads to inhibition. The yellow connection indicates findings that are inconsistent with state of downstream molecule. Black connections mean that effects cannot be predicted based on data provided.

4.3.5 **T cell co cultures**

Following on from the gene array studies, results indicated that the stimulatory polymers treated DCs were able to more efficiently interact with T cells than TCP cultured DCs. To investigate this further in a functional assay, autologous co-cultures between various T cell subsets and polymer treated DCs were set up to measure the rate of T cell proliferation and production of cytokines (e.g., IFN-γ, IL-10 or IL-17). Polymers used in this set of experiments were the 3 hit

polymers identified in the previous chapter, constituting of two stimulatory and oner regulatory polymers. For these functional assays the regulatory polymer ZnA was included even without having any gene array data.

4.3.5.1 Polymer culture influences DC interaction with CD3+ T cells

To look at the entity of T cells, all CD3+ T cells were used from the same blood donor. Monocytes were differentiated into DCs and immature DCs conditioned for 24 hours on flat polymer coatings, followed by co-culture with CD3+ T cells in a 1:10 ratio (DC: T cell) for 8 days. Co-cultures were cultured in compete media, but instead of FBS human AB serum has been used. On day 3 and 6 co-cultures had half their media removed and substituted with fresh media containing 20 IU of IL-2.

CD3+ T cells that were co-cultured with DEAEA and HFiPMA conditioned DCs showed higher proliferation levels than TCP (and in case of some donors higher than TCP + LPS) (Figure 4-25). Generally, the green blood donor showed more response to DC conditioning and in effect the conditions of stimulatory polymers, as well as the stimulation controls were more easily modulated in this donor (showed higher proliferation rates).

DEAEA conditioned DCs induced higher proliferation levels than TCP DCs, but this modulation was not significant. The combined effect of DEAEA coating together with LPS stimulation of DCs increased the proliferation level significantly ($p<0.001$). HFiPMA coatings induced CD3+ T cell proliferation of roughly the same level as DEAEA + LPS condition, also significantly ($p<0.01$). The HFiPMA + LPS condition showed similar proliferation level as DEAEA +

LPS, as the combined effect of polymer and LPS increased CD3+ T cell proliferation significantly ($p<0.001$). The regulatory polymer ZnA conditioned DCs induced lower CD3+ T cell proliferation levels over most of the 4 donors, with the blue donor having higher CD3+ T cell proliferation than the TCP control. Similar behaviour was observed for ZnA + LPS.

The secretion of IFN-γ in the cell culture supernatant was measured after 8 days of culture by ELISA. DEAEA and HFiPMA conditioned DCs increased the IFN-γ secretion of CD3+ T cells above the TCP levels, but not significantly. Combining the stimulatory polymer treatment with LPS increased the IFN-γ secretion significantly (DEAEA $p<0.0001$ and HFiPMA $p<0.05$). The regulatory polymer coating ZnA induced CD3+ T cells to secrete low levels of IFN-γ in both the polymer only and the combination of polymer and LPS condition. The ZnA only condition secreted IFN-γ below TCP, while the addition of LPS slightly increased it above TCP levels.

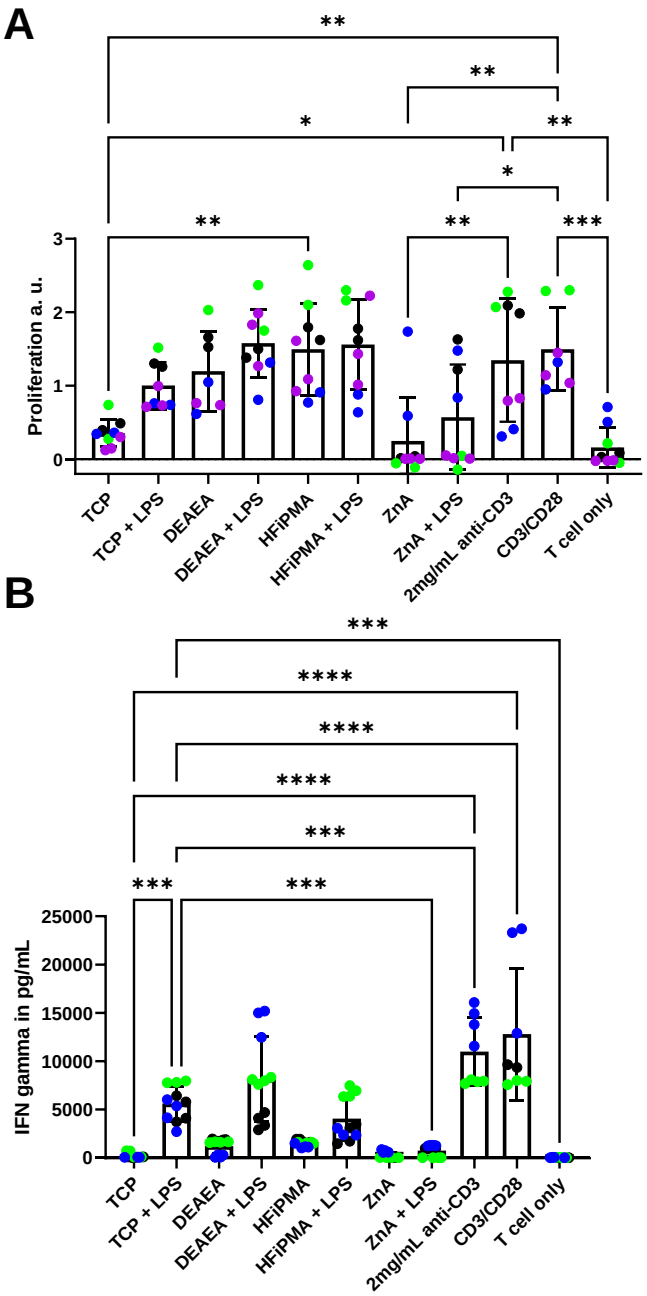


Figure 4-25: Polymer treatment influences the outcome of DC-T cell interactions

(**A)** T-cell proliferation assay using CD3+ T cells as responder cells after 8 days of co-culture; The proliferation was measured by BrdU colorimetric assay **(B)** IFN-γ production of CD3+ T cell-Polymer DC cultures. Data is of 4 independent blood donors, with 2-4 technical repeats each. TCP – tissue culture polystyrene, and data is presented as mean + SD. Statistical analysis was performed using one-way ANOVA with Tukey's post hoc multiple comparison tests. * $p< 0.05$, ** $p<0.01$, *** $p < 0.001$ and **** $p < 0.0001$.

4.3.5.2 Stimulatory polymers significantly improve DC ability to activate naïve T cells and induce higher proliferation levels

Taking a decisive look at the subset of naïve T cells the same experimental set up as for CD3+ T cells was used. Monocytes and naïve T cells were isolated from the same donor, and monocytes were differentiated into DCs and immature DCs conditioned for 24 hours on flat polymer coatings, followed by co-culture with naive T cells in a 1:10 ratio (DC: T cell) for 8 days. Co-cultures were cultured in complete media, but instead of FBS human AB serum was used. On day 3 and 6 co-cultures had half their media removed and substituted with fresh media containing 20 IU of IL-2.

The results show co-cultures with DC conditioned on DEAEA and HFiPMA significantly upregulated T cell proliferation levels, $p<0.01$ and $p<0.001$ respectively. While LPS stimulation did upregulate the proliferation of TCP + LPS compared to TCP control condition it did not do so significantly, DEAEA and HFiPMA however showed combinatorial effect with LPS to highly significantly upregulate the proliferation of naïve T cells ($p<0.001$ and $p<0.0001$ respectively). The proliferation rate of HFiPMA + LPS was close to anti-CD3 and anti-CD28 positive control. ZnA and ZnA + LPS conditions showed similar or less proliferation than the TCP control, although not significantly decreased.

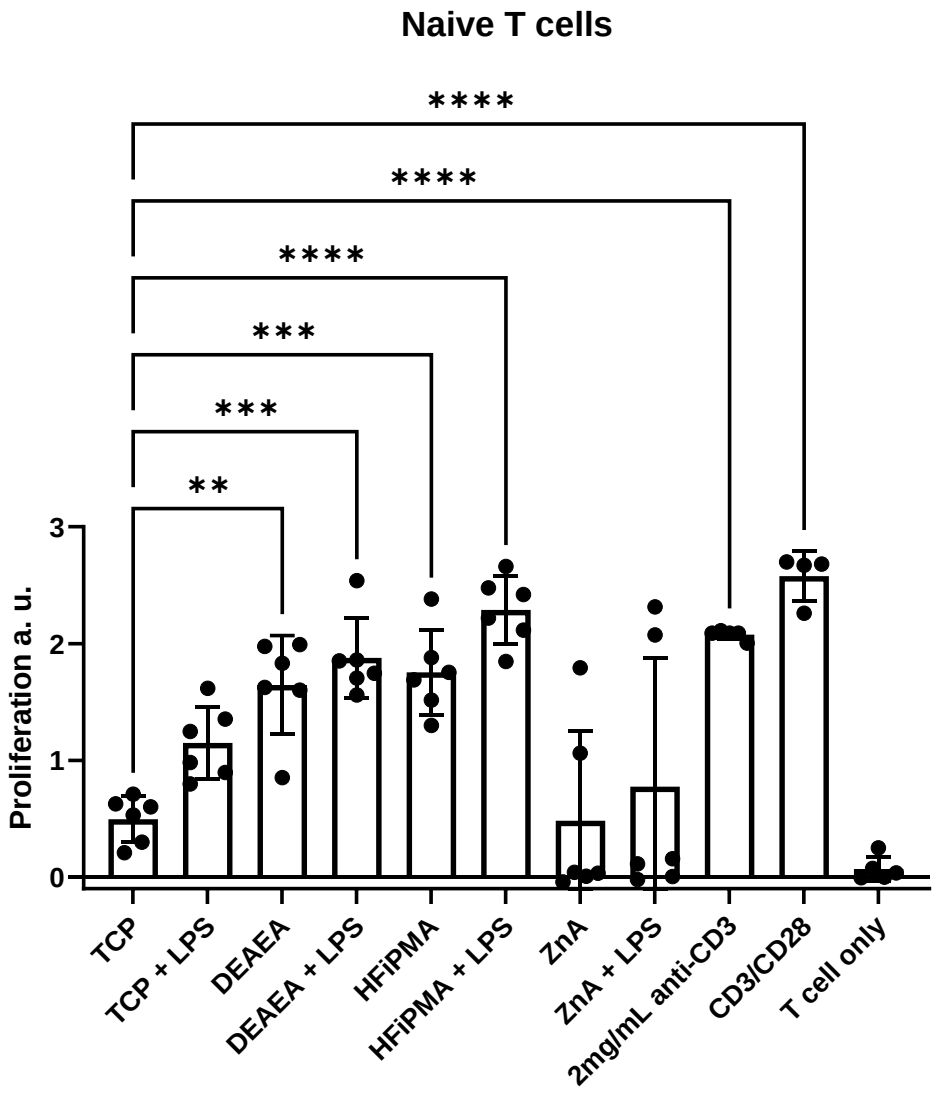


Figure 4-26: Polymer treatment influences DC interaction with naïve T cells and modulates naïve T cell proliferation rates

Autologous naïve T cell were co cultured with polymer treated DCs for 8 days. The proliferation of naïve T cells was measured by BrdU proliferation assay (Roche). Data is of 3 independent experiments, with 2 technical repeats each. TCP – tissue culture polystyrene, and data is presented as mean + SD. Statistical analysis was performed using one-way ANOVA with Dunnet's post hoc multiple comparison tests. * $p< 0.05$, ** $p<0.01$, *** $p < 0.001$ and **** $p < 0.0001$.

The secretion of IFN-γ was shown to be modulated by DCs cultured on polymers. Both DEAEA and HFiPMA conditioning induced higher secretion of

IFN-γ by naïve T cells, although not significantly. ZnA conditioning maintained IFN-γ secretion levels similar to TCP. TCP + LPS and DEAEA + LPS highly upregulated the secretion towards around 7000 pg/mL, with HFiPMA + LPS up to 6300 pg/mL (all $p<0.0001$). ZnA + LPS maintained similar IFN-γ levels as the negative TCP control. The two positive controls anti-CD3 and combination with anti-CD28 upregulated the secretion of IFN-γ up to 8000 and 11,000 pg/mL, significant upregulation ($p<0.0001$) compared to TCP negative control.

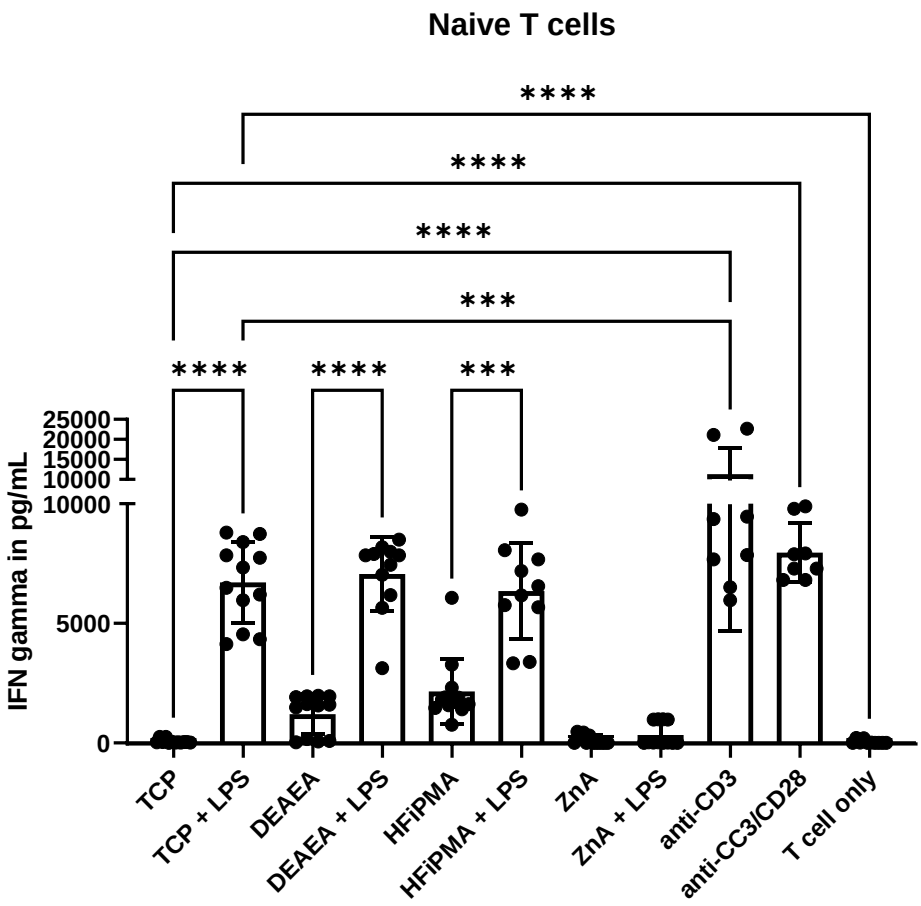


Figure 4-27: Polymer treatment influences DC interaction with naïve T cells and modulates naïve T cell IFN gamma secretion

Autologous naïve T cells were co cultured with polymer treated DCs for 8 days. The secretion of IFN-γ was measured by DuoSet ELISA. Data is from 3 independent experiments with 4 technical repeats each and presented as mean + SD. Statistical analysis was performed using one-way ANOVA with Dunnet's post hoc multiple comparison tests. * $p< 0.05$, ** $p<0.01$, *** $p < 0.001$ and **** $p < 0.0001$.

4.3.5.3 Memory T cells expand more rapidly when DCs have been cultured on stimulatory polymers

Memory T cells react to antigens they know, therefore introducing an antigen that is widespread in the population will give insight into the ability of polymers

to modulate the response to antigens which an adaptive immune response was already build against.

To use a common antigen, it was decided to use tetanus toxin (TT). The tetanus vaccine is a vaccination widespread in the population in the UK, and therefore the immunity should exist within the donor population. Memory T cells and monocytes originated from the same blood donor. Monocytes were differentiated into DCs and iDCs were conditioned for 24 hours on flat polymer coatings, followed by co-culture with memory T cells in a 1:10 ratio (DC: T cell) for either 48 or 72 hours. Co-cultures were cultured in complete media, but instead of FBS human AB serum was used.

As memory T cells react quickly the timescale for these experiments was 48 and 72 hours. Generally, after 48 hours of culture there was little proliferation modulation by the polymer treated DCs. HFiPMA showed some non-significant upregulation of proliferation, with DEAEA to a lesser amount and ZnA showed less proliferation (also non-significant) than the TCP condition. The T cell only condition did not proliferate to a measurable amount (Figure 4-28). After 72 hours however, both DEAEA and HFiPMA treated DCs induced higher proliferation rates in memory T cells compared to TCP in both the condition with and without the TT, with the HFiPMA condition being significant in the non-TT condition. ZnA treated DCs showed similar proliferation rates as the T cell only condition.

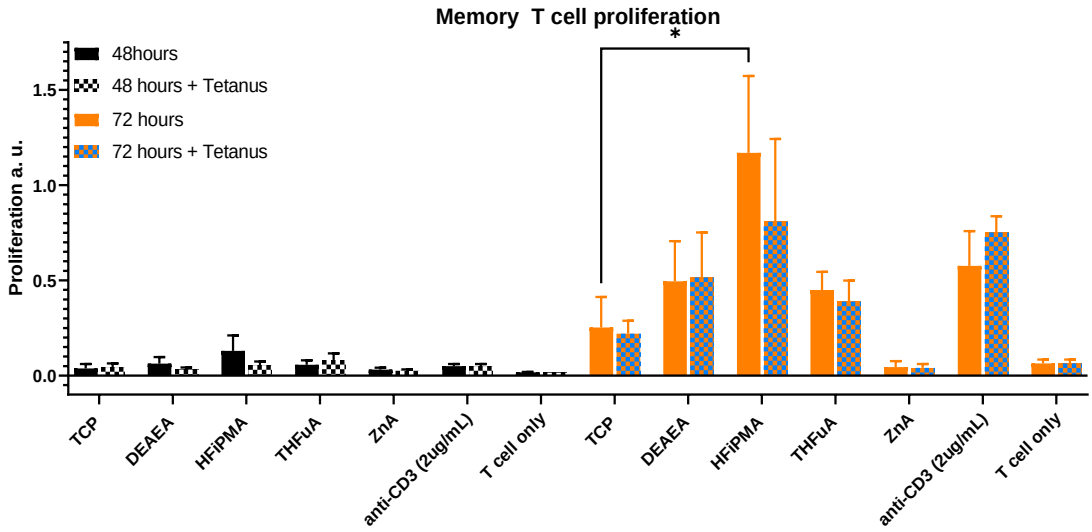


Figure 4-28: Polymer treatment influences DC interaction with memory T cells and modulates their proliferation rates

Autologous memory T cells were co cultured with polymer treated DCs for 48 and 72 hours. The proliferation of memory T cells was measured by BrdU proliferation assay (Roche). Data is of 3 independent blood donors, with 2 technical repeats each. TCP – tissue culture polystyrene, and data is presented as mean + SD. * p< 0.05, ** p<0.01, *** p < 0.001 and **** p < 0.0001. Statistical analysis was performed using one-way ANOVA with Dunnet's post hoc multiple comparison tests.

From these co-cultures the cell culture supernatant was harvested and used to investigate the amount of IFN-γ secreted by Memory T cells. After 48 hours most polymer treated DCs induced no big modulation of IFN-γ secretion, apart from HFiPMA treatment, where 1 donor shows to be more sensitive to polymer treatment. After 72 hours of co-culture the HFiPMA treatment condition is the one that is most upregulating IFN-γ, close to the levels of anti-CD3 (positive control) conditions (Figure 4-29).

The presence of TT antigen does not seem to have an impact on IFN-γ production over the polymer, meaning that polymer effect overpowers any TT

response. After 48hours stimulatory polymer conditions were found to proliferate less when DCs were cultured with TT, which is a disconnect from the IFNg secretion data, where there was no difference seen after 48hrs. After 72hrs every condition with TT proliferated at similar level or less than the non TT condition. The presence of TT does not seem to have an impact on IFN-g production over the polymer, indicating that the stimulatory polymers in conjunction with TT do not show a combinatorial effect. Interestingly, THFuA and ZnA conditions show a significantly increased IFNg secretion after 72hrs, when DCs were cultured with TT. At 48 hours this effect is not yet visible.

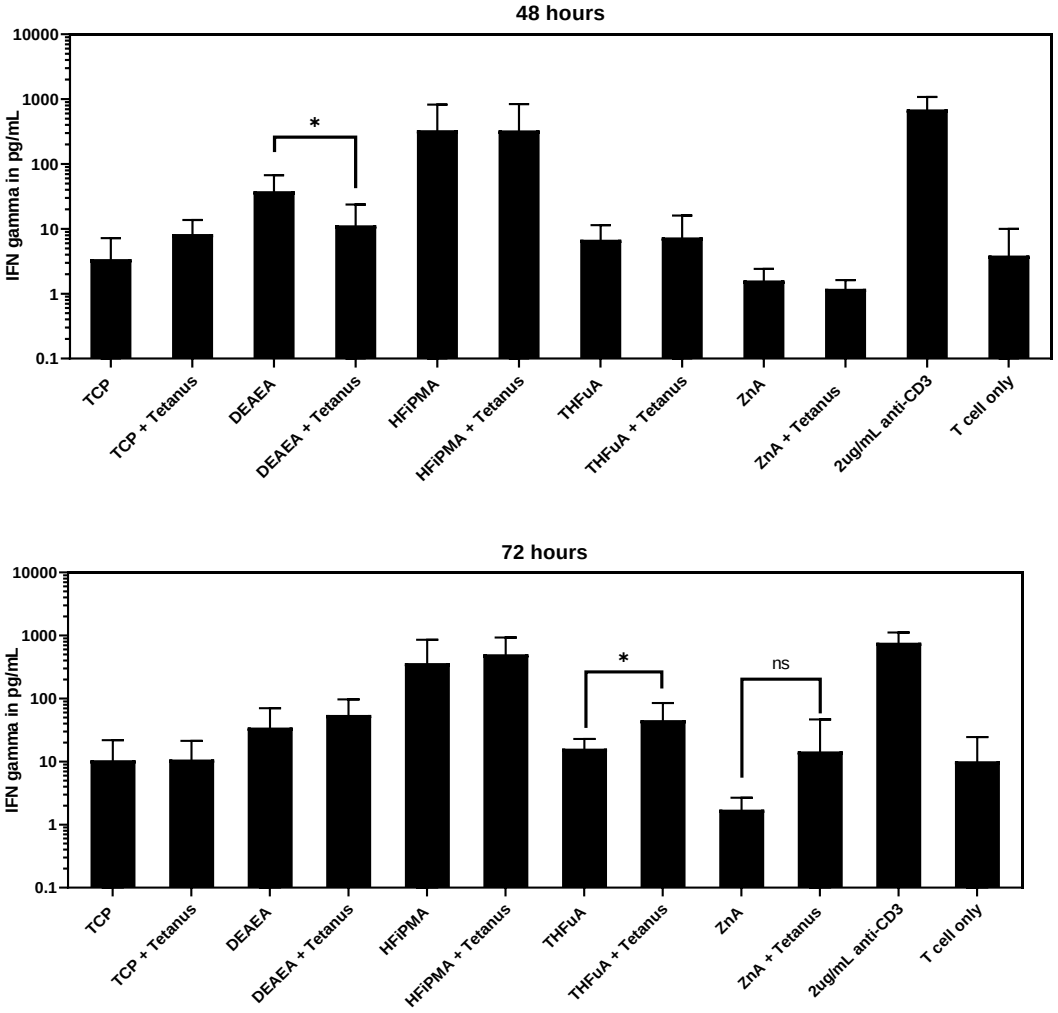


Figure 4-29: Polymer treatment influences interaction of DCs with memory T cells and modulates their IFN-γ secretion

Autologous memory T cells were co cultured with polymer treated DCs for 48 and 72 hours. The secretion of IFN-γ was measured by DuoSet ELISA. Data is from 3 independent biological donors, with 4 technical repeats each. TCP – tissue culture polystyrene. Statistical analysis was performed using one-way ANOVA with Dunnet's post hoc multiple comparison tests and is shown as * p< 0.05, ** p<0.01, *** p < 0.001 and **** p < 0.0001.

4.3.6 **Tumour killing assay**

Following the results of the T cell co-cultures, as well as the promising indications of the gene array, I looked at whether stimulatory polymer cultured

DCs are able to induce tumour specific cytotoxic T lymphocytes (CTLs), as this will determine whether they are good candidates for cancer immunotherapy. For this, DCs were cultured on flat polymer coatings for 24 hours, followed by addition of MCF7 (a breast cancer cell line) cells that have been rendered non-proliferative by mitomycin c (MMC) for another 24 hours. These DCs were then co-cultured with autologous naïve CD8 T lymphocytes for 8 days in a 1:10 ratios (DC: T cells). Every 2-3 days 100µl of cell culture media was removed and substituted with fresh media containing 200 IU/mL IL-2. Proliferated tumour specific CTLs were then seeded on MCF7 monolayers for 6 hours in differing ratios (1:5 to 1:20) and assessed for the ability to kill MCF7 cells. Representative images of the MCF7 monolayer after 6hours culture can be seen in Figure 4-30: .

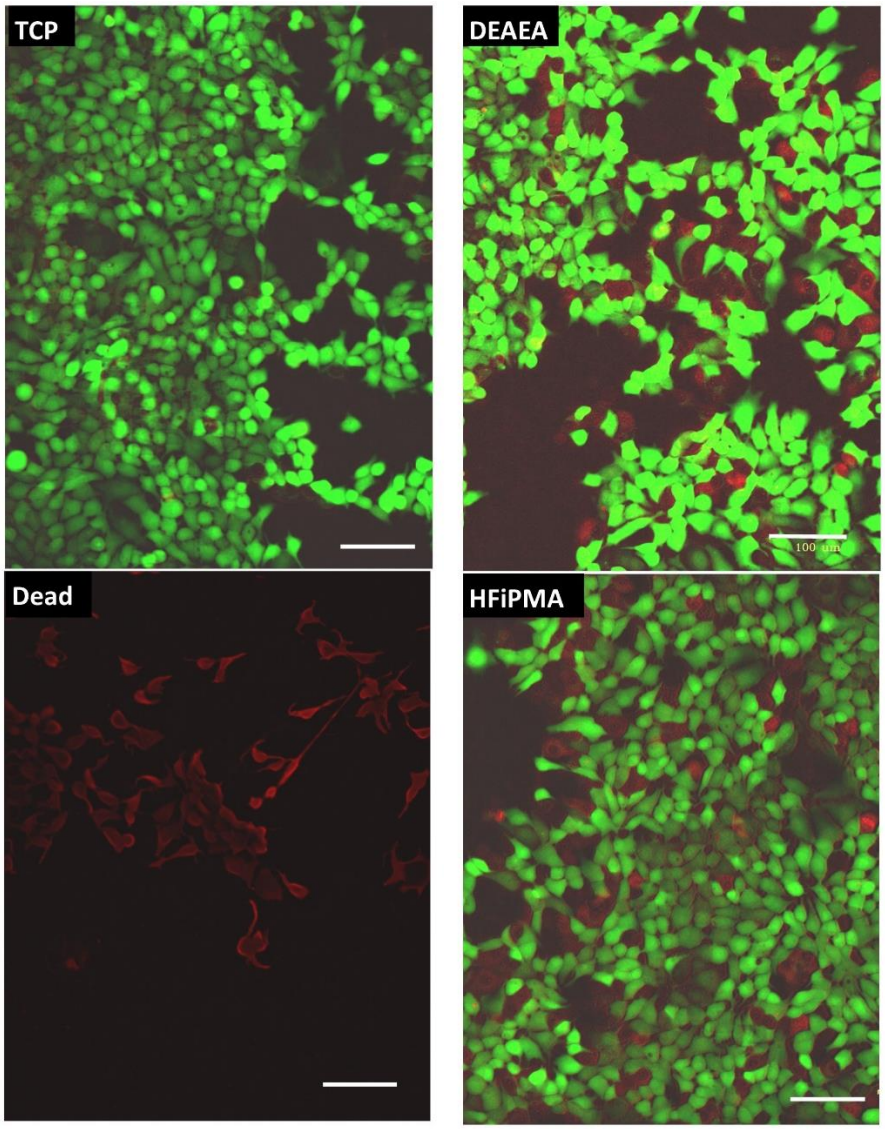


Figure 4-30: MCF7 monolayer shows dead cells after CTL-coculture

DCs were first cultured on polymer coatings, then co-cultured with naïve CD8 T cells to generate CTLs. CTLS were then seeded on MCF7 monolayers for 6 hours. Images are representative of 4 independent experiments. MCF7- were stained by CalceinAM (CaAM) and ethidium homodimer-1 (EthD-1) to determine live/dead cells. CaAM stains alive cells (green) and EthD-1 (red) stains dead cells. (scale bar = 100 µm).

Culturing the CTLs for 6hrs on the MCF7 monolayer showed, that stimulatory polymer conditions induced CTLs are significantly more efficient in killing MCF7 cells than the TCP condition, as well as IFN-γ DC induced condition

(Figure 4-31). This is most prominent in the 1:5 ratio of MCF7 to CTLs but still indicates very high tumour killing at the 1:20 ratio. Highest tumour killing measured at 1:20 was 73% dead MCF7 cells.

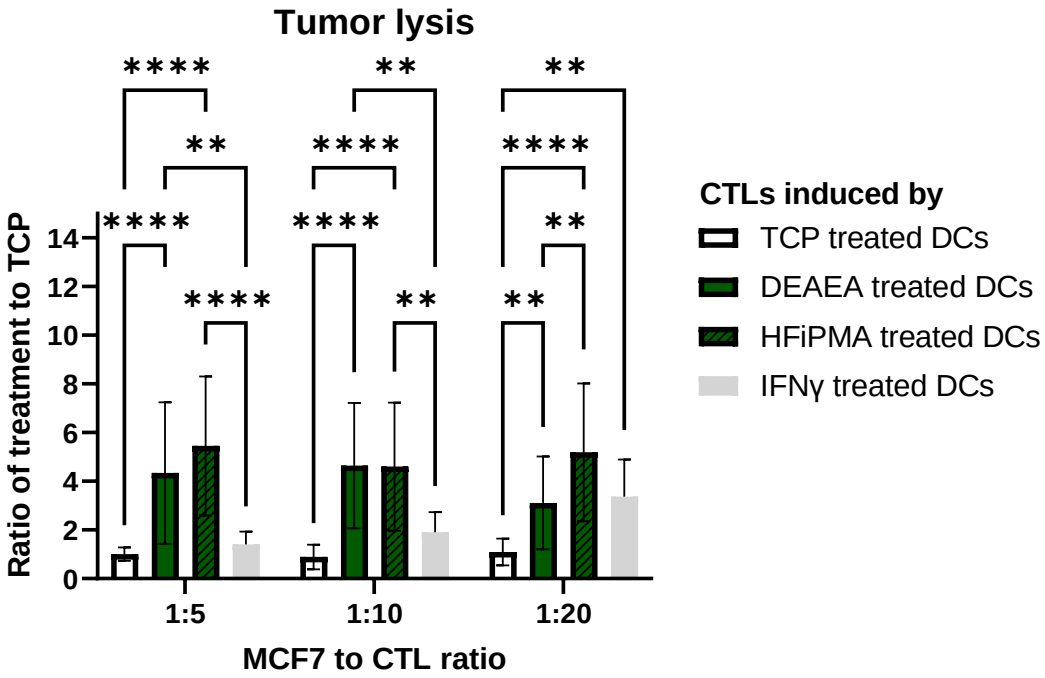


Figure 4-31: Tumour specific lysis is increased ratio-dependent in conditions where DCs were conditioned on polymers

Specific lysis is measured by dividing dead/total cell numbers for each condition in at least 2 images per well (2 technical replicates each). Lysis is normalised per donor and per ratio for better comparison. n=4 with 2 wells per condition and at least 3 ROIs per well. Statistical analysis was performed using one-way ANOVA with Dunnet's post hoc multiple comparison tests and is shown as * p< 0.05, ** p<0.01, *** p < 0.001 and **** p < 0.0001.

4.3.7 **Immunomodulatory properties of ZnA**

The regulatory polymer ZnA was in earlier chapters shown to induce a less mature DC phenotype, even in the presence of LPS. There have already been studies about the effect of soluble Zinc (and $ZnSO_4$) on macrophages and DCs

[223]–[226]. Zinc supplementation induces tolerogenic DCs and skews the T cell balance between Th17 and Tregs, with increases of Tregs [224]. In another study, $ZnSO_4$ supplementation induced Tregs in animal models [223]. Zinc homeostasis has previously been found to be essential for adequate immune functions. Zinc deficiency has been documented to lead to several immune disorders. Earlier studies have attributed zinc administration (at physiological doses) a beneficial effect in autoimmune diseases like multiple sclerosis, allergies, or graft versus host disease. In addition, zinc mediates the stability of Foxp3, which can be inhibited by the transcription factor IRF-1 and the induction of KLF-10 [227].

ZnA cultured DCs showed lower HLA-DR expression levels than TCP cultured DCs, which becomes more apparent with the addition of LPS to both systems. For ZnA + LPS the HLA-DR levels were significantly reduced compared to TCP+ LPS (Figure 4-32). The expression of programmed death ligand 2 (PD-L2) was significantly increased when cultured on ZnA (both without and with LPS stimulation).

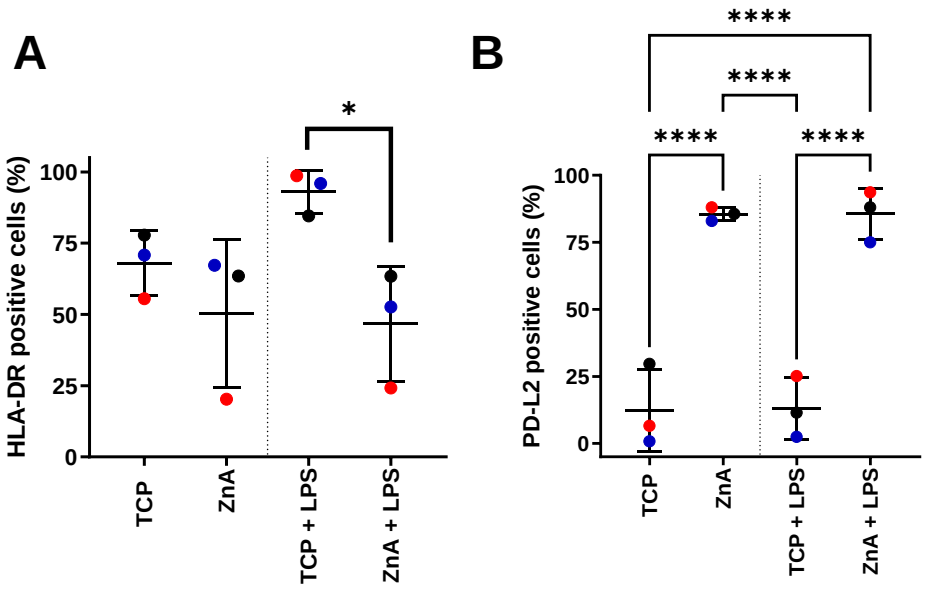


Figure 4-32: ZnA modulates HLA-DR and PD-L2 expression

DCs were cultured on ZnA for 24hours with and without LPS stimulation. Data is from 3 independent experiments with 10,000 events routinely acquired in each sample. TCP – tissue culture polystyrene, and data is presented as mean ± SD. Donor were colour coded for better visualisation. Statistical analysis was performed using one-way ANOVA with Dunnet's post hoc multiple comparison tests and is shown as * $p< 0.05$, ** $p<0.01$, *** $p < 0.001$ and **** $p < 0.0001$.

Indoleamine 2,3 dioxygenase (IDO) is a tryptophan degrading enzyme that has been implicated in inducing T cell tolerance. IDO was significantly modulated after DC culture on ZnA coatings. ZnA culture alone increased IDO activity nearly 6 times above the level of TCP culture, which is highly significant. Addition of LPS stimulation showed a less dominant but significant difference between TCP and ZnA (Figure 4-33).

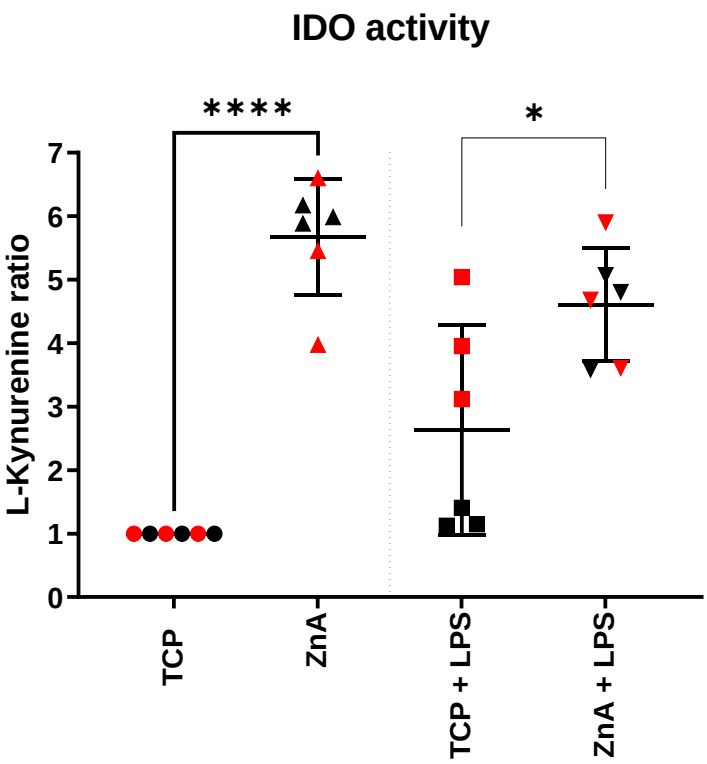


Figure 4-33: ZnA treatment increased IDO activity

DCs were cultured on ZnA for 24 hours in the presence of tryptophane. Cell supernatant was used to measure kynurenine production using a colorimetric assay; known standard concentrations were used to establish a standard curve. Values are the mean of triplicate wells ± SD. Data is representative of 2 independent experiments that are colour coded. Statistical analysis was performed using one-way ANOVA with Dunnet's post hoc multiple comparison tests and is shown as * p< 0.05, ** p<0.01, *** p < 0.001 and **** p < 0.0001.

4.4 Discussion

The polymers characterised in this chapter offer a novel, cytokine-free DC modulation that is entirely based on polymer properties. This presents several advantages over cytokine based therapies, as cytokine-monotherapies are known to have low response rates and have high toxicities associated with them [76], [77]. To better understand these effects, the material characterisations studied in this chapter give indications of how DCs could potentially be modulated by the polymers surface characteristics. Stimulatory polymers were shown to be stiffer and had a thinner bio-adsorbate layer, with regulatory polymer being softer with a thicker bio-adsorbate layer [174], [228]. A recent study on polydimethylsilaoxane (PDMS) hydrogel-coated plates have indicated similar effects on DCs, where stiffer materials (although only in kPA range) induced pro-inflammatory DC responses as well as increased DC metabolic activity [173], [229] which is comparable to the effect of the stimulatory polymers observed here.

As the polymers from the library used here have not been widely used or investigated in context with biomedical applications, not much information is known about their effects on (immune) cells as well as their chemical characteristics. In a separate study, the same library was used to research their effect on macrophage attachment and polarisation. In that study, DEAEA was identified as a pro-attachment polymer for macrophages [230]. Ultimately, this polymer was not investigated further but might be of interest for additional macrophage studies.

Two stimulatory polymers were identified which activate DCs and downstream T cell response as evidenced by higher pro-inflammatory cytokine secretion, as well as non-significant increases of CD80, HLA-ABC and DEC-205. The global effects of the stimulatory polymers on DC gene expression corroborated earlier phenotype data, as we all as gave reason to believe that stimulatory polymer cultured DCs are more efficient in inducing T cell activation, proliferation, and as well as tumour specific CTLs. The functional data once more corroborated results from the gene microarray study reported in this chapter. The gene array study showed that HFiPMA cultured DCs were very distinct from TCP cultured iDCs by a large number of uniquely expressed genes, and more similar to TCP + LPS cultured mDCs than the other stimulatory polymer DEAEA. Both stimulatory polymers gave indications for enhanced DC-T cell interactions by upregulating genes such as MYOG1, as well as other genes related to T cell signalling. At the same time, genes relating to cross presentation (NCF1) were upregulated which predicts the increased ability to induce CTLs and other anti-tumour genes (CXCL8 and IL2RA), which the functional data corroborated. NCF1 expression has been shown to be required for activation and effector function of CD8+ Tcells in other studies, agreeing with data presented here [198].

In summary, the gene array study in this chapter confirmed that stimulatory polymers significantly activated DC maturation, adaptive immune responses, as well as antigen presentation (in particular cross presentation pathways). Additionally, HFiPMA showed upregulated genes that are specifically involved in DC maturation and NFκB signalling. There seem to be some mixed

responses in integrin signalling, requiring further in-dept studies to elucidate how integrin signalling is modulated (e.g., ITBG8 is highly upregulated, however it is mainly involved in the induction of tolerance, which has not been observed here). The generated data from this microarray study is vast and only a snapshot of its size is presented in this study, therefore, further work can reveal more information comparing polymer cultured DCs in the future. A phenotype classification study mainly focused on murine DCs, ran a data mining protocol to elucidate specific genes that can determine an inflammatory phenotype validated their findings in human DCs and found CD40 and Socs3 to be master genes of activation/inflammation in DCs [231]. Both CD40 signalling and IL12b expression were found to be upregulated in DEAEA and HFiPMA-cultured DCs, which agrees with the literature that these two genes might serve as molecular markers for DC activation. Therefore, I conclude that many of the functional and phenotypical observations are proven by the microarray data, e.g., increased DC maturation, T cell crosspriming, T cell activation and anti-tumour responses.

The tumour killing data showed that stimulatory polymer cultured DCs, that were used to prime naïve CD8+ T cells, were more efficient than TCP cultured DCs to induce CTLs, even more so at an increasing ratio of effector to target cells. The stimulatory polymers were comparatively more efficient in % of killed tumour cells than several approaches described in the literature (such as antigen pulsing or conjugation of antigen to virus-like particles) [232], [233]. Thus, it can be concluded that the findings here provide rationale for the stimulatory polymers to be tested *in vivo* for their ability in developing anti-

tumour responses in an animal model. The next step in this process will be the development of a deliverable format of those polymers for application *in vivo*. Examples of this could be macroporous scaffolds or particulates, which have already found application in acute myeloid leukaemia and breast cancer [144], [234]. Another possible application for these polymers could be particulates that can be used as adjuvants for vaccinations.

The regulatory polymer ZnA was found here to portray several indicators of a tolerance inducing material with lower T cell activation and proliferation. On a phenotypical level, ZnA downregulated HLA-DR and HLA-ABC expression, as well as increased IDO activity and PD-L2 expression. Thus, induction of tolerogenic DC by ZnA appears to be a promising strategy of modulating immune responses to biomaterials to improve biocompatibility. Zinc has previously been found to modulate the adverse immune responses in transplantation, and is crucial in the homeostasis and optimal function of the innate and adaptive parts of the immune system. Other materials such as $ZnSO_4$, 10-Hydroxy-2-Decenoid acid have shown the same phenotypical modulation in the literature[235]. In agreement to my observations of ZnA culture of DCs, the same phenotype modulation were seen by ZnSO4 culture (dimished MHC II and increased PD-L1/L2 expression with elevated IDO activity). Intruigingly, LPS stimulation was also found to be dimished in the ZnSO4 addition study. Overall, it can be assumed that ZnSO4 and ZnA have similar, if not the same effect on DC function and phenotype. In an in vivo studythe induction of T_{regs} cells and dampening of the pro- inflammatory immune response was observed. The mechanism of which Zinc modulates DC

phenotype remains largely unknown [224]. Understanding the complex immune modulation by zinc may establish zinc as a new therapeutic tool in transplantation medicine and autoimmune disorders. The connection between uptake of $ZnSO_4$ in the study mentioned, and the outside-in signalling found here with ZnA, is still elusive. ZnA could become of high interest, as combined zinc and immunosuppressive therapy seem to be greatly beneficial, due to their ability to induce immune tolerance without completely abrogating antigenic immune defence. This might guarantee exceeded long-term graft survival, and hence is a topic of broad interest, which warrants further investigation of the polymer.

Recent research on MyD88 and TLR knock out mice demonstrated that DCs use TLR-2, -4, and -6, as a response to a group of chemically and physically diverse biomaterials. Mice lacking any of these TLRs, or MyD88, showed impaired expression of activation markers and reduced production of pro-inflammatory cytokines relative to the wild-type controls [139]. An explanation for the modulatory ability of polymers would be that their surface presents itself as ligands to TLRs expressed on DCs. It is highly likely that surface properties do not directly influence immune cell response and rather, that these surface properties can alter the composition, conformation and concentration of proteins adsorbed on surfaces – and the immune cells then react to changes of protein adsorption on varying surfaces. Through XPS analysis, the regulatory polymer identified here was shown to significantly adsorb more proteins than both stimulatory polymers, which could easily be the source of polymer-dependant modulation of DC phenotype and function. DC

phagocytosis has been previously shown to be positively correlated with increased protein attachment to microparticles, and can be seen in agreement to data in this study on high endocytosis levels of DCs on ZnA coatings [236]t. In contrast to my findings here, a recent publication found thicker protein layers to relate more with pro-inflammatory M1 macrophages and thinner protein layers with anti-inflammatory M2 macrophages [174]. This could be attributed to the difference in cell type, but most probably is due to a difference in which proteins have adsorbed on the respective polymers. To elucidate which proteins specifically are adsorbed on these polymers, more assays, such as proteomics analysis, will have to be performed. Interestingly, the gene array data showed that TLR-1, -3, -4, and -6, were downregulated after DC stimulatory polymer culture, for which the reason is yet unknown.

This chapter further underlines the earlier assertion of stimulatory and regulatory polymers from chapter 3 and shows that the initial phenotype-based screen has successfully translated into functional DC modulation. This work may provide the basis for further development of deliverable formats, such as 3D particulates and macroporous scaffold systems to evaluate the capability of materials *in vivo* for clinical applications mainly for immune stimulation in cancer settings, but also to further investigate the feasibility of the regulatory polymer in autoimmune settings.

Chapter 5: From 2D to 3D structures – polymeric scaffolds as new tools for immunomodulation

Chapter 5 From 2D to 3D structures – Polymeric scaffolds as new tools for immunomodulation

5.1 Introduction

In situ cell modulation requires a highly defined microenvironment to control cell behaviour. Three dimensional (3D) scaffolds might be ideal for this purpose. 3D biomaterials, such as scaffolds have been a focus due to their use in controlled drug and cell delivery. They have also been developed for tissue regeneration to act as a template for new growing tissues. These templates (are often used as biological substitutes) aim to restore, maintain or improve tissue function [237], [238].

Macroporous scaffolds essentially act as a template for tissue formation and are typically seeded with cells and occasionally growth factors, or chemokines that provide a chemokine gradient upon implantation to recruit immune cells. These cell-seeded scaffolds are either cultured *in vitro* to synthesize tissues which can then be implanted into an injured site, or are implanted directly into the injured site, using the body's own system, where regeneration of tissues or organs is induced *in vivo*.

Several criteria are important for scaffold suitability in tissue engineering. They need to be biocompatible and allow cells to adhere, migrate through and function normally. This leads to another criteria: scaffold architecture. The architecture, specifically the pore structure is important as pores must be interconnected and the system altogether highly porous. This allows cellular

penetration, but also more importantly the adequate diffusion of nutrients (such as oxygen or nitrogen) to and from cells situated within the scaffold construct. On a similar topic, only a porous interconnected structure allows the diffusion of waste products out of the scaffold [239], [240]. Pores need to be large enough for cells to migrate through the structure, but small enough to establish efficient binding of a critical number of cells to the scaffold [241]–[243]. In this sense, a critical range of pore size exists for each scaffold system, depending on cell type being used and application required [244], [245]. A study into porous implants demonstrated that the minimum pore size for significant bone growth is 75 – 100 µm with an optimum around 100 – 135 µm [246], [247]. Many different methods of fabrication are able to produce scaffolds: solvent casting & particulate leaching, gas foaming, freeze drying, nanofiber self-assembly, electrospinning and thermally induced phase separation [248].

As with scaffold architecture, the material it is made off also depends largely on the final application. Many scaffolds have been fabricated from the PLGA family of polymers. For example, tuning of the lactide/glycolide ratio has engineered scaffolds to be more inductive and conductive for cellular growth and tissue formation – especially for bone tissue engineering applications [249], [250]. Materials widely used for scaffold fabrication are generally immune – inert materials, the resulting scaffolds are then often loaded with immune modulating agents, such as cytokines or stimulating/modulating agents others [251], [252].

Due to their wide versatility, scaffolds have been used in many different settings. One of the main applications is bone growth induction. Immune-

mediated tissue regeneration is one of the main applications biomaterial's scaffolds have been used for. A study revealed, that bone – and muscle-derived tissue ECM scaffolds can induce a pro-regenerative response, that is characterized by an mTOR/Rictor-dependent T helper 2 pathway guiding IL-4 dependent macrophage polarisation [253]. A PLG scaffold has proven to support growth and proliferation of a pre-osteoblast cell line leading to mineralisation of the deposited collagen that increased over time and resulted in the formation of a 3-D tissue with architecture similar to native bone [254].

In another study collagen sponges implanted into rats with partial thickness, full thickness and full thickness infected wounds were found to promote cellular motility, which in turn lead to the infiltration of neutrophils and macrophages resulting in increased phagocytosis and decreased bacterial loads. The collagen sponges also led to vascularised granulation tissue being formed, which stimulated the formation of new granulation tissue and epithelial layers [255]. Bone marrow mesenchymal stem cells seeded on PLCL/Collagen nanofibrous scaffolds were shown to differentiate with the help of an induction cocktail into neuronal cells, which also adds therapy of neurodegenerative diseases on the list of scaffold applications [256].

In an earlier study, the phenotype of DCs upon seeding the cells on PLGA or agarose scaffolds was examined [128]. It was found that, similar to treatment of DCs with the film versions of these polymers, DCs seeded on PLGA scaffolds displayed a moderately mature phenotype with dendritic processes, elevated expression of maturation markers and increased secretion of pro-inflammatory cytokines to the level similar to cells treated with PLGA films,

while the agarose scaffold did not induce DC maturation [128]. It was also found that biomaterial scaffolds engineered with an authentic lymphoid microenvironment allow DC migration and interaction with T-cells, which represents a promising strategy to create ectopic lymphoid tissue [142].

High-aspect-ratio mesoporous silica rods that are injected and self-assemble *in vivo* form macroporous structures that provide a 3D cellular microenvironment for host immune cells, specially DCs [257]. This murine study presented substantial DC infiltration into the scaffold construct, while also stimulating the infiltrated DCs via the scaffold–loaded inflammatory agents and adjuvants. As a result, a consistent induction of an adaptive immune response of Th1, Th2 and even CTLs was observed, suggesting that these scaffolds can serve as a multifunctional vaccine platform.

In more recent DC scaffold work David Mooney developed PLG scaffolds that were loaded with GM-CSF and tumour antigens to first recruit DCs and present easily accessible antigens [143]. These scaffolds were shown to be stimulatory for DCs and induce anti-tumour immune responses. In another study crosslinked methacrylated PEG and methacrylated alginate was prepared into macroporous scaffolds, which were then loaded with GM-CSF, CpG-ODN (a toll-like receptor (TLR) ligand), and tumour antigens [144]. With this, a biomaterial-based acute myeloid leukaemia (AML) vaccine was developed, which demonstrated to induce robust immune responses against AML and was able to prevent AML engraftment in a prophylactic study [144]. This approach of *in vivo* DC modulation is thought to improve poor functionality and the low persistence of DCs. In DC-based immunotherapies against cancer, DCs are

usually isolated from the patient and are treated with tumour antigen and other activating agents *ex vivo* to be later transferred back into the patient, with the goal of inducing strong antigen-specific anti-tumour immune responses. In the past, this has proven to be successful, albeit the clinical efficacy was low due to decreased DC persistence and their poor functionality [145]–[147].

In this chapter the previously identified stimulatory polymer HFiPMA was fabricated into macroporous polymeric scaffolds to act as a proof-of-concept study for the feasibility of translatability of DC modulatory effect from coating to 3D scaffold. Pore size optimisation, as well as initial DC viability and cytokine secretion are being presented.

5.2 Methods

5.2.1 Scaffold fabrication

Scaffolds were fabricated by first UV polymerising HFiPMA in a polypropylene well plate and then scraping off the polymer. The scraped of HFiPMA was then dissolved in 1,4 – dioxane at specific weight percentages and frozen in a Nalgene™ Cryo 1°C Freezing Container (Mr Frosty™) in either -20° or -80°C freezer. The frozen mix was then freeze dried overnight.

A 6 mm biopsy punch was utilised to punch out reproducible sized circular scaffold wafers for cell culture.

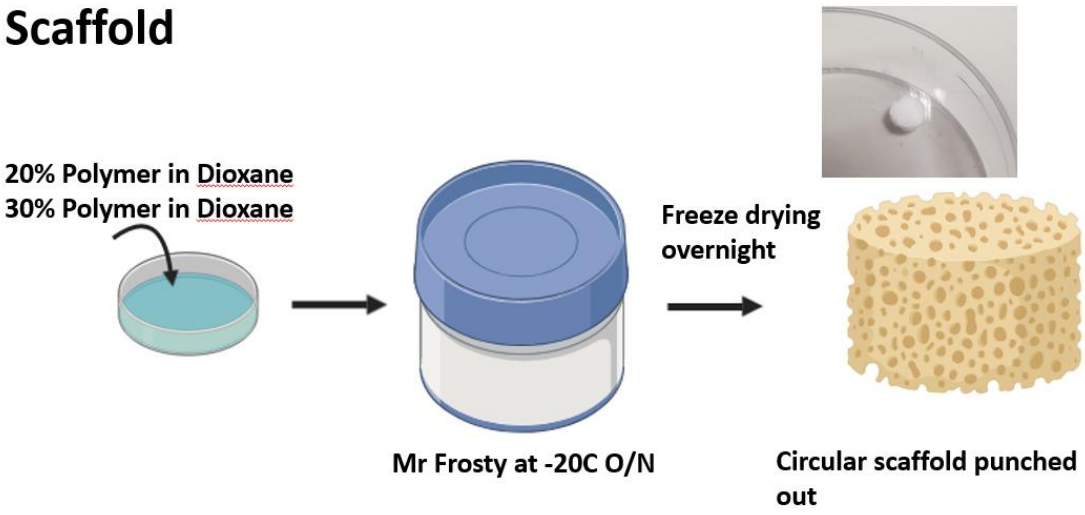


Figure 5-1 Methodology of scaffold fabrication

Scaffolds were produced by dissolving polymer in 1,4-dioxane, poured into 35mm petri dishes and frozen at -20°C. Frozen petri dishes were then freeze dried overnight and following the freeze-drying step the scaffolds were finished. Figure generated in Biorender.

5.2.2 **Monocyte isolation**

Monocytes were isolated from buffy coat as described in general methods section 2.2 and differentiated into DCs as described in section 2.2.1.

5.2.3 **Viability assay**

Viability was assessed by ToxiLight ®. ToxiLight is a non-destructive bioluminescent cytotoxicity assay that measures the release of adenylate kinase (AK) from damaged cells. AK is present in all cells and loss of cell integrity, through damage to the plasma membrane, results in the leakage of a number of factors from cells cultured into the surrounding medium. For the assay ADP is added as a substrate of AK. When AK is present the ADP is converted to ATP for assay by bioluminescence.

$$Mg^{2+}\ ADP + ADP \leftrightarrow Mg^{2+}\ ATP + AMP$$

The bioluminescence utilises the enzyme luciferase, which catalyses the formation of light from ATP and luciferin. Combining these two reactions the emitted light is linearly related to the AK concentration.

5.2.4 **Cell culture**

Scaffolds were UV sterilised and pre-soaked with complete media before seeding 5 x 10^5 DCs per scaffold and culturing 24 hours.

5.2.5 **ELISA**

Cytokine production was measured as described in section 2.2.2.

5.2.6 **SEM**

Samples were air dried, mounted to SEM stubs affixed with carbon tabs and gold coated via a polaron E5175 sputter coater at 2.2 Kv for 90 seconds. Samples were loaded into and imaged with a JEOL 770 SEM at 10Kv with a 10 mm working distance under high vacuum.

5.2.7 **Statistical analysis**

All graphs were prepared, and all statistical analysis was carried out using Prism 8 (GraphPad software, Inc., USA). Student T-test or one-way-ANOVA and multiple comparisons post-tests were performed and are stated below each graph.

A p value $p<0.05$ was considered statistically significant. For significance: *<0.05; **<0.01; ***<0.001; ****<0.0001.

5.3 Results

To fabricate polymeric macroporous scaffolds several methods of fabrication were attempted. The experimental methodology that worked for HFiPMA was a modified version of the ice-templating process [250]. The UV polymerised polymer was prepared at varying weight percentages (dissolved in 1,4 dioxane), poured into a 35 mm petri dish and frozen in a Mr Frosty (gradient freezing inducer) inside the freezer for 24 hours, followed by overnight freeze drying. Afterwards, polymer scaffold wafers were punched out with a 6 mm biopsy puncher to have comparable size between scaffolds.

5.3.1 Optimisation of pore size

To optimise scaffold fabrication and size of pores, different weight percentages and freezing temperatures were compared for their effect on pore size development.

To analyse pore size, fabricated scaffolds were punched into 6mm wide discs using a biopsy puncher, cut horizontally and vertically with a scalpel, and both the surface and the inner sections were imaged by SEM. The size of pores was determined manually in ImageJ (each pore was measured for their minimal and maximal axis length). To determine the impact of freezing temperature, scaffolds were fabricated according to previously described methodology with freezing temperature used -20°C or -80°C. Scaffolds that were frozen at -20°C developed larger pore sizes than to -80°C (see Figure 5-2). The freezing temperature of -80°C had a gradient increase of pore size with a decrease of polymer weight percentage used. Freezing at -20°C

however showed a spike in pore size at 25%$_{wt,}$ while both 20%$_{wt}$ and 30%$_{wt}$ had smaller pores, with 30%$_{wt}$ having the smallest pores. Altogether pore size ranged between 22 µm for 30%$_{wt}$ at -80°C and 65µm for 25%$_{wt}$ at -20°C.

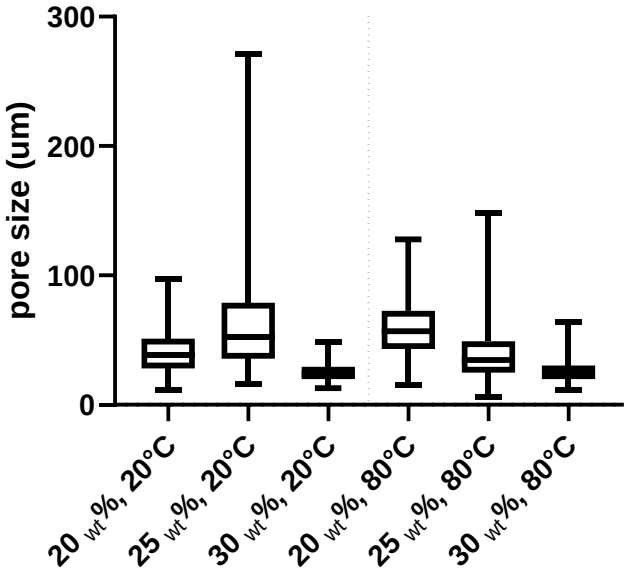


Figure 5-2: HFiPMA-Comparison of pore size between different weight percentages and freezing temperatures

Scaffolds from 3 different fabrication days, 30 < N < 250 pore measurements per scaffold, pores measured via ImageJ both in minimal and maximal axis.

Due to published findings on the effect of pore size on DC activation the 20%$_{wt}$ (41 µm) and 30%$_{wt}$ (25 µm) frozen at -20°C were chosen to go forward, due to their small and very consistent pore size. The process was shown to be reproducible with limited variation between different fabrication days (Figure 5-3).

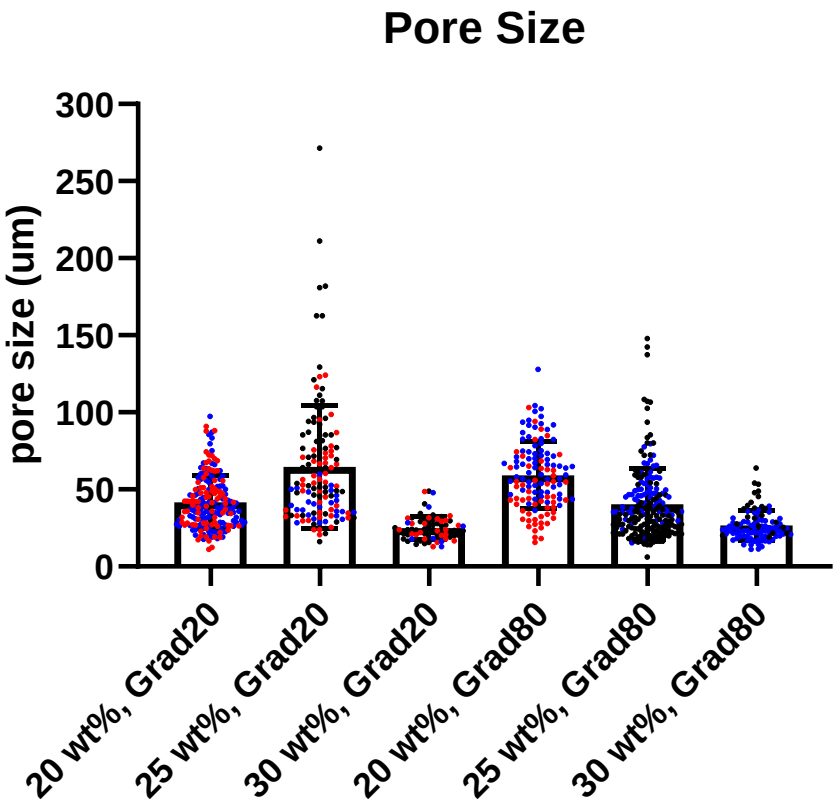


Figure 5-3: HFiPMA-scaffolds comparison between fabrication days

Scaffolds are from 3 different fabrication days, 30 < N < 250 pore measurements per scaffold, pores measured via ImageJ both in minimal and maximal axis. Colour coding for different fabrications days of scaffolds. Each dot represents one measurement.

Representative SEM images of both chosen scaffolds are shown in Figure 5-4.

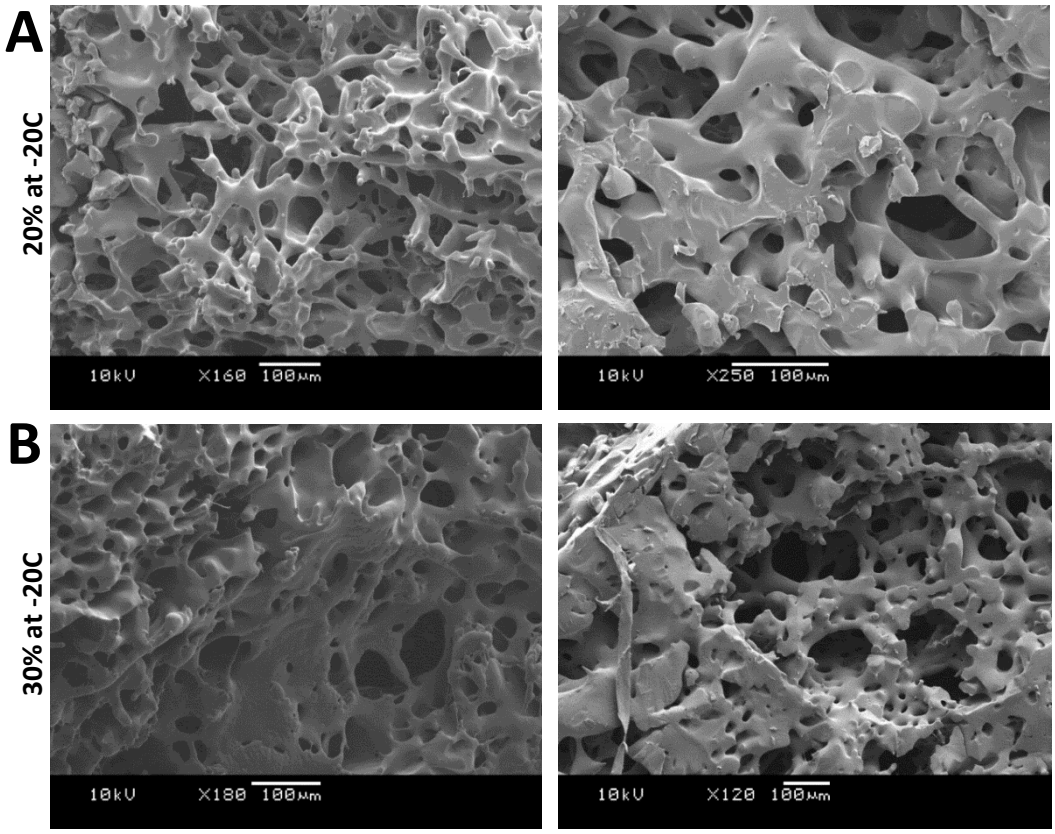


Figure 5-4: Representative images of HFiPMA scaffolds by SEM

Two representative images from scaffolds fabricated on different days. Scale bar is 100um and images were taken on a JEOL 770 SEM machine. A is 20%$_{wt}$ at -20°C freezing temperature, B is 30%$_{wt}$ at -20°C.

5.3.2 HFiPMA scaffold did not negatively impact DC viability

Immature DCs were seeded onto the HFiPMA scaffolds and cultured for 24 hours. Viability after 24 hours was not significantly decreased when compared to the TCP culture condition control (Figure 5-5). Interestingly the viability of DCs cultured with the scaffold was increased compared to TCP.

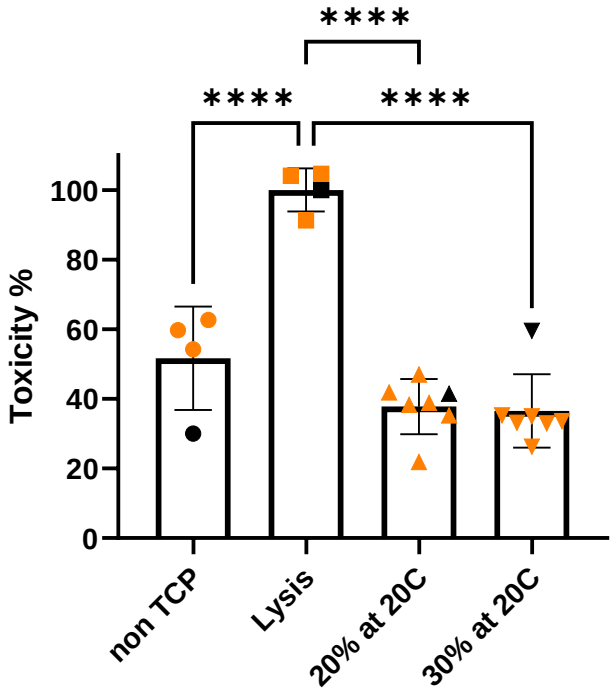


Figure 5-5: Impact of HFiPMA scaffolds on DC viability

Scaffold toxicity measured by ToxiLight assay. Data is from 2 biological donors with 2 scaffolds per donor. Donors are colour coded and each donor normalised to lysis maximum baseline. Statistical analysis was performed using one-way ANOVA with Dunnet's post hoc multiple comparison tests and is shown as * p< 0.05, ** p<0.01, *** p < 0.001 and **** p < 0.0001.

5.3.3 DCs cultured in HFiPMA scaffold increase cytokine secretion

To determine whether HFiPMA was still bioactive after transformation into a 3D construct, iDCs were seeded onto the scaffolds for 24 hours. The media was then used for cytokine analysis by ELISA.

Both scaffolds increased TNF-α levels in the media above the TCP control (Figure 5-6), with the smaller pore size (30_{wt}%) inducing more TNF- α secretion than the bigger pore size (20_{wt}%).

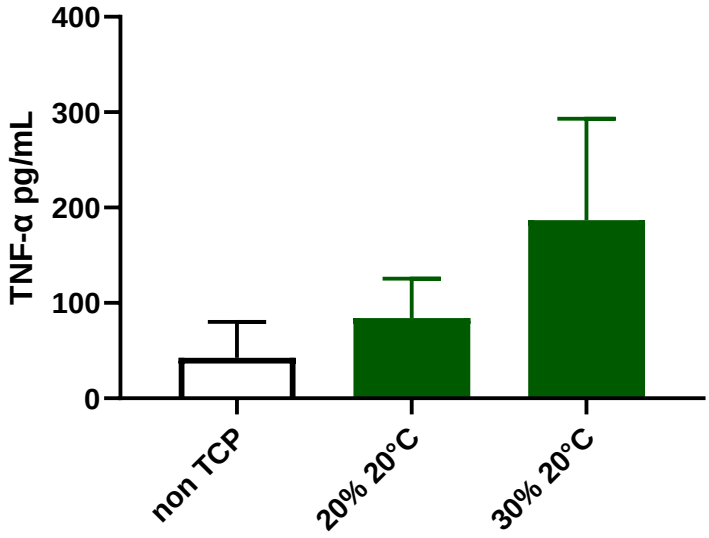


Figure 5-6: TNF-α secretion within scaffolds

Immature DCs were cultured in the scaffolds for 24 hours on. Experimental conditions are compared to the TCP iDC control. Data is from 2 independent experiments with 2 technical repeats each and data presented as mean ± SD.

Similar behaviour was observed for IL-1β (Figure 5-7), with the smaller pore size inducing higher pro-inflammatory cytokine secretion than bigger pores, but both scaffolds higher then non detectable TCP levels.

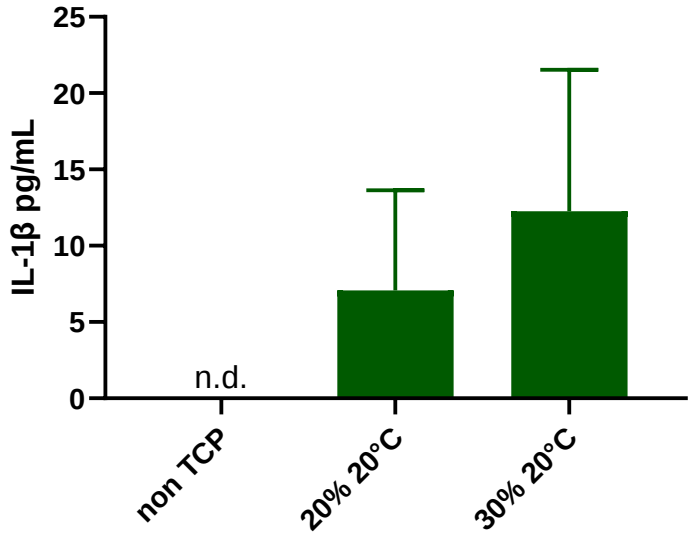


Figure 5-7: IL-1β secretion within scaffolds

iDCs were cultured in the scaffolds for 24 hours on. Non-TCP iDC condition had non-detectable IL-1β secretion levels. Data is from 2 independent experiments with 2 technical repeats each and data presented as mean ± SD.

Scaffolds induced significantly higher IL-6 secretion than the TCP condition (Figure 5-8), with the bigger pore size inducing 140 pg/mL and the smaller pore size inducing 120 pg/mL IL-6 secretion.

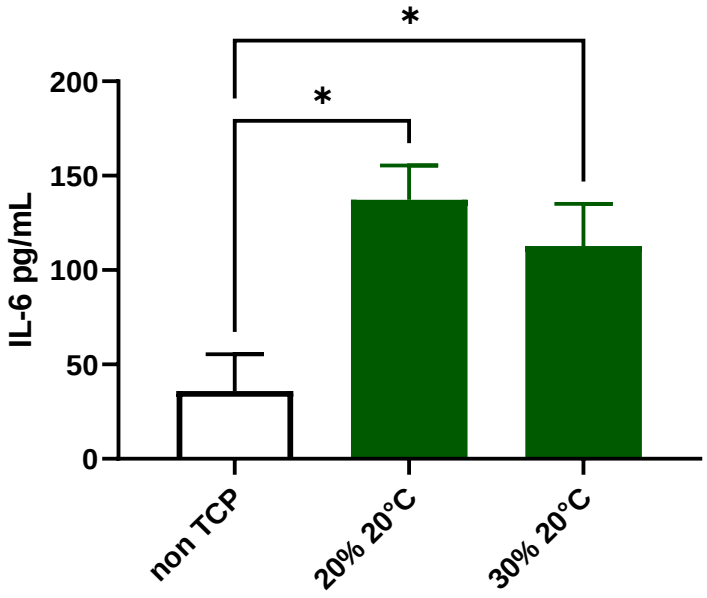


Figure 5-8: IL-6 secretion within scaffolds

Immature DCs were cultured in the scaffolds for 24 hours on. Experimental conditions are compared to the TCP iDC control. Data is from 2 independent experiments with 2 technical repeats each and data presented as mean ± SD. Statistical analysis was performed using one-way ANOVA with Dunnet's post hoc multiple comparison tests and is shown as * p< 0.05, ** p<0.01, *** p < 0.001 and **** p < 0.0001.

5.4 Discussion

Scaffolds for cell modulation have been used widely in the last years. Various fabrication methods were trialled in order to provide functioning scaffolds for all 3 hit polymers. HFiPMA was the only polymer that was able to be easily translated into a 3D scaffold due to several technical difficulties. DEAEA coatings were earlier found to be very thin and therefore could not be collected for scaffold fabrication. Therefore, to gain more polymer material DEAEA was tried to polymerise thermally. Several attempts were made with the thermal polymerisation of DEAEA, but low conversion rates and low yields unfortunately did not give enough polymer product to fabricate scaffolds.

With ZnA the initial technical issue was to dissolve the polymer, as it was not soluble in any of the solvents trialled. In the end a mix of acetic acid and water was able to dissolve the ZnA, but when the gel-like mixture was freeze-dried a very thin-walled scaffold with large inconsistent pores was produced that cracked on touch. This meant, that it was unable to be used for cell culture. Therefore, only HFiPMA was chosen to act as a proof-of-concept model, with plans to go back to the other two polymers in the future.

In contrast to earlier published studies about the effect of pore size on DC phenotype, where an optimal pore size of 40 µm was found to induce the highest level of DC migration and maturation, here a smaller 25 µm pore size was found to induce higher cytokine secretion levels than 41 µm pore size scaffold [258], [259]. A possible explanation of this could be the higher concentration of the polymer material included in the scaffold having a higher stimulator effect than the 20_{wt}% scaffold, although previous literature

hypothesied that smaller pore sizes might prevent DCs to infiltrate into the scaffold [259]c. On the other hand DC enrichment and actication was found to be increased on 20 µm pore scaffolds, so the throat size of the small pore assumeably not prevent DCs to infiltrate, and that maybe porosity in addition to pores could play a role in the level on infiltration and activation.Different to most other scaffold used in immune-therapy approaches, the scaffolds presented here were not loaded with bioactive agents (GM-CSF, a TLR 9 agonist, and tumour lysates) [260]. This means that the material used in this study is the sole source of the modulatory effect on DCs.

In Chen *et al.* different pore sizes were shown to have varying effects on DC cytokine secretion, whilst different scaffold materials also had an effect [259]. Scaffolds made from PDMS and pore sizes in 20 µm and 40 µm showed similar levels of TNF-α and IL-6 secretion. More TNF-α was secreted by 40µm pore sized scaffold seeded cells while IL-6 had higher levels in smaller pore size scaffolds. In general the Chen study showed that smaller pore size scaffold promoted more pro-inflammatory responses in both macrophages and DCs [259], which is in agreement to the cytokine data presented here. More DC phenotyping will have to be performed to determine the inflammatory phenotype of DCs infiltrated into the scaffolds.

The next steps in this project will be to validate the phenotype of the DCs within the scaffolds, followed by testing of T cell co-cultures which then hopefully would be validated in an animal model for cancer. Luckily HFIPMA is also the best performing polymer in the tumour killing assays, which means it would be

a great option to be used in an *in vivo* model for validating its effect for clinical use.

Chapter 6: Particulate systems – Is 2D effect of polymer coatings translated into 3D particulates?

Chapter 6 Particulate system - Is 2D effect of polymer coatings translated into 3D particulates?

6.1 Introduction

Biomaterial-based strategies to engineer the immune system have gathered widespread attention and have opened new avenues to modulate the immune system to fight cancer, be utilised in vaccine delivery or in the treatment of autoimmune diseases. Biomaterial particles are generated either on purpose or accidentally through wear and tear of implants. This wear debris has been found to induce acute inflammation of the surrounding tissue [72], [75]. Release of debris' particles and adsorption of host proteins initiate an inflammatory cascade upon phagocytosis by macrophages and have effect on osteoblasts.

Recently there has been a growing interest to utilise particles (either in nano or micro scale) with diverse size and chemistry in vaccine delivery, oncology, and autoimmune disease treatment. Not only the particle size has a critical impact on exerted functions and modulations but also particle shape [261]. The particle shape can influence the cellular uptake by immune cells, release of loaded immune-modulatory agents and also cell targeting. As such the surface properties of particles can significantly affect phagocytosis [262].

Microparticles in particular have been a fascinating area of research: They are small enough to be used as injectable drug delivery vehicles – which makes application easy as their high surface area allows surface functionalisation to

target specific cells, tissues or organs; and they can be loaded with a drug or fluorescent molecules [263], [264]. Systemic application requires particles of less than 500 nm in diameter, while for intramuscular application or oral delivery particles in diameter 1 µm to 125 µm can be utilised [264].

Commonly, PLGA, PLA, PGA have been used to fabricate microparticles and very often these microparticles were loaded with drugs for easier drug delivery. Due to PLGAs excellent biocompatibility and the ability to fine tune its monomer ratio to obtain varying degradation abilities, PLGA has been studied extensively for delivery of a range of biomolecules, including nucleic acids, proteins and peptides, and hydrophilic and hydrophobic drugs [265]. Fabrication methods range from single and double emulsion solvent evaporation, spray drying, gelation and more recently micro fluidics [266].

Microparticles have found application in various fields of research. With focus on DC modulation, Jamal Lewis and his research group have performed extensive research on loaded PLGA microparticles. Their attempt to present a dual-sized, microparticle “regulatory vaccine” that passively targets DCs for antigen-specific biomaterial immunotherapy of rheumatoid arthritis (RA) has proven successful in both *in vitro* and murine *in vivo* studies [135]. MPs were loaded with a DC chemoattractant, potent immunosuppressive molecule (1α,25-dihydroxycholecalciferol-Vitamin D3, TGF-β1 and/or GM-CSF) and an RA-relevant autoantigen to provide a multifaceted approach for the treatment of collagen-induced arthritis. Immunological assessment showed a decreased expression of CD80, CD86 and MHC-II on CD11c+ DCs in joint-associated lymph nodes. Additionally, a significant increase in $CD25^{+}FOXP3^{+}$ T regulatory

cells as well as PD-1 expressing $CD4^+$ T cells in joint-proximal lymph nodes and the spleen were found. Inflammatory cytokine expression (IL-6) was significantly decreased, while IL-10 mRNA levels were significantly increased. Similar routes of application of this MP system have shown great success for type 1 diabetes, multiple sclerosis, and autoimmune encephalomyelitis in murine *in vivo* models. For the diabetes model, phagocytosable ~1 µm and non phagocytosable ~30 µm MPs were used to deliver tolerance – promoting factors both intracellularly and extracellularly, in addition to type 1 diabetes autoantigen, and insulin to DCs [134]. This delivery was used to reprogram the immune response, remediated autoimmunity and was successfully shown to prevent the development of diabetes in 60% of animals in a murine model.

In a bid for smaller applications: Nanoparticles (NPs) and nanomedicine are a recent focus of regenerative medicine and biomaterial research. Nanoparticles are generally particles smaller than 1000 nm and can be theoretically produced out of any material. NPs are small enough to interact with DNA, while their small size also allows the much larger cells to uptake NPs.

Size determines how nanoparticles are distributed in the blood stream and also how well they are taken up by cells and especially regulates the mode of transportation within the cell [267]. A peak of particle circulation is achieved when particles are 30-300 nm big. Smaller particles < 20 nm are quickly cleared through kidney filtration and the ideal balance between prolonged circulation and desired biodistribution lies somewhere between 100-200 nm [268], [269]. Spherical nanoparticles may persist longer in the circulation due to their tendency to localize to the site of the fastest flow. This positions

spheroids toward the centre of the blood vessel, permitting minimum NP interaction with the vessel wall [270]. NPs larger than 200 nm tend to accumulate in the red pulp of the spleen, therefore presenting a perfect location for immune cell – NP interaction [271]. Generally, all NPs will eventually be taken up by phagocytes, which is mediated by classical non-specific internalisation pathways such as micropinocytosis, clathrin-mediated and caveolin-mediated endocytosis [272]. Another internalisation process is also via scavenger receptors by immune cells [273], [274].

The impact of NPs on the immune system (and specially on DCs) is yet to be fully understood. Studies investigating PLGA, Silica or PS NPs cultured with DCs have shown that particles of specific size and material modulate DCs in different ways [275]. Spherical silica and PLGA NPs between 100-160 nm size did not show any effect on DC phenotype and function, while same size particles made of PS and larger PLGA NPs induced significant changes in DC phenotype and function (respectively, suppression and upregulation of activation markers such as CD83) [275]. Another study revealed further, how hydrophobicity and functionalisation can enhance protein adsorption and this way influence nanoparticle interaction with DCs [276]. This elucidates the complex relationship between DC activation and polymer chemistry and functionalisation. It is known that serum proteins adsorb onto the surfaces of parenterally administered NPs and affect how NPs interact with DCs and the nature of the resulting immune response [276]. One of the downsides of NPs is the suspected negative impact they can have on health and environment, e.g. due to aggregation toxicity [277]. A prolonged presence and particularly

accumulation renders smaller NPs toxic to the host cells [267]. Recent advancements in nanoparticle synthesis have enabled surface functionalization of particles that mimic the diversity of ligands on the cell surface [278].

With flat coatings having a significant effect on DC phenotype and function the various identified polymers were attempted to be translated into NPs and MPs for proof-of-concept studies investigating particulate interactions with DCs.

In this chapter I present several proof-of-concept studies into particulate effect on DCs. Micron-sized particles that were fabricated by a collaborator were probed for their impact on DC viability, as well as for modulation of DC phenotype and cytokine secretion. Additionally, polymer were trialled to be fabricated into NPs with initial attempts presented here.

6.2 Methods

6.2.1 Monocyte isolation

Monocytes were isolated from buffy coat as described in general methods section 2.2 and differentiated into DCs as described in section 2.2.1.

6.2.2 Viability assay

Viability was assessed by ToxiLight ® as described in section 5.2.3.

6.2.3 Cell culture

DCs were cultures with MP at specific concentrations for 24 hours.

6.2.4 Microparticle fabrication

Microparticles were fabricated by collaborators at the Centre of Additive Manufacturing, as previously described [266]. In brief, the polymer microparticles were produced using a 100µm hydrophilic 3D flow-focusing microfluidic droplet generator, with the continuous phase as distilled water and the dispersed phase containing the monomer (1,6 hexanediol diacrylate, (HMDA)) with 2% w/v polymer surfactant (THFuA-co-MPEGMA, DEAEA-co-MPEGMA, and HFiPMA-co-MPEGMA)) and 1% w/v photoinitiator (2,2 dimethoxy-2-phenylacetophenone). The emulsions were then collected in distilled water and irradiated with UV light at 365nm.

6.2.5 Immunofluorescence staining

DC-MP culture was fixed with 4% PFA and the plates centrifuged after each staining step to prevent DCs and MP from being washed away. DCs were stained with anti-CD86 (mouse anti-human) primary antibody overnight and secondary (rabbit anti-mouse) Alexa 488 and DAPI on the next day. Images were acquired with a Zeiss LSM710 microscope (Carl Zeiss GmbH) with a 40x objective. Zen 2010 software (v6.0; Carl Zeiss GmbH) was used to capture images and for image stacks, slices were captured at 1-micron intervals. All data was processed using Image J (version 1.52p; Java 1.8.0_172 (64 bit)) and ZEN Zeiss LSM 700 imaging software.

6.2.6 Flow cytometry

DCs were detached from MPs by incubating the culture with TripleE for 20min. Cell-MP-mix was then filtered through a 30 µm filter mesh, allowing cells to pass through and leaving MPs behind. Wells were rinsed with PBS, and this was mix was filtered again. Cells were then stained for flow cytometer acquisition according to procedure described in section 2.2.3.

6.2.7 Single step nanoprecipitation

For the fabrication of NPs UV-polymerised polymers were scraped from polystyrene plates and dissolved in an organic solvent. Different volumes for the solutions and the addition rate can be seen in Table 12.

Table 12: Nanoparticle single step nanoprecipitation volumes and addition rates

Polymer	Weight	Organic Solvent	Vol organic solvent	Addition time	Aqueous phase	Vol aqueous phase
DEAEA	20 mg	Acetone	2 mL	135 sec	MilliQ H_2O	5 mL
HFiPMA	20 mg	Acetone	2 mL	160 sec	MilliQ H_2O	5 mL
THFuA	20 mg	Acetone	3 mL	160 sec	MilliQ H_2O	5 mL

The dissolved polymer-solvent mix was then dropwise added into a beaker filled with MilliQ water, that was continuously stirred at 1200rpm. The addition rate was specifically noted down as this can change the size of forming nanoparticles. The beaker was stirred continuously overnight in a chemical cabinet until the solvent evaporated. Formed NPs remained in water until analysis in ZetaSizer suite.

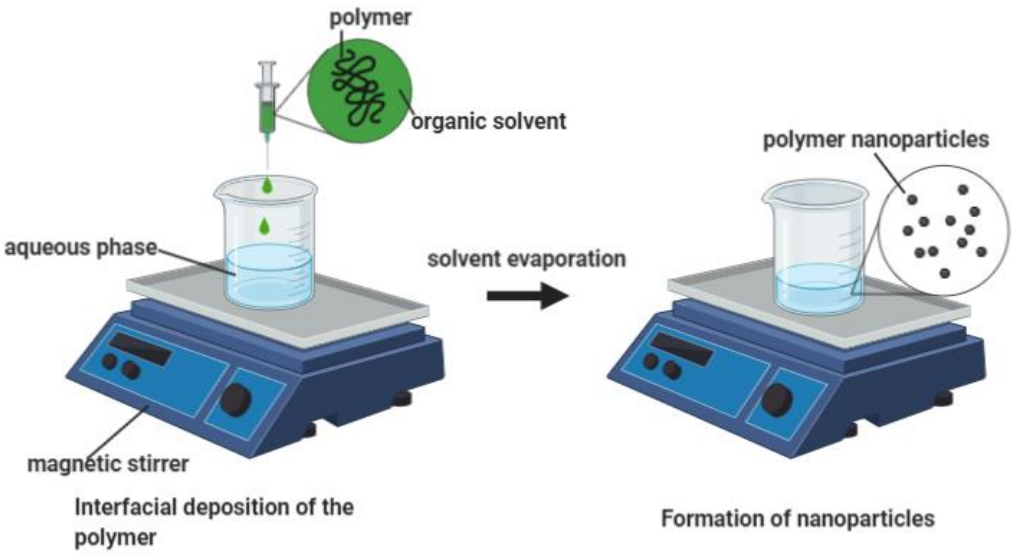


Figure 6-1: Single step nanoprecipitation methodology

Polymers were dissolved in an organic solvent and then dropwise pipetted into an aqueous solution stirring continuously. The nanoprecipitate method is a 'simple and reproducible technique that produces particles with narrow size distribution' [271], [272]. This is due to a phenomenon called supersaturation and is defined by the ratio of polymer concentration to polymer solubility in the organic solvent. The nucleation rate is also defined by supersaturation: The mixing of organic and solvent phases and the process of fluid dynamics are essential factors. This means, that poor mixing produces few and big nanoparticles (a low nucleation rate), whereas good mixing conditions bring about high nucleation rates with large numbers of small, distributed NPs [273]. Figure generated in Biorender.

6.3 Results

6.3.1 Polymeric microparticles for DC modulation

6.3.1.1 Assessing impact of microparticles on dendritic cell viability

To assess the impact of the different polymeric MPs on DC viability, cells were cultured with MPs at different concentrations (1 mg/mL up to 10 mg/mL).

For this, cells were seeded in duplicate wells and tissue culture plastic wells were used as a 2D background control. HMDA (the core material of the MP) MPs were utilised as a 3D material control. The HMDA, HFiPMA and THFuA MPs did not show any significant cytotoxic effect on DCs in any concentration tested (see Figure 6-2- A, B, D). Interestingly DEAEA MPs showed slight cytotoxic effects on DCs after 24 hours of culture on a dosage dependent gradient (see Figure 6-2C). DEAEA MPs at the highest concentration (10 mg/mL) showed the highest toxicity, however this was still at a non-significant level towards TCP control.

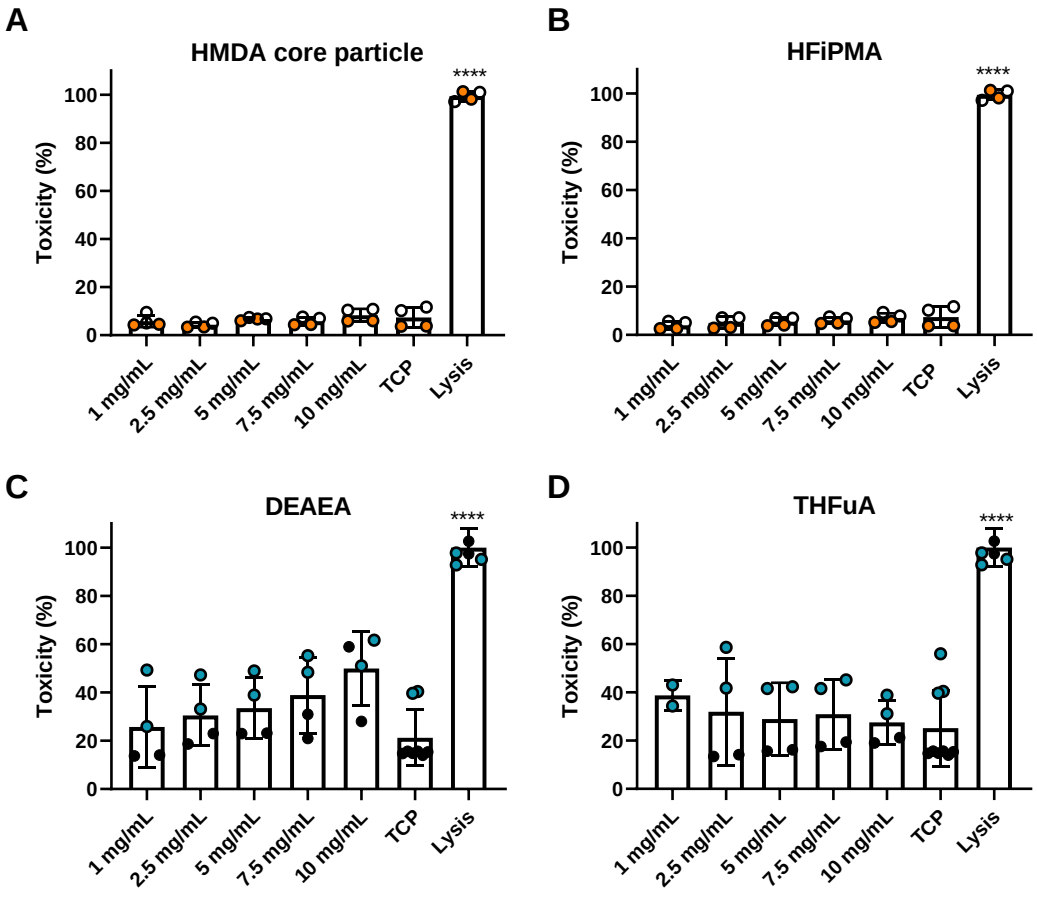


Figure 6-2: Impact of microparticles on DC viability

Immature DCs were cultured with microparticles for 24 hours and then their viability was assessed with ToxiLight. Data is from 2 independent biological experiments with 2 technical repeats each. Points are colour coding per donor. Statistical analysis was performed using one-way ANOVA with Dunnet's post hoc multiple comparison tests and is shown as * p< 0.05, ** p<0.01, *** p < 0.001 and **** p < 0.0001. * compared to TCP.

6.3.1.2 Microparticles induce differential attachment behaviour of DCs

After 24 hours culture of DCs on MPs, cells were fixed and stained with DAPI (Figure 6-3). Stimulatory polymers were observed to be pro-attachment in a MP format towards DCs. Both DEAEA and HFiPMA MPs induced attachment of 30-40 DCs per particle. The polymer THFuA, formerly characterised as a

regulatory polymer (rendering DCs less able to be activated by LPS), showed significantly less DC attachment (averaging 6 cells attached per particle). DEAEA MP + LPS maintained pro-attachment, with cell attachment similar to the non-stimulation MP – significantly more than THFuA MP. LPS stimulation decreased the attachment of DC on HFiPMA by roughly half (attachment in the range between 10 and 30). Conversely, LPS stimulation increased DC attachment on THFuA MP to more than double the initial amount (to 15 cells per particle).

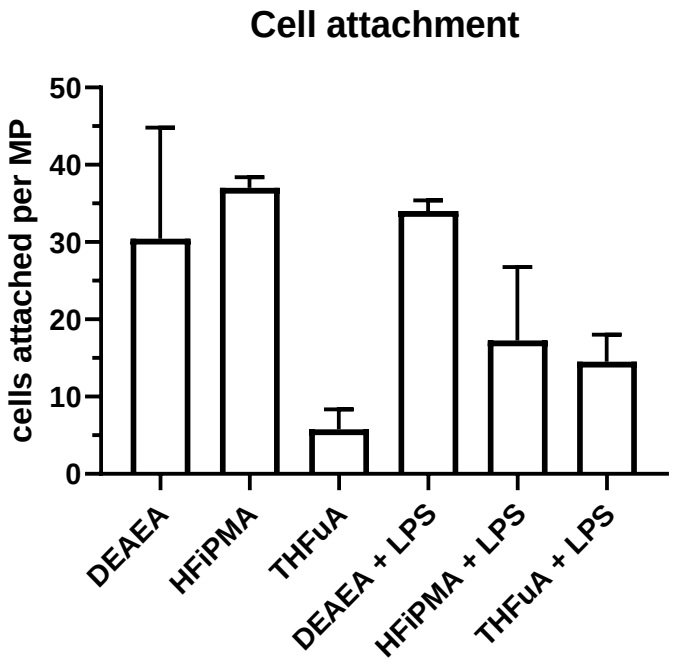


Figure 6-3: DC attachment to polymer microparticles

DCs were cultured for 24 hours with 2.5mg/mL of microparticles. They were then fixed, stained with DAPI and CD86 and imaged on a confocal microscope. DAPI-stained nuclei were counted per particle, with usually 2 particles per image. Cells were counted after z-stacks were stitched together as a 3D projection. Data is from 2 independent biological experiments with at least 2 ROIs each.

6.3.1.3 Microparticles induce upregulation of CD86 on DCs

MP-DC cultures were seeded at a concentration of 2.5 mg/mL of polymeric MPs. To perform phenotyping assays the cells were either fixed, stained for immunofluorescence based staining readout or alternatively cells were detached from MPs, filtered to isolate cells only and then further stained for flow cytometric analysis.

With these two different approaches it was possible to investigate the surface expression of specific activation markers that were previously shown to be modulated after 2D polymer coated culture. With the immunofluorescent approach the attachment of cells and the expression levels of CD86 was primarily investigated, while with the flow cytometry approach a wider panel of surface markers were investigated.

6.3.1.3.1 DEAEA MP increase CD86 mean fluorescence intensity

Staining the fixed cells adhered to the MPs for immunofluorescence, showed the upregulation of CD86 on the surface of cells adhered to the DEAEA MPs – similarly as observed earlier on the flat DEAEA coatings. DCs on DEAEA MPs showed high CD86 expression, while the non-tissue culture plastic control only showed single cells intermediately expressing CD86. The THFuA MPs had only few cells attached to them and in line with previous observations these cells did not show significant CD86 expression (in contrast, the expression is comparable to the non-tissue culture plastic control).

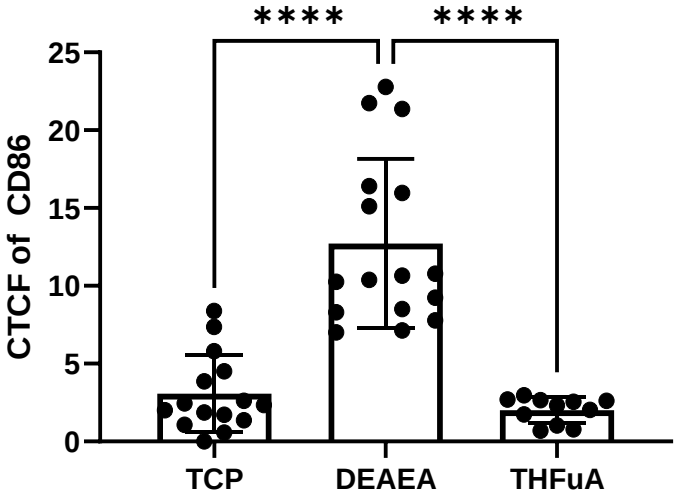


Figure 6-4: CTCF of DCs adhered to microparticles.

DCs were cultured for 24 hours with 2.5mg/mL of microparticles. They were then fixed, stained with DAPI and CD86 and imaged on a confocal microscope. Corrected total cell fluorescence (CTCF) was calculated according to formulas previously published: CTCF = Integrated Density - (Area of selected cell X Mean fluorescence of background readings). Each dot represents a single cell attached to a microparticle. Data is from 2 independent biological experiments with at least 2 ROIs each. Statistical analysis was performed using one-way ANOVA with Dunnet's post hoc multiple comparison tests and is shown as * $p< 0.05$, ** $p<0.01$, *** $p < 0.001$ and **** $p < 0.0001$.

6.3.1.3.2 Assessed by flow cytometry

Assessing the expression of more activation markers by flow cytometry paint a different picture: After 24 hours THFuA MPs induced similar CD86 expression levels as TCP control (Figure 6-5B). In contrast, DEAEA MPs showed higher levels of CD86 surface expression (from 5% at TCP to 36% for DEAEA MPs at 24 hours. These CD86 positive cell populations from the DEAEA MPs are around the same percentages as the positive control that was stimulated with LPS. DEAEA MPs showed a combinatorial effect with LPS

stimulation at 24 hours – as DEAEA MPs cultured DCs, that have been additionally stimulated with LPS show a greater CD86 positive population than the TCP DCs that have been stimulated with LPS. The DEAEA MP condition induced very high variability between donors. HMDA and HFiPMA MP were only included later on during this study and no conclusive results were observed.

The previously observed modulatory behaviours did not translate from a flat coating to a particulate system for CD83 expression. For both DEAEA and THFuA MPs the CD83 positive populations hovered around the negative TCP control with very high donor to donor variability; and much below the TCP + LPS positive control Figure 6-5A). In complete contrast to earlier observations on the flat surface coatings, THFuA MPs cultured DCs that were additionally stimulated with LPS did not show any suppression of either CD83 or CD86 upregulation.

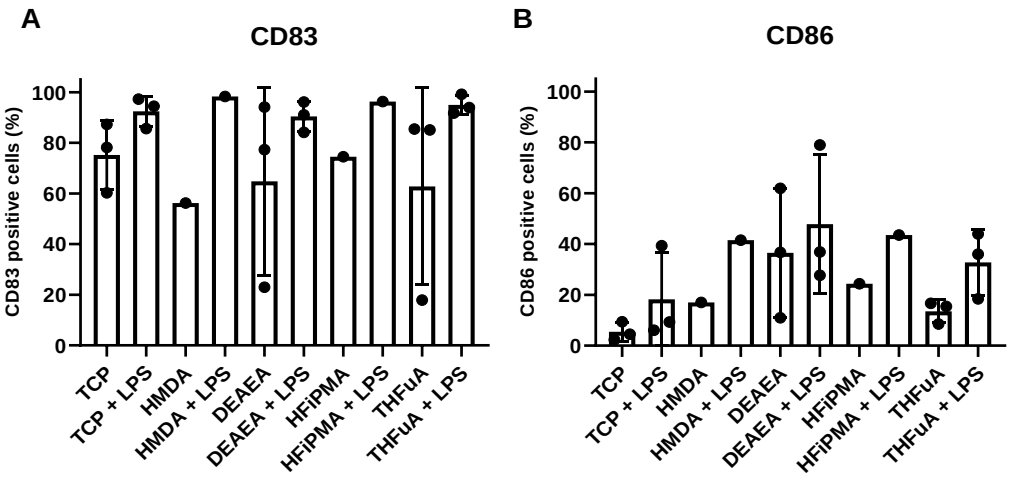


Figure 6-5: Effect of 2.5 mg/mL microparticle culture on DC activation

DCs were cultured with MPs at 2.5 mg/mL for 24 hours. Data points are from 3 independent experiments (HMDA, HFiPMA only n=1, due to MP availability) with 10,000 events routinely acquired in each sample. TCP – tissue culture polystyrene, and data is presented as mean + SD.

To test a higher concentration of MPs, DCs were cultured with 10mg/mL MPs for 24 hours. Results can be seen in Figure 6-6 and compare the effect of 2.5 mg/mL and 10 mg/mL MPs on DC phenotype. In contrast to earlier findings, THFuA MPs induced at both concentrations' higher expression levels of CD83 and CD86 than the 2D non-tissue culture plastic control. In general, the 10 mg/mL concentration induced lower levels of activation surface marker expression throughout most MP conditions (except CD86 THFuA MP). No significant up- or downregulation of CD83 and CD86 expression was observed after MP culture.

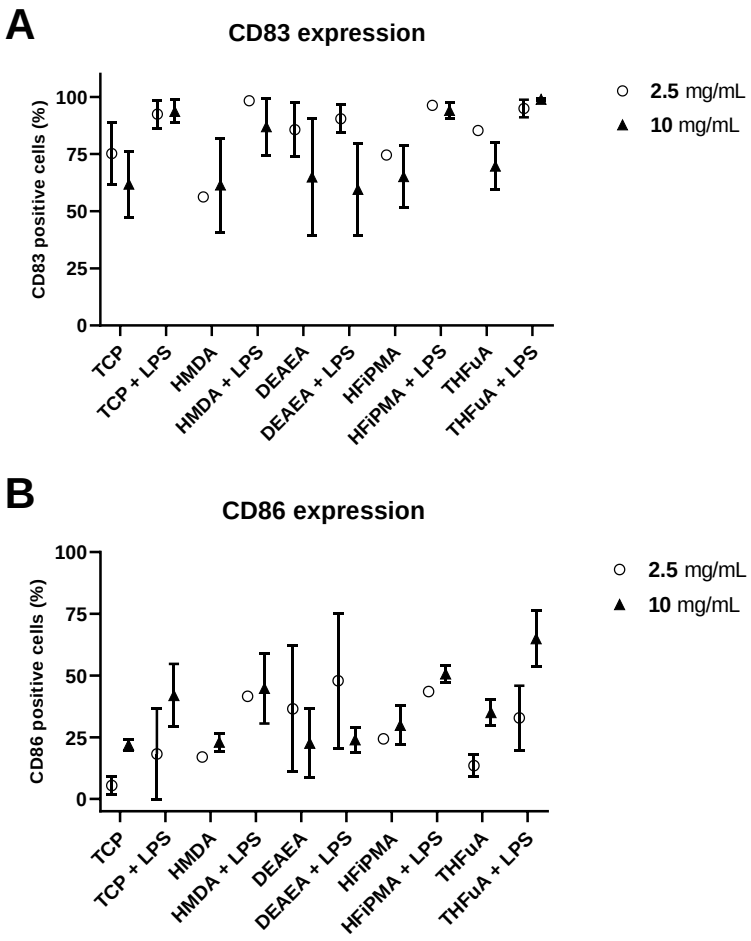


Figure 6-6: Comparison between 2.5 mg/mL and 10 mg/mL microparticle culture on DC activation

DCs were cultured with MPs at 2.5 mg/mL and 10 mg/mL for 24 hours. Data points are from 3 independent experiments (HMDA, HFiPMA only n=1, due to MP availability) with 10,000 events routinely acquired in each sample. TCP – tissue culture polystyrene, and data is presented as mean + SD.

6.3.1.4 Microparticle induce modulated cytokine secretion

DCs secrete cytokines to polarise T cells and, and to determine whether MP culture has an effect on cytokine secretion, the supernatant of 24 hours DC-

MP cultures was analysed. Specifically, the pro-inflammatory cytokines TNF-α and IL-1β were investigated.

TNFα was secreted at the TCP base level at 67 pg/mL, TCP+ LPS was 140 pg/mL (Figure 6-7). The core particle HMDA increased this to 183 pg/mL at 2.5 mg/mL and to 98 pg/mL at 10 mg/mL. HMDA + LPS stimulation to 123 pg/mL at 2.5mg/mL and 205 pg/mL at 10 pg/mL. DEAEA MP increased TNFα to 125 pg/mL and 210 pg/mL respectively, maintaining similar levels when stimulated with LPS (115 pg/mL and 240 pg/mL). HFiPMA MPs at both concentrations were around 200 pg/mL. Whilst 2.5 mg/mL of THFuA MP increased TNFα secretion to 125 pg/mL, 10 mg/mL induced around 115 pg/mL secretion. Addition of LPS to THFuA MPs maintained levels around 130 pg/mL.

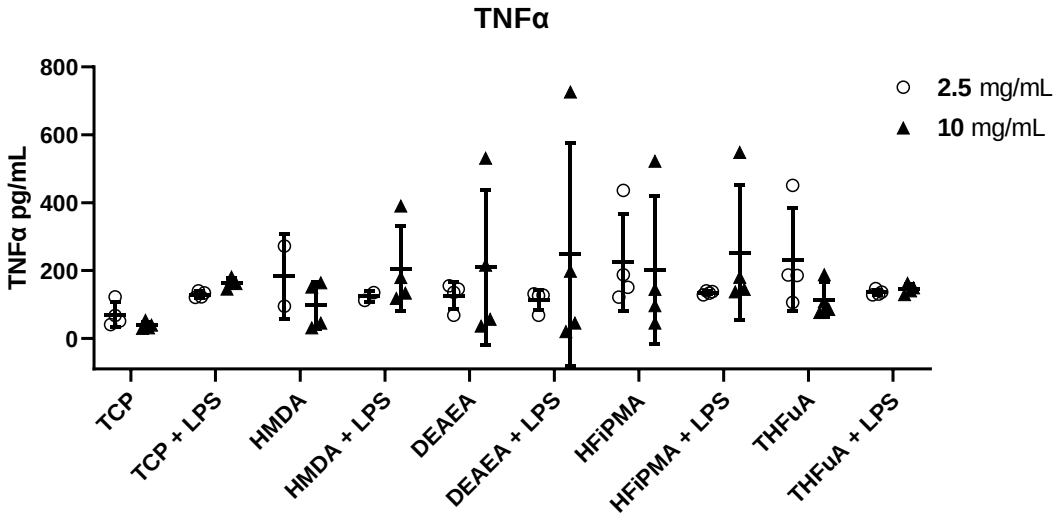


Figure 6-7: TNFα secretion after microparticle culture

Immature DCs were cultured with 2.5 and 10mg/mL MPs (without and with LPS) for 24 hours. Cell culture supernatants were then analysed by ELISA for cytokine secretion. Data is from 1-3 independent experiments with 2 technical repeats each and data presented as mean ± SD.

IL-1β was secreted at the TCP base level at non detectable levels, TCP+ LPS was 80 pg/mL. The core particle HMDA did not increase IL-1β secretion, while DEAEA MP, DEAEA MP + LPS and HFiPMA MP, THFuA MP increased it to around 40 pg/mL. HFiPMA and THFuA MP + LPS at 2.5 mg/mL increased to 250 and 310 pg/mL but with large variation between donors (Figure 6-8). MPs at 10 mg/mL did not induce any modulatory IL-1β secretion levels.

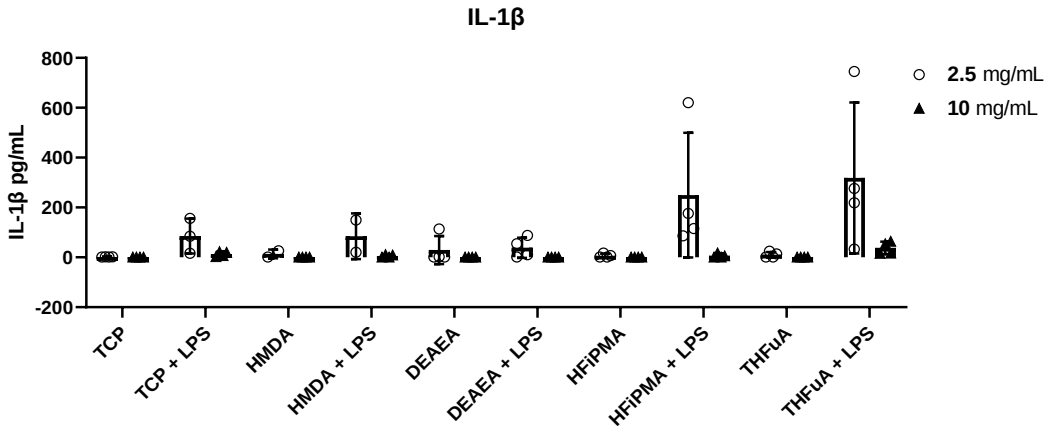


Figure 6-8: IL-1β secretion after microparticle culture

Immature DCs were cultured with 2.5 and 10mg/mL MPs (without and with LPS) for 24 hours. Cell culture supernatants were then analysed by ELISA for cytokine secretion. Data is from 1-3 independent experiments with 2 technical repeats each and data presented as mean ± SD.

6.3.2 **Polymeric nanoparticles for DC modulation**

In order to test the ability of polymeric NPs made from the hit materials to modulate DCs, these polymers first had to be fabricated in a NP format. For this, the polymers were UV pre-polymerised in well plates and washed according to previously described methods. Polymer's coatings were then scraped off the plates and via single-step nanoprecipitation methodology made into nanoparticles (see Figure 6-1). As the polymers chosen for this have not

been previously used to fabricate NPs, this series of experiments was seen as proof-of-concept on whether it was possible to achieve this. For analysis of particulate diameter and checking of the uniformity of particle dispersion, aliquots of the were measured in a ZetaSizer Suite (Malvern).

Exemplary depictions of diameter and dispersion can be seen in Figure 6-9 until Figure 6-11. The amounts of polymers, solvents and stirring/addition rates used are noted in Table 12. DEAEA NPs analysed by the ZetaSizer showed, that two populations with different diameters were formed (43 nm and 272 nm). Formation of DEAEA NPs was shown to be not reproducible over multiple repeats.

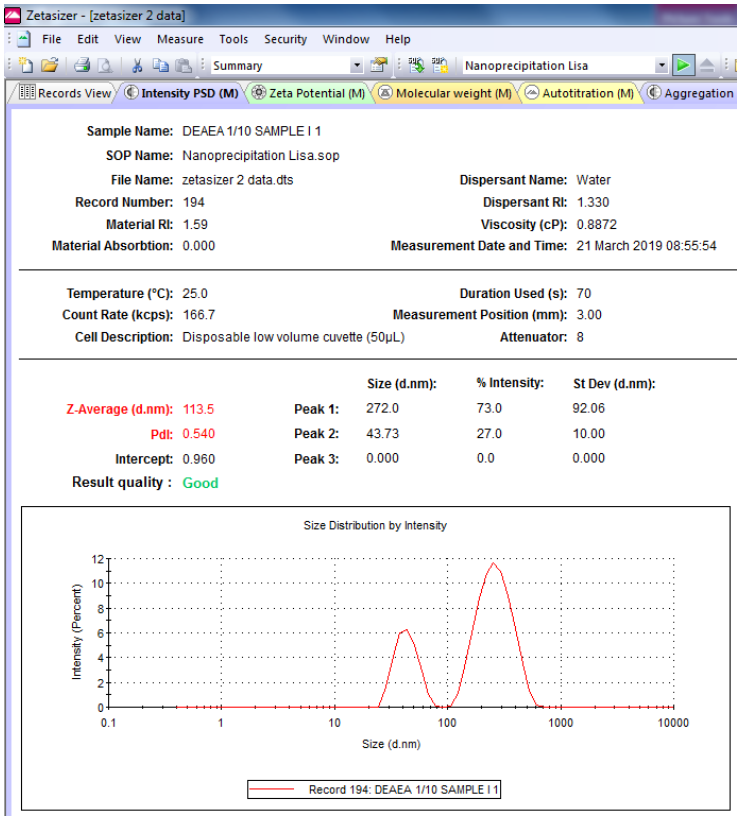


Figure 6-9: Preliminary fabrication of DEAEA nanoparticles

Representative image of multiple repeats.

HFiPMA formed 131 nm big NPs, with a very low standard derivation symbolising a uniform dispersion of particles. This was reproduced multiple times.

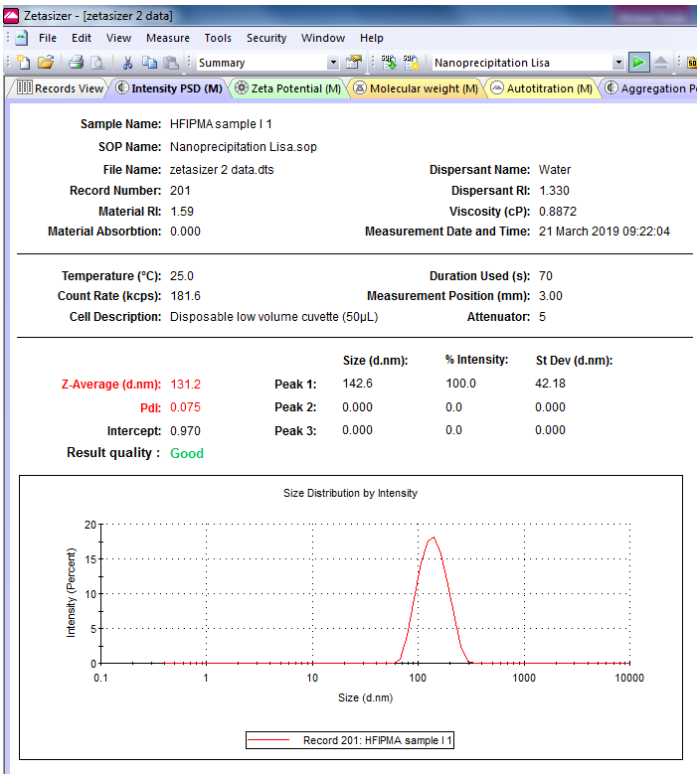


Figure 6-10: Preliminary fabrication of HFiPMA nanoparticles

Representative image of multiple repeats.

THFuA was used for the regulatory polymer, as ZnA was unable to be dissolved in the organic solvents for the single step nanoprecipitation method. THFuA formed NPs in a mono-dispersed population of a size around 100 nm. This was able to be reproduced multiple times.

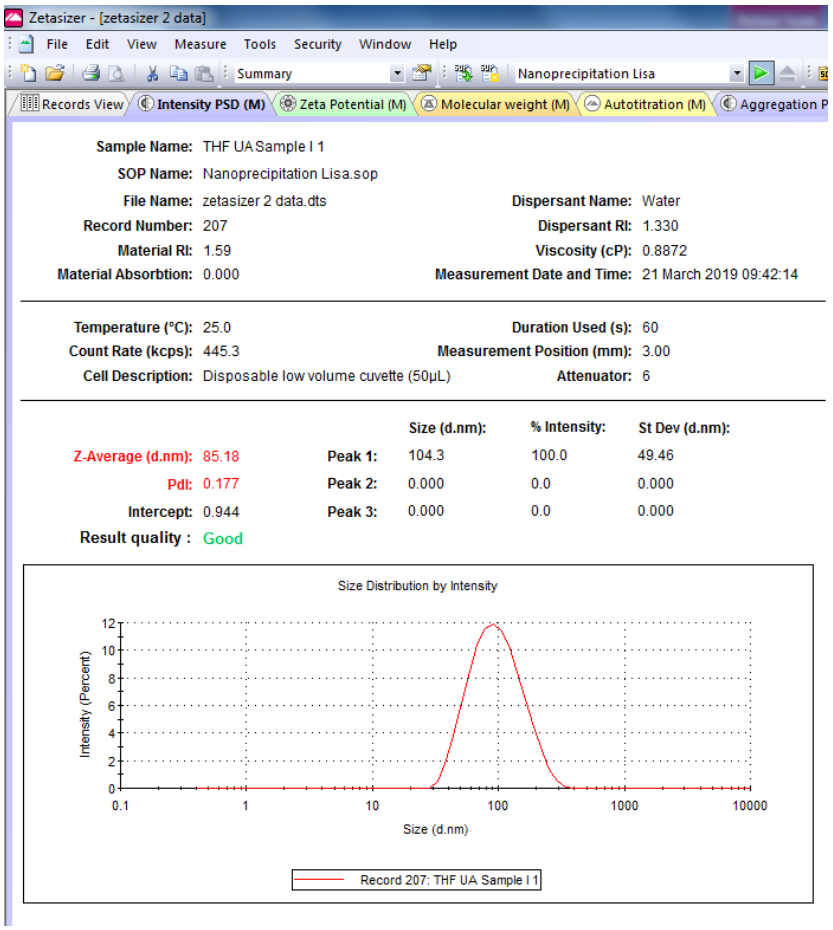


Figure 6-11: Preliminary fabrication of THFuA nanoparticles

Representative image of multiple repeats.

Freeze drying is generally used to determine the weight of the NPs and then utilise this to use a consistent concentration in cell culture experiments. Freeze drying also allows visualisation of nanoparticles via SEM imaging.

Initial SEM imaging revealed that HFiPMA NPs aggregated together in the freeze-drying process (Figure 6-12). HFiPMA NP were not able to be distinguished easily, but circular shape and aggregations of circular shapes were visualised. The aggregates were roughly around the size of 1 µm. Higher magnification burned the materials; therefore, no higher magnification images were taken.

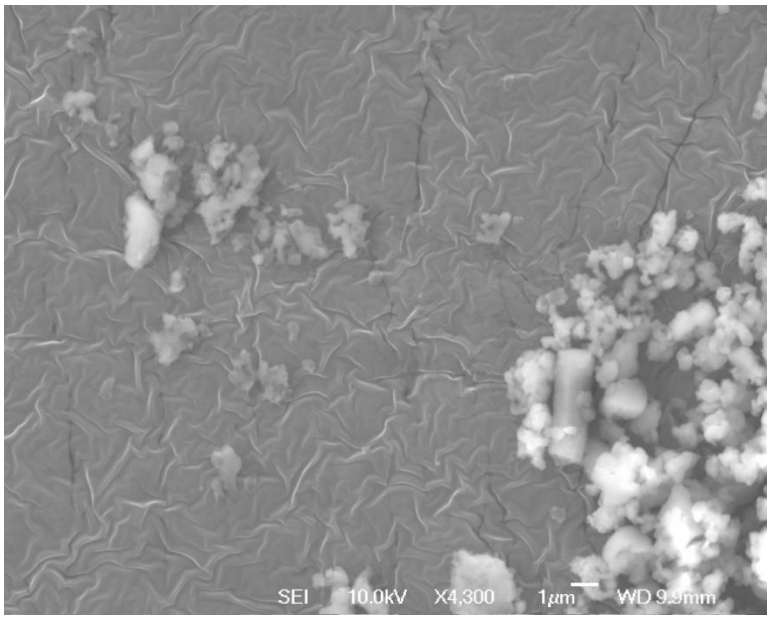


Figure 6-12: HFiPMA nanoparticle aggregates by SEM

Representative images from HFiPMA nanoparticles. Scale bar is 1µm and images were taken on a JEOL 770 SEM machine.

In order to be able to assess size and structure of single NPs, a different approach was envisioned: Freshly fabricated HFiPMA particles were diluted in water/solvent and imaged on TEM. Images taken (Figure 6-13) confirmed the particle size to be smaller than previously obtained by the ZetaSizer (mid 40 nm instead of 140 nm), while NP shape was confirmed to be circular as was assumed from SEM images.

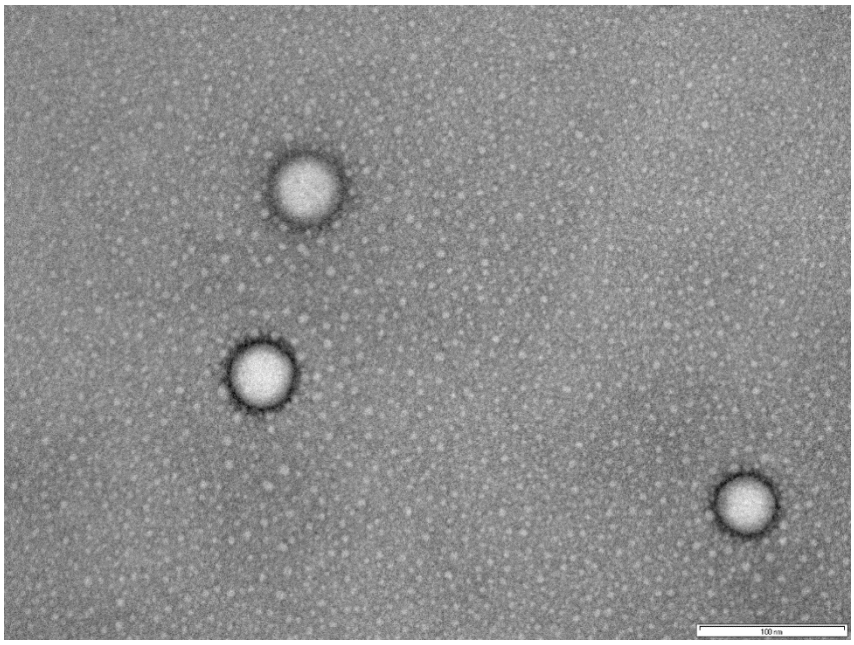


Figure 6-13: TEM of HFiPMA nanoparticle

Representative images of HFiPMA nanoparticles. Scale bar is 100nm and images were taken on a transmission electron microscope.

6.4 Discussion

Investigating both NPs and MPs made from the hit polymers did not translate the whole modulatory function from the flat coatings.

The proof-of-concept experiments of NP fabrication were stopped as only HFiPMA out of the hit materials was able to be reproduced in a consistent size and monodispersed population. HFiPMA NPs analysed in the ZetaSizer gave a size around 140 nm while TEM images revealed a much smaller diameter for the particles. As the ZetaSizer measures the diffusion speed of an ensemble group (many millions or billions) of particles. The protective layer (e.g., surfactant or PEG) on top of a core particle will influence this diffusion and thus the interpretation of the nanoparticle size. Electron microscopy on the other hand will explore the electron-rich core of the particle. Visualisation of the nanoparticles is therefore essential, and this can only be achieved by EM or AFM in the nanometre region. This interesting juxtaposition of size needs to be evaluated further, but initially indicates a true smaller size of HFiPMA NPs than found in ZetaSizer measurements. Polymeric NPs have in the past few years found to have modulatory and activatory effects on DCs with focus on both cancer immunology and autoimmune diseases research. Further research on these polymeric NPs would be fascinating, but unfortunately not the scope of this PhD project due to time and that it would have been a change from surface material effect to a material that would be phagocytosed by the DCs.

Increased cytotoxic effects of DEAEA microparticles above 7.5 mg/mL can potentially be linked to not using catalytic chain transfer polymerisation (CCTP;

a specific material in the fabrication process) in the production of the surfactant used; meaning a different thiol agent was used in the surfactant production and potentially introducing an accumulation of toxic contaminants when using the particles in a higher concentration. Unfortunately, MPs did not have the same effect on DCs as flat coatings. Literature research found that, MPs had generally been used in concentrations ranging from 0.6 mg – 3 mg/mL with DCs [135], therefore here it was initially decided on using a concentration of 2.5 mg/mL as a non-toxic but still expected to be very effective concentration. After observing no significant modulations by MP concentrations of 2.5 mg/mL a higher concentration of 10 mg/mL was trialled. This however also did not show to have any effect on both cytokine secretion, as well as surface marker expression analysed by flow cytometry. In complete contrast to the flow cytometry results the immunofluorescence images revealed a fascinating connection between ability of DCs to attach to polymeric MPs and also increased CD86 expression of adhered DCs. DEAEA MPs were observed to be highly pro-attachment and also showed significantly higher CTCF of CD86, whereas THFuA MPs were observed to do the opposite (little DC attachment and low levels of CD86 expression). Both stimulatory polymer MPs (DEAEA and HFiPMA) were not able to translate the 2D coating effect into a 3D MP system. THFuA MPs did not induce an immunosuppressive behaviour as previously observed for the flat coatings, but instead increased both CD83 and CD86 expression measured from flow cytometry. This is a completely different behaviour as expected. This might stem from the fact, that particulate systems as such are already known to have a minimal pro-inflammatory effect on DC activation, function and behaviour. This might be shown to overpower the

material-induced effect. On the other hand the aspect of particle size might be the issue here, as most MP studies in the past years utilised MPs that were much smaller in size than the ones used here (sizes of 0.5 to 5 µm compared to 70 µm here) and often focused more on the uptake and delivery of drugs or other loads [279]. Additionally, MPs in DC studies were often loaded with tolerogenic or stimulatory agents which is very different from MP used here. Size could also play a role in the modulatory effect on DCs. Here, particles of 70 µm size were used that are much larger than the DCs interacting with them. A recent study investigating MPs around 10 µm of size interestingly found the tentacular morphology of MP (and surface roughness) to have a modulatory effect on DC activation, which was unfortunately not looked at here [280]. Ultimately, the largest difference from the study presented here and studies in the literature are the size of MPs, which I hypothesise to be the main reason that I believe MPs do not have an effect on DC activation. Another explanation could be a low concentration of polymer surfactant on the surface which would be significantly less than the high concentration that is usual on flat UV polymerised coatings.

Overall, the proof-of-concept studies of particulate systems showed that modulatory effects from the flat coatings were not successfully translatable into microparticle format. Further studies are needed to gain more insight into how NPs could have an effect on DCs (with more time and expertise for fabricating NPs), and how smaller MPs and MPs with higher surfactant polymer concentrations could have a different effect on DCs than the here trialled larger MPs.

Chapter 7: Investigation of topography-induced modulation of DC behaviour and function

Chapter 7 Investigation of topography – induced modulation of DC behaviour and function

7.1 Introduction

It is well recognised that biomaterial surface properties influence cell responses, and specifically recent research into physical properties has shown that surface topographies have the ability to modulate cellular behaviour and phenotype [96], [109], [281]–[283]. The term surface topography can range from surface roughness to defined structure-like features such as grooves, wells and more complex - 3 dimensional features. These might occur naturally (structures found in nature), accidentally or can be carefully designed [99]. Micron-scale surface topography is an independent parameter that can be modified without affecting the bulk mechanical or chemical properties of a target substrate. Specifically, a rational design of regular topographic features can reduce the adhesion, spreading and/or the differentiation of several cell types, including fibroblasts, inflammatory precursors, and others. Examples of such geometries include dots, cones, pyramids, pits, funnels, circular elements and inverted pyramids [284]–[288]. These surfaces are often or usually sensed by cells through mechanoreceptors, while the process as such is termed mechanotransduction.

Recent endeavours into topographical research have used acid-etching of surfaces to change the roughness of material surfaces, modelling grooves or wells on the material surface – however, with new advances in manufacturing and fabrication technologies the design and development of complex

nano/micro sized surface features has become possible. 3D printing or heat moulding are now widely used techniques to generate carefully designed topographies [109], [289]. Through these methods researchers have been able to generate diverse platforms to investigate the effect of surface structures on cellular behaviour. The TopoChip, 3DArchiChip, and other platforms have been able to give a screening overview of the gradients of different structures or the complex design of topographies [107], [108]. The TopoChip is a 2 by 2 cm^2 chip made from polystyrene (PS) in areas of 290 by 290 μm^2, designated as 'TopoUnits'. The TopoChip holds 2176 distinct, randomly designed surface topographies using a mathematical algorithm as a design tool. Topographic features are built up using three types or microscale primitive shapes: circles, isosceles triangles (with one angle of 36° and two angles of 72°), and thin rectangles (3µm width) [109]. With this approach several cell types have been successfully investigated in how they react to these TopoUnits. Attempts to increase functionality of assays, and the use of other (non-adherent) cell types have been the TopoWellPlate, scaling up into the Phenome platform and also the combination of chemistry and topography in the ChemoTopoChip [114], [282].

Earliest research about surface topographies, centred around contact guidance in the developing and regenerating nervous system. When cultured on different topographies (grooved surfaces, aligned fibres, guidance conduits, nanorough surfaces and pillars/posts) neuron growth direction was modulated, it was found that topographical cues exert powerful effects on neurons and glia [290]. In comparison, microfabricated pillars (with varied diameter, length and

spacing) affected fibroblast shape and migration, leading to fewer actin stress fibres on the micropillars than on flat surfaces; similar results have been found when looking at topography islets [284], [291], [292]. On a smaller scale, nano-topographies have in the past shown to maintain stem cell proliferation or induce differentiation into a plethora of distinct cell types [103], [292], [293]. Keratocytes, the major cellular component of the eyes stroma have recently been proven to be respond to PDMS micropatterns (lines, lattices or micropits) [294]. The linear patterns resulted in elongated and aligned cells along the microchannels, whereas the lattice and micropit patterns lead to more spread cells with less alignment. Surprisingly, proliferation was the same on all surfaces [294].

Similarly, macrophages, a cell type of the innate immune system have been shown to be polarized into pro- or anti-inflammatory phenotypes depending on the topography feature cultured upon [283], [295]. Investigating macrophages, the effect of titanium surface modifications (roughness and hydrophobicity) has shown, that smooth titanium induced inflammatory macrophage activation (as sensed by increased pro-inflammatory cytokine secretion IL-1β, IL-6 and TNFα, a “M1”phenotype), while hydrophilic rough titanium induced anti-inflammatory macrophage activation (also known as “M2” wound healing state) [296]. These results demonstrate that macrophages cultured on high surface wettability materials produce an anti-inflammatory microenvironment. With these promising results, looking at parallel gratings (250 nm-1 µm line width) showed that cell morphology as well as TNFα and VEGF secretion levels were significantly modulated [117].

DCs are the bridge between the innate and the adaptive arm of the immune system, and therefore essential for the induction and regulation of any immune response. In steady-state conditions, DCs maintain immune tolerance against self-antigens; however, when DCs encounter pathogen they will uptake the foreign pathogen, internally process it and present antigen fragments on their MHCs. This process is also termed DC activation– these activated DCs then migrate to the lymph nodes where they will interact with naïve T cells. While several studies have looked at macrophage polarisation and function, little is known about the immunomodulatory properties of topographies on DCs. Utilising complex topographies to investigate their impact on DC motility has not yet been attempted. DCs contain mechanosensitive adhesive structures called podosomes which consist of actin-rich core surrounded by integrins, adaptor proteins and actin network filaments [297]. They facilitate cell migration via localized degradation of extracellular matrix [297]. It has been shown, that DCs can sense 3-dimensional (3-D) geometry by aligning podosomes along the edges of 3-D micropatterned surfaces [298]. Podosomes of DCs also primarily locate to spots of low physical resistance in the substrate. The main function of DCs is presenting antigens, for this the receptors with which DCs present antigens locate to these protrusive structures, where they can trigger receptor-mediated uptake of antigen [297]. The expression of c-type lectin on iDCs has been found to be regulated by substrate stiffness, resulting in differential antigen internalisation [173]. Furthermore, substrate stiffness is shown to affect β2-integrin expression and podosome formation by iDCs, while influencing CD83 and CCR7 expression on mature DCs [173]. These results showed that DCs can sense substrate

stiffness during differentiation and maturation, leading to altered DC phenotype and function.

Apart from these observations, no studies are known to me about the influence of topographic features on DCs. Driven by the results of some of van den Dries *et al* work [298] and the emergence of screening platforms such as the TopoChip and Phenome28, this project is an attempt to establish a small-scale screen of the effect of topographic features on DCs and elucidate whether a more in-depth study will be useful. Earlier attempts to culture KG-1 cells (a cell line, that is supposed to be of similar function than primary DCs) on the TopoChip were unsuccessful due to their non-adherent properties [128]. With the recent fabrication of the Phenome28 platform allowing small scale culture and allowing to use non adherent cells, new possibilities for analysing different cell types have opened. Given the limited understanding of the interaction between DCs and the topographical cues of their environment, in this chapter I chose to pursue an unbiased, proof-of-concept screening approach using a topographical Chip (MiniTopoChip), as well as the Phenome 28 platform. The aim of these experiments was to investigate topographic influence on DC phenotype, function, and motility behaviour.

7.2 Methods

7.2.1 Topography fabrication

Both Phenome and MiniTopoChip topographies were fabricated by collaborators from Jan de Boers laboratory (MERLN institute) at Maastricht University, Netherlands. The topographies were fabricated by Ormo-stamp molding as previously described [299]. Finalised topographies were send my postal mail to Nottingham and utilised in cell culture experiments. Large magnification of the different topographic features can be seen in Appendix 8 and Appendix 9.

7.2.2 Topography preparation

Phenome topography wafers (made from polystyrene (PS)) were received from MERLN and punched out by manual punching with a hammer and a puncher. Wafers were then carefully washed with 70 % EtOH, PBS (1x), sterilized by UV radiation followed by a priming step with complete media overnight.

Wafers were punched out in a diameter of 12 mm and put into 24 wellplates of a non-tissue culture plastic kind in order to facilitate more interaction with the topographies.

For the MiniTopoChip the same cell culture preparation as for the Phenome platform was used, with the MiniTopoChip platform having a base chemistry composed of an alkyl sulphide.

7.2.3 Cell culture on topographies

DCs were cultured at $1x10^6$ DCs/mL for 24 hours on the oxygen plasma treated polystyrene Topo chips. 1 repeat of the topographies was stimulated with 100 ng/mL LPS after 6 hours of DC conditioning on the topographies.

7.2.4 DC staining

DCs were stained with Hoechst nuclear stain (400 ng/mL) for 20 minutes as well as CFSE cytoplasmic stain (according to manufacturers instruction) for 15 minutes in serum-free media, followed by 30 minutes incubation to induce CFSE hydrolysis.

7.2.5 Live cell imaging

Cells were seeded at $1x10^6$ cells/mL onto a uniform chemistry topography chip and left to settle for 30 minutes before live imaging started. Different regions of interest were programmed into the ROI manager, so the view field will cover the entire 350µm of the squared topography unit at 4x magnification. To cover all 36 positions (including a flat control) the interval of images was set to 7 minutes and set to record for 3 hours in total. Images were acquired in brightfield, Hoechst and CFSE channels on a DeltaVision set up. Cells were kept at 37°C and 5% CO_2 throughout the entire imaging process.

7.2.6 Flow cytometry staining

To assess modulation of surface maker expression DCs were harvested, washed with PBA, and stained with CD83-FITC, CD86-PE, PD-L1 APC, CCR7-PE-Cy7 and HLA-DR PerCP antibodies for 20 minutes. Cells were then

again washed with PBA, fixed in 1% PFA and acquired on a Canto flow cytometer.

7.2.7 ELISA

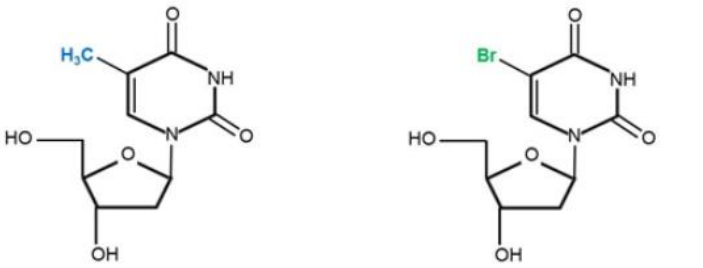
Cell culture supernatant was harvested after 24 hours of cell culture and stored at -20°C until further use. IL-10, IL-12p70, IFN-γ and IL-17 assays were run in a 384- wellplate format (R&D Systems).

7.2.8 $CD3^+$ T cell co-culture

DCs were co-cultured in a 1:10 ratio with $CD3^+$ T cells in human serum supplemented complete media for 8 days. On day 3 100 µL of the cell culture was removed and substituted with fresh media supplemented with 5 ng/mL IL-2. On day 7 the positive controls were stimulated with 2 µg/mL anti-CD3 and 2 µg/mL anti-CD28 monoclonal antibodies (Sigma Aldridge). After 8 days, the cell culture supernatant was harvested and stored at -20°C until further use.

7.2.9 T cell proliferation assay

On Day 7 of the DC- CD3+-T cell co cultures 20 µL of prepared Bromodeoxyuridine (BrdU)-labelling solution was added into the wells. BrdU is a synthetic nucleoside and an analog for thymidine. During the S phase of the cell cycle (when the DNA is replicated) BrdU will incorporate itself into the newly synthesized DNA of replicating cells instead of thymidine. BrdU-specific antibodies can then be used to detect and quantify the level of incorporation.



Thymidine 5′-bromo-2′-deoxyuridine (BrdU)

The wellplates were dried in the oven for 1 hour at 60C, after which they can be stored for up to 1 week in the fridge. In order for the BrdU-antibody to be able to bind to the incorporated BrdU the DNA has to be denatured by heat or acid (in this case fixative/denaturation solution consisting of acid). After denaturation of the DNA the anti-BrdU antibody can bind to the BrdU incorporated in the DNA. The anti-BrdU antibody which was used here is conjugated to peroxidase (POD). Following washing steps and addition of the colourless substrate solution (TMB/peroxide) which the peroxidase conjugated to the antibody will catalyse to a colour change. To stop this colorimetric reaction H2SO4 (1M) is added and absorbance levels measured at 450nm and for reference at 600nm.

7.2.10 **Statistics**

Data points were analysed using GraphPad Prism version 8.01; results are presented as mean ± SD. Statistical differences between the experimental conditions were determined using one-way ANOVA with Dunnett's multiple comparisons as indicated. A level of $p<0.05$ was considered statistically significant.

7.3 Results

7.3.1 Motility of immature dendritic cells on topographic features

To determine the effect of topography on DC movement, the speed of cells moving in different TopoUnits in comparison to a flat PS surface were assessed. Cells were fluorescently labelled as described in 7.2.4 to visualise the cytoplasm and nucleus of DCs.

After live imaging the fluorescently labelled cells for 3 hours the images were stacked together in the ImageJ-Fiji program and analysed by the TrackMate PlugIn. With the help of the PlugIn the movement of the seeded cells were tracked across the stacks and the cell movement quantified. Non-moving cells (that had not moved in 3 hours= moving but in in one area, movement < 10 µm) were removed from the analysis. From this analysis nine 'hit' topographies have been identified to very significantly slow down DC motility and reduce length of travel in comparison to the on-chip flat surface control ($p < 0.001$) (**** in both conditions, see Figure 7-1 and Figure 7-2). Both motility readouts correlated well with each other (R^2=0.7821, see Figure 7-3).

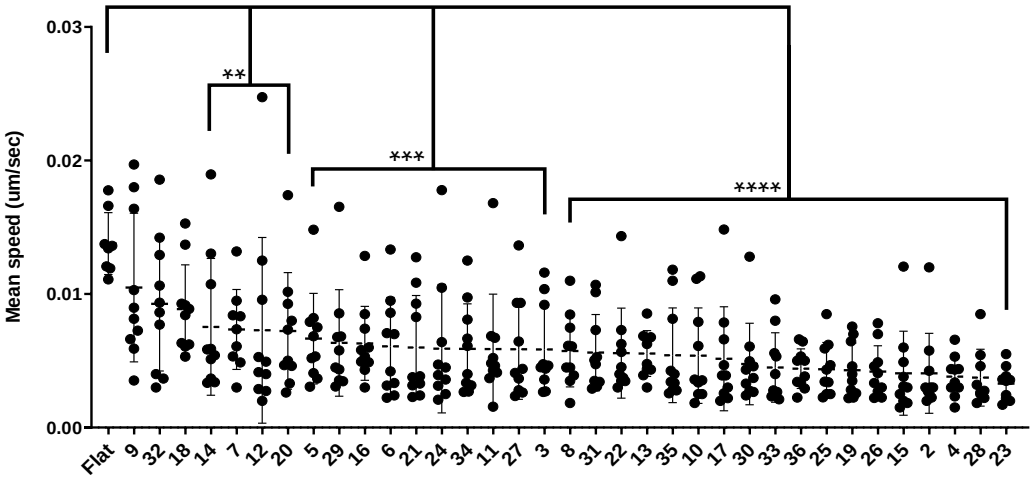


Figure 7-1: Mean speed per Track from each topographic pattern.

PS TopoChips were seeded with Hoechst (nuclear stain) stained DCs and live imaged for 3 hours in 7 min intervals. Tracks per unit were determined and motility calculated with TrackMate in ImageJ – speed per cell was averaged per topographic unit. 10 chips from 6 different biological donors were imaged and data presented as mean ± SD. Units are arranged in a ranked order from fast to slow motility. For significance a ONE-way with Dunnet multiple comparison test was performed and significantly (*= p<0.05; **=p<0.01; ***= p<0.001; ****=p<0.0001) changed motilities have been highlighted.

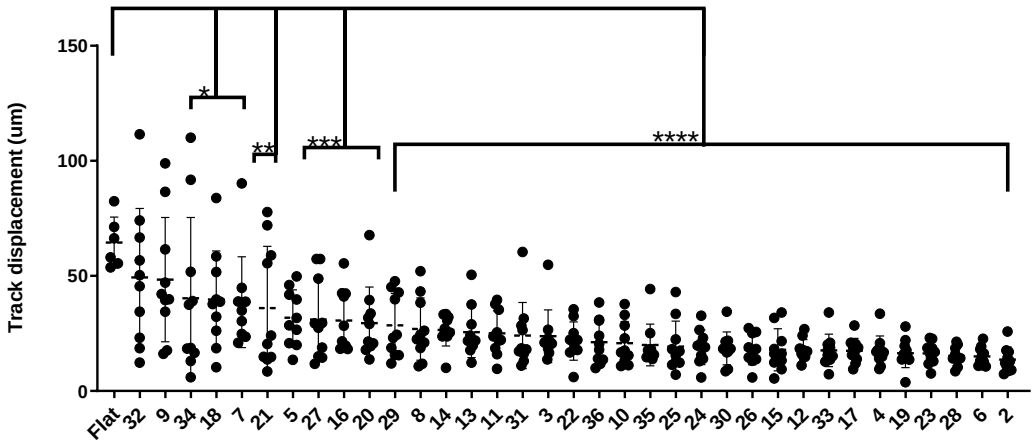


Figure 7-2: Track displacement from each topographic pattern**.**

PS TopoChips were seeded with Hoechst (nuclear stain) stained DCs and live imaged for 3 hours in 7 min intervals. Tracks per unit were determined and track displacement calculated with TrackMate in ImageJ – displacement per cell track was averaged per topographic unit. 10

chips from 6 different biological donors were imaged and data presented as mean ± SD. Units are arranged in a ranked order from fast to slow motility. For significance a ONE-way with Dunnet multiple comparison test was performed and significantly (*= p<0.05; **=p<0.01; ***= p<0.001; ****=p<0.0001) changed track displacements have been highlighted.

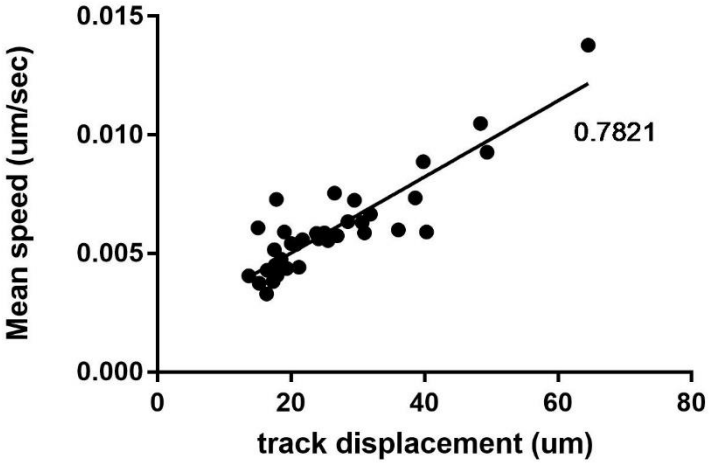


Figure 7-3: Correlation between mean speed and track displacement of cells on topographies.

Correlation the values of mean speed and track displacement in the different topography units gives a good correlation of R^2 of 0.7821, made by a linear standard curve.

Analysis of the topographic features of the most motility-wise distinct topographies has shown the spacing of ‘fast’ features to be more distant and more complex in comparison to the five ‘slowest’ topographic features (Figure 7-4 and Figure 7-5).

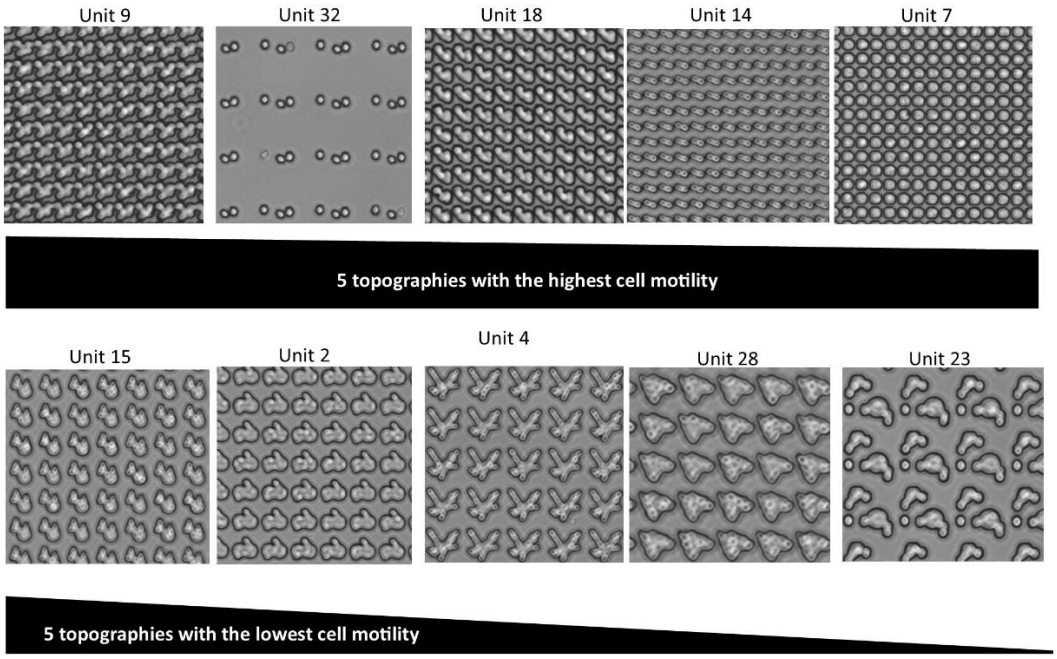


Figure 7-4: Five fastest and five slowest motility generating topographies

Features are magnified and ranked from fast to slow cell motility.

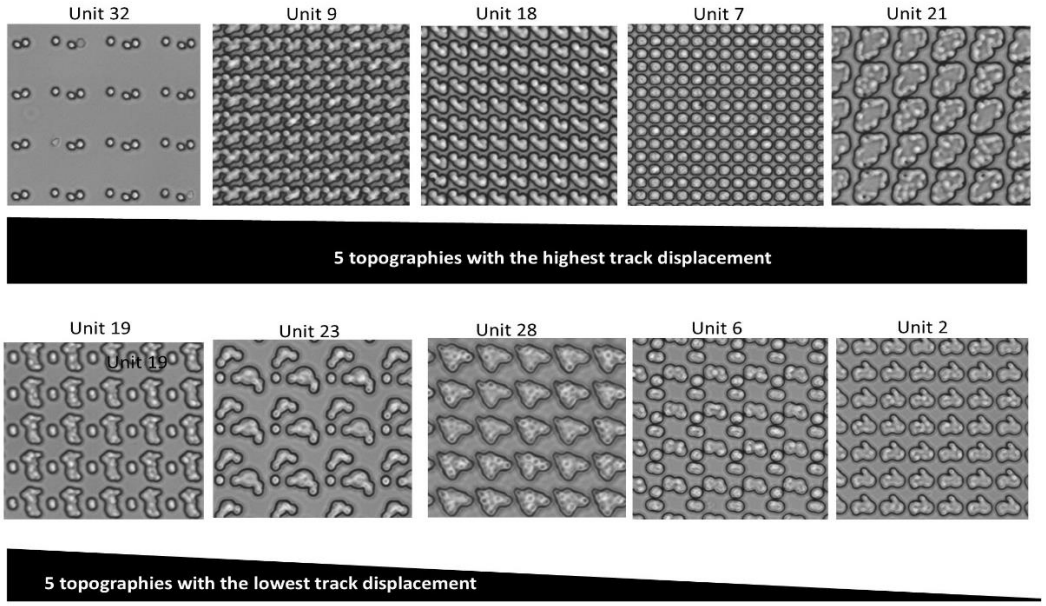


Figure 7-5: Five topographic features that support the most movement and five that support least cell movement

Features are magnified and ranked from furthest displacement to smallest displacement.

Looking at the topographies portrayed in Figure 7-4 and Figure 7-5 a topography pattern became visible. Therefore, the mean speed cells moved on those topographies with the diagonal spacing in between topographic features was correlated (see Figure 7-6). Different groups can easily be classified with this graph and good correlation of R^2 of 0.6782 (deriving from a non-linear regression standard curve).

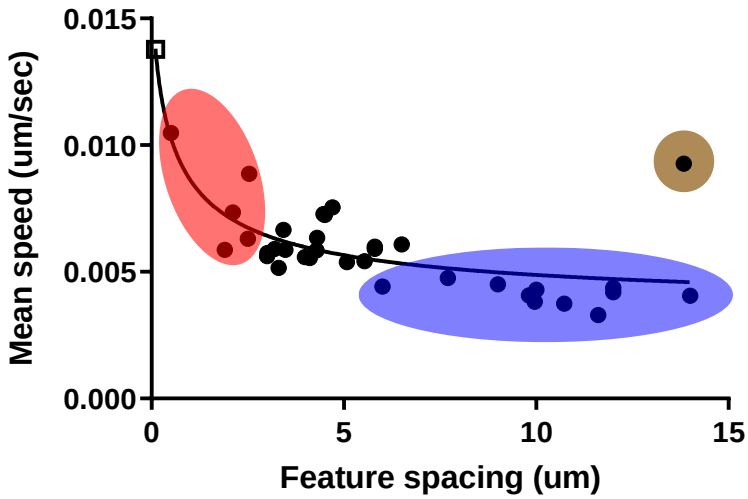


Figure 7-6: Mean speed can be correlated to feature spacing

The flat surface is visualised as the square. The feature spacing is defined by the diagonal space between features. A nonlinear regression curve is fitted to provide a standard curve.

These data indicate that features that are very close to each other ('little spacing') have similar movement behaviour as the flat surface, because cells will mostly move on top of the features; **red area.** However, features with 'intermediate spacing' slow down movement and also restrict how far cells will move in between them: cells are going through a 'labyrinth'; **blue area.** Finally, features that are spaced very far apart ('far spaced'), let cells move freely in between them, cells move unrestricted similar to flat surface; **brown area.**

Examples of these classifications can be seen in Figure 7-7.

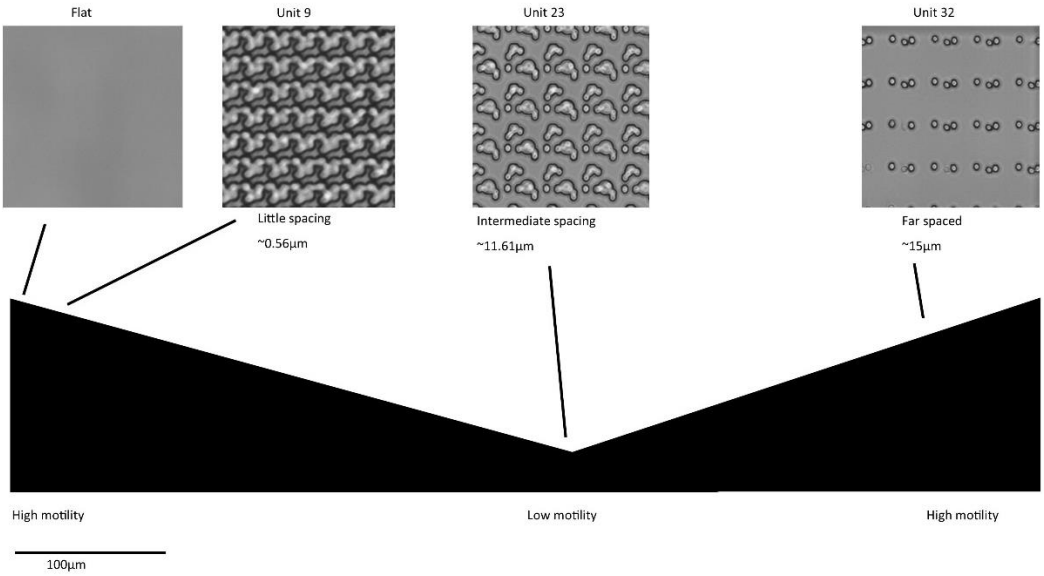


Figure 7-7: Examples of feature spacing classes

Features are classed into three groups (little, intermediate and far spacing) and have distinct effects on DC motility, with intermediate spacing slowing down DC movement the most.

After classifying the units/features into these three classes and referring these classes back into the correlation between mean speed and track displacement, it becomes obvious that the red and brown areas (standing for little spacing and very far spacing) are very similarly located in that correlation graph – whereas the little spacing class is also mixing in with the non- classed features (Figure 7-8). The blue area (intermediate spacing) however, presents itself as a tight cluster with the least speed and displacement.

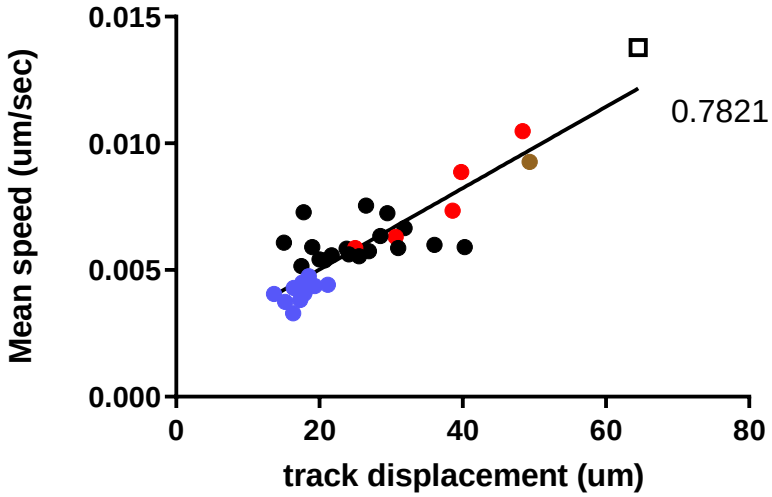


Figure 7-8:Mean speed vs track displacement

Modification of correlation between mean speed and track displacement from Figure 7-3 with the classes from Figure 7-6.The flat surface is visualised as a square. A linear regression curve was fitted into the graph, resulting in a R2 value of 0.7821 of correlation between mean speed and track displacement of DCs.

7.3.2 Topography culture decreases HLA-DR expression on iDCs

To assess the impact of topographic features on DC phenotype $6.5x10^5$ immature DCs were cultured for 24 hours on the punched-out wafers as described in 7.2.3. To account for donor-to-donor variations, each donor was normalised to its flat PS control condition to provide a baseline for each donor.

Only HLA-DR was shown to be modulated in expression level strength (Figure 7-9), with several features suppressing HLA-DR expression – 990, 1130, 2113 and I decreased the expression of HLA-DR significantly. The suppression of HLA-DR expression for topography 1130 was 40% less than the flat PS control. Following topography culture, the phenotype of DCs was not significantly

modulated in the expression levels of other investigated surface markers CD83, CD86, CCR7 and PD-L1 (Figure 7-10).

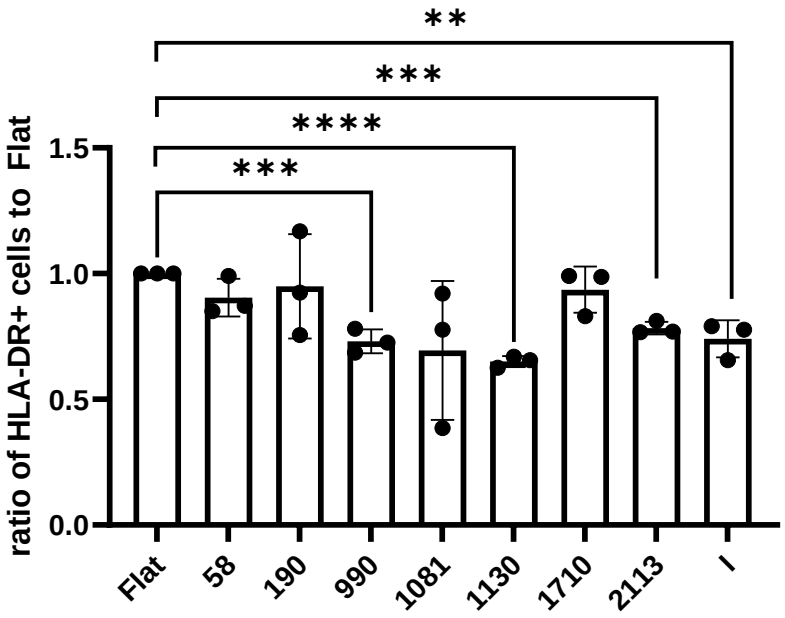


Figure 7-9: Modulation of HLA-DR expression on immature DCs following 24 hours culture on topographies.

DCs were stained for HLA-DR and analysed via flow cytometry. Data is from 3 independent experiments and shows the ratio of HLA-DR+ cells compared to the flat condition as mean ± SD. For significance: *<0.05; **<.01; ***<0.001; ****<0.0001, by Students T-Test.

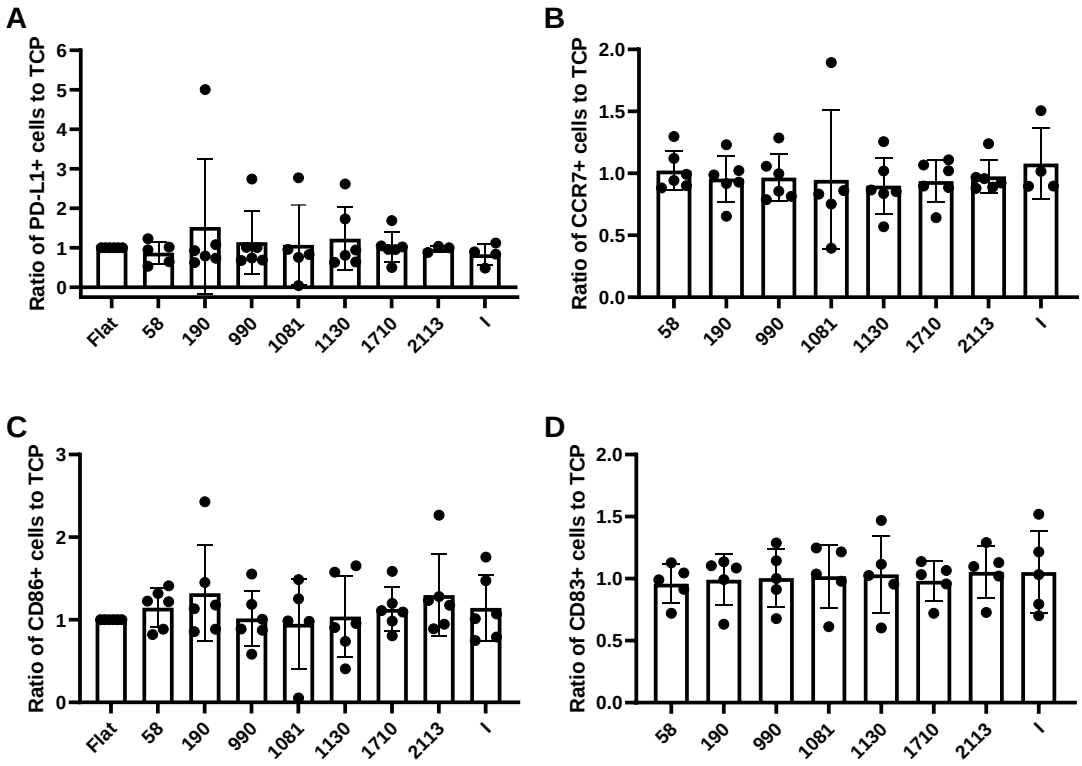


Figure 7-10: No modulation of PD-L1, CCR7, CD83 and CD86 after iDC topography culture.

DCs were stained for respective antibodies and acquired by flow cytometry. Data is from 5 independent donors and shows the ratio of percentage of positive cells normalised to the flat condition and shown as mean ± SD.

7.3.3 **LPS stimulation DCs on topographies leads to less activated DCs**

Seeing how HLA-DR expression was decreased on immature DCs after topography culture, a new hypothesis whether topographies might influence the stimulation of TLRs on DCs was formed. In this experimental set-up LPS (*e.coli*) was used as a model stimulant to engage the TLR-4 - pathway.

Immature DCs were cultured for 6 hours on the topographic wafers, and then stimulated with LPS for a further 18 hours – they were then assessed for the

expression levels of CD83, CD86, HLA-DR, CCR7 and PD-L1. HLA-DR was observed to be decreased after culture on two specific topographies (990 and 1130), a reduction of 20% compared to flat PS (Figure 7-11). Interestingly one topography increased HLA-DR expression slightly, but significantly (1081).

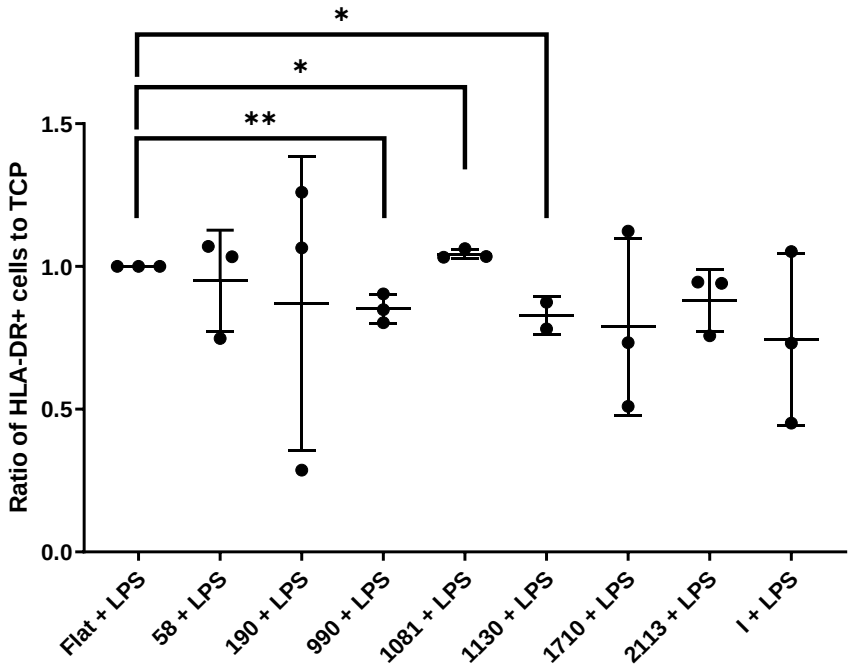


Figure 7-11: HLA-DR expression is modulated when DCs are stimulated with LPS on topographies

Cells were stained for HLA-DR and analysed via flow cytometry. Data is from 3 independent experiments and shows ratio of HLA-DR+ cells compared to flat condition and presented as mean ± SD. Experimental conditions are compared to the flat surface control to compare fold changes over different donors. For significance T-tests were performed and significance highlighted: *<0.05; **<.01; ***<0.001; ****<0.0001.

Topography 1130 induced lower CCR7 and CD83 expression in DCs stimulated on that topographic feature. Topography 1710 induced lower C83 and CD86 expression in LPS-stimulated DCs, while roman number I feature

downregulated CD86 expression significantly. PD-L1 expression showed no changes in expression following LPS stimulation on topographies (Figure 7-12).

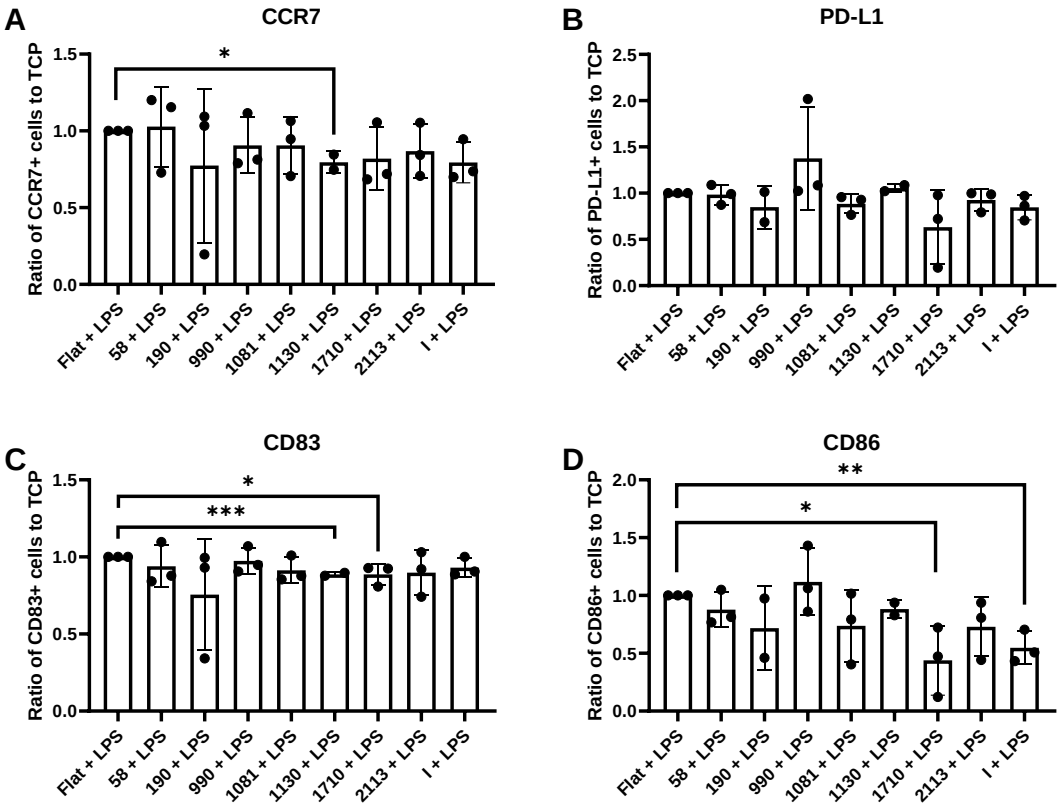


Figure 7-12: CCR7, PD-L1, CD83 and CD86 expression in LPS-stimulated DCs on topographies

Cells were stained for respective antibodies and analysed via flow cytometry. Data is from 3 independent experiments and shows ratio of positive cells compared to flat condition and presented as mean ± SD. Experimental conditions are compared to the flat surface control to compare fold changes over different donors. For significance: *<0.05; **<.01; ***<0.001; ****<0.0001, by Students T-Test.

7.3.4 **Assessing cytokine secretion on topographies**

Following the observations of DC phenotype and movement behaviours, the levels of pro-inflammatory (IL-12p70) and anti-inflammatory (IL-10) cytokines secreted into the culture medium were quantified.

Due to biological variations observed across donors tested, cytokine concentrations were normalised to flat PS control to allow for a more accurate comparison of culture conditions. Following normalisation, no statistically significant differences were observed in the levels of IL-12p70 and IL-10 produced by unstimulated DC on topographic features compared to the flat polystyrene (Figure 7-13 A and B). Only topography 190 very slightly decreased the fold change of IL-10 concentration. For the stimulated conditions, topography 190 again decreased slightly the fold change for IL-10 concentration between topography and flat PS control (Figure 7-13 C and D). Topography 1710 + LPS induced slight elevated levels of IL-12p70 secretion.

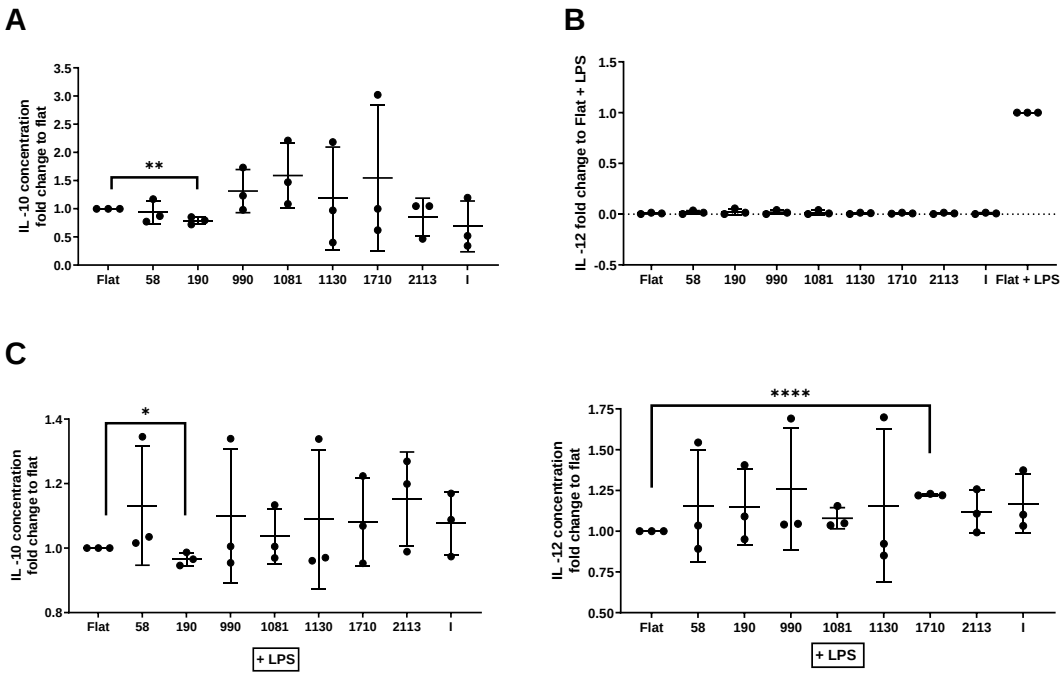


Figure 7-13: IL-10 and IL-12 secretion after DC culture on topographies with and without LPS stimulation

Topographies are investigated for their ability to modulate IL-10 and IL-12 secretion. Experimental conditions are compared to the flat surface control, except for B when compared to Flat + LPS, as Flat cytokine levels were non-detectable. Data is from 3 independent experiments and represented as mean ± SD and fold change normalised to flat control. ONE-way ANOVA with Bonferroni multiple comparisons test. For significance: *<0.05; **<.01; ***<0.001; ****<0.0001, by Students T-Test.

7.3.5 Effect of topography culture on DC ability to initiate T cell response

In order to assess the possible functional modulation of DCs by topographic features, the ability of topography cultured DCs to interact with CD3+ T cells in a co-culture system was assessed.

After 8 days of co-culture T cells showed to have proliferated more with topography 1130 and topography 1710-modulated DCs, when compared to

flat polystyrene (Figure 7-14). However, only the 1710-culture condition was statistically significant. The LPS stimulated DCs on the same topographies were on the same proliferation levels as the non-stimulated DCs.

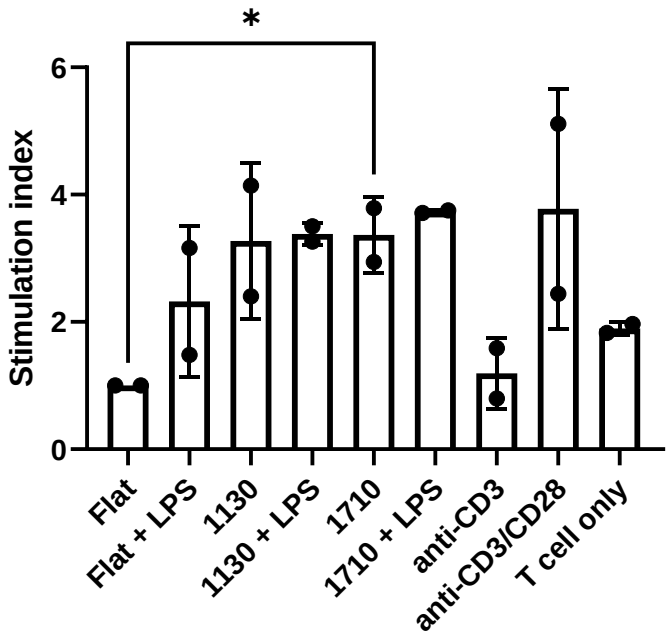


Figure 7-14: CD3+ T cell proliferation for topography modulated DCs.

Proliferation was assessed by BrdU incorporation and then calculated into a stimulation index. Data is from 1 biological donor with 2 technical repeat wells. Data is presented as mean ± SD. Significance is determined by t-test. For significance: *<0.05; **<.01; ***<0.001; ****<0.0001, by Students T-Test.

DC culture on topography 1710 significantly decreased IFN-γ secretion in both the unstimulated condition (Figure 7-15 A). Both culture on topography 1130 and 1710 significantly reduced IL-10 secretion by T cells, while IL-17 secretion was shown to be not modulated by topography cultures.

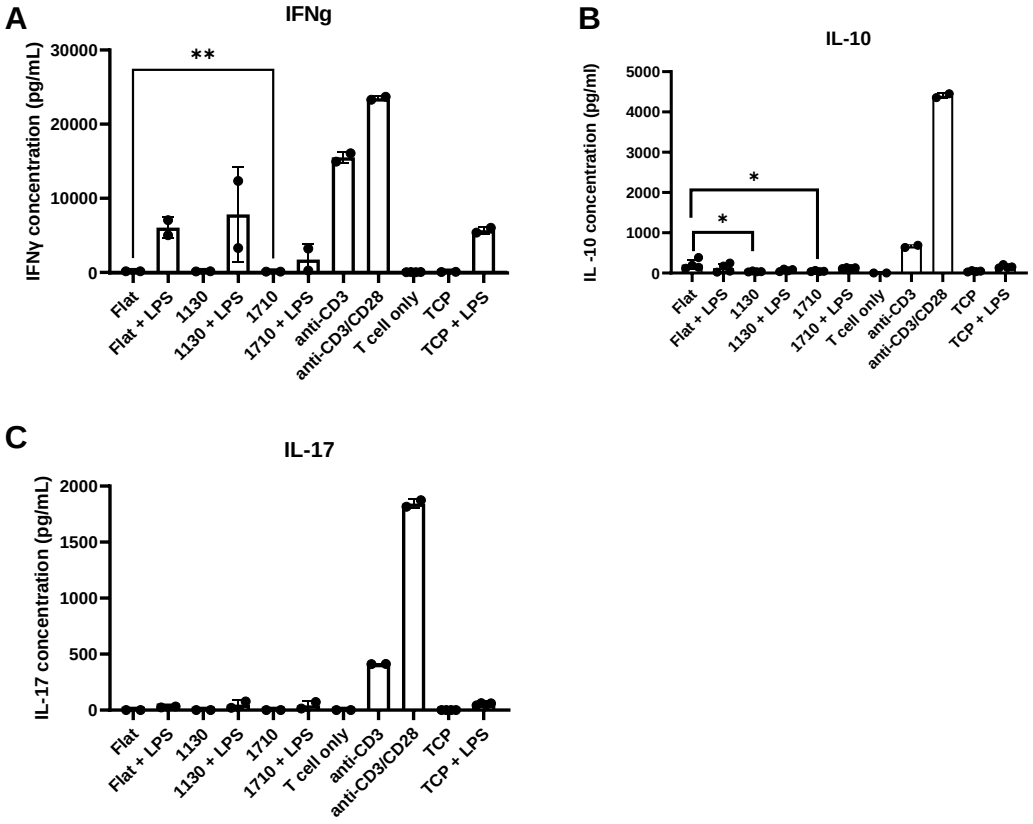


Figure 7-15: Topography-treated DCs induce modulated T cell secretion

Cytokine secretion was assessed by ELISA technique. **A** IFN-γ, **B** IL-10 and **C** IL-17. Data is from 1 biological donor and 2 technical repeats. Data is presented as mean ± SD. For significance: *<0.05; **<.01; ***<0.001; ****<0.0001, by Students T-Test.

7.4 Discussion

A potential strategy to control immune cell responses is the manipulation of biomaterial surface topography. Despite recent interest on topographical control of cells, little attention has been given to whether complexly designed topographic features can modulate DC phenotype and function. This chapter therefore presents the first data in a directed approach on the response of human moDC to topographic features.

The modulatory effects of topographic features on DC phenotype and function were assessed by quantifying the levels of key cytokines (IL-10 and IL-12), as well as the surface marker expression of a panel of markers that are known to characterise DC activation levels (CD83, CD86, CCR7, HLA-DR and PD-L1). Due to their function to patrol tissues to find pathogens, DCs are very motile cells. Change of DC motility can therefore have a big impact on immunity and its regulation.

Results generated from this investigation show, that there is a direct correlation between the spacing in between features and slowing down of DC movement – cells that have tighter spaces to navigate through, will move less and at a much slower speed. This can likely be attributed to the ‘3D environment’ cells are encountering inside the morphological architecture design. If feature height is greater than DC height and the spacing between the features big enough for cells to fall into the gaps, they would experience a maze-like environment surrounding them. However, features that are narrowly spaced will not give cells the opportunity to easily move between the features and cells will more likely move on top of the features (e.g., using it as a solid surface). In

agreement to my study here, another study looking at DC migration through microchannel (smooth or with different separation periods that look like compressed channels) showed that bone marrow derived DCs migrated fastest in the smooth channel and slowest in the microchannels with the most ‘hindrance’through the environment. This can be compared to our topography features, where cells moved slower through the maze of features with slowest movement at feature spacings of 5-13 µm, which is in agreement to the slowest migration in microchannels with separators in every 6-12 µm [300].

For the Phenom28 study, initially 34 different surfaces were used and 9 topographies with potential immune modulatory effects were identified and investigated further. Ensuing experiments s were therefore run with 9 different topographies. T cells are known to recognize mechanical forces through mechanical triggering of their T cell receptors (TCR) and integrin LFA-1 [301], [302]. By fabrication of scaffolds with varying stiffnesses, it was observed that T cells cultured in stiffer 3D matrices proliferated at a higher rate and showed more activation [303]. With the addition of APCs (both natural and artificial beads), the immune synapses were shown to be bigger in the stiffer matrices leading to increased T cell activation. Taken together, T cells are observed to sense 3D environmental micromechanical stiffness whether the stimulatory signal come from APCs or artificial APC beads [303]. APCs used in that study were I-A^b-bearing B-cell lymphoma line LB27.4 and were incubated with OVA as a model peptide and therefore cannot be compared to the DCs used during this study.

There were no obvious induction or suppression of IL-10 and IL-12 production for both unstimulated and LPS stimulated DCs for most topographies; however, topography 190 showed less IL-10 secretion both in the unstimulated and LPS stimulated condition. This could be due to the fact, that Topo190 was the topographic surface with the least donor-to-donor-variation. Although this slight suppression of IL-10 secretion is statistically significant, its biological relevance needs to be determined.

Phenotype investigations show that topographic features decrease the expression of HLA-DR, while other surface markers are not modulated in non-activated DCs. A limited number of topographies inhibit the upregulation of CCR7, CD86 and CD83 slightly; with HLA-DR most potently being modulated when DCs were stimulated with LPS on top the topographies.

Remarkably, even though activation markers and antigen-presentation markers were less expressed, DCs cultured on 2 chosen topographic features induced higher CD3+ T cell proliferation than the flat planar control surface, when subjected to investigation of their T cell interaction and activation capability. Interestingly, topography-modulated DCs were observed to increase the proliferation of CD3+T cells in an 8-day co-culture, as well as moderate cytokine secretion modulation. T cell co-cultures on topography 1710 significantly decreased IL-10 and IFN-γ secretion in the unstimulated condition (Figure 7-15 A), with its biological relevance unclear.

Using screening platforms with non-adherent cells is problematic, as an *in-situ* immunofluorescence readout is nearly impossible. For this situation alternative readouts, such as the ones utilized here had to be identified. Flow cytometry

is an efficient analytical tool to show surface marker expression on non-adherent cells harvested from topographic features. Although flow cytometry can be used in 96-well plates, this is still only a semi-high throughput screen and better tools are needed. Therefore, a final answer cannot be given to the question whether DCs get influenced by topography culture – solely, these limited number of features investigated here can be ascertained to not show any appreciable modulation of DC phenotype or function. As there has not been any studies conducted of DC phenotype modulation by surface topographies, it is difficult to evaluate this study in comparison to the literature. Less complex surface features such as roughness have been shown to modulate the state of DC activation, but on the more complex side (at least on the few features investigated here) no clear correlations were able to be made [121], [304]. A study investigating DC response to surface properties of clinical titanium surfaces showed that surface roughness induced higher expression levels of CD86, but had no effect on CD83 or any of the MHC molecules. While in contrast to this study I found HLA-DR to be modulated by surface topographies, I also did not find CD83 to be altered. In agreement to some of my data, the clinical titanium surfaces in that study were shown to not suppress DC's capability to respond to bacterial stimulie (e.g., LPS), I however found a topography that significantly lowered HLA-DR expression on DCs after LPS-stimulation (but induced increased T cell proliferation levels) [305].

In conclusion in this chapter, it was observed that topographical features can modulate the speed at which DCs move and that a clear relationship between feature spacing and speed can be established. The phenotype data shows

several features to be slightly immune modulatory while no conclusive relationship or pattern was found. These modulations induce a more tolerogenic phenotype, making DCs cultured on them express a less mature phenotype. Tolerogenic DCs are able to induce tolerance in the body against specific antigens, which is useful in the treatment of autoimmune diseases. Following the observation of more T cell proliferation after DC topography culture, it would be interesting to investigate whether topography-DCs polarize naïve T cells into regulatory T cells and in turn induce antigen-specific tolerance. Overall, topographies appear to only have a limited effect on DC phenotype and function, with implications into the antigen-presenting process being the most potently observed ones. The inconclusive relationship between decreased antigen-presentation of topography-modulated DCs and increased CD3+ T cell proliferation will need to be further investigated.

Chapter 8: General Discussion

Chapter 8 **General Discussion**

Overview

With most cytokine-based immunotherapies not fulfilling the promise of efficacy seen in pre-clinical experiments, and often being associated with severe dose-limiting toxicities, biomaterial-based immunotherapies have emerged as a powerful tool in different clinical settings, including cancer vaccines, inflammatory diseases, and autoimmune diseases. DCs are crucial immune cells linking the innate and adaptive immunity, playing an important role in the orchestration of the response to specific antigens and are therefore ideal targets for immune modulation. Notably, DC phenotype is a powerful indicator of their downstream effector functions. The discovery of the ability to modulate these functions has revealed a new avenue of immune system targeted therapies. Biomaterials have in the past been found to modulate host immune responses, as well as the phenotypic state of DCs. Various biomaterial polymers (alginate, agarose, chitosan, HA, PLGA) have been shown to exert differential effects on DC activation levels [89], [123], [167]. In the past ten years, established libraries of combinatorial polymers have created opportunities to identify simple polymers with bio-instructive interactions with great success [148]–[153]. As far as it is known to me, there has been no attempt yet to have a directed screen to identify new biomaterials to bring into clinical use for DC modulation.

Major findings

By screening a polymer library constituted of acrylates, methacrylates, and acrylamides, both, stimulatory and regulatory polymers, were found to enable the instruction and inhibition of DC activation, respectively. From the 222 polymers investigated, a number of polymers instructed an immunogenic DC phenotype in the absence of any other exogenous stimulus. They significantly upregulated CD83 and CD86 expression, and showed modulations of antigen uptake ability and cytokine secretion. By reducing the number of polymers to investigate, more in-depth/complex experiments were possible, allowing global gene expression studies and mixed lymphocyte reactions. Specially in the case of DEAEA and HFiPMA, which were additionally tested as DC modulators in a breast cancer-based tumour assay, showing the efficient induction of tumour specific CTLs. Thus, making them very promising candidates for future animal cancer studies. Additionally, DEAEA and HFiPMA were tested using microarray platform/technologies, showing evidence that supports the phenotypical and functional findings, as well as revealing new details about activated DC phenotype, increased NFκB signalling, and the functional downstream effects such as antigen cross-presentation. Upregulated canonical pathways involving B cells, and natural killer cells, gave indications of other DC-immune cell interactions which should be investigated. The HFiPMA gene array data revealed mixed expression levels of integrin signalling, implicating a potential role of integrin in DC response to HFiPMA, which fits to earlier studies but requires further experiments [140]. This may support earlier findings by Rogers *et al*. but requires further experiments as

findings from the gene array study were not able to give conclusive results towards integrin signalling due to mixed expression levels [121], [140].

A limited number of polymers were able to induce a tolerogenic DC phenotype, and hence, immune tolerance, showing potential for applications in autoimmune disease settings. The data presented here provide a good basis to support future research into seeking further understanding of the function of ZnA as an inducer of immune tolerance. Unfortunately, this was not followed up more closely in this project due to a higher focus on the stimulatory polymers.

Strengths and limitations of the research

The strength of material based immune instruction is, that it does not rely on cytokines to modulate the immune response. Cytokine based immunotherapy can be detrimental for cells and lead to toxicity issues. Additionally, no delivery systems as such are needed to uphold modulation capability, as the material itself can be implanted as a scaffold, negating the need for slow-release platforms.

Interestingly, culture on 33% of the investigated polymers showed a higher DC survival efficiency in comparison to the tissue culture plastic (Figure 3-2). A possible explanation for this might be that proteins adsorbed on these polymers induce higher DC viability, in comparison to the surface chemistry of the tissue culture plastic polystyrene. Previously, gas permeable hydrophobic culture bags have been found to be superior for viability, yield, and function of DCs cultured in plastic tissue culture flasks, or well plates. Comparing various

well plate formats and plate materials, a study concluded that DCs cultured and assayed under conditions that minimise cell adherence were functionally better, as well as conferring more viability [170]. These polymers were not further investigated in this setting; however, they could prove to be relevant for *ex vivo* experiments using DC cultures as an alternative culture surface (such as Polyolefin bags) instead of tissue culture plastic.

Something not investigated previously about these polymers, is the mechanical interaction of DCs with the polymers. Are they due to integrin attachment or TLR engagement? At least for HFiPMA, the gene microarray data indicated an involvement of integrins, which should be investigated further.

One limitation of this large number polymer approach was that few specific markers were chosen to determine the positive 'hits' of the search. This means that some polymers might have been efficient bio-instructive materials in modulating DCs, but not significant on CD83 and CD86 expression. Further analysis of some of these polymers will be more than likely to reveal DC modulation, which would have been not previously discovered due to the limited nature of this study.

Future avenues of this research

Future efforts should focus more on translating the 3 hit polymer coatings into deliverable formats, such as 3D particulates, or macroporous scaffolds, to evaluate the ability of materials to modulate the immune system *in vivo*. These 3D formats could then find application in cancer therapy and vaccine adjuvants.

The scaffolds developed here showed promising initial data, which will hopefully lead to more successful research in the future.

Moving to appropriate animal models to validate the shown tumour killing effect *in vivo* would be a next step in the application for cancer treatment. The further development of the fabricated stimulatory HFiPMA scaffolds could be advantageous in these animal models, simplifying the experiments by implanting a small scaffold instead of giving a DC vaccine. Furthermore, the gene microarray has more information hidden in its vast amount of data, which has been analysed only at its surface, revealing some of the most impactful genes, however, deeper analysis could reveal even more genes or canonical pathways. More scrutiny of these data sets might be able to reveal more details on how DCs interact with the polymers, or even implementation of more in-depth techniques such as RNA sequencing, or single cell sequencing, might reveal more details on how DCs interact with the polymers at a genetic level.

Since the regulatory polymers were not the main focus of this study, more functional studies to assess the functional modulatory capabilities of these polymers would be suggested. Following on from the functional results, results could be used to translate the polymers into appropriate disease 2D and 3D models for the next steps of immune tolerance validation.

Further material characterisation might involve water contact angle measurements, which will reveal the materials hydrophobicity, and additional investigations towards the polymer's composition of adsorbed proteins onto its surface. Material hydrophobicity has previously been implicated in immune cell modulation, so might be a useful material characterisation to add more insight

of polymer induced DC modulations. Several studies have reported the use proteomics-based approaches, such as Liquid Chromatography-Tandem Mass Spectrometry, to identify proteins adsorbed onto biomaterials [174]. Future work on these polymers could involve proteomics analysis of protein adsorbates, for the identification of proteins that are unique to the different polymers. This would provide more insight on the molecular mechanisms through which polymers influence DC behaviour.

Topography study

The motility study on topographies has shown that there is a clear relationship between feature spacing, and speed of DCs, due to the 3D environment the cell encountered. Analysis of DC phenotype indicated several features to be slightly immune modulatory, while no conclusive relationship or pattern was found. These modulations induce a more tolerogenic phenotype, making DCs cultured express a less mature phenotype. Overall, more insight is needed into topography effects on DC, although findings from this thesis suggest that topographies have only a limited impact on DC phenotype and function, with implications into the antigen-presenting process being the most potently observed ones. The inconclusive relationship between decreased antigen-presentation of topography-modulated DCs, and increased CD3+ T cell proliferation, will need to be further investigated.

Conclusion

This research project has shown the feasibility of DC – polymer/material screenings in order to identify novel materials for clinical use. Whereas

previously all DC-materials studies where done on selected few materials, this study has proven the feasibility to pursue larger number screenings. Specially, metabolites, cytokines (soluble factors), but also cell-specific factors, such as surface marker expression levels are able to be assayed on hundreds of polymers – as long as sufficient cell numbers and distinction of materials (by well separation) are given. It is expected that further large-scale screens should come to fruition based on this project. There is already another PhD project, which is currently pursuing the fabrication of printed polymer coatings within 96 and 384-WPs to follow on from data from this study, while also trying to modify the fabrication approach taken here (UV polymerisation), that unfortunately introduced some cell toxicities by solvent and monomer trapping.

The clinical applicability of the identified immune-instructive polymers and fabricated polymeric scaffolds has been pursued by finalising a grant application that is aimed at investigating the efficacy of polymer scaffolds against breast cancer in a mouse model. Utilisation of immune instructive polymers in 3D formats, such as scaffolds, can find application in the treatment of cancer (in the case of stimulatory polymers) or autoimmune diseases (in the case of regulatory polymers), or in particulate format polymers could be used as adjuvants in vaccines.

In this research project, I have discovered polymers that induce pro- or anti-inflammatory phenotypes in human DCs *in vitro*. These polymer-primed DCs induce differentiation of CD8 T cells with robust tumour killing activity in an in vitro breast cancer tumour killing assay. Intriguingly, the performance of polymers-primed DCs in these assays is better than cytokine-primed DCs with

potent pro-inflammatory function. I have also successfully fabricated macroporous scaffolds using these polymers and now hypothesise that when implanted adjacent to tumour environment such 3D scaffold can induce *in situ* anti-tumour immune responses *in vivo*. The use of 'immune-instructive' polymers for *in situ* immune modulation presents a step change in the current immunotherapy approaches that rely on use of biologics and cytokines that are associated with high cost and extensive side/off-target effects. While the initial hypothesis is on breast cancer the tools and data generated further on in this project will have wider applications in cancer immunotherapy for other solid cancers as well as other indications of organ specific *in situ* immunotherapy.

Current treatments for breast cancer include surgery, chemo and radiotherapy. These usually induce severe side effects in most of the patients, and treatment efficiency is often insufficient too, with high rates of cancer recurrence. Additionally, breast cancer therapies put substantial burden the NHS.

The recent development of immunotherapies has already led to clinical use of checkpoint inhibitors, however, most of these drugs are only focused on specific cohorts of patients (e.g., PD-L1 positive patients) [281]. DC based cancer vaccines have also shown great promise however generating DC vaccines is not efficient and e*x vivo* generated DCs often do not induce robust anti-tumor responses due to poor migration and weak immune-stimulatory effects. On the other hand, systemic or local use of immunostimulatory cytokines to activate DCs requires multiple applications, is expensive and importantly can cause severe side effects [306]. There is therefore significant

scope for developing novel solutions to allow *in situ* immune-stimulation to promote anti-tumor immunity without relying on cytokines or biologics.

The here presented solution involves using simple, inexpensive and scalable polymers for *in situ* immune-stimulation of DCs to develop tools for the next generation of DC based vaccines. This could lead to a step-change in delivering local immune modulation. The pre-clinical application of implantable cytokine loaded polymeric scaffolds for cancer has been trialled by Mooney group in the last years successfully, as well as currently investigated in clinical phase I trials [307], [308]. However, the fundamental advantage of the here presented polymers is their inherent 'immune-instructiveness' eliminating the need for addition of exogenous cytokines and chemokines. In our case, we solely plan to introduce the scaffold itself, providing a template for DCs to get activated on their own without exogenous stimulus. This should offer simpler regulatory approval process further along the development pathway.

In conclusion, findings from this thesis demonstrate the ability of surface chemistries to manipulate physiological phenomena: activating DCs towards a mature state that is able to induce efficient tumour killing via cytotoxic T cells.

Chapter 9 **References**

[1] J. Parkin and B. Cohen, “An overview of the immune system,” *Lancet*, vol. 357, no. 9270, pp. 1777–1789, 2001.

[2] J. Canton, D. Neculai, and S. Grinstein, “Scavenger receptors in homeostasis and immunity,” *Nat. Rev. Immunol.*, vol. 13, no. 9, pp. 621–634, 2013.

[3] R. C. Davicino, R. J. Eliçabe, M. S. Di Genaro, and G. A. Rabinovich, “Coupling pathogen recognition to innate immunity through glycan-dependent mechanisms,” *Int. Immunopharmacol.*, vol. 11, no. 10, pp. 1457–1463, 2011.

[4] C. A. Janeway, “Approaching the asymptote? Evolution and revolution in immunology,” in *Cold Spring Harbor Symposia on Quantitative Biology*, 1989.

[5] L. A. J. O’Neill and E. J. Pearce, “Immunometabolism governs dendritic cell and macrophage function,” *Journal of Experimental Medicine*, vol. 213, no. 1. 2016.

[6] S. Akira, K. Takeda, and T. Kaisho, “Toll-like receptors: Critical proteins linking innate and acquired immunity,” *Nature Immunology*. 2001.

[7] B. Beutler, “ScienceDirect - Molecular Immunology : Innate immunity: an overview,” *Mol. Immunol.*, 2004.

[8] C. A. Janeway and R. Medzhitov, “Innate immune recognition,” *Annu. Rev. Immunol.*, vol. 20, no. 1, pp. 197–216, Apr. 2002.

[9] W. I. Weis, M. E. Taylor, and K. Drickamer, “The C-type lectin superfamily in the immune system,” *Immunological Reviews*. 1998.

[10] C. G. Figdor, Y. Van Kooyk, and G. J. Adema, “C-type lectin receptors on dendritic cells and langerhans cells,” *Nature Reviews Immunology*. 2002.

[11] H. Kato *et al.*, “Differential roles of MDA5 and RIG-I helicases in the recognition of RNA viruses,” *Nature*, 2006.

[12] N. Inohara and G. Nunez, “Cell death and immunity: NODs: intracellular proteins involved in inflammation and apoptosis.,” *Nat. Rev. Immunol.*, 2003.

[13] A. Takaoka *et al.*, “DAI (DLM-1/ZBP1) is a cytosolic DNA sensor and an activator of innate immune response,” *Nature*, 2007.

[14] F. Y. and F. K., *Microbial Glycoconjugates Recognition with TLRs and NLRs in Innate Immunity*. Springer, Tokyo, 2015.

[15] T. B. . Geijtenbeek *et al.*, “Identification of DC-SIGN, a Novel Dendritic Cell–Specific ICAM-3 Receptor that Supports Primary Immune Responses,” *Cell*, vol. 100, no. 5, pp. 575–585, 2000.

[16] E. J. Soilleux, L. S. Morris, S. Rushbrook, B. Lee, and N. Coleman, “Expression of human immunodeficiency virus (HIV)-binding lectin DC-SIGNR: Consequences for HIV infection and immunity,” *Hum. Pathol.*, vol. 33, no. 6, pp. 652–659, 2002.

[17] C. Guzzi *et al.*, “Detection and quantitative analysis of two independent binding modes of a small ligand responsible for DC-SIGN clustering,” *Org. Biomol. Chem.*, vol. 14, no. 1, pp. 335–344, 2016.

[18] L. Wu *et al.*, “Rhesus macaque dendritic cells efficiently transmit primate lentiviruses independently of DC-SIGN.,” *Proc. Natl. Acad. Sci. U. S. A.*, vol. 99, no. 3, pp. 1568–1573, 2002.

[19] J. Geurtsen, N. N. Driessen, and B. J. Appelmelk, “Mannose–fucose recognition by DC-SIGN,” in *Microbial Glycobiology*, vol. 21, no. 1, Elsevier, 2010, pp. 673–695.

[20] D. Delcassian, S. Sattler, and I. E. Dunlop, “T cell immunoengineering with advanced biomaterials,” *Integr Biol*, vol. 9, no. 3, pp. 211–222, 2017.

[21] F. Ouaaz, J. Arron, Y. Zheng, Y. Choi, and A. A. Beg, “Dendritic cell development and survival require distinct NF-κB subunits,” *Immunity*, 2002.

[22] J. H. Niess and H. C. Reinecker, “Dendritic cells in the recognition of intestinal microbiota,” *Cell. Microbiol.*, vol. 8, no. 4, pp. 558–564, 2006.

[23] M. Haniffa *et al.*, “Human Tissues Contain CD141 hi Cross-Presenting Dendritic Cells with Functional Homology to Mouse CD103 + Nonlymphoid Dendritic Cells,” *Immunity*, vol. 37, no. 1, pp. 60–73, 2012.

[24] O. P. Joffre, E. Segura, A. Savina, and S. Amigorena, “Cross-presentation by dendritic cells,” *Nat Rev Immunol*, vol. 12, no. 8, pp. 557–569, Aug. 2012.

[25] M. Embgenbroich and S. Burgdorf, “Current concepts of antigen cross-presentation,” *Frontiers in Immunology*, vol. 9, no. JUL. 2018.

[26] F. Benencia, M. Muccioli, and M. Alnaeeli, “Perspectives on Reprograming Cancer-Associated Dendritic Cells for Anti-Tumor Therapies.,” *Front. Oncol.*, vol. 4, no. April, p. 72, 2014.

[27] K. Palucka and J. Banchereau, “Cancer immunotherapy via dendritic cells,” *Nat. Rev. Cancer*, vol. 12, no. 4, pp. 265–277, 2012.

[28] P. Gogolak *et al.*, “Differentiation of CD1a- and CD1a+ monocyte-derived dendritic cells is biased by lipid environment and PPARγ,” *Blood*, vol. 109, no. 2, pp. 643–652, 2007.

[29] D. F. Legler, E. Uetz-Von Allmen, and M. A. Hauser, “CCR7: Roles in cancer cell dissemination, migration and metastasis formation,” *Int. J. Biochem. Cell Biol.*, vol. 54, pp. 78–82, 2014.

[30] A. Ager and M. J. May, “Understanding high endothelial venules: Lessons for cancer immunology,” *Oncoimmunology*, vol. 4, no. 6, pp. 1–14, 2015.

[31] A. D. McLellan, A. Heiser, and D. N. J. Hart, “Induction of dendritic cell costimulator molecule expression is suppressed by T cells in the absence of antigen-specific signalling: Role of cluster formation, CD40 and HLA-class II for dendritic cell activation,” *Immunology*, vol. 98, no. 2, pp. 171–180, 1999.

[32] C. Aerts-Toegaert *et al.*, “CD83 expression on dendritic cells and T cells: Correlation with effective immune responses,” *Eur. J. Immunol.*, vol. 37, no. 3, pp. 686–695, 2007.

[33] J. S. Suwandi, T. Nikolic, and B. O. Roep, “Translating mechanism of regulatory action of tolerogenic dendritic cells to monitoring endpoints in clinical trials,” *Front. Immunol.*, vol. 8, no. NOV, pp. 1–8, 2017.

[34] J. S. Suwandi, R. E. M. Toes, T. Nikolic, and B. O. Roep, “Inducing tissue specific tolerance in autoimmune disease with tolerogenic dendritic cells,” *Clin. Exp. Rheumatol.*, vol. 33, pp. 97–103, 2015.

[35] K. Steinbrink, M. Wölfl, H. Jonuleit, J. Knop, and A. H. Enk, “Induction of tolerance by IL-10-treated dendritic cells.,” *J. Immunol.*, 1997.

[36] A. Vanherwegen, C. Gysemans, and L. Overbergh, “Dendritic cell metabolism: immunity and tolerance,” *Oncotarget*, vol. 6, no. 33, pp. 34039–34040, 2015.

[37] S. Solano-Gálvez *et al.*, “Human Dendritic Cells: Ontogeny and Their Subsets in Health and Disease,” *Med. Sci.*, vol. 6, no. 4, p. 88, 2018.

[38] J. Lee *et al.*, “Restricted dendritic cell and monocyte progenitors in human cord blood and bone marrow,” *J. Exp. Med.*, vol. 212, no. 3, pp. 385–399, 2015.

[39] G. Breton, J. Lee, K. Liu, and M. C. Nussenzweig, “Defining human dendritic cell progenitors by multiparametric flow cytometry,” *Nat. Protoc.*, vol. 10, no. 9, pp. 1407–1422, 2015.

[40] K. Liu *et al.*, “In Vivo Analysis of Dendritic Cell Development and Homeostasis,” *Science (80-.).*, vol. 123, no. 19, pp. 2145–2156, Mar. 2009.

[41] K. P. A. MacDonald, D. J. Munster, G. J. Clark, A. Dzionek, J. Schmitz, and D. N. J. Hart, “Characterization of human blood dendritic cell subsets,” *Blood*, vol. 100, no. 13, pp. 4512–4520, 2002.

[42] Y. J. Liu, “Dendritic cell subsets and lineages, and their functions in innate and adaptive immunity,” *Cell*, vol. 106, no. 3, pp. 259–262, 2001.

[43] M. Colonna, G. Trinchieri, and Y. J. Liu, “Plasmacytoid dendritic cells in immunity,” *Nat. Immunol.*, vol. 5, no. 12, pp. 1219–1226, 2004.

[44] J.-F. Fonteneau *et al.*, “Activation of influenza virus–specific CD4+ and CD8+ T cells: a new role for plasmacytoid dendritic cells in adaptive immunity,” *Blood*, vol. 101, no. 9, pp. 3520–3526, 2003.

[45] F. Ginhoux *et al.*, “Langerhans cells arise from monocytes in vivo,” *Nat. Immunol.*, vol. 7, no. 3, pp. 265–273, 2006.

[46] L. Chorro *et al.*, “Langerhans cell (LC) proliferation mediates neonatal development, homeostasis, and inflammation-associated expansion of the epidermal LC network,” *J. Exp. Med.*, vol. 206, no. 13, pp. 3089–3100, 2009.

[47] H. Hemmi *et al.*, “Skin antigens in the steady state are trafficked to regional lymph nodes by transforming growth factor-β1-dependent cells,” *Int. Immunol.*, vol. 13, no. 5, pp. 695–704, 2001.

[48] M. L. Kripke, C. G. Munn, A. Jeevan, J. M. Tang, and C. Bucana, “Evidence that cutaneous antigen-presenting cells migrate to regional lymph nodes during contact sensitization.,” *J. Immunol.*, 1990.

[49] F. Sallusto and A. Lanzavecchi, “Efficient presentation of soluble antigen by cultured human dendritic cells is maintained by granulocyte/macrophage colony-stimulating factor plus iuterleukin 4 and downregulated by tumor necrosis factor α,” *J. Exp. Med.*, vol. 179, no. 4, pp. 1109–1118, 1994.

[50] B. León, M. López-Bravo, and C. Ardavín, “Monocyte-derived dendritic cells,” *Semin. Immunol.*, vol. 17, no. 4, pp. 313–318, 2005.

[51] L. J. Zhou and T. F. Tedder, “CD14+ blood monocytes can differentiate into functionally mature CD83+ dendritic cells,” *Proc. Natl. Acad. Sci. U. S. A.*, 1996.

[52] L. Klein, B. Kyewski, P. M. Allen, and K. A. Hogquist, “Positive and negative selection of the T cell repertoire: what thymocytes see (and don’t see),” *Nat. Rev. Immunol.*, vol. 14, no. 6, pp. 377–391, 2014.

[53] K. Murphy, *Janeway’s Immunobiology*, 8 edition. Garland Science, 2011.

[54] P. Blanco, A. K. Palucka, V. Pascual, and J. Banchereau, “Dendritic cells and cytokines in human inflammatory and autoimmune diseases,” *Cytokine Growth Factor Rev.*, vol. 19, no. 1, pp. 41–52, 2008.

[55] G. E. Kaiko, J. C. Horvat, K. W. Beagley, and P. M. Hansbro, “Immunological decision-making: How does the immune system decide to mount a helper T-cell response?,” *Immunology*, vol. 123, no. 3, pp. 326–338, 2008.

[56] K. P. Walsh and K. H. G. Mills, “Dendritic cells and other innate determinants of T helper cell polarisation,” *Trends Immunol.*, vol. 34, no. 11, pp. 521–530, 2013.

[57] A. Berger, “Science commentary: Th1 and Th2 responses: what are they?,” *Br. Med. J.*, vol. 321, no. 7258, pp. 424–424, 2000.

[58] C. Dong, “TH17 cells in development: An updated view of their molecular identity and genetic programming,” *Nature Reviews Immunology*. 2008.

[59] L. E. Harrington *et al.*, “Interleukin 17-producing CD4+ effector T cells develop via a lineage distinct from the T helper type 1 and 2 lineages,” *Nat. Immunol.*, 2005.

[60] J. Tabarkiewicz, K. Pogoda, A. Karczmarczyk, P. Pozarowski, and K. Giannopoulos, “The Role of IL-17 and Th17 Lymphocytes in Autoimmune Diseases,” *Arch. Immunol. Ther. Exp. (Warsz).*, vol. 63, no. 6, pp. 435–449, 2015.

[61] B. Farhood, M. Najafi, and K. Mortezaee, “CD8+ cytotoxic T lymphocytes in cancer immunotherapy: A review,” *Journal of Cellular Physiology*, vol. 234, no. 6. 2019.

[62] D. A. Thomas and J. Massagué, “TGF-β directly targets cytotoxic T cell functions during tumor evasion of immune surveillance,” *Cancer Cell*, vol. 8, no. 5, 2005.

[63] J. C. Wang *et al.*, “Metformin’s antitumour and anti-angiogenic activities are mediated by skewing macrophage polarization,” *J. Cell. Mol. Med.*, vol. 22, no. 8, 2018.

[64] P. Kalinski, “Dendritic cells in immunotherapy of established cancer: Roles of signals 1,2,3 and 4,” *Curr. Opin. Investig. Drugs*, vol. 10, no. 6, pp. 1–17, Aug. 2010.

[65] D. Piccioli *et al.*, “Functional specialization of human circulating CD16 and CD1c myeloid dendritic-cell subsets,” *Blood*, vol. 109, no. 12, pp. 5371–5379, 2007.

[66] P. Kalinski, J. Urban, R. Narang, E. Berk, E. Wieckowski, and R. Muthuswamy, “Dendritic cell-based therapeutic cancer vaccines: what we have and what we need,” *Futur. Oncol.*, vol. 5, no. 3, pp. 379–390, Apr. 2009.

[67] B. D. Ratner, “A History of Biomaterials,” *Biomater. Sci. An Introd. to Mater. Third Ed.*, pp. xli–liii, 2013.

[68] A. S. Hoffman, *Introduction: The Diversity and Versatility of Biomaterials*, Third Edit. Elsevier, 2013.

[69] F. J. Schoen, *Introduction: “Biological Responses to Biomaterials,”* Third Edit. Elsevier, 2013.

[70] J. M. Anderson, A. Rodriguez, and D. T. Chang, “Foreign Body Reaction to Biomaterials,” *Semin. Immunol.*, vol. 20, no. 2, pp. 86–100, Apr. 2008.

[71] J. M. Anderson, *Inflammation, Wound Healing, and the Foreign-Body Response*, Third Edit., no. 2005. Elsevier, 2013.

[72] C. Nich *et al.*, “Macrophages - Key cells in the response to wear debris from joint replacements,” *Journal of Biomedical Materials Research - Part A*. 2013.

[73] L. Samelko, S. Landgraeber, K. McAllister, J. Jacobs, and N. J. Hallab, “Cobalt alloy implant debris induces inflammation and bone loss primarily through danger signaling, not TLR4 activation: Implications for DAMP-ening implant related inflammation,” *PLoS One*, 2016.

[74] N. J. Hallab and J. J. Jacobs, “Biologic effects of implant debris,” in *Bulletin of the NYU Hospital for Joint Diseases*, 2009.

[75] L. Zhang *et al.*, “The Effects of Biomaterial Implant Wear Debris on Osteoblasts,” *Front. Cell Dev. Biol.*, vol. 8, no. June, pp. 1–17, 2020.

[76] T. A. Waldmann, “Cytokines in cancer immunotherapy,” *Cold Spring Harb. Perspect. Biol.*, vol. 10, no. 12, pp. 1–23, 2018.

[77] P. Sharma and J. P. Allison, “The future of immune checkpoint therapy,” *Science (80-.).*, vol. 348, no. 6230, pp. 56–61, 2015.

[78] V. A. Schulte, M. Díez, M. Möller, and M. C. Lensen, “Surface topography induces fibroblast adhesion on intrinsically nonadhesive poly(ethylene glycol) substrates,” *Biomacromolecules*, 2009.

[79] S. Franz, S. Rammelt, D. Scharnweber, and J. C. Simon, “Immune responses to implants - A review of the implications for the design of immunomodulatory biomaterials,” *Biomaterials*, vol. 32, no. 28, pp. 6692–6709, 2011.

[80] T. O. Collier and J. M. Anderson, “Protein and surface effects on monocyte and macrophage adhesion, maturation, and survival,” *J. Biomed. Mater. Res.*, vol. 60, no. 3, pp. 487–496, Jun. 2002.

[81] M. Ventre and P. A. Netti, “Engineering Cell Instructive Materials to Control Cell Fate and Functions through Material Cues and Surface Patterning,” *ACS Appl. Mater. Interfaces*, 2016.

[82] P. . H. Thevenot W.; Tang, L., “Surface chemistry influence implant biocompatibility,” *Curr. Top. Med. Chem.*, vol. 8, no. 4, p. 11, 2008.

[83] K. G. Battiston, R. S. Labow, and J. P. Santerre, “Protein binding mediation of biomaterial-dependent monocyte activation on a degradable polar hydrophobic ionic polyurethane,” *Biomaterials*, 2012.

[84] S. Bose, S. F. Robertson, and A. Bandyopadhyay, “Surface modification of biomaterials and biomedical devices using additive manufacturing,” *Acta Biomater.*, vol. 66, no. 3, pp. 6–22, Jan. 2018.

[85] L.-C. Xu, J. W. Bauer, and C. A. Siedlecki, “Proteins, platelets, and blood coagulation at biomaterial interfaces,” *Colloids Surfaces B Biointerfaces*, vol. 124, no. 12, pp. 49–68, Dec. 2014.

[86] P. Roach, D. Eglin, K. Rohde, and C. C. Perry, “Modern biomaterials: a

review{\textemdash}bulk properties and implications of surface modifications," *J. Mater. Sci. Mater. Med.*, vol. 18, no. 7, pp. 1263–1277, Apr. 2007.

[87] P. M. Kou and J. E. Babensee, "Macrophage and dendritic cell phenotypic diversity in the context of biomaterials," *J. Biomed. Mater. Res. - Part A*, vol. 96 A, no. 1, pp. 239–260, 2011.

[88] A. P. Acharya, M. J. Clare-Salzler, and B. G. Keselowsky, "A high-throughput microparticle microarray platform for dendritic cell-targeting vaccines," *Biomaterials*, vol. 30, no. 25, pp. 4168–4177, 2009.

[89] M. Yoshida and J. E. Babensee, "Poly(lactic-co-glycolic acid) enhances maturation of humanmonocyte-derived dendritic cells," *J. Biomed. Mater. Res. Part A*, 2004.

[90] J. Koerner, D. Horvath, and M. Groettrup, "Harnessing Dendritic Cells for Poly (D,L-lactide-co-glycolide) Microspheres (PLGA MS)—Mediated Anti-tumor Therapy," *Front. Immunol.*, vol. 10, no. April, pp. 1–16, 2019.

[91] M. Nikkhah, F. Edalat, S. Manoucheri, and A. Khademhosseini, "Engineering microscale topographies to control the cell-substrate interface," *Biomaterials*. 2012.

[92] R. O. Hynes, "The extracellular matrix: Not just pretty fibrils," *Science*. 2009.

[93] H. S. Dhowre, S. Rajput, N. A. Russell, and M. Zelzer, "Responsive cell-material interfaces," *Nanomedicine*. 2015.

[94] P. Rørth, "Whence Directionality: Guidance Mechanisms in Solitary and Collective Cell Migration," *Developmental Cell*. 2011.

[95] K. Metavarayuth, P. Sitasuwan, X. Zhao, Y. Lin, and Q. Wang, "Influence of Surface Topographical Cues on the Differentiation of Mesenchymal Stem Cells in Vitro," *ACS Biomater. Sci. Eng.*, vol. 2, no. 2, pp. 142–151, 2016.

[96] G. Abagnale *et al.*, "Surface Topography Guides Morphology and Spatial Patterning of Induced Pluripotent Stem Cell Colonies," *Stem Cell Reports*, vol. 9, no. 2, pp. 654–666, 2017.

[97] G. Abagnale *et al.*, "Surface topography enhances differentiation of mesenchymal stem cells towards osteogenic and adipogenic lineages," *Biomaterials*, vol. 61, pp. 316–326, 2015.

[98] A. English *et al.*, "Substrate topography: A valuable in vitro tool, but a clinical red herring for in vivo tenogenesis," *Acta Biomater.*, 2015.

[99] S. Vermeulen *et al.*, "Expanding Biomaterial Surface Topographical Design Space through Natural Surface Reproduction," *bioRxiv*, 2020.

[100] S. Pacelli *et al.*, "Tailoring biomaterial surface properties to modulate host-implant interactions: Implication in cardiovascular and bone therapy," *J. Mater. Chem. B*, vol. 4, no. 9, pp. 1586–1599, 2016.

[101] A. F. L. Fernando A. Lasagi, "Fabrication and Characterization in the Micro-Nano Range," *Springer*, 2011.

[102] Y. Zhao, R. Truckenmuller, M. Levers, W. S. Hua, J. de Boer, and B. Papenburg, "High-definition micropatterning method for hard, stiff and brittle polymers," *Mater. Sci. Eng. C*, vol. 71, pp. 558–564, 2017.

[103] F. F. B. Hulshof *et al.*, “NanoTopoChip: High-throughput nanotopographical cell instruction,” *Acta Biomater.*, vol. 62, pp. 188–198, 2017.

[104] X. M. Zhao, “Soft lithographic methods for nano-fabrication,” *J. Mater. Chem.*, 1997.

[105] K. M. Tanvir Ahmmed, C. Grambow, and A. M. Kietzig, “Fabrication of micro/nano structures on metals by femtosecond laser micromachining,” *Micromachines*. 2014.

[106] H. N. Hansen, R. J. Hocken, and G. Tosello, “Replication of micro and nano surface geometries,” *CIRP Ann. - Manuf. Technol.*, 2011.

[107] T. A. B. van der Boon *et al.*, “Well Plate Integrated Topography Gradient Screening Technology for Studying Cell-Surface Topography Interactions,” *Adv. Biosyst.*, vol. 4, no. 1, 2020.

[108] D.-H. Kim, K. Han, K. Gupta, K. W. Kwon, K.-Y. Suh, and A. Levchenko, “Mechanosensitivity of fibroblast cell shape and movement to anisotropic substratum topography gradients,” *Biomaterials*, vol. 30, no. 29, pp. 5433–5444, Oct. 2009.

[109] H. V. Unadkat *et al.*, “An algorithm-based topographical biomaterials library to instruct cell fate,” *Proc. Natl. Acad. Sci.*, vol. 108, no. 40, pp. 16565–16570, 2011.

[110] A. Reimer *et al.*, “Scalable topographies to support proliferation and Oct4 expression by human induced pluripotent stem cells.,” *Sci. Rep.*, vol. 6, no. January, p. 18948, 2016.

[111] S. Vermeulen *et al.*, “Identification of topographical architectures supporting the phenotype of rat tenocytes,” *Acta Biomater.*, vol. 83, pp. 277–290, 2019.

[112] F. F. B. Hulshof *et al.*, “Mining for osteogenic surface topographies: In silico design to in vivo osseo-integration,” *Biomaterials*, vol. 137, pp. 49–60, 2017.

[113] A. S. Vasilevich *et al.*, “Designed Surface Topographies Control ICAM-1 Expression in Tonsil-Derived Human Stromal Cells,” *Front. Bioeng. Biotechnol.*, vol. 6, no. June, pp. 1–14, 2018.

[114] N. R. M. Beijer *et al.*, “TopoWellPlate : A Well-Plate-Based Screening Platform to Study Cell – Surface Topography Interactions,” *Adv. Biosyst.*, pp. 1–8, 2017.

[115] W. G. Brodbeck *et al.*, “Biomaterial adherent macrophage apoptosis is increased by hydrophilic and anionic substrates in vivo,” *Proc. Natl. Acad. Sci. U. S. A.*, vol. 99, no. 16, pp. 10287–10292, 2002.

[116] H. M. Rostam *et al.*, “The impact of surface chemistry modification on macrophage polarisation,” *Immunobiology*, vol. 221, no. 11, pp. 1–10, 2016.

[117] S. Chen, J. A. Jones, Y. Xu, J.-Y. Low, J. M. Anderson, and K. W. Leong, “Characterisation of topographical effects on macrophage behaviour in a foreign body response model,” *Biomaterials*, vol. 31, no. 13, pp. 3479–3491, 2010.

[118] T. U. Luu, S. C. Gott, B. W. K. Woo, M. P. Rao, and W. F. Liu, “Micro- and Nanopatterned Topographical Cues for Regulating Macrophage Cell Shape and Phenotype,” *ACS Appl. Mater. Interfaces*, vol. 7, no. 51, pp. 28665–28672, Dec. 2015.

[119] F. Y. McWhorter, T. Wang, P. Nguyen, T. Chung, and W. F. Liu, “Modulation of macrophage phenotype by cell shape,” *Proc. Natl. Acad. Sci. U. S. A.*, 2013.

[120] H. M. Rostam *et al.*, “Immune-Instructive Polymers Control Macrophage Phenotype

and Modulate the Foreign Body Response In Vivo," *Matter*, vol. 2, no. 6, pp. 1564–1581, Jun. 2020.

[121] B. G. Keselowsky and J. S. Lewis, "Dendritic cells in the host response to implanted materials," *Semin. Immunol.*, vol. 29, no. November 2016, pp. 33–40, 2016.

[122] S. Vasilijić *et al.*, "Dendritic cells acquire tolerogenic properties at the site of sterile granulomatous inflammation," *Cell. Immunol.*, vol. 233, no. 2, pp. 148–157, 2005.

[123] J. Babensee and A. Paranjpe, "Differential levels of dendritic cell maturation on different biomaterials used in combination products," *J Biomed Mater Res A.*, vol. 4, no. 74, pp. 503–10, 2005.

[124] J. E. Babensee and J. Park, "Differential Functional Effects of Biomaterials on Dendritic Cell Maturation," *Acta Biomater.*, vol. 8, no. 10, pp. 3606–3617, 2012.

[125] M. Yoshida and J. E. Babensee, "Differential effects of agarose and poly(lactic-co-glycolic acid) on dendritic cell maturation," *J. Biomed. Mater. Res. - Part A*, 2006.

[126] E. Mariani, G. Lisignoli, R. M. Borzì, and L. Pulsatelli, "Biomaterials: Foreign bodies or tuners for the immune response?," *International Journal of Molecular Sciences*, vol. 20, no. 3. 2019.

[127] H. Knopf-Marques *et al.*, "Hyaluronic Acid and Its Derivatives in Coating and Delivery Systems: Applications in Tissue Engineering, Regenerative Medicine and Immunomodulation," *Advanced Healthcare Materials*. 2016.

[128] P. M. Kou, "Elucidation of dendritic cell response-material property relationships using high-throughput methodologies," Georgia Institute of Technology, 2011.

[129] P. M. Kou, "Elucidation of dendritic cell response-material property relationships using high throughput methodoligies," pp. 1–239, 2011.

[130] J. Park and J. E. Babensee, "Differential functional effects of biomaterials on dendritic cell maturation," *Acta Biomater.*, vol. 8, no. 10, pp. 3606–3617, 2012.

[131] Y. Hori, A. M. Winans, C. C. Huang, E. M. Horrigan, and D. J. Irvine, "Injectable dendritic cell-carrying alginate gels for immunization and immunotherapy," *Biomaterials*, vol. 29, no. 27, pp. 3671–3682, 2008.

[132] F. A. Sharp *et al.*, "Uptake of particulate vaccine adjuvants by dendritic cells activates the NALP3 inflammasome," *Proc. Natl. Acad. Sci. U. S. A.*, 2009.

[133] C. Fang, B. Shi, Y. Y. Pei, M. H. Hong, J. Wu, and H. Z. Chen, "In vivo tumor targeting of tumor necrosis factor-α-loaded stealth nanoparticles: Effect of MePEG molecular weight and particle size," *Eur. J. Pharm. Sci.*, 2006.

[134] J. S. Lewis *et al.*, "Dual-Sized Microparticle System for Generating Suppressive Dendritic Cells Prevents and Reverses Type 1 Diabetes in the Nonobese Diabetic Mouse Model," *ACS Biomater. Sci. Eng.*, vol. 5, no. 5, pp. 2631–2646, 2019.

[135] R. Allen, S. Chizari, J. A. Ma, S. Raychaudhuri, and J. S. Lewis, "Combinatorial, Microparticle-Based Delivery of Immune Modulators Reprograms the Dendritic Cell Phenotype and Promotes Remission of Collagen-Induced Arthritis in Mice," *ACS Appl. Bio Mater.*, vol. 2, no. 6, pp. 2388–2404, 2019.

[136] J. S. Lewis *et al.*, "A combination dual-sized microparticle system modulates dendritic cells and prevents type 1 diabetes in prediabetic NOD mice," *Clin. Immunol.*, vol. 160,

no. 1, pp. 90–102, Sep. 2015.

[137] J. J. Cho *et al.*, “An antigen-specific semi-therapeutic treatment with local delivery of tolerogenic factors through a dual-sized microparticle system blocks experimental autoimmune encephalomyelitis,” *Biomaterials*, vol. 143, pp. 79–92, 2017.

[138] B. Shokouhi *et al.*, “The role of multiple toll-like receptor signalling cascades on interactions between biomedical polymers and dendritic cells,” *Biomaterials*, vol. 31, no. 22, pp. 5759–5771, 2010.

[139] A. P. Acharya, N. V Dolgova, M. J. Clare-Salzler, and B. G. Keselowsky, “Adhesive substrate-modulation of adaptive immune responses,” *Biomaterials*, vol. 29, no. 36, pp. 4736–4750, 2008.

[140] T. H. Rogers and J. E. Babensee, “The role of integrins in the recognition and response of dendritic cells to biomaterials,” *Biomaterials*, vol. 32, no. 5, pp. 1270–1279, 2011.

[141] F. G. Giancotti and E. Ruoslahti, “Integrin signaling,” *Science (80-.).*, vol. 285, no. 5430, pp. 1028–1032, Aug. 1999.

[142] A. N. Stachowiak and D. J. Irvine, “Inverse opal hydrogel-collagen composite scaffolds as a supportive microenvironment for immune cell migration,” *J. Biomed. Mater. Res. - Part A*, vol. 85, no. 3, pp. 815–828, 2008.

[143] J. Kim, W. A. Li, W. Sands, and D. J. Mooney, “Effect of Pore Structure of Macroporous Poly (Lactide-co- Glycolide) Scaffolds on the In Vivo Enrichment of Dendritic Cells Effect of Pore Structure of Macroporous Poly (Lactide-co- Glycolide) Scaffolds on the In Vivo Enrichment of Dendritic Cells,” *ACS Appl. Mater. Interfaces*, vol. 6, no. 11, pp. 8505–8512, 2014.

[144] N. J. Shah *et al.*, “A biomaterial-based vaccine eliciting durable tumour-specific responses against acute myeloid leukaemia,” *Nat. Biomed. Eng.*, 2020.

[145] P. J. Tacken, I. J. M. De Vries, R. Torensma, and C. G. Figdor, “Dendritic-cell immunotherapy: From ex vivo loading to in vivo targeting,” *Nat. Rev. Immunol.*, vol. 7, no. 10, pp. 790–802, 2007.

[146] A. D. Garg, P. G. Coulie, B. J. Van den Eynde, and P. Agostinis, “Integrating Next-Generation Dendritic Cell Vaccines into the Current Cancer Immunotherapy Landscape,” *Trends Immunol.*, vol. 38, no. 8, pp. 577–593, 2017.

[147] J. Calmeiro, M. Carrascal, C. Gomes, A. Falcão, M. T. Cruz, and B. M. Neves, “Biomaterial-based platforms for in situ dendritic cell programming and their use in antitumor immunotherapy,” *J. Immunother. Cancer*, vol. 7, no. 1, pp. 1–11, 2019.

[148] A. D. Celiz *et al.*, “Discovery of a Novel Polymer for Human Pluripotent Stem Cell Expansion and Multilineage Differentiation,” *Adv. Mater.*, vol. 27, no. 27, pp. 4006–4012, 2015.

[149] A. K. Patel *et al.*, “A defined synthetic substrate for serum-free culture of human stem cell derived cardiomyocytes with improved functinoal maturity identified using combinatorial materials microarrays,” vol. 61, pp. 257–265, 2016.

[150] A. L. Hook *et al.*, “Combinatorial discovery of polymers resistant to bacterial attachment,” *Nat. Biotechnol.*, vol. 30, no. 9, pp. 867–874, 2012.

[151] A. L. Hook, D. G. Anderson, R. Langer, P. Williams, M. C. Davies, and M. R. Alexander, “High throughput methods applied in biomaterial development and discovery,”

Biomaterials, vol. 31, no. 2, pp. 187–198, 2010.

[152] J. Yang *et al.*, “Polymer surface functionalities that control human embryoid body cell adhesion revealed by high throughput surface characterization of combinatorial material microarrays,” *Biomaterials*, vol. 31, no. 34, pp. 8827–8838, 2010.

[153] A. Mant, G. Tourniaire, J. J. Diaz-Mochon, T. J. Elliott, A. P. Williams, and M. Bradley, “Polymer microarrays: Identification of substrates for phagocytosis assays,” *Biomaterials*, vol. 27, no. 30, pp. 5299–5306, 2006.

[154] L. Burroughs *et al.*, “Discovery of synergistic material-topography combinations to achieve immunomodulatory osteoinductive biomaterials using a novel in vitro screening method: The ChemoTopoChip,” *Biomaterials*, vol. 271, no. February, p. 120740, 2021.

[155] N. H. Turner, “Surface Analysis: X-ray Photoelectron Spectroscopy and Auger Electron Spectroscopy,” *Anal. Chem.*, 1986.

[156] Kratos Analytical, “X-ray Photoelectron Spectroscopy (XPS),” 2021. [Online]. Available: https://www.kratos.com/applications/techniques/x-ray-photoelectron-spectroscopy. [Accessed: 27-Jan-2021].

[157] D. Briggs, “X-ray photoelectron spectroscopy (XPS),” in *Handbook of Adhesion: Second Edition*, 2005.

[158] D. M. Mattox, “Substrate (‘Real’) Surfaces and Surface Modification,” in *Handbook of Physical Vapor Deposition (PVD) Processing*, 2010.

[159] S. L. McArthur, G. Mishra, and C. D. Easton, “Applications of XPS in biology and biointerface analysis,” in *Surface Analysis and Techniques in Biology*, 2014.

[160] S. Ray and A. G. Shard, “Quantitative analysis of adsorbed proteins by X-ray photoelectron spectroscopy,” *Anal. Chem.*, vol. 83, no. 22, pp. 8659–8666, 2011.

[161] R. N. Foster, E. T. Harrison, and D. G. Castner, “ToF-SIMS and XPS Characterization of Protein Films Adsorbed onto Bare and Sodium Styrenesulfonate-Grafted Gold Substrates,” *Langmuir*, 2016.

[162] R. A. Zangmeister, “Application of x-ray photoelectron spectroscopic analysis to protein adsorption on materials relevant to biomanufacturing,” *J. Pharm. Sci.*, 2012.

[163] M. S. Wagner and D. G. Castner, “Characterization of adsorbed protein films by time-of-flight secondary ion mass spectrometry with principal component analysis,” *Langmuir*, 2001.

[164] S. S. N. E. V. M. R. A. A. M. G. H M Rostam, “Impact of surface chemistry and topography on the function of antigen presenting cells,” *Biomater. Sci.*, vol. 3, no. 3, pp. 424–441, 2015.

[165] D. M. Higgins, R. J. Basaraba, A. C. Hohnbaum, E. J. Lee, D. W. Grainger, and M. Gonzalez-Juarrero, “Localized immunosuppressive environment in the foreign body response to implanted biomaterials.,” *Am. J. Pathol.*, vol. 175, no. 1, pp. 161–170, 2009.

[166] I. Firkowska-Boden, X. Zhang, and K. D. Jandt, “Controlling Protein Adsorption through Nanostructured Polymeric Surfaces,” *Adv. Healthc. Mater.*, vol. 7, no. 1, pp. 1–19, 2018.

[167] J. E. Babensee, “Interaction of dendritic cells with biomaterials,” *Semin. Immunol.*, vol. 20, no. 2, pp. 101–108, Apr. 2008.

[168] S. O. Neves *et al.*, “Composite-derived monomers affect cell viability and cytokine expression in human leukocytes stimulated with porphyromonas gingivalis,” *J. Appl. Oral Sci.*, vol. 27, 2019.

[169] N. Pradeep and A. V. Sreekumar, “An in vitro investigation into the cytotoxicity of methyl methacrylate monomer,” *J. Contemp. Dent. Pract.*, vol. 13, no. 6, 2012.

[170] C. A. Guyre *et al.*, “Advantages of hydrophobic culture bags over flasks for the generation of monocyte-derived dendritic cells for clinical applications,” *J. Immunol. Methods*, vol. 262, no. 1–2, pp. 85–94, 2002.

[171] S. Garcia-Nieto *et al.*, “Laminin and Fibronectin Treatment Leads to Generation of Dendritic Cells with Superior Endocytic Capacity,” *PLoS One*, vol. 5, no. 4, pp. e10123--10, Apr. 2010.

[172] P. J. Mannon *et al.*, “Anti–Interleukin-12 Antibody for Active Crohn’s Disease,” *N. Engl. J. Med.*, vol. 351, no. 20, pp. 2069–2079, 2004.

[173] S. F. B. Mennens, M. Bolomini-Vittori, J. Weiden, B. Joosten, A. Cambi, and K. Van Den Dries, “Substrate stiffness influences phenotype and function of human antigen-presenting dendritic cells,” *Sci. Rep.*, vol. 7, no. 1, pp. 1–14, 2017.

[174] H. M. Rostam *et al.*, “Immune-Instructive Polymers Control Macrophage Phenotype and Modulate the Foreign Body Response In Vivo,” *Matter*, vol. 2, no. 6, 2020.

[175] J. Dannull *et al.*, “Gene Expression Profile of Dendritic Cell-Tumor Cell Hybrids Determined by Microarrays and Its Implications for Cancer Immunotherapy,” *J. Immunol. Res.*, vol. 2015, 2015.

[176] K. Schinnerling, P. García-González, and J. C. Aguillón, “Gene expression profiling of human monocyte-derived dendritic cells - Searching for molecular regulators of tolerogenicity,” *Frontiers in Immunology*, vol. 6, no. OCT. 2015.

[177] Q. Qiu, M. Sayer, M. Kawaja, X. Shen, and J. E. Davies, “Attachment, morphology, and protein expression of rat marrow stromal cells cultured on charged substrate surfaces,” *J. Biomed. Mater. Res.*, vol. 42, no. 1, 1998.

[178] F. Salazar, D. Awuah, O. H. Negm, F. Shakib, and A. M. Ghaemmaghami, “The role of indoleamine 2,3-dioxygenase-aryl hydrocarbon receptor pathway in the TLR4-induced tolerogenic phenotype in human DCs,” *Sci. Rep.*, vol. 7, no. March, pp. 1–11, 2017.

[179] F. Salazar *et al.*, “The mannose receptor negatively modulates the Toll-like receptor 4-aryl hydrocarbon receptor-indoleamine 2,3-dioxygenase axis in dendritic cells affecting T helper cell polarization,” *J. Allergy Clin. Immunol.*, vol. 137, no. 6, pp. 1841-1851.e2, 2016.

[180] Y. Tomita, E. Watanabe, M. Shimizu, Y. Negishi, Y. Kondo, and H. Takahashi, “Induction of tumor-specific CD8+ cytotoxic T lymphocytes from naïve human T cells by using Mycobacterium-derived mycolic acid and lipoarabinomannan-stimulated dendritic cells,” *Cancer Immunol. Immunother.*, vol. 68, no. 10, pp. 1605–1619, 2019.

[181] S. Cho *et al.*, “Combinatorial development of biomaterials for clonal growth of human pluripotent stem cells,” *Nat. Mater.*, vol. 9, no. 9, pp. 768–778, 2010.

[182] D. T. Butcher, T. Alliston, and V. M. Weaver, “A tense situation: forcing tumour progression,” *Nat. Rev. Cancer*, vol. 9, no. 2, pp. 108–122, Feb. 2009.

[183] T. R. Cox and J. T. Erler, “Remodeling and homeostasis of the extracellular matrix:

Implications for fibrotic diseases and cancer," *DMM Disease Models and Mechanisms*. 2011.

[184] L. J. Russell *et al.*, "Deregulated expression of cytokine receptor gene, CRLF2, is involved in lymphoid transformation in B-cell precursor acute lymphoblastic leukemia," *Blood*, vol. 114, no. 13, 2009.

[185] T. Miwa *et al.*, "Identification of NCCRP1 as an epigenetically regulated tumor suppressor and biomarker for malignant phenotypes of squamous cell carcinoma of the esophagus," *Oncol. Lett.*, vol. 14, no. 4, 2017.

[186] Z. Shi, S. Jiao, and Z. Zhou, "STRIPAK complexes in cell signaling and cancer," *Oncogene*, vol. 35, no. 35. 2016.

[187] L. M. Qiu, Y. H. Sun, T. T. Chen, J. J. Chen, and H. T. Ma, "STRIP2, a member of the striatin-interacting phosphatase and kinase complex, is implicated in lung adenocarcinoma cell growth and migration," *FEBS Open Bio*, vol. 10, no. 3, 2020.

[188] J. G. Zeevaart *et al.*, "Detection of Rare Antigen Presenting Cells through T cell-intrinsic meandering motility, mediated by Myo1g," *Cell*, vol. 158, no. 3, pp. 492–505, 2014.

[189] A. I. Chen *et al.*, "Ox40-ligand has a critical costimulatory role in dendritic cell:T cell interactions," *Immunity*, vol. 11, no. 6, 1999.

[190] Y. Ohshima, Y. Tanaka, H. Tozawa, Y. Takahashi, C. Maliszewski, and G. Delespesse, "Expression and Function of OX40 Ligand on Human Dendritic Cells," *J. Immunol.*, vol. 159, no. 8, 1997.

[191] I. Mizoguchi *et al.*, "Prediction of chemical respiratory and contact sensitizers by OX40L expression in dendritic cells using a novel 3D coculture system," *Front. Immunol.*, vol. 8, no. AUG, 2017.

[192] R. Förster, A. C. Davalos-Misslitz, and A. Rot, "CCR7 and its ligands: Balancing immunity and tolerance," *Nature Reviews Immunology*, vol. 8, no. 5. pp. 362–371, 2008.

[193] D. R. Saban, "The chemokine receptor CCR7 expressed by dendritic cells: A key player in corneal and ocular surface inflammation," *Ocular Surface*, vol. 12, no. 2. 2014.

[194] L. Riol-Blanco *et al.*, "The Chemokine Receptor CCR7 Activates in Dendritic Cells Two Signaling Modules That Independently Regulate Chemotaxis and Migratory Speed," *J. Immunol.*, vol. 174, no. 7, 2005.

[195] C. Louvet, "Dendritic cells require TMEM176A / B ion channels for optimal MHC II antigen presentation to naive CD4 + T cells," pp. 1–48, 2020.

[196] T. Condamine *et al.*, "Tmem176B and Tmem176A are associated with the immature state of dendritic cells," *J. Leukoc. Biol.*, vol. 88, no. 3, pp. 507–515, 2010.

[197] X. Ma *et al.*, "Regulation of IL-10 and IL-12 production and function in macrophages and dendritic cells," *F1000Research*, vol. 4. 2015.

[198] C. Liu *et al.*, "Neutrophil cytosolic factor 1 in dendritic cells promotes autoreactive CD8+ T cell activation via cross-presentation in type 1 diabetes," *Front. Immunol.*, vol. 10, no. MAY, 2019.

[199] R. Aviner, A. Shenoy, O. Elroy-Stein, and T. Geiger, "Uncovering Hidden Layers of Cell Cycle Regulation through Integrative Multi-omic Analysis," *PLoS Genet.*, vol. 11, no. 10, 2015.

[200] A. Jayo, C. Isabel, L. Pedro, J.-Y. Victor, and C. Gonzalez-Manchon, “Possible role for cellular FXIII in monocyte-derived dendritic cell motility,” *bioRxiv*, 2020.

[201] Z. H. Zhang and G. L. Song, “Roles of Selenoproteins in Brain Function and the Potential Mechanism of Selenium in Alzheimer’s Disease,” *Frontiers in Neuroscience*, vol. 15. 2021.

[202] F. F. Ma *et al.*, “Dysregulated NF-κB signal promotes the hub gene PCLAF expression to facilitate nasopharyngeal carcinoma proliferation and metastasis,” *Biomed. Pharmacother.*, vol. 125, 2020.

[203] J. N. Cao, A. Agrawal, E. Sharman, Z. Jia, and S. Gupta, “Alterations in gene array patterns in dendritic cells from aged humans,” *PLoS One*, vol. 9, no. 9, 2014.

[204] J. C. Valle-Casuso *et al.*, “p21 Restricts HIV-1 in Monocyte-Derived Dendritic Cells through the Reduction of Deoxynucleoside Triphosphate Biosynthesis and Regulation of SAMHD1 Antiviral Activity,” *J. Virol.*, vol. 91, no. 23, 2017.

[205] J. Y. Im *et al.*, “DNA damage-induced apoptosis suppressor (DDIAS), a novel target of NFATc1, is associated with cisplatin resistance in lung cancer,” *Biochim. Biophys. Acta - Mol. Cell Res.*, vol. 1863, no. 1, 2016.

[206] J. Park *et al.*, “The MCM8-MCM9 Complex Promotes RAD51 Recruitment at DNA Damage Sites To Facilitate Homologous Recombination,” *Mol. Cell. Biol.*, vol. 33, no. 8, 2013.

[207] M. L. Guler *et al.*, “Tpm1, a locus controlling IL-12 responsiveness, acts by a cell-autonomous mechanism,” *J. Immunol.*, vol. 162, no. 3, 1999.

[208] E. Li *et al.*, “CXCL8 Associated Dendritic Cell Activation Marker Expression and Recruitment as Indicators of Favorable Outcomes in Colorectal Cancer,” *Front. Immunol.*, vol. 12, 2021.

[209] S. C. Wuest *et al.*, “A role for interleukin-2 trans-presentation in dendritic cell-mediated T cell activation in humans, as revealed by daclizumab therapy,” *Nat. Med.*, vol. 17, no. 5, 2011.

[210] M. Boucard-Jourdin *et al.*, “β8 Integrin Expression and Activation of TGF-β by Intestinal Dendritic Cells Are Determined by Both Tissue Microenvironment and Cell Lineage,” *J. Immunol.*, vol. 197, no. 5, 2016.

[211] M. Yasuda-Yamahara *et al.*, “FERMT2 links cortical actin structures, plasma membrane tension and focal adhesion function to stabilize podocyte morphology,” *Matrix Biol.*, vol. 68–69, 2018.

[212] M. de la Fuente-Granada, R. Olguín-Alor, S. Ortega-Francisco, L. C. Bonifaz, and G. Soldevila, “Inhibins regulate peripheral regulatory T cell induction through modulation of dendritic cell function,” *FEBS Open Bio*, vol. 9, no. 1, 2019.

[213] W. C. Huang *et al.*, “Sphingosine-1-phosphate phosphatase 2 promotes disruption of mucosal integrity, and contributes to ulcerative colitis in mice and humans,” *FASEB J.*, vol. 30, no. 8, 2016.

[214] L. Kui, G. C. Chan, and P. P. W. Lee, “TSG-6 Downregulates IFN-Alpha and TNF-Alpha Expression by Suppressing IRF7 Phosphorylation in Human Plasmacytoid Dendritic Cells,” *Mediators Inflamm.*, vol. 2017, 2017.

[215] D. M. Elizondo, T. Andargie, C. M. Lee, W. A. Anderson, and M. W. Lipscomb, “AIF1

expression regulates differentiation of dendritic cells from hematopoietic stem cell multipotent progenitor subsets and regulates antigen presentation capacity," *J. Immunol.*, vol. 198, no. 1, 2017.

[216] D. M. Elizondo, N. Z. D. Brandy, R. L. Da Silva, T. R. De Moura, and M. W. Lipscomb, "Allograft inflammatory factor-1 in myeloid cells drives autoimmunity in type 1 diabetes," *JCI Insight*, vol. 5, no. 10, 2020.

[217] G. Ferrero *et al.*, "The macrophage-expressed gene (mpeg) 1 identifies a subpopulation of B cells in the adult zebrafish," *J. Leukoc. Biol.*, vol. 107, no. 3, 2020.

[218] T. Nikolic *et al.*, "Differential transcriptome of tolerogenic versus inflammatory dendritic cells points to modulated T1D genetic risk and enriched immune regulation," *Genes Immun.*, vol. 18, no. 3, pp. 176–183, 2017.

[219] G.-X. Shi, K. Harrison, S.-B. Han, C. Moratz, and J. H. Kehrl, "Toll-Like Receptor Signaling Alters the Expression of Regulator of G Protein Signaling Proteins in Dendritic Cells: Implications for G Protein-Coupled Receptor Signaling," *J. Immunol.*, vol. 172, no. 9, 2004.

[220] M. A. R. Ferreira *et al.*, "Gene-based analysis of regulatory variants identifies 4 putative novel asthma risk genes related to nucleotide synthesis and signaling," *J. Allergy Clin. Immunol.*, vol. 139, no. 4, 2017.

[221] M. F. Elshal, A. M. Aldahlawi, O. I. Saadah, and J. P. McCoy, "Reduced dendritic cells expressing CD200R1 in children with inflammatory bowel disease: Correlation with Th17 and regulatory T cells," *Int. J. Mol. Sci.*, vol. 16, no. 12, 2015.

[222] J. S. Shin and A. M. Greer, "The role of FcεRI expressed in dendritic cells and monocytes," *Cellular and Molecular Life Sciences*, vol. 72, no. 12. 2015.

[223] M. Maywald, "Zinc supplementionation induces regulatory T cells in vitro and in vivo," 2017.

[224] M. M. George, G. S. Deepe Jr, J. A. Caruso, K. S. Vignesh, and J. A. Landero Figueroa, "Zinc induces dendritic cell tolerogenic phenotype and skews regulatory T cell - Th17 balance," *J. Immunol.*, vol. 197, no. 5, pp. 1864–1876, 2016.

[225] T. Hirano, M. Murakami, T. Fukada, K. Nishida, S. Yamasaki, and T. Suzuki, "Roles of Zinc and Zinc Signaling in Immunity: Zinc as an Intracellular Signaling Molecule," *Adv. Immunol.*, vol. 97, no. 08, pp. 149–176, 2008.

[226] H. Kitamura *et al.*, "Toll-like receptor-mediated regulation of zinc homeostasis influences dendritic cell function," *Nat. Immunol.*, vol. 7, no. 9, pp. 971–977, 2006.

[227] A. Fragale *et al.*, " IFN Regulatory Factor-1 Negatively Regulates CD4 + CD25 + Regulatory T Cell Differentiation by Repressing Foxp3 Expression ," *J. Immunol.*, vol. 181, no. 3, pp. 1673–1682, 2008.

[228] R. Sridharan, B. Cavanagh, A. R. Cameron, D. J. Kelly, and F. J. O'Brien, "Material stiffness influences the polarization state, function and migration mode of macrophages," *Acta Biomater.*, vol. 89, pp. 47–59, 2019.

[229] M. Chakraborty *et al.*, "Mechanical Stiffness Controls Dendritic Cell Metabolism and Function," *Cell Rep.*, vol. 34, no. 2, 2021.

[230] C. Mbadugha, "Biomaterial Surface Chemistry as a Cue for the Modulation of Macrophage Polarisation," University of Nottingham, 2019.

[231] G. Tuana, V. Volpato, P. Ricciardi-Castagnoli, F. Zolezzi, F. Stella, and M. Foti, “Classification of dendritic cell phenotypes from gene expression data,” *BMC Immunol.*, vol. 12, 2011.

[232] S. J. Win *et al.*, “Enhancing the immunogenicity of tumour lysate-loaded dendritic cell vaccines by conjugation to virus-like particles,” *Br. J. Cancer*, vol. 106, no. 1, pp. 92–98, 2012.

[233] M. Schnurr *et al.*, “Tumor cell lysate-pulsed human dendritic cells induce a T-cell response against pancreatic carcinoma cells: An in vitro model for the assessment of tumor vaccines,” *Cancer Res.*, vol. 61, no. 17, pp. 6445–6450, 2001.

[234] O. A. Ali, E. Doherty, D. J. Mooney, and D. Emerich, “Relationship of vaccine efficacy to the kinetics of DC and T-cell responses induced by PLG-based cancer vaccines.,” *Biomatter*, vol. 1, no. 1, pp. 66–75, 2011.

[235] F. Eslami-kaliji, M. Sarafbidabad, A. Kiani-Esfahani, S. Z. Mirahmadi-Zare, and K. Dormiani, “10-Hydroxy-2-Decenoic Acid a Bio-Immunomodulator in Tissue Engineering; Generates Tolerogenic Dendritic Cells By Blocking the Toll-Like Receptor4,” *J. Biomed. Mater. Res. - Part A*, 2021.

[236] L. Thiele, J. E. Diederichs, R. Reszka, H. P. Merkle, and E. Walter, “Competitive adsorption of serum proteins at microparticles affects phagocytosis by dendritic cells,” *Biomaterials*, vol. 24, no. 8, pp. 1409–1418, 2003.

[237] R. Langer, “Biomaterials in drug delivery and tissue engineering: One laboratory’s experience,” *Acc. Chem. Res.*, vol. 33, no. 2, pp. 94–101, 2000.

[238] A. Atala, “Tissue Engineering and Regenerative Medicine: Concepts for Clinical Application,” *Rejuvenation Res.*, vol. 7, no. 1, pp. 15–31, May 2004.

[239] E. A. Phelps and A. J. Garcia, “Update on therapeutic vascularization strategies,” *Regen. Med.*, vol. 4, no. 1, pp. 65–80, 2009.

[240] H. C. H. Ko, B. K. Milthorpe, and C. D. McFarland, “Engineering thick tissues - The vascularisation problem,” *Eur. Cells Mater.*, vol. 14, pp. 1–18, 2007.

[241] F. J. O’Brien, B. A. Harley, I. V. Yannas, and L. J. Gibson, “The effect of pore size on cell adhesion in collagen-GAG scaffolds,” *Biomaterials*, vol. 26, no. 4, pp. 433–441, 2005.

[242] F. J. O’Brien, B. A. Harley, M. A. Waller, I. V. Yannas, L. J. Gibson, and P. J. Prendergast, “The effect of pore size on permeability and cell attachment in collagen scaffolds for tissue engineering,” in *Technology and Health Care*, 2007, vol. 15, no. 1, pp. 3–17.

[243] I. V. Yannas, E. Lee, D. P. Orgill, E. M. Skrabut, and G. F. Murphy, “Synthesis and characterization of a model extracellular matrix that induces partial regeneration of adult mammalian skin,” *Proc. Natl. Acad. Sci. U. S. A.*, vol. 86, no. 3, pp. 933–937, 1989.

[244] C. M. Murphy, M. G. Haugh, and F. J. O’Brien, “The effect of mean pore size on cell attachment, proliferation and migration in collagen-glycosaminoglycan scaffolds for bone tissue engineering,” *Biomaterials*, vol. 31, no. 3, pp. 461–466, 2010.

[245] C. M. Murphy and F. J. O’Brien, “Understanding the effect of mean pore size on cell activity in collagen-glycosaminoglycan scaffolds,” *Cell Adhes. Migr.*, vol. 4, no. 3, pp. 377–381, 2010.

[246] HULBERT SF, YOUNG FA, MATHEWS RS, KLAWITTER JJ, TALBERT CD, and STELLING FH, “POTENTIAL OF CERAMIC MATERIALS AS PERMANENTLY IMPLANTABLE SKELETAL PROSTHESIS,” 1970.

[247] J. J. Klawitter, J. G. Bagwell, A. M. Weinstein, B. W. Sauer, and J. R. Pruitt, “An evaluation of bone growth into porous high density polyethylene,” *J. Biomed. Mater. Res.*, 1976.

[248] G. Lutzweiler, A. N. Halili, and N. E. Vrana, “The overview of porous, bioactive scaffolds as instructive biomaterials for tissue regeneration and their clinical translation,” *Pharmaceutics*, vol. 12, no. 7, pp. 1–29, 2020.

[249] L. P. Corrales, M. L. Esteves, and J. aime E. . Vick, “Scaffold design for bone regeneration. Journal of nanoscience and nanotechnology,” *J Nanosci Nanotechnol*, vol. 14, no. 1, pp. 15–56, 2014.

[250] A. G. Guex *et al.*, “Highly porous scaffolds of PEDOT:PSS for bone tissue engineering,” *Acta Biomater.*, vol. 62, pp. 91–101, 2017.

[251] C. Yang, N. T. Blum, J. Lin, J. Qu, and P. Huang, “Biomaterial scaffold-based local drug delivery systems for cancer immunotherapy,” *Science Bulletin*. 2020.

[252] M. Milosevic *et al.*, “Preparation and modeling of three-layered PCL/PLGA/PCL fibrous scaffolds for prolonged drug release,” *Sci. Rep.*, 2020.

[253] K. Sadtler *et al.*, “Developing a pro-regenerative biomaterial scaffold microenvironment requires T helper 2 cells,” *Science (80-.).*, vol. 2, no. 2, pp. 147–185, 2015.

[254] L. D. Shea, D. Wang, R. T. Franceschi, and D. J. Mooney, “Engineered bone development from a pre-osteoblast cell line on three-dimensional scaffolds,” *Tissue Eng.*, vol. 6, no. 6, pp. 605–617, 2000.

[255] M. Chvapil, T. A. Chvapil, and J. A. Owen, “Reaction of various skin wounds in the rat to collagen sponge dressing,” *J. Surg. Res.*, 1986.

[256] M. P. Prabhakaran, J. R. Venugopal, and S. Ramakrishna, “Mesenchymal stem cell differentiation to neuronal cells on electrospun nanofibrous substrates for nerve tissue engineering,” *Biomaterials*, vol. 30, no. 28, pp. 4996–5003, 2009.

[257] J. Kim *et al.*, “Injectable, spontaneously assembling, inorganic scaffolds modulate immune cells in vivo and increase vaccine efficacy,” *Nat. Biotechnol.*, vol. 33, no. 1, pp. 64–72, 2015.

[258] C. S. Verbeke and D. J. Mooney, “Injectable, Pore-Forming Hydrogels for In Vivo Enrichment of Immature Dendritic Cells,” *Adv. Healthc. Mater.*, vol. 4, no. 17, pp. 2677–2687, 2015.

[259] R. Chen, H. Ma, L. Zhang, and J. D. Bryers, “Precision-porous templated scaffolds of varying pore size drive dendritic cell activation,” *Biotechnol. Bioeng.*, vol. 115, no. 4, pp. 1086–1095, 2018.

[260] J. Kim, W. A. Li, W. Sands, and D. J. Mooney, “Effect of pore structure of macroporous poly(lactide-co-glycolide) scaffolds on the in vivo enrichment of dendritic cells,” *ACS Appl. Mater. Interfaces*, vol. 6, no. 11, pp. 8505–8512, 2014.

[261] J. A. Champion, Y. K. Katare, and S. Mitragotri, “Making polymeric micro- and nanoparticles of complex shapes,” *Proc. Natl. Acad. Sci. U. S. A.*, 2007.

[262] H. Gelb, H. R. Schumacher, J. Cuckler, P. Ducheyne, and D. G. Baker, “In vivo inflammatory response to polymethylmethacrylate particulate debris: effect of size, morphology, and surface area.[Erratum appears in J Orthop Res 1994 Jul;12(4):598],” *J. Orthop. Res.*, 1994.

[263] S. Suri, G. Ruan, J. Winter, and C. E. Schmidt, *Microparticles and Nanoparticles*, Third Edit., no. 2000. Elsevier, 2013.

[264] R. A. Jain, “The manufacturing techniques of various drug loaded biodegradable poly(lactide-co-glycolide) (PLGA) devices,” *Biomaterials*, 2000.

[265] A. Singh, H. Nie, B. Ghosn, H. Qin, L. W. Kwak, and K. Roy, “Efficient modulation of T-cell response by dual-mode, single-carrier delivery of cytokine-targeted siRNA and DNA vaccine to antigen-presenting cells,” *Mol. Ther.*, 2008.

[266] A. A. Dundas *et al.*, “Achieving Microparticles with Cell-Instructive Surface Chemistry by Using Tunable Co-Polymer Surfactants,” *Adv. Funct. Mater.*, vol. 30, no. 36, p. 2001821, Sep. 2020.

[267] E. B. Thorp, C. Boada, C. Jarbath, and X. Luo, “Nanoparticle Platforms for Antigen-Specific Immune Tolerance,” *Front. Immunol.*, vol. 11, no. May, pp. 1–12, 2020.

[268] J. D. Heidel *et al.*, “Administration in non-human primates of escalating intravenous doses of targeted nanoparticles containing ribonucleotide reductase subunit M2 siRNA,” *Proc. Natl. Acad. Sci. U. S. A.*, 2007.

[269] D. Wang *et al.*, “Erythrocyte-Cancer Hybrid Membrane Camouflaged Hollow Copper Sulfide Nanoparticles for Prolonged Circulation Life and Homotypic-Targeting Photothermal/Chemotherapy of Melanoma,” *ACS Nano*, 2018.

[270] P. Decuzzi *et al.*, “Size and shape effects in the biodistribution of intravascularly injected particles,” *J. Control. Release*, 2010.

[271] P. Serra and P. Santamaria, “Nanoparticle-based autoimmune disease therapy,” *Clin. Immunol.*, vol. 160, no. 1, pp. 3–13, 2015.

[272] A. Syed and W. C. W. Chan, “How nanoparticles interact with cancer cells,” *Cancer Treat. Res.*, 2015.

[273] H. Wang, L. Wu, and B. M. Reinhard, “Scavenger receptor mediated endocytosis of silver nanoparticles into J774A.1 macrophages is heterogeneous,” *ACS Nano*, 2012.

[274] P. C. Patel, D. A. Giljohann, W. L. Daniel, D. Zheng, A. E. Prigodich, and C. A. Mirkin, “Scavenger receptors mediate cellular uptake of polyvalent oligonucleotide-functionalized gold nanoparticles,” *Bioconjug. Chem.*, 2010.

[275] R. Y. Al-zahri, “Immune modulatory properties of nanoparticles on human Dendritic Cells,” 2018.

[276] J. T. Goodman *et al.*, “Nanoparticle chemistry and functionalization differentially regulates dendritic cell-nanoparticle interactions and triggers dendritic cell maturation,” *Part. Part. Syst. Charact.*, vol. 31, no. 12, pp. 1269–1280, 2014.

[277] V. Ravinayagam and B. R. Jermy, “Nanomaterials and Their Negative Effects on Human Health,” in *Applications of Nanomaterials in Human Health*, pp. 249–273.

[278] J. Youshia, M. E. Ali, V. Stein, and A. Lamprecht, “Nanoparticles’ properties modify cell type-dependent distribution in immune cells,” *Nanomedicine Nanotechnology, Biol.*

Med., p. 102244, Jun. 2020.

[279] J. S. Lewis, T. D. Zaveri, C. P. Crooks, and B. G. Keselowsky, “Microparticle surface modifications targeting dendritic cells for non-activating applications,” *Biomaterials*, vol. 33, no. 29, pp. 7221–7232, 2012.

[280] M. Hussain *et al.*, “Biodegradable Polymer Microparticles with Tunable Shapes and Surface Textures for Enhancement of Dendritic Cell Maturation,” *ACS Appl. Mater. Interfaces*, vol. 11, no. 45, pp. 42734–42743, 2019.

[281] A. Vishwakarma *et al.*, “Engineering Immunomodulatory Biomaterials To Tune the Inflammatory Response,” *Trends Biotechnol.*, vol. 34, no. 6, pp. 470–482, 2016.

[282] L. Burroughs *et al.*, “Synergistic Material-Topography Combinations to Achieve Immunomodulatory Osteogenic Biomaterials,” *bioRxiv*, p. 2020.04.29.067421, 2020.

[283] M. J. Vassey *et al.*, “Immune Modulation by Design: Using Topography to Control Human Monocyte Attachment and Macrophage Differentiation,” *Adv. Sci.*, vol. 1903392, p. 1903392, Apr. 2020.

[284] M. J. Dalby, S. Childs, M. O. Riehle, H. J. H. Johnstone, S. Affrossman, and A. S. G. Curtis, “Fibroblast reaction to island topography: Changes in cytoskeleton and morphology with time,” *Biomaterials*, vol. 24, no. 6, pp. 927–935, 2003.

[285] M. J. Dalby *et al.*, “The control of human mesenchymal cell differentiation using nanoscale symmetry and disorder,” *Nat. Mater.*, vol. 6, no. 12, pp. 997–1003, 2007.

[286] S. Singh *et al.*, “Unbiased Analysis of the Impact of Micropatterned Biomaterials on Macrophage Behavior Provides Insights beyond Predefined Polarization States,” *ACS Biomater. Sci. Eng.*, vol. 3, no. 6, pp. 969–978, 2017.

[287] V. Malheiro, F. Lehner, V. Dinca, P. Hoffmann, and K. Maniura-Weber, “Convex and concave micro-structured silicone controls the shape, but not the polarization state of human macrophages,” *Biomater. Sci.*, vol. 4, no. 11, pp. 1562–1573, 2016.

[288] T. L. Downing *et al.*, “Biophysical regulation of epigenetic state and cell reprogramming,” *Nat. Mater.*, vol. 12, no. 12, pp. 1154–1162, 2013.

[289] Y. Park *et al.*, “Microtopography-Guided Conductive Patterns of Liquid-Driven Graphene Nanoplatelet Networks for Stretchable and Skin-Conformal Sensor Array,” *Adv. Mater.*, vol. 29, no. 21, 2017.

[290] D. Hoffman-Kim, J. A. Mitchel, and R. V. Bellamkonda, “Topography, Cell Response, and Nerve Regeneration,” *Annu. Rev. Biomed. Eng.*, vol. 15, no. 12, pp. 203–231, 2010.

[291] M. Ghibaudo, L. Trichet, J. Le Digabel, A. Richert, P. Hersen, and B. Ladoux, “Substrate topography induces a crossover from 2D to 3D behavior in fibroblast migration,” *Biophys. J.*, vol. 97, no. 1, pp. 357–368, 2009.

[292] T. U. Luu, S. C. Gott, B. W. K. Woo, M. P. Rao, and W. F. Liu, “Micro and Nano-patterned Topographical Cues for Regulating Macrophage Cell Shape and Phenotype,” *ACS Appl. Mater. Interfaces*, vol. 7, no. 51, pp. 28665–28672, 2015.

[293] K. W. Kwon *et al.*, “Nanotopography-Guided Migration of T Cells,” *J. Immunol.*, vol. 189, no. 5, pp. 2266–2273, 2012.

[294] P. Bhattacharjee, B. L. Cavanagh, and M. Ahearne, “Influence of micropatterned substrates on keratocyte phenotype,” *Sci. Rep.*, vol. 10, no. 1, pp. 1–11, 2020.

[295] T. Schmitz *et al.*, “Nanotopographical coatings induce an early phenotype-specific response of primary material-resident M1 and M2 macrophages,” *Materials (Basel).*, vol. 13, no. 5, pp. 1–20, 2020.

[296] K. M. Hotchkiss *et al.*, “Titanium surface characteristics, including topography and wettability, alter macrophage activation,” *Acta Biomater*, vol. 31, pp. 425–434, 2016.

[297] M. V Baranov, M. Ter Beest, I. Reinieren-Beeren, A. Cambi, C. G. Figdor, and G. van den Bogaart, “Podosomes of dendritic cells facilitate antigen sampling.,” *J. Cell Sci.*, vol. 127, no. Pt 5, pp. 1052–64, 2014.

[298] K. Van Den Dries *et al.*, “Geometry sensing by dendritic cells dictates spatial organization and PGE 2-induced dissolution of podosomes,” *Cell. Mol. Life Sci.*, vol. 69, no. 11, pp. 1889–1901, 2012.

[299] F. Hulshof, “TOPOCHIP: TECHNOLOGY FOR INSTRUCTING CELL FATE AND MORPHOLOGY VIA DESIGNED SURFACE TOPOGRAPHY,” 2017.

[300] A. Reversat *et al.*, “Cellular locomotion using environmental topography,” *Nature*, no. January 2018, May 2020.

[301] K. H. Hu and M. J. Butte, “T cell activation requires force generation,” *J. Cell Biol.*, vol. 213, no. 5, pp. 535–542, 2016.

[302] W. Chen and C. Zhu, “Mechanical regulation of T-cell functions,” *Immunol. Rev.*, vol. 256, no. 1, pp. 160–176, 2013.

[303] F. S. Majedi, M. M. Hasani-Sadrabadi, T. J. Thauland, S. Li, L. S. Bouchard, and M. J. Butte, “T-cell activation is modulated by the 3D mechanical microenvironment,” *Biomaterials*, vol. 252, no. April, p. 120058, 2020.

[304] T. Roch, K. Kratz, N. Ma, and A. Lendlein, “Inflammatory responses of primary human dendritic cells towards polydimethylsiloxane and polytetrafluoroethylene,” *Clin. Hemorheol. Microcirc.*, vol. 64, no. 4, pp. 899–910, 2016.

[305] P. M. Kou, Z. Schwartz, B. D. Boyan, and J. E. Babensee, “Dendritic cell responses to surface properties of clinical titanium surfaces,” *Acta Biomater.*, vol. 7, no. 3, pp. 1354–1363, Mar. 2011.

[306] S. K. Wculek, F. J. Cueto, A. M. Mujal, I. Melero, M. F. Krummel, and D. Sancho, “Dendritic cells in cancer immunology and immunotherapy,” *Nat. Rev. Immunol.*, vol. 20, no. 1, pp. 7–24, 2020.

[307] H. Wang *et al.*, “Biomaterial-based scaffold for in situ chemo-immunotherapy to treat poorly immunogenic tumors,” *Nat. Commun.*, vol. 11, no. 1, 2020.

[308] M. O. Dellacherie *et al.*, “Single-Shot Mesoporous Silica Rods Scaffold for Induction of Humoral Responses Against Small Antigens,” *Adv. Funct. Mater.*, vol. 30, no. 38, pp. 1–14, 2020.

[309] S. Majumder, S. Bhattacharjee, B. Paul Chowdhury, and S. Majumdar, “CXCL10 Is Critical for the Generation of Protective CD8 T Cell Response Induced by Antigen Pulsed CpG-ODN Activated Dendritic Cells,” *PLoS One*, vol. 7, no. 11, 2012.

[310] M. Metzemaekers, V. Vanheule, R. Janssens, S. Struyf, and P. Proost, “Overview of the mechanisms that may contribute to the non-redundant activities of interferon-inducible CXC chemokine receptor 3 ligands,” *Frontiers in Immunology*, vol. 8, no. JAN. 2018.

[311] N. Krishnamoorthy, T. Oriss, M. Paglia, A. Ray, and P. Ray, “A critical role for IL-6 secretion by dendritic cells promoting Th2 and limiting Th1 response (95.24),” *J. Immunol.*, vol. 178, no. 1, 2007.

[312] M. Le Borgne *et al.*, “Dendritic cells rapidly recruited into epithelial tissues via CCR6/CCL20 are responsible for CD8+ T cell crosspriming in vivo,” *Immunity*, vol. 24, no. 2, 2006.

[313] J.-H. Sheen *et al.*, “TLR-Induced Murine Dendritic Cell (DC) Activation Requires DC-Intrinsic Complement,” *J. Immunol.*, vol. 199, no. 1, 2017.

[314] F. R. Fischer, Y. Luo, M. Luo, L. Santambrogio, and M. E. Dorf, “RANTES-Induced Chemokine Cascade in Dendritic Cells,” *J. Immunol.*, vol. 167, no. 3, 2001.

[315] V. Chabot, “CCL5-enhanced human immature dendritic cell migration through the basement membrane in vitro depends on matrix metalloproteinase-9,” *J. Leukoc. Biol.*, vol. 79, no. 4, 2006.

[316] M. J. Young, K. C. Hsu, T. E. Lin, W. C. Chang, and J. J. Hung, “The role of ubiquitin-specific peptidases in cancer progression,” *Journal of Biomedical Science*, vol. 26, no. 1. 2019.

[317] K. Shen, W. Yu, Y. Yu, X. Liu, and X. Cui, “Knockdown of TMEM45B inhibits cell proliferation and invasion in gastric cancer,” *Biomed. Pharmacother.*, vol. 104, 2018.

[318] E. Schmid *et al.*, “Serum- and glucocorticoid-inducible kinase 1 sensitive NF-κB signaling in dendritic cells,” *Cell. Physiol. Biochem.*, vol. 34, no. 3, 2014.

[319] R. W. DePaolo *et al.*, “Toll-Like Receptor 6 Drives Differentiation of Tolerogenic Dendritic Cells and Contributes to LcrV-Mediated Plague Pathogenesis,” *Cell Host Microbe*, vol. 4, no. 4, 2008.

[320] Y. Nakao *et al.*, “Surface-Expressed TLR6 Participates in the Recognition of Diacylated Lipopeptide and Peptidoglycan in Human Cells,” *J. Immunol.*, vol. 174, no. 3, 2005.

[321] S. L. Stafford *et al.*, “Metal ions in macrophage antimicrobial pathways: emerging roles for zinc and copper,” *Biosci. Rep.*, vol. 33, no. 4, pp. 541–554, 2013.

[322] W. Ren *et al.*, “Amino-acid transporters in T-cell activation and differentiation,” *Cell Death and Disease*, vol. 8, no. 3. 2017.

[323] Y. D. Bhutia, E. Babu, and V. Ganapathy, “Interferon-γ induces a tryptophan-selective amino acid transporter in human colonic epithelial cells and mouse dendritic cells,” *Biochim. Biophys. Acta - Biomembr.*, vol. 1848, no. 2, 2015.

[324] L. Heger *et al.*, “CLEC10A Is a specific marker for human CD1c+ dendritic cells and enhances their toll-like receptor 7/8-Induced cytokine secretion,” *Front. Immunol.*, vol. 9, no. APR, 2018.

Appendix 1: Polymer library with viability values

Acronym	Name	Viability 1	Viability 2
13BDDA	Butanediol-1,3 diacrylate	87.17949	83.33333
13BDDMA	1,3-Butanediol dimethacrylate, 98%	96.15385	94.87179
AAcAm	Diacetone acrylamide	101.2821	92.30769
AcAPAm	N-[2-(Acryloylamino)phenyl]acrylamide	97.4359	96.15385
AEMA.C	2-Aminoethyl methacrylate hydrochloride,	70.51282	73.07692
AODMBA	(R)-α-Acryloyloxy-β,β-dimethyl-γ-butyrolactone	34.61538	29.48718
AOHPA	Acryloyloxy-2-hydroxypropyl acrylate	100	106.4103
AOHPMA	Acryloyloxy-2-hydroxypropyl methacrylate	52.5641	41.02564
BA	Butyl acrylate	84.61538	83.33333
BACOEA	Butylamino carbonyl oxy ethyl acrylate	64.10256	80.76923
BAGDA	Bisphenol A glycerolate diacrylate	105.1282	103.8462
BAPODA	Bisphenol A propoxylate diacrylate	102.5641	101.2821
BDDA	Butanediol diacrylate	97.4359	93.58974
BFEODA	Bisphenol F ethoxylate diacrylate	103.8462	100
BHMA	Benzhydryl methacrylate	103.8462	98.71795
BMA	Butyl methacrylate	66.66667	71.79487
BMAM	N-Benzylmethacrylamide	107.6923	101.2821
BMAOEP	Bis[2-(methacryloyloxy)ethyl] phosphate	76.92308	98.71795
BMENBC	Bis(2-methacryloxyethyl) N,N'-1,9-nonylene biscarbamate	92.30769	100
BnA	Benzyl acrylate	98.71795	98.71795
BnMA	Benzyl methacrylate	105.1282	105.1282
BOEMA	Butoxyethyl methacrylate	48.71795	46.15385
BPAPGDA	Bisphenol A propoxylate glycerolate diacrylate	98.71795	96.15385
BPDMA	Bisphenol A dimethacrylate	85.89744	82.05128
BPEODA	Bisphenol A ethoxylate diacrylate	92.30769	84.61538
BzHPEA	Benzoyl-3-hydroxy-phenoxy)ethyl acrylate	83.33333	79.48718
CEA	Carboxyethyl acrylate	103.8462	103.8462
CHA	Cyclohexyl acrylate	58.97436	69.23077
CHMA	Cyclohexyl methacrylate	97.4359	84.61538
CHMA 66%, DMAEMA33%		98.71795	98.71795
CHMA 66%, iDMA 33%		84.61538	70.51282
CHPMA	Chloro-2-hydroxy-propyl methacrylate	100	102.5641
CMAOE	Caprolactone 2-(methacryloyloxy)ethyl ester	70.51282	69.23077
CNEA	Cyanoethyl acrylate	105.1282	105.1282

COEA	2-Cinnamoyloxyethyl acrylate	101.2821	101.2821
COMAm		69.23077	75.64103
CzEA	Carbazol-9-yl ethyl acrylate	94.87179	103.8462
DAAM	N,N-Diallylacrylamide	96.15385	96.15385
DDDMA	1,10-Decanediol dimethacrylate	64.10256	70.51282
DEAEA	Diethylamino ethyl acrylate	101.2821	88.46154
DEAEMA	Diethylaminoethyl methacrylate	61.53846	60.25641
DEGDA	Di(ethylene glycol) diacrylate	97.4359	101.2821
DEGDMA	Diethylene glycol dimethacrylate	98.71795	114.1026
DEGEEA	Di(ethylene glycol) ethyl ether acrylate	76.92308	66.66667
DEGEHA	Di(ethylene glycol) 2-ethylhexyl ether acrylate	73.07692	76.92308
DEGMA	Di(ethylene glycol) methyl ether methacrylate	78.20513	74.35897
DFFMOA	Dodecafluoro-7-(trifluoromethyl)-octyl acrylate	102.5641	100
DFHA	Dodecafluoroheptyl acrylate	105.1282	112.8205
DFHNMA	Dodecafluoro-2-hydroxy-8-(trifluoromethyl)nonyl methacrylate	93.58974	74.35897
DiPEMA	2-Diisopropylaminoethyl methacrylate	62.82051	75.64103
DMA	Decyl methacrylate	56.41026	57.69231
DMAEMA	Dimethylamino-ethyl methacrylate	37.17949	41.02564
DMAPA	Dimethylamino-propyl acrylate	85.89744	73.07692
DMEMAm	N-[2-(N,N-Dimethylamino)ethyl]methacrylamide	32.05128	39.74359
DMMAm	N,N-Dimethylmethacrylamide	96.15385	89.74359
DMPAm	N-[3-(Dimethylamino)propyl]acrylamide	32.05128	58.97436
DMPMAm	N-[3-(Dimethylamino)propyl]methacrylamide	91.02564	80.76923
DPEPHA	Dipentaerythritol penta/hexa-acrylate	97.4359	100
DVAd	Divinyl Adipate	111.5385	96.15385
E3GDA	Triethylene glycol diacrylate	91.02564	98.71795
EA	Ethyl acrylate	98.71795	85.89744
EaNIA	Ethyl trans-a-cyano-3-indole-acrylate	102.5641	107.6923
EbCNA	Ethyl-cis-B-cyano-acrylate	103.8462	101.2821
EEMA	Ethoxyethyl methacrylate	64.10256	75.64103
EG3DMA	Tri(ethylene glycol) dimethacrylate	98.71795	91.02564
EG4DMA	Tetraethylene glycol dimethacrylate	98.71795	100
EGDA	Ethylene {glycol} diacrylate	46.15385	44.87179
EGDCMA	Ethylene glycol dicyclopentenyl ether methacrylate	84.61538	70.51282
EGDMA 66%, HDFDA 33%		105.1282	105.1282
EGDPEA	Ethylene glycol dicyclopentenyl ether acrylate	92.30769	85.89744

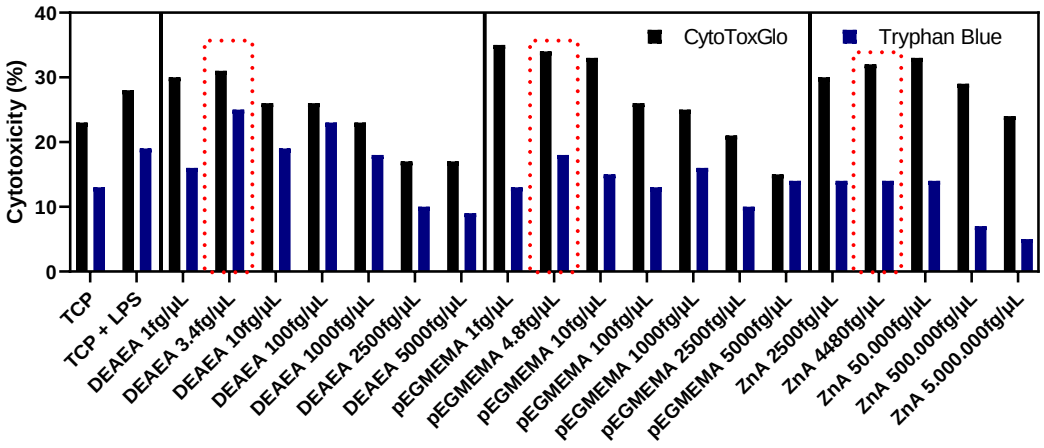
EGMEA	Ethylene glycol methyl ether acrylate	76.92308	48.71795
EGMMA	Ethylene glycol methyl ether methacrylate	98.71795	105.1282
EGPEA	Ethylene glycol phenyl ether acrylate	98.71795	97.4359
EGPhMA	Ethylene glycol phenyl ether methacrylate	102.5641	105.1282
EHA	Ethylhexyl acrylate	70.51282	66.66667
EHMA	Ethylhexyl methacrylate	47.4359	44.87179
EMA	Ethyl methacrylate	103.8462	105.1282
EOEA	Ethoxyethyl acrylate	29.48718	55.12821
ExA	Epoxidized acrylate	92.30769	98.71795
F6BA	Hexafluorobutyl acrylate	96.15385	53.84615
F6BMA	Hexafluorobutyl methacrylate	80.76923	100
F7BA	Heptafluorobutyl acrylate	101.2821	100
F7BMA	Heptafluorobutyl methacrylate	98.71795	92.30769
FMHPNMA	Trifluoro-2′-(trifluoromethyl)-2′-hydroxy)propyl]-3-norbornyl methacrylate	78.20513	80.76923
FuMA	Furfuryl methacrylate	103.8462	107.6923
GDGDA	Glycerol 1,3-diglycerolate diacrylate	103.8462	105.1282
GDMA	Glycerol dimethacrylate	85.89744	84.61538
HA	Hexyl acrylate	48.71795	56.41026
HBA	Hydroxybutyl acrylate	97.4359	106.4103
HBMA	Hydroxybutyl methacrylate	93.58974	87.17949
HBOPBA	Hexanediylbis[oxy(2-hydroxy-3,1-propanediyl)] bisacrylate	100	103.8462
HDDMA	1,6-Hexanediol dimethacrylate,	79.48718	82.05128
HDFDA	Heptadecafluorodecyl acrylate	103.8462	101.2821
HDFDMA	Heptadecafluorodecyl methacrylate	87.17949	96.15385
HDFHUA	Heptadecafluoro-2-hydroxyundecyl acrylate	101.2821	89.74359
HDMPDA	Hydroxy-2,2-dimethylpropyl 3-hydroxy-2,2-dimethylpropionate diacrylate	47.4359	23.07692
HEA	Hydroxyethyl acrylate	98.71795	105.1282
HEAm	N-Hydroxyethyl acrylamide	100	100
HEODA	Hexanediol ethoxylate diacrylate	101.2821	101.2821
HfCEA	Hafnium carboxyethyl acrylate	83.33333	102.5641
HFHUMA	Hexadecafluoro-2-hydroxy-10-(trifluoromethyl)undecyl methacrylate	76.92308	82.05128
HFiPA	Hexafluoroisopropyl acrylate	103.8462	101.2821
HFiPMA	Hexafluoroisopropyl methacrylate	98.71795	105.1282
HFPDA	Hexafluoropent-1,5-diyl diacrylate	94.87179	97.4359
HMA	Hexyl methacrylate	48.71795	39.74359
HPA	Hydroxypropyl acrylate	103.8462	102.5641
HPhMA	N-(4-Hydroxyphenyl)methacrylamide	101.2821	92.30769
HPhOPA	Hydroxy-3-phenoxypropyl acrylate	93.58974	102.5641

HPHPBAH	Hydroxypivalyl hydroxypivalate bis[6-(acryloyloxy)hexanoate]	89.74359	106.4103
HPMA	Hydroxypropyl methacrylate	92.30769	89.74359
HPMAP	Hydroxypropyl 2-(methacryloyloxy)ethyl phthalate	97.4359	100
iBA	Isobutyl acrylate	74.35897	89.74359
iBMA	Isobornyl methacrylate	92.30769	91.02564
iBOA	Isobornyl acrylate	92.30769	79.48718
iBOMAm	N-(Isobutoxymethyl)acrylamide	101.2821	97.4359
iDA	Isodecyl acrylate	98.71795	94.87179
iDMA	Isodecyl methacrylate	65.38462	58.97436
iDMA 66%, HPMA33%		83.33333	64.10256
iOA	Isooctyl acrylate	76.92308	74.35897
iPAm	N-Isopropylacrylamide	85.89744	82.05128
LaA	Lauryl acrylate	89.74359	74.35897
TCP		101.2821	100
LMA	Lauryl methacrylate	57.69231	71.79487
MA	Methyl acrylate	101.2821	106.4103
MAAH	Methacrylic anhydride	98.71795	94.87179
MAAHS	Methacrylic acid N-hydroxysuccinimide ester	106.4103	101.2821
MAEA	Methacryloyloxy)ethyl acetoacetate	98.71795	87.17949
MAEACl	[2-Methacryloyloxy)ethyl] trimethylammonium chloride solution	57.69231	55.12821
MAHBP	4-Methacryloxy-2-hydroxybenzophenone	88.46154	91.02564
Mam	Methacrylamide	93.58974	94.87179
MAPtMA	Methacrylamidopropyltrimethylammonium chloride,	102.5641	101.2821
MAPU	2-methacryloxyethyl phenyl urethane	97.4359	105.1282
MBMAm	N,N'-Methylenebismethacrylamide	107.6923	106.4103
MHMB	Methyl 3-hydroxy-2-methylenebutyrate	101.2821	102.5641
MMA	Methyl methacrylate	106.4103	94.87179
mMAOEM	mono-2-(Methacryloyloxy)ethyl maleate	94.87179	98.71795
Mmam	N-Methyl methacrylamide	101.2821	103.8462
mMAOES	mono-2-(Methacryloyloxy)ethyl succinate	88.46154	91.02564
MOPAm	N-(3-Methoxypropyl)acrylamide	101.2821	105.1282
MSPMA	Methyldiethoxysilyl-propyl methacrylate	97.4359	92.30769
MTEMA	Methylthioethyl methacrylate	101.2821	96.15385
NAM	N-Acryloylmorpholine	102.5641	107.6923
NBnMA	o-Nitrobenzyl methacrylate, . 95%	78.20513	79.48718
NDMAm	N-Dodecylmethacrylamide	76.92308	61.53846
NGDA	Neopentyl glycol diacrylate	102.5641	96.15385
NGPDA	Neopentyl glycol propoxylate diacrylate	102.5641	100

NMEMA	2-N-Morpholinoethyl methacrylate, 95%	97.4359	106.4103
nOcMA	n-Octyl methacrylate,	46.15385	42.30769
NpMA	Naphthyl methacrylate	105.1282	107.6923
NPhPMA	Nitrophenyl-2-pyrrolidonemethyl acrylate	60.25641	117.9487
ODA	Octadecyl acrylate	101.2821	101.2821
OFPA	Octafluoropentyl acrylate	78.20513	92.30769
OFPMA	Octafluoropentyl methacrylate	100	92.30769
PA	Propargyl acrylate	82.05128	94.87179
PAHEMA	Phosphoric acid 2-hydroxyethyl methacrylate ester	102.5641	98.71795
PDA	1,4-Phenylene diacrylate	69.23077	46.15385
PDDMA	1,5-Pentanediol dimethacrylate	62.82051	62.82051
PEDAM	Pentaerythritol diacrylate monostearate	97.4359	102.5641
pEGDA	Polyethylene glycol diacrylate	102.5641	94.87179
pEGDMA	Poly(ethylene glycol) (600) dimethacrylate	102.5641	96.15385
pEGMEMA	Poly(ethylene glycol) methyl ether methacrylate	96.15385	96.15385
pEGPhEA	Poly(ethylene glycol) phenyl ether acrylate	89.74359	94.87179
PETA	Pentaerythritol tetraacrylate	94.87179	98.71795
PETrA	Pentaerythritol triacrylate	100	97.4359
pFDA	Perfluorodecyl acrylate	100	101.2821
PFPA	Pentafluoropropyl acrylate	98.71795	97.4359
PFPhA	Pentafluorophenyl acrylate	96.15385	89.74359
PFPhMA	Pentafluorophenyl methacrylate, 95%	98.71795	96.15385
PFPMA	Pentafluoropropyl methacrylate	91.02564	93.58974
PhA	Phenyl acrylate, 95%	96.15385	96.15385
PhEA	2-Phenylethyl acrylate	112.8205	100
PhEMA	2-Phenylethyl methacrylate	101.2821	96.15385
PhMA	Phenyl methacrylate	96.15385	96.15385
PhMA 66%, iDMA33%		101.2821	96.15385
PhMAm	N-Phenylmethacrylamide	94.87179	98.71795
PMA	Propargyl methacrylate	92.30769	98.71795
PMAm	N-(Phthalimidomethyl)acrylamide	101.2821	98.71795
PMMA	1-Pyrenylmethyl methacrylate	93.58974	91.02564
pPGA	Poly(propylene glycol) acrylate	87.17949	88.46154
pPGDA	Poly(propylene glycol) diacrylate	103.8462	98.71795
pPGDMA	Poly(propylene glycol) (400) dimethacrylate	89.74359	100
pPGNEA	Poly(propylene glycol) 4-nonylphenyl ether acrylate	58.97436	62.82051
SEMA	2-Sulfoethyl methacrylate	94.87179	80.76923
SMA	Stearyl methacrylate	100	88.46154
SPAK	Sulfopropyl acrylate potassium salt	105.1282	108.9744

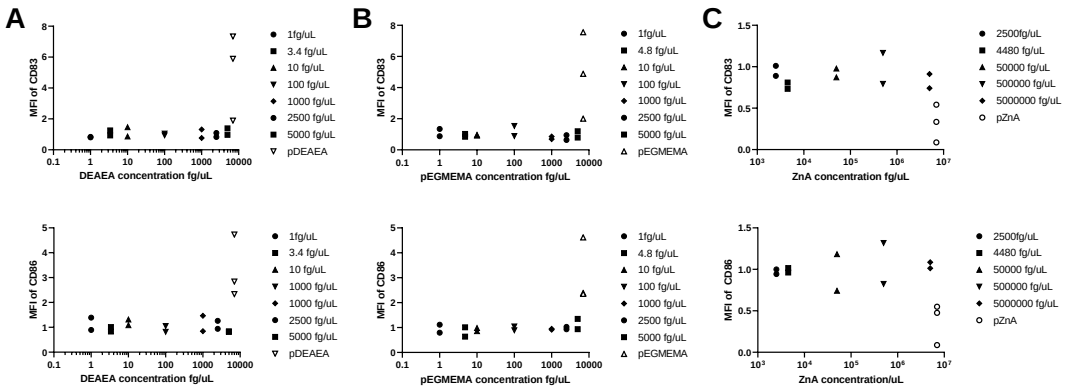
SPMAK	3-Sulfopropyl methacrylate potassium salt	107.6923	103.8462
TAHTA	1,3,5-Triacryloylhexahydro-1,3,5-triazine	119.2308	70.51282
TAIC	Tris[2-(acryloyloxy)ethyl] isocyanurate	106.4103	102.5641
tBA	Tert-butyl acrylate	87.17949	89.74359
tBAEMA	Tert-butylamino-ethyl methacrylate	42.30769	46.15385
tBCHA	Tert-butylcyclohexylacrylate	91.02564	98.71795
tBCHMA	Tertbutylcyclohexyl methacrylate	96.15385	70.51282
tBMAm	N-tert-Butylmethacrylamide	75.64103	83.33333
TBNpMA	Tribromoneopentyl methacrylate	85.89744	97.4359
tBOCAPAm	N-(t-BOC-aminopropyl)methacrylamide	100	79.48718
TBPhA	2,4,6-Tribromophenyl acrylate	91.02564	88.46154
TCDMDA	Tricyclodecane-dimethanol diacrylate	96.15385	94.87179
TDFOMA	Tridecafluorooctyl methacrylate	83.33333	102.5641
TEGDA	Tetra(ethylene glycol) diacrylate	105.1282	105.1282
TEGMA	Tri(ethylene glycol) methyl ether methacrylate	102.5641	106.4103
TFPMA	Tetrafluoropropyl methacrylate	93.58974	94.87179
THFuA	Tetrahydrofurfuryl acrylate	102.5641	103.8462
THFuMA	Tetrahydrofurfuryl methacrylate	106.4103	106.4103
TMCHMA	Trimethylcyclohexyl methacrylate	83.33333	96.15385
TMHA	Trimethylhexyl acrylate	85.89744	92.30769
TMOBDA	Trimethylolpropane benzoate diacrylate	101.2821	106.4103
TMPDAE	Trimethyl propane diallyl ether	101.2821	92.30769
TMPETA	Trimethylolpropane ethoxylate triacrylate	103.8462	98.71795
TMPOTA	Trimethylolpropane propoxylate triacrylate	98.71795	98.71795
TMPTA	Trimethylolpropane triacrylate	98.71795	96.15385
TPGDA	Tri(propylene glycol) diacrylate	105.1282	100
VMA	Vinyl methacrylate	100	101.2821
ZnA	Zinc acrylate	100	92.30769
ZrCEA	Zirconium carboxyethyl acrylate	107.6923	110.2564

Appendix 2: Cytotoxicity of monomer in media



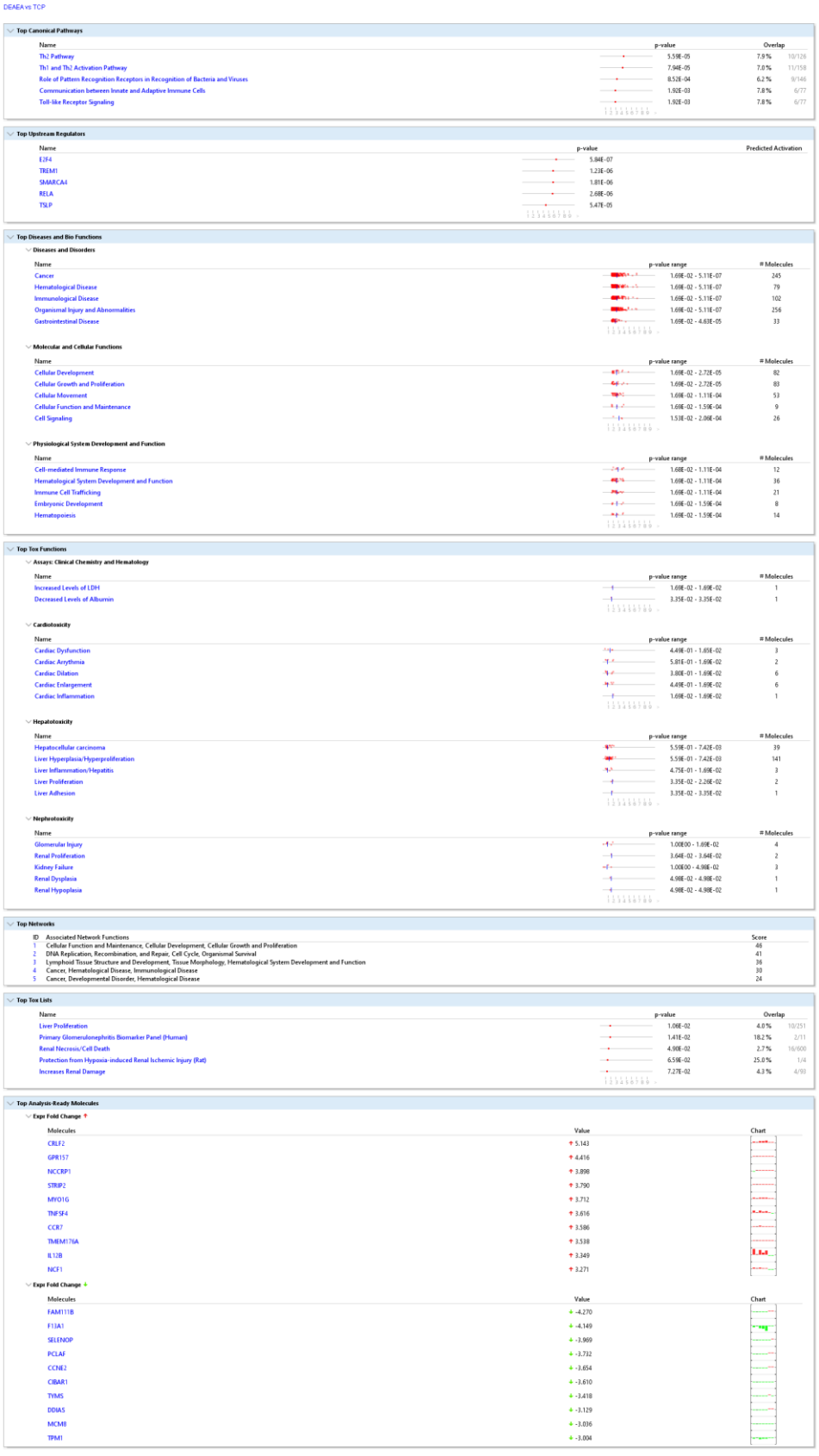
Traditional cytotoxicity assay (CytoToxGlo) and metabolic assay (Tryphan blue) of monomer diluted in complete media. Concentrations were chosen just below, and up to factor 1500 (DEAEA and pEGMEMA) and factor 1000 (ZnA) above monomer levels observed in media washing procedure. The observed monomer level for each monomer is highlighted with a red ticked box. Data is from n=1, immature DCs were cultured in 96 well plate.

Appendix 3: Comparison of monomer effect to polymerised surface coatings on iDCs



The same concentrations used in Appendix 2 were investigated for their effect on DC phenotype; CD83 and CD86 expression on immature DCs after 24 hours culture with monomer in the media or on top of polymerised surface coating.

Appendix 4: DEAEA vs TCP – summary of IPA analysis



DEAEA vs TCP

Top Canonical Pathways

Name	p-value	Overlap
Th2 Pathway	5.59E-05	7.9% 10/126
Th1 and Th2 Activation Pathway	7.94E-05	7.0% 11/158
Role of Pattern Recognition Receptors in Recognition of Bacteria and Viruses	8.52E-04	6.2% 9/146
Communication between Innate and Adaptive Immune Cells	1.92E-03	7.8% 6/77
Toll-like Receptor Signaling	1.92E-03	7.8% 6/77

Top Upstream Regulators

Name	p-value	Predicted Activation
E2F4	5.84E-07	
TREM1	1.23E-06	
SMARCA4	1.81E-06	
RELA	2.68E-06	
TSLP	5.47E-05	

Top Diseases and Bio Functions

Diseases and Disorders

Name	p-value range	# Molecules
Cancer	1.69E-02 - 5.11E-07	245
Hematological Disease	1.69E-02 - 5.11E-07	79
Immunological Disease	1.69E-02 - 5.11E-07	102
Organismal Injury and Abnormalities	1.69E-02 - 5.11E-07	256
Gastrointestinal Disease	1.69E-02 - 4.63E-05	33

Molecular and Cellular Functions

Name	p-value range	# Molecules
Cellular Development	1.69E-02 - 2.72E-05	82
Cellular Growth and Proliferation	1.69E-02 - 2.72E-05	83
Cellular Movement	1.69E-02 - 1.11E-04	53
Cellular Function and Maintenance	1.69E-02 - 1.59E-04	9
Cell Signaling	1.53E-02 - 2.00E-04	26

Physiological System Development and Function

Name	p-value range	# Molecules
Cell-mediated Immune Response	1.69E-02 - 1.11E-04	12
Hematological System Development and Function	1.69E-02 - 1.11E-04	36
Immune Cell Trafficking	1.69E-02 - 1.11E-04	21
Embryonic Development	1.69E-02 - 1.59E-04	8
Hematopoiesis	1.69E-02 - 1.59E-04	14

Top Tox Functions

Assays: Clinical Chemistry and Hematology

Name	p-value range	# Molecules
Increased Levels of LDH	1.69E-02 - 1.69E-02	1
Decreased Levels of Albumin	3.35E-02 - 3.35E-02	1

Cardiotoxicity

Name	p-value range	# Molecules
Cardiac Dysfunction	4.49E-01 - 1.65E-02	3
Cardiac Arrythmia	5.81E-01 - 1.69E-02	2
Cardiac Dilation	3.80E-01 - 1.69E-02	6
Cardiac Enlargement	4.49E-01 - 1.69E-02	6
Cardiac Inflammation	1.69E-02 - 1.69E-02	1

Hepatotoxicity

Name	p-value range	# Molecules
Hepatocellular carcinoma	5.59E-01 - 7.42E-03	39
Liver Hyperplasia/Hyperproliferation	5.59E-01 - 7.42E-03	141
Liver Inflammation/Hepatitis	4.75E-01 - 1.69E-02	3
Liver Proliferation	3.35E-02 - 2.20E-02	2
Liver Adhesion	3.35E-02 - 3.35E-02	1

Nephrotoxicity

Name	p-value range	# Molecules
Glomerular Injury	1.00E00 - 1.69E-02	4
Renal Proliferation	3.64E-02 - 3.64E-02	2
Kidney Failure	1.00E00 - 4.98E-02	3
Renal Dysplasia	4.98E-02 - 4.98E-02	1
Renal Hypoplasia	4.98E-02 - 4.98E-02	1

Top Networks

ID	Associated Network Functions	Score
1	Cellular Function and Maintenance, Cellular Development, Cellular Growth and Proliferation	46
2	DNA Replication, Recombination, and Repair, Cell Cycle, Organismal Survival	41
3	Lymphoid Tissue Structure and Development, Tissue Morphology, Hematological System Development and Function	36
4	Cancer, Hematological Disease, Immunological Disease	30
5	Cancer, Developmental Disorder, Hematological Disease	24

Top Tox Lists

Name	p-value	Overlap
Liver Proliferation	1.06E-02	4.0% 10/251
Primary Glomerulonephritis Biomarker Panel (Human)	1.41E-02	18.2% 2/11
Renal Necrosis/Cell Death	4.90E-02	2.7% 16/600
Protection from Hypoxia-induced Renal Ischemic Injury (Rat)	6.59E-02	25.0% 1/4
Increases Renal Damage	7.27E-02	4.3% 4/93

Top Analysis-Ready Molecules

Expr Fold Change ↑

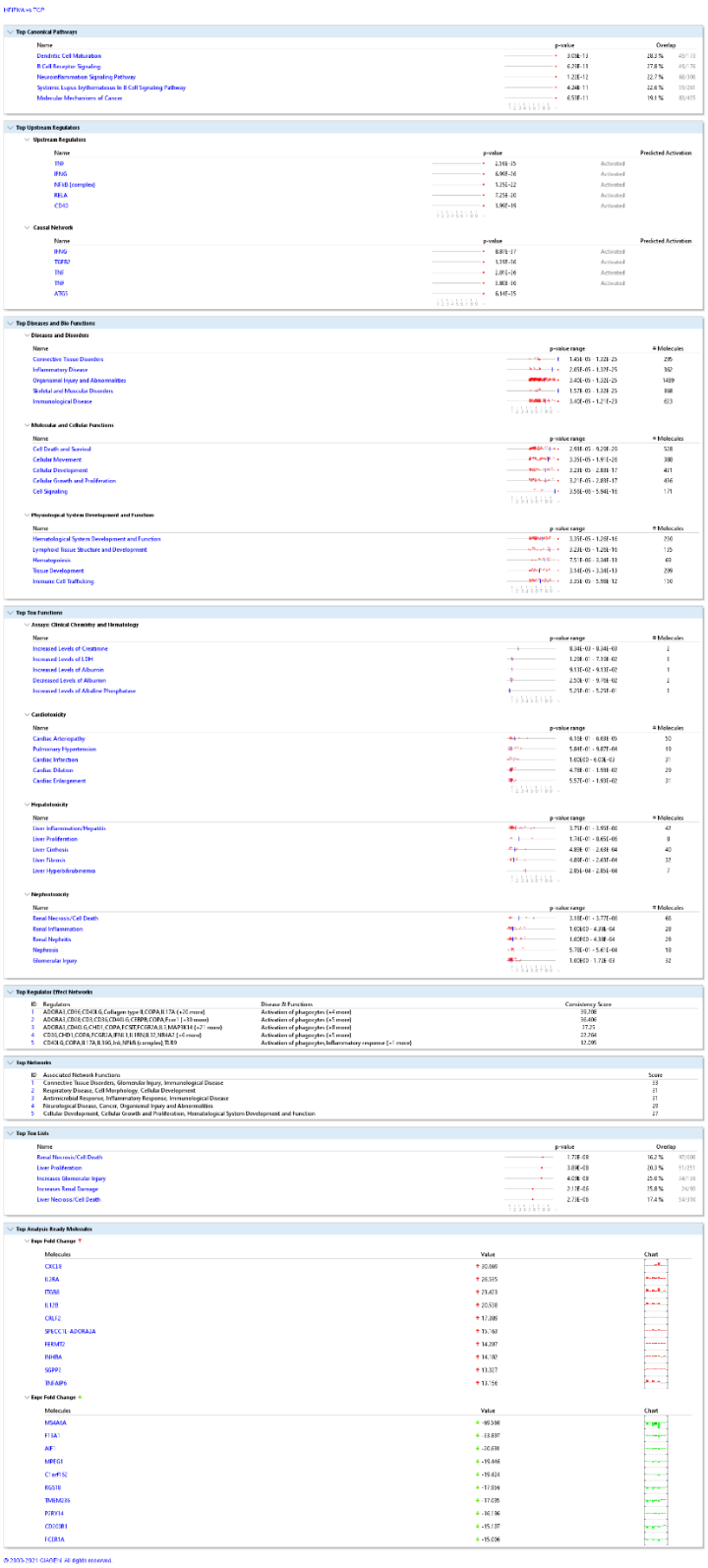
Molecules	Value	Chart
CRLF2	↑ 5.143	
GPR157	↑ 4.416	
NCCRP1	↑ 3.898	
STRIP2	↑ 3.790	
MYO1G	↑ 3.712	
TNFSF4	↑ 3.616	
CCR7	↑ 3.586	
TMEM176A	↑ 3.538	
IL12B	↑ 3.349	
NCF1	↑ 3.271	

Expr Fold Change ↓

Molecules	Value	Chart
FAM111B	↓ -4.270	
F13A1	↓ -4.149	
SELENOP	↓ -3.969	
PCLAF	↓ -3.732	
CCNE2	↓ -3.654	
CIBAR1	↓ -3.610	
TYMS	↓ -3.418	
DDIAS	↓ -3.129	
MCM8	↓ -3.036	
TPM1	↓ -3.004	

© 2000-2021 QIAGEN. All rights reserved.

Appendix 5: HFiPMA vs TCP – summary of IPA analysis



Appendix 6: Canonical pathways summary

Canonical Pathways	TCP + LPS vs TCP	HFiPMA vs TCP	DEAEA vs TCP
	z-value		
Dendritic Cell Maturation	2.994	2.429	1.89
Production of Nitric Oxide and Reactive Oxygen Species in Macrophages	2.722	2.335	1.633
FAT10 Cancer Signaling Pathway	1.807	2.324	2
Superpathway of Inositol Phosphate Compounds	-3.042	-1.671	-1.342
Th17 Activation Pathway	2.828	1.941	1
Oxidative Phosphorylation	-3.71	-1.633	N/A
IL-17 Signaling	2.611	1.732	1
Role of Hypercytokinemia/hyperchemokinemia in the Pathogenesis of Influenza	4.271	0.943	0
Role of IL-17F in Allergic Inflammatory Airway Diseases	2.53	2.646	N/A
3-phosphoinositide Degradation	-2.414	-1.4	-1.342
Role of Pattern Recognition Receptors in Recognition of Bacteria and Viruses	0.784	-2.4	-1.89
Fcγ Receptor-mediated Phagocytosis in Macrophages and Monocytes	-1.633	-1.961	-1.342
PPAR Signaling	-1.886	-3	N/A

PI3K/AKT Signaling	2.524	2.236	N/A
FAT10 Signaling Pathway	2.646	2	N/A
4-1BB Signaling in T Lymphocytes	2.121	2.449	N/A
Superpathway of Cholesterol Biosynthesis	2.324	2.236	N/A
fMLP Signaling in Neutrophils	-1.569	-2.524	-0.447
Complement System	-2.236	-2.236	N/A
Crosstalk between Dendritic Cells and Natural Killer Cells	2.858	1.606	N/A
Systemic Lupus Erythematosus In B Cell Signaling Pathway	2.557	1.192	0.632
Small Cell Lung Cancer Signaling	2.668	1.604	N/A
Coronavirus Pathogenesis Pathway	0.508	1.521	2.236
Differential Regulation of Cytokine Production in Intestinal Epithelial Cells by IL-17A and IL-17F	2	2.236	N/A
Acute Phase Response Signaling	1.512	2.711	N/A
PD-1, PD-L1 cancer immunotherapy pathway	-1.8	-1.043	-1.342
B Cell Activating Factor Signaling	2.496	1.667	N/A
FLT3 Signaling in Hematopoietic Progenitor Cells	2.524	1.604	N/A
IL-15 Signaling	2.5	1.604	N/A
Regulation of IL-2 Expression in Activated and Anergic T Lymphocytes	1.89	2.183	N/A
Cell Cycle Control of Chromosomal Replication	-1.387	-1.667	-1

Phospholipase C Signaling	-1.64	-1.947	0.447
Role of NFAT in Regulation of the Immune Response	-1.441	-2.121	0.447
Systemic Lupus Erythematosus In T Cell Signaling Pathway	1	1.809	1.134
3-phosphoinositide Biosynthesis	-2.121	-0.816	-1
Melatonin Signaling	-1.807	-2.111	N/A
GNRH Signaling	-2.475	-1.4	N/A
Breast Cancer Regulation by Stathmin1	-2.393	-1.179	-0.277
TNFR2 Signaling	1.732	2.111	N/A
IL-6 Signaling	1.569	2.236	N/A
Signaling by Rho Family GTPases	-1.183	-1.8	0.816
D-myo-inositol-5-phosphate Metabolism	-2.556	-1.225	N/A
Factors Promoting Cardiogenesis in Vertebrates	-2.065	-1.706	N/A
Endothelin-1 Signaling	-1.3	-2.449	N/A
Role of NFAT in Cardiac Hypertrophy	-1.761	-1.961	N/A
CD27 Signaling in Lymphocytes	1.213	2.496	N/A
Fc Epsilon RI Signaling	-1.633	-2.065	N/A
IL-22 Signaling	1.667	2	N/A
ERK/MAPK Signaling	-0.378	-1.8	-1.342

Endoplasmic Reticulum Stress Pathway	1.414	2	N/A
CXCR4 Signaling	-1	-1.964	-0.447
Integrin Signaling	-0.73	-1.671	-1
OX40 Signaling Pathway	1.732	1.667	N/A
RANK Signaling in Osteoclasts	1.3	2.065	N/A
IL-8 Signaling	-1.333	-1	-1
Role of PKR in Interferon Induction and Antiviral Response	2.694	-0.626	0
HOTAIR Regulatory Pathway	2.065	0.229	-1
Tumour Microenvironment Pathway	1.298	1.567	0.378
Senescence Pathway	-0.962	-0.885	-1.342
iNOS Signaling	2.111	1	N/A
Neuroinflammation Signaling Pathway	1.806	0.911	-0.378
p53 Signaling	-1.877	-1.213	N/A
Protein Kinase A Signaling	-0.63	-2.064	-0.378
Interferon Signaling	2.524	0.447	N/A
Estrogen-Dependent Breast Cancer Signaling	1.508	1.387	N/A
Calcium-induced T Lymphocyte Apoptosis	-1.5	-1.387	N/A
TNFR1 Signaling	1.698	1.069	N/A

UVA-Induced MAPK Signaling	-0.302	-2.449	N/A
Inhibition of ARE-Mediated mRNA Degradation Pathway	1.461	1.213	N/A
Semaphorin Neuronal Repulsive Signaling Pathway	0.784	1.877	N/A
Reelin Signaling in Neurons	-0.784	-1.877	N/A
IL-23 Signaling Pathway	1.387	1.265	N/A
Cholesterol Biosynthesis I	2.646	N/A	N/A
Cholesterol Biosynthesis III (via Desmosterol)	2.646	N/A	N/A
Cholesterol Biosynthesis II (via 24,25-dihydrolanosterol)	2.646	N/A	N/A
Sperm Motility	-0.626	-2	N/A
D-myo-inositol (1,4,5,6)-Tetrakisphosphate Biosynthesis	-1.961	-0.655	N/A
D-myo-inositol (3,4,5,6)-tetrakisphosphate Biosynthesis	-1.961	-0.655	N/A
IL-1 Signaling	1.213	1.387	N/A
PPARα/RXRα Activation	-1.257	-1.342	N/A
NGF Signaling	0.853	1.732	N/A
Rac Signaling	-1.279	-1.291	N/A
Toll-like Receptor Signaling	1.732	0.832	N/A
Macropinocytosis Signaling	-1.265	-1.265	N/A
Type II Diabetes Mellitus Signaling	1.213	1.291	N/A

Role of RIG1-like Receptors in Antiviral Innate Immunity	2.496	0	N/A
Neuropathic Pain Signaling In Dorsal Horn Neurons	-0.471	-2	N/A
T Cell Exhaustion Signaling Pathway	1.029	1.4	0
T Cell Receptor Signaling	1.571	0.469	0.378
Autophagy	1	1.414	N/A
P2Y Purigenic Receptor Signaling Pathway	-0.626	-1.698	N/A
SPINK1 General Cancer Pathway	-1.5	-0.816	N/A
IL-7 Signaling Pathway	1	1.291	N/A
Antioxidant Action of Vitamin C	-1.342	-0.943	N/A
Non-Small Cell Lung Cancer Signaling	-1.134	-1.134	N/A
Apelin Pancreas Signaling Pathway	-0.832	-1.414	N/A
Pyridoxal 5'-phosphate Salvage Pathway	-0.832	-1.414	N/A
Role of MAPK Signaling in Inhibiting the Pathogenesis of Influenza	1.964	0.277	N/A
Th2 Pathway	1.569	0.655	0
Myc Mediated Apoptosis Signaling	-0.832	-1.387	N/A
April Mediated Signaling	1.291	0.905	N/A
HMGB1 Signaling	1.134	0.6	0.447
Xenobiotic Metabolism AHR Signaling Pathway	-0.277	1.897	N/A

PFKFB4 Signaling Pathway	-0.905	-1.265	N/A
Erythropoietin Signaling Pathway	-0.48	-0.686	-1
Colorectal Cancer Metastasis Signaling	1.151	-0.174	-0.816
Paxillin Signaling	-1.069	-1.069	N/A
Endocannabinoid Cancer Inhibition Pathway	1.347	0.784	N/A
D-myo-inositol (1,4,5)-Trisphosphate Biosynthesis	-2.121	N/A	N/A
Type I Diabetes Mellitus Signaling	1.177	0.943	N/A
NRF2-mediated Oxidative Stress Response	-1.789	-0.258	N/A
Cdc42 Signaling	-1.213	-0.832	N/A
Ephrin B Signaling	-1.732	-0.302	N/A
Renin-Angiotensin Signaling	-0.816	-1.213	N/A
ILK Signaling	1.461	0.557	0
Induction of Apoptosis by HIV1	0	0	2
MSP-RON Signaling In Macrophages Pathway	0	0	-2
NF-κB Activation by Viruses	1.5	0.5	N/A
iCOS-iCOSL Signaling in T Helper Cells	0.962	-0.218	0.816
Pancreatic Adenocarcinoma Signaling	1.213	0.775	N/A
Cholecystokinin/Gastrin-mediated Signaling	-1.528	-0.447	N/A

VDR/RXR Activation	1.155	0.816	N/A
Activation of IRF by Cytosolic Pattern Recognition Receptors	1.633	-0.333	N/A
cAMP-mediated signaling	-0.949	-0.557	-0.447
Phospholipases	-0.632	-1.265	N/A
Lymphotoxin β Receptor Signaling	1.265	0.632	N/A
IL-9 Signaling	1.508	0.378	N/A
STAT3 Pathway	-1.091	0.775	N/A
Cardiac Hypertrophy Signaling	-1.265	-0.6	N/A
TREM1 Signaling	1.633	0.218	N/A
Regulation of Actin-based Motility by Rho	-1	-0.832	N/A
IL-17A Signaling in Gastric Cells	0.816	1	N/A
Tumouricidal Function of Hepatic Natural Killer Cells	0.816	-1	N/A
Cardiac Hypertrophy Signaling (Enhanced)	-1.294	-0.492	0
Ephrin Receptor Signaling	-1.528	-0.218	N/A
p38 MAPK Signaling	-1.043	-0.688	N/A
Leptin Signaling in Obesity	-0.378	-1.342	N/A
Antiproliferative Role of TOB in T Cell Signaling	-1.387	-0.333	N/A
Death Receptor Signaling	0.962	-0.728	N/A

Sirtuin Signaling Pathway	0.686	0	-1
Salvage Pathways of Pyrimidine Ribonucleotides	1.091	-0.577	N/A
Fatty Acid β-oxidation I	-1.265	-0.378	N/A
HER-2 Signaling in Breast Cancer	-0.333	-1.3	0
Inflammasome pathway	0.632	-1	N/A
Acute Myeloid Leukemia Signaling	1.147	-0.471	N/A
Role of BRCA1 in DNA Damage Response	-0.775	-0.816	N/A
Cell Cycle: G1/S Checkpoint Regulation	0.728	0.832	N/A
NF-κB Signaling	0.469	0	-1
Amyotrophic Lateral Sclerosis Signaling	0.243	-1.213	N/A
Cytotoxic T Lymphocyte-mediated Apoptosis of Target Cells	0.447	-1	N/A
RhoA Signaling	-0.894	-0.535	N/A
Unfolded protein response	-0.277	1.134	N/A
Osteoarthritis Pathway	-0.522	-0.87	N/A
Apelin Endothelial Signaling Pathway	0	-1.387	N/A
PAK Signaling	0	-1.387	N/A
Th1 Pathway	0.707	0.655	0
GM-CSF Signaling	0.775	-0.577	N/A

Choline Biosynthesis III	N/A	-1.342	N/A
Regulation Of The Epithelial Mesenchymal Transition By Growth Factors Pathway	0.949	0.392	N/A
ERK5 Signaling	-1	0.333	N/A
Tryptophan Degradation III (Eukaryotic)	-0.333	1	N/A
Hepatic Fibrosis Signaling Pathway	-0.384	-0.128	0.816
LPS-stimulated MAPK Signaling	-0.258	-1.069	N/A
HGF Signaling	-0.626	-0.688	N/A
AMPK Signaling	1.069	0.243	N/A
HIF1α Signaling	-0.949	-0.343	N/A
Ceramide Signaling	0	1.291	N/A
IL-17A Signaling in Airway Cells	1.291	0	N/A
Gα12/13 Signaling	0.626	0.655	N/A
Cyclins and Cell Cycle Regulation	0.258	-1	N/A
Sumoylation Pathway	0.243	0	-1
JAK/Stat Signaling	1.225	0	N/A
Role of PI3K/AKT Signaling in the Pathogenesis of Influenza	0.577	-0.632	N/A
Pyrimidine Deoxyribonucleotides De Novo Biosynthesis I	-0.378	-0.816	N/A
Chemokine Signaling	-0.688	-0.5	N/A

SAPK/JNK Signaling	-0.894	-0.277	N/A
PI3K Signaling in B Lymphocytes	0.48	-0.686	0
Relaxin Signaling	0	-1.155	N/A
CD40 Signaling	0.894	0.258	N/A
TGF-β Signaling	-0.894	-0.258	N/A
BEX2 Signaling Pathway	1.147	0	N/A
MIF-mediated Glucocorticoid Regulation	1.134	0	N/A
Natural Killer Cell Signaling	-0.143	-0.174	-0.816
MSP-RON Signaling In Cancer Cells Pathway	0.688	0.426	N/A
PEDF Signaling	0	-1.069	N/A
Sphingosine-1-phosphate Signaling	-0.408	0.655	N/A
Estrogen-mediated S-phase Entry	-0.333	-0.707	N/A
Necroptosis Signaling Pathway	0.845	-0.192	N/A
Tec Kinase Signaling	1.029	0	N/A
Role of CHK Proteins in Cell Cycle Checkpoint Control	-0.632	-0.378	N/A
ATM Signaling	-0.229	-0.775	N/A
Aryl Hydrocarbon Receptor Signaling	0.784	-0.218	N/A
MIF Regulation of Innate Immunity	1	0	N/A

Bile Acid Biosynthesis, Neutral Pathway	N/A	1	N/A
Ketolysis	-1	N/A	N/A
Role of IL-17A in Psoriasis	N/A	1	N/A
Folate Transformations I	-1	0	N/A
Apoptosis Signaling	0	-1	N/A
Endocannabinoid Developing Neuron Pathway	-0.218	-0.775	N/A
Gαq Signaling	-0.378	-0.6	0
Cell Cycle: G2/M DNA Damage Checkpoint Regulation	-0.632	-0.333	N/A
Ovarian Cancer Signaling	0.632	-0.333	N/A
PTEN Signaling	0.218	-0.728	N/A
Nur77 Signaling in T Lymphocytes	-0.943	0	N/A
Neuregulin Signaling	-0.632	0.302	N/A
Glioma Invasiveness Signaling	0.577	-0.333	N/A
CD28 Signaling in T Helper Cells	0	-0.894	N/A
B Cell Receptor Signaling	0.137	-0.309	-0.447
BMP signaling pathway	0.258	0.632	N/A
Glioma Signaling	-0.302	-0.577	N/A
Wnt/Ca+ pathway	0.277	-0.577	N/A

Glioblastoma Multiforme Signaling	0.209	-0.626	N/A
Cell Cycle Regulation by BTG Family Proteins	-0.378	0.447	N/A
γ-linolenate Biosynthesis II (Animals)	0.816	N/A	N/A
Ceramide Degradation	-0.816	N/A	N/A
Regulation of Cellular Mechanics by Calpain Protease	-0.816	0	N/A
Glutaryl-CoA Degradation	-0.816	N/A	N/A
Inhibition of Angiogenesis by TSP1	0.333	0.447	N/A
Adrenomedullin signaling pathway	0.169	-0.6	N/A
Thrombin Signaling	0.186	-0.577	N/A
Netrin Signaling	0	-0.707	N/A
LPS/IL-1 Mediated Inhibition of RXR Function	0	0.707	N/A
Superpathway of Geranylgeranyldiphosphate Biosynthesis I (via Mevalonate)	0.707	N/A	N/A
Growth Hormone Signaling	0	-0.707	N/A
IL-3 Signaling	0.688	0	N/A
IL-15 Production	0.209	0.471	N/A
Actin Nucleation by ARP-WASP Complex	-0.302	-0.302	N/A
Ferroptosis Signaling Pathway	0.6	0	N/A
Regulation Of The Epithelial Mesenchymal Transition In Development Pathway	0.577	0	N/A

TWEAK Signaling	0.258	-0.277	N/A
LXR/RXR Activation	0.229	-0.258	N/A
Leukocyte Extravasation Signaling	-0.302	0.169	0
Fatty Acid Activation	0.447	N/A	N/A
Phenylalanine Degradation IV (Mammalian, via Side Chain)	-0.447	N/A	N/A
Eicosanoid Signaling	-0.447	N/A	N/A
Ketogenesis	-0.447	N/A	N/A
Salvage Pathways of Pyrimidine Deoxyribonucleotides	0.447	N/A	N/A
Sphingosine and Sphingosine-1-phosphate Metabolism	-0.378	N/A	N/A
Mevalonate Pathway I	0.378	N/A	N/A
NAD Signaling Pathway	0.378	0	N/A
Angiopoietin Signaling	0	-0.277	N/A
PKCθ Signaling in T Lymphocytes	0.169	0	0

Appendix 7: LPS stimulated DCs lead to typical maturation gene responses

Microarray analysis of DCs stimulated with LPS on TCP showed high transcription levels of chemokines CXCL9/10/11/20/5 and IL-6 all promoting interaction with T cells, as wells as other adaptive immune responses (Table 13).

Table 13: TCP + LPS - Top 10 upregulated genes

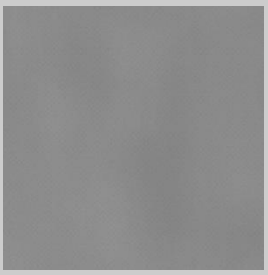
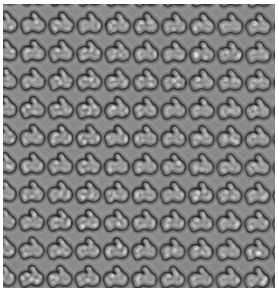
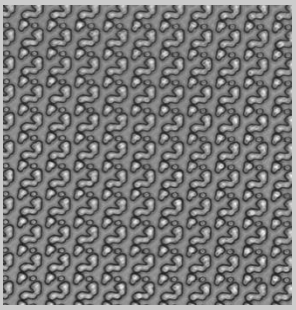
Gene	Expression Foldchange	Function	Ref
CXCL10	+216.445	Required for CD8+ T cells and contributes to granzyme B and Perforin generation	[309]
CXCL11	+138.587	Chemotactic for activated T cells, binds CXCR3, correlated with antitumour activity	[310]
CXCL9	+126.666	Regulates immune migration, differentiation, and activation	[208]
IL6	+102.637	Promotes Th2 and limits Th1 responses	[311]
CCL20	+68.757	Recruits DC and LC precursors to the skin and is required for CD8+ T cell crosspriming, CCR6/CCL20 is needed by most adjuvants for crosspriming	[312]
TNFAIP6	+64.977	Key regulator of inflammation and downregulates IFN-α and TNF-α by suppressing IRF7 phosphorylation	[214]
ITGB8	+62.923	Encodes Integrin β8-subunit, involved in inducing tolerogenic function and Tregs	[210]
CFB	+62.432	Complement factor B, from alternative pathway of complement activation, and forms C3 convertase, involved in proliferation of preactivated B cells	[313]
CCL5	+60.376	Chemoattractant for iDCs and other immune cells	[314], [315]
USP41	+55.949	Involved in processing of poly-ubiquitin precursors as well as ubiquitinated proteins	[316]

Several PRRs had lower transcription levels as well as other genes involved in immune system related genes (Table 14).

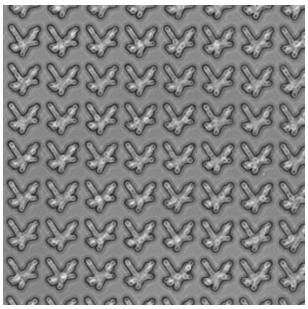
Table 14: TCP + LPS - Top 10 downregulated genes

Gene	Expression Foldchange	Function	Ref
MS4A6A	-63.113	Signal transduction, unknown	
TMEM45B	-62.121	Knockdown inhibits cell proliferation and invasion in gastric cancer	[317]
SGK1	-59.651	Participates in NFκb signalling and DC maturation	[318]
CD200R1	-56.252	Expression positively correlated with Tregs and negatively with Th17; CD200R1 decrease therefore increases Th17 and decreases Tregs	[221]
TLR6	-48.677	Induces IL-10 producing DCs and type-1 regulatory T cells, recognises diacylated lipopeptide and peptidoglycan	[319], [320]
TMEM236	-48.627	Unknown function	
SLC7A8	-45.539	Sodium independent neutral amino acid transporter that is induced by IFN-γ, also known as LAT2	[321] – [323]
CLEC10A	-45.213	CLR and Specific marker for CD1c+ DCs and enhances TLR7,8 induced cytokine secretion	[324]
RGS18	-37.169	Engagement of TLR3 or TLR4 reduces RGS18 without modifying other RGS proteins, RGS18 inhibits Gα signalling and this reduces CXCL12-,19,21Ligand mediated DC migration	[219]
GASK1B	-35.755	Unknown function	

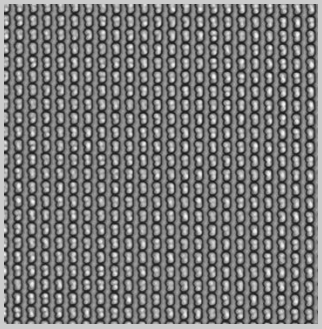
Appendix 8: Mini TopoChip unit numbering with corresponding features

Topography ID	Feature
Unit 1 (=flat)	
Unit 2	
Unit 3	

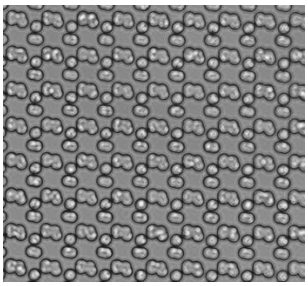
Unit 4



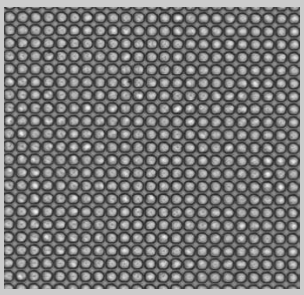
Unit 5



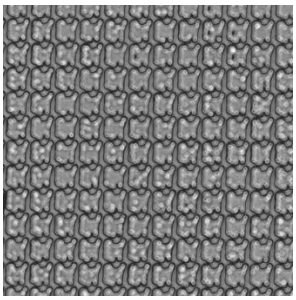
Unit 6



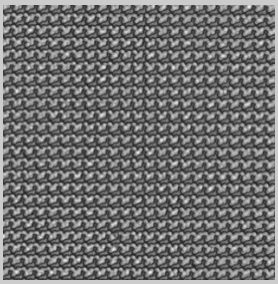
Unit 7



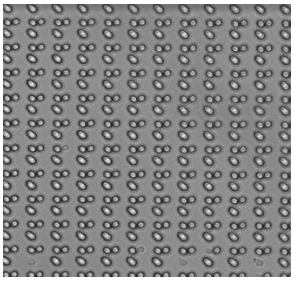
Unit 8



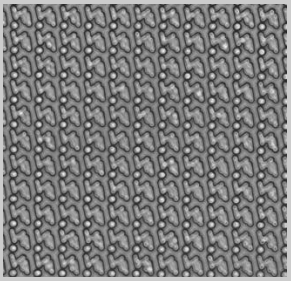
Unit 9



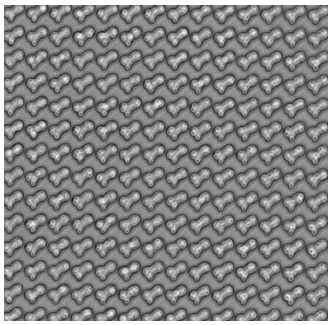
Unit 10



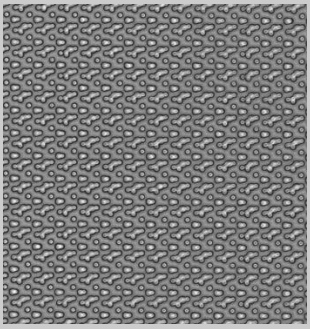
Unit 11



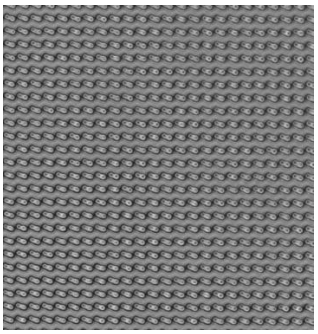
Unit 12



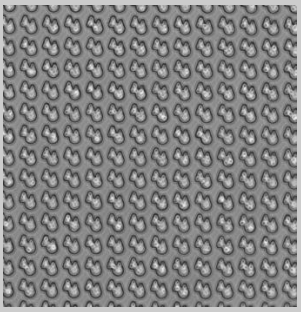
Unit 13



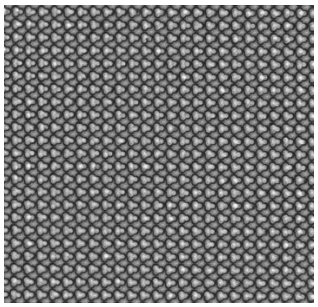
Unit 14



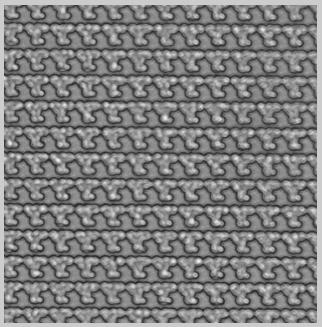
Unit 15



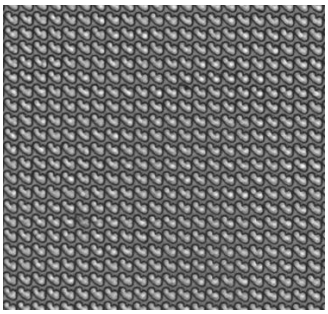
Unit 16



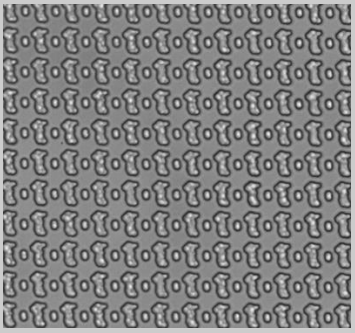
Unit 17



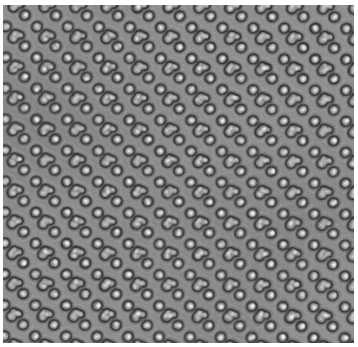
Unit 18



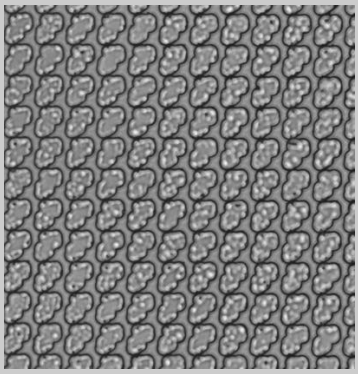
Unit 19



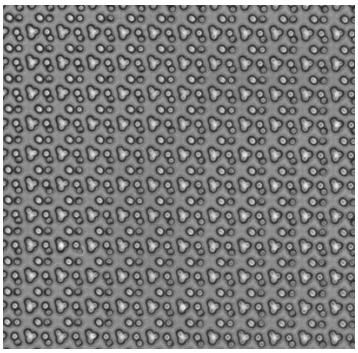
Unit 20



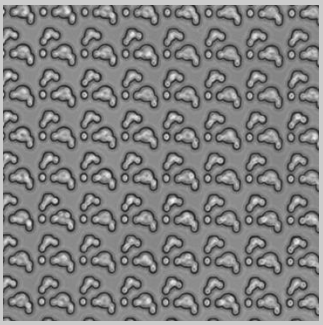
Unit 21



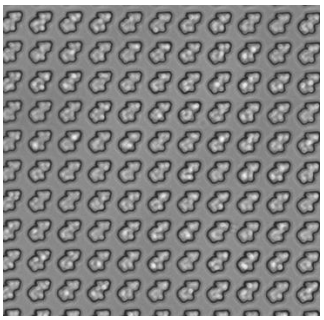
Unit 22



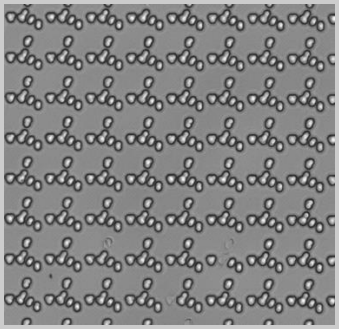
Unit 23



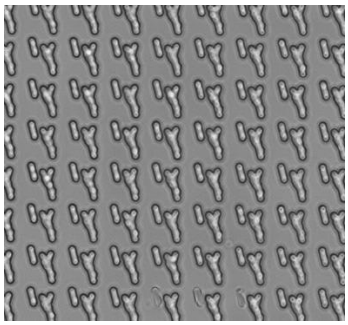
Unit 24



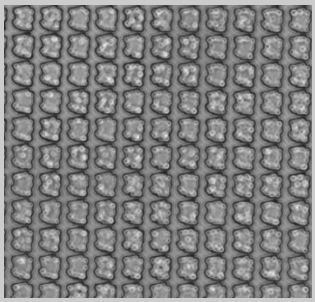
Unit 25



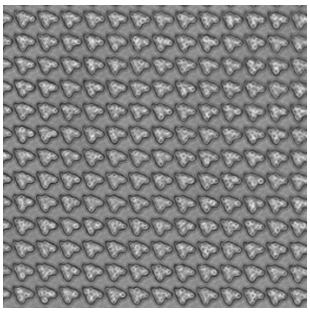
Unit 26



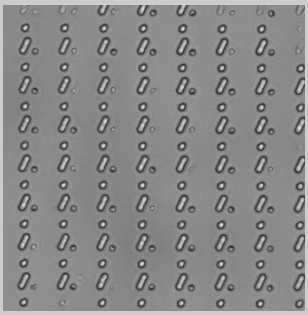
Unit 27



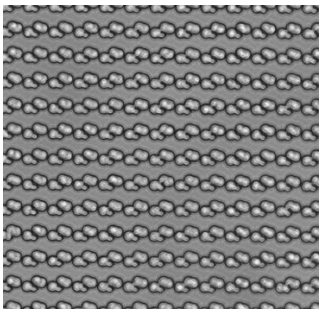
Unit 28



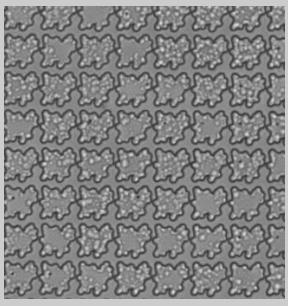
Unit 29



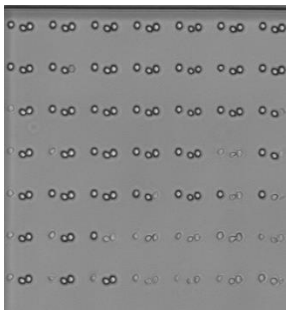
Unit 30



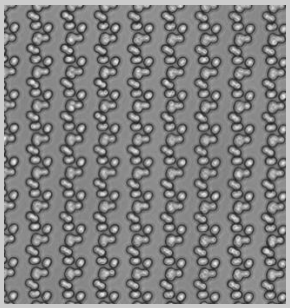
Unit 31



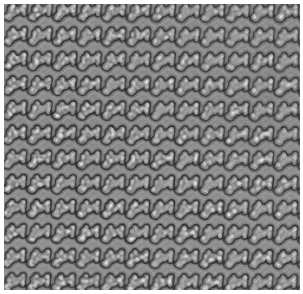
Unit 32



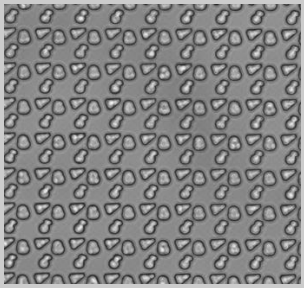
Unit 33



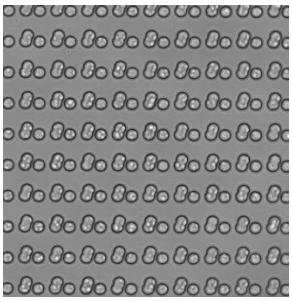
Unit 34



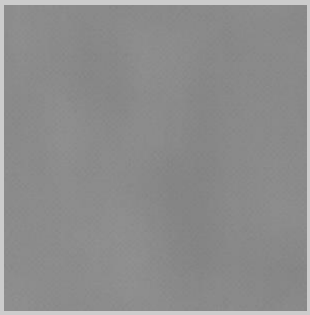
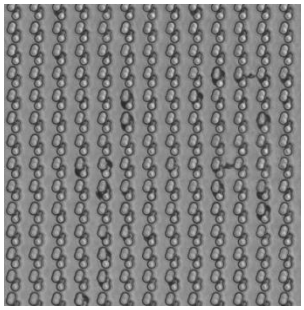
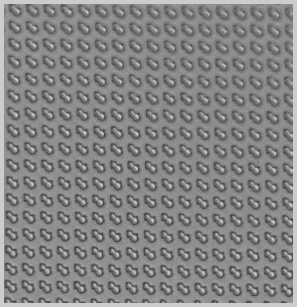
Unit 35



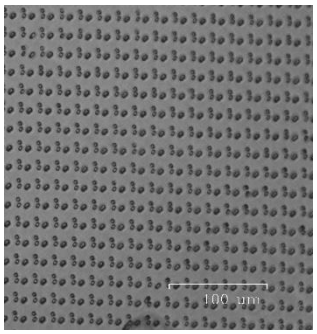
Unit 36



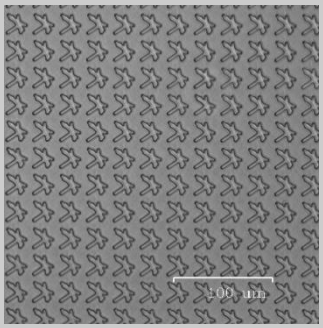
Appendix 9: Phenome topographies with corresponding topography IDs

Topography ID	Feature
Flat	
58	
190	

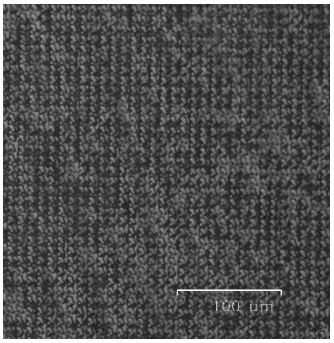
1081



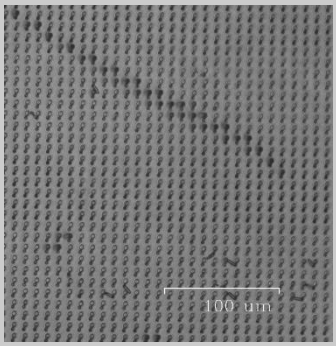
1130



1710



2113



I

